FAN DESIGN AND OPERATION FOR ULTRA LOW NOISE

Daniel Crichton

Trinity Hall

A dissertation submitted for the degree of

Doctor of Philosophy

UNIVERSITY OF CAMBRIDGE

Department of Engineering

2007

Preface

The work described in this dissertation was carried out at the Cambridge University Engineering Department between January 2004 and April 2007. It is the original work of the author and includes nothing which is the outcome of work done in collaboration. The one exception is the higher fidelity noise calculations in §6.5.4 which were created collaboratively with SAI colleagues Dr Elena de la Rosa Blanca, Dr Jim Hileman and Thomas Law. It contains approximately 64,000 words and 91 figures.

I would like to take this opportunity to thank all of the people who have helped me in any way during my time here: Firstly Liping Xu, my supervisor, for helping and guiding me throughout, but equally for encouraging me to set my priorities and explore areas as and when I wanted. Secondly, everyone on the Silent Aircraft Initiative; it was a great three years even if research and design conflicted at times! In particular, I would like to thank my advisor Tom Hynes, Chez Hall, Tom Law, Elena de la Rosa Blanca and Tom Reynolds from Cambridge, Jim Hileman from MIT and Joe Walsh at Rolls Royce. At the Whittle Laboratory, where I spent the last eighteen months of my time, I would like to thank Tony Dickens, Bromwyn Power, Davide Giacche, Graham Pullan and Ed Naylor amongst others for assisting me with the various CFD codes, also Chris Freeman for taking the time to go through my results and make suggestions. The project was funded by the Cambridge MIT Institute and I am very grateful for their support.

Finally, I would like to thank Lucy, my wife, for her love and support throughout.

Daniel Crichton
April 2007

Summary

In this thesis, a new approach to the selection of key fan design parameters is presented and a methodology to optimise engine operation for minimum take-off noise is developed. These techniques are applied to the detailed design of a fan system for the Cambridge-MIT Silent Aircraft Initiative engine in which ultra low noise is the principal design objective.

Reduction of jet mixing noise is identified as being crucial to the design process leading to jet area at take-off having to be increased significantly compared to current trends. Whilst increasing the number of engines from two to three and optimisation of the departure profile reduced this area increase, the introduction of variable cycle technology is required in order to deliver low cruise fuel burn. A variable area nozzle, identified as the most promising technology, is linked to operation of the fan through a simple model. This is used to show that it is possible to enable large increases in exit nozzle area at take-off without compromising fan performance at cruise.

For the fan design, stage loading is shown to be a critical parameter as it impacts competing requirements: Increasing loading increases efficiency and part speed capacity but makes designing fixed outlet guide vanes harder. Fan noise, dominant in this design once jet noise is minimised, is also impacted by loading and a final value of 0.52 is selected, slightly higher than current designs. With high part speed capacity essential for delivering low jet noise, further increased above those obtained through the selection of stage loading are achieved through the use of forward sweep and modification to the blade sections. It is also shown how the outlet guide vane and duct design can be refined to support the high incidence range that results from changes in the exhaust nozzle area.

The method to optimise the departure profile was combined with the completed fan design and extended to include fan and airframe noise sources. The results of this show that, by modifying the nozzle area at all times during take-off to maximise mass flow rate, the final podded SAI design is estimated to have a noise footprint of approximately 65.5 dBA outside the baseline airport at take-off. This leads to an ICAO take-off certification noise level of approximately 73 EPNdB at both flyover and sideline, 23 dB below existing requirements at each measuring location.

Overall, this thesis shows how the additional degree of freedom introduced with a variable area nozzle can be exploited in the design and operation of a fan for a low noise turbofan engine. As well as providing a design solution for the SAI engine, the findings are applicable to any future engine design in which low noise is a key requirement.

Contents

Nomenclature

Symbols

a	speed of sound
A	area
C_{FG}	thrust coefficient
D	drag
f	frequency, Hz
FPR	fan pressure ratio (of bypass flow across stage unless specified otherwise)
g	acceleration due to gravity
h	specific enthalpy
htr	hub to tip radius ratio
I	turbulent intensity
k	turbulent kinetic energy
l	length
L	lift
m	mass
M	Mach number
n	number of engines
N	noise level, dBA
p	pressure
PR	pressure recovery
r	radius
R	gas constant for air = 287 kJ/kgK
Q	fan capacity, $\dot{m}\sqrt{c_p T_0}\,/\,Ap_0$
T	temperature, thrust
T_{ij}	stress tensor
U	blade speed
V	velocity
W	force from aircraft to ground through wheels
α	angle of attack, degrees
β	thrust vector angle in vertical plane, degrees
δ	thrust vector angle in aircraft plane, also duct swirl angle, degrees
ε	turbulent dissipation rate
γ	ratio of specific capacities of heat

φ	azimuthal angle (degrees), flow coefficient
θ	climb angle (degrees), temperature correction $T_0/T_{0,ref}$
ρ	density
η	efficiency
μ	coefficient of friction, viscosity
ω	polar angle (degrees, ahead equals zero)
ψ	stage loading

Subscripts

0	stagnation
01	inlet
2	initial climb
den	day, evening and night
eq	equivalent
EF	engine failure
ff	fan face
G	gross
j	jet
noz	nozzle
N	net
p	polytropic
ref	reference conditions, ISA sea level
R	rotation
s	source
t	turbulent
T/O	take-off
ToC	top of climb
x	axial
∞	free stream

Superscripts

n	velocity exponent
*	critical engine out

Abbreviations

ACARE	Advisory Council for Aeronautics Research in Europe
ATTCS	Automatic Take-off Thrust Control System
BPR	Bypass Ratio
BPF	Blade Passing Frequency
DNL	Day Night Level
EPN	Effective Perceived Noise
ESDU	Engineering Sciences Data Unit
ESS	Engine Section Stator
FAA	Federal Aviation Administration
FAR	Federal Aviation Regulations
JAA	Joint Aviation Authorities
JAR	Joint Aviation Regulations
ICAO	International Civil Aviation Organisation
ISA	International Standard Atmosphere
MTOW	Maximum Take-off Weight
LPT	Low Pressure Turbine
OGV	Outlet Guide Vane
OASPL	Overall Sound Pressure Level
SAI	Silent Aircraft Initiative
SID	Standard Instrument Departure
VAN	Variable Area Nozzle
WAT	Weight – Altitude - Temperature

1. Introduction

Whilst aircraft noise has been reduced by ~20dB since the dawn of the jet age (Smith 1989, Green *et al.* 2001), this has primarily been as a result of the introduction of low and then high bypass engines which are now at optimum ratios for current technologies and installations. The rate of noise exposure reduction has tailed off over recent years with current trends predicting an inflection point being reached in the future. This is illustrated by figure 1-1 which plots noise exposure from all aircraft in service around the world with the drop from 2000 due to the final retirement of non ICAO chapter 3 aircraft (ICAO 1993). Beyond this point, the increase in air traffic is expected to offset the shrinking reductions in noise footprint of new aircraft entering service.

To continue a downward trend in overall noise exposure new aircraft will need to have significantly lower noise footprints than current trends suggest. To drive this reduction the Advisory Council for Aeronautics Research in Europe (ACARE) has created a series of goals for the year 2020 (ACARE 2000) which include efficiency and emissions targets in addition to a 50% reduction in perceived noise relative to 2000 technology levels. Meeting these goals is proving to be extremely challenging and it has been argued that revolution rather than evolution in airframe and engine concepts is required (Smith 2005).

The research presented in this thesis was completed under the auspices of the Silent Aircraft Initiative whose 2025 goal is the reduction in airframe and engine noise sources to a point where they are inaudible outside of the airport boundary in an urban environment. As shown in figure 1-2 this is considerably more challenging in terms of target noise level than the ACARE target. By taking noise reduction as the primary design driver alongside mission requirements and fuel burn, the intention is to explore innovative solutions applicable within the ACARE2020 timeframe and beyond.

This thesis looks at how a drastic reduction in overall aircraft noise to that deemed 'functionally silent' would impact the design and operation of the propulsion system, primarily the fan and exit nozzle.

1.1. What is noise and how is it quantified?

Noise is annoying sound. The threshold of human hearing is generally regarded as fluctuations in pressure of magnitude 20 μPa with over a millionfold increase in magnitude tolerable before the

onset of pain. A logarithmic scale is used to cover this wide range in pressure fluctuations with the sound power of a source and the sound pressure fluctuations heard both described in decibels.

$$PWL = 10\log_{10}\left(\frac{sound\ power}{10^{-12}\ watts}\right) \qquad SPL = 20\log_{10}\left(\frac{p'_{rms}}{20\mu Pa}\right)$$

A change in PWL or SPL of 3dB is generally considered the limit of perceptibility although much smaller reductions in noise than this are still cherished when trying to reduce engine noise. In terms of the audible frequency range, frequencies as low as 20Hz can be sensed as sound with an upper limit for young people of up to 20kHz although this deteriorates down to 10kHz by midlife. Generally, when looking at annoyance, only frequencies from 44.7Hz up to 11220Hz are considered, split into 24 third-octave bands (centred on 50Hz, 63Hz, 80Hz, …, 8kHz, 10kHz). The perception and annoyance of sound is different at different frequencies and therefore, when integrating across the frequency range to give an overall noise level, weighting is applied to the different frequencies. Perceived Noise Level (PNdB) and A-weighted decibels (dBA) are the two most commonly used weighting schemes although others do exist.

Research has found that noise at discrete tones can be more annoying than noise spread across a range of frequencies and therefore tone corrections can be applied to these weighted levels. Further, when looking at the annoyance of aircraft which fly overhead, the noise is commonly integrated over a timeframe rather than just expressed as a peak value. Effective Perceived Noise Level (EPNdB) utilises this approach plus tone corrections and is the value used for aircraft certification (ICAO 1993). Finally, when looking at the annoyance caused by a series of events, such as aircraft periodically flying overhead throughout the day, a correction or integration of the sound over a longer period is required. Examples of such readings include the Noise Number Index (NNI), Day-Night Sound Level (DNL) and the equivalent continuous sound level (L_{eq}). L_{eq} can be calculated for an entire day or just part of the day with weighting sometimes applied for different periods (as is the case for L_{den} in which 5dB is added to evening values and 10dB to night time values). A value of 57 dBA L_{eq} between the hours of 7am and 11pm is used by the UK Government to mark the onset of significant community annoyance (Government 2003a).

For the purposes of this thesis, in which the noise from a single aircraft is of concern, peak A-weighted decibel (dBA) will be used as the target metric. This is because it does not require prior knowledge of flight profiles or the frequency of operation and is therefore easy to design against.

1.2. Benefits of noise reduction

From the entry into service of the first jet powered commercial aircraft in 1952 until today, aircraft noise has been a constraint on the growth of the civil aviation industry. Regulation on acceptable aircraft noise first came into force in the United States in 1969 in the form of FAR part 36 (FAA) and soon after elsewhere in the world in the form of Annex 16 of the 1944 Chicago Convention on Civil Aviation (ICAO 1993). These regulations have become nearly identical and more stringent over time with all current aircraft operating in the developed world conforming to 'chapter 3' requirements and 'chapter 4' now in force for all new aircraft. In recent years more stringent regulation and restrictions relating to aircraft noise have been enforced at the local level. A key example of this is the Quota Count (QC) system in operation at London Heathrow since 1993. Only aircraft that meet the QC2 limit are permitted to land during the night and, for the long haul sector of the market, this has become a *de facto* world wide standard as it is more stringent than the chapter 4 requirements (UK Government 2003b). These regulations have an economic cost in that they affect the design of aircraft, restrict the number of aircraft movements allowed and lead to retirement of aircraft earlier than might otherwise have occurred. For example, the fan diameter of the Airbus A380 was increased beyond what was considered optimum for low fuel burn so that the target quota count band could be achieved (Donoghue 2004).

Another key constraint that aircraft noise has on the growth of the civil aviation industry is in restricting the construction of new runways and terminals. Whilst aircraft noise is by no means the only limiting factor in this respect (increased road traffic and pollution also being critical), it does create a large amount of local opposition to new construction projects. The UK Government in a recent White Paper has recognised that extra runway capacity is required especially in the south east of England (UK Government 2003a) and has stated that a new runway at Heathrow would bring the biggest direct net economic benefit to the UK. Due to local opposition though, the government has decided that this runway will only be constructed 'on the basis that it resulted in no net increase in the total area of the 57dBA L_{eq} noise contour [around Heathrow] compared with summer 2002'.

If a functionally silent aircraft could be developed that also met other environmental requirements whilst remaining economic, one of the key constraints on the growth of civil aviation would be lifted. Whilst small incremental reductions in aircraft noise do help, it has been seen over the years that regulation and more recently local view on what level of noise is acceptable moves to limit

any benefit. Only a step change in noise emission could remove the constraint of aircraft noise on growth altogether.

1.3. What do we mean by 'ultra low noise'?

The Silent Aircraft Initiative aims 'to discover ways to reduce aircraft noise dramatically, to the point where it would be virtually unnoticeable to people outside the airport perimeter in a typical built-up area'. Whilst this is not silence *per se*, it is an extremely ambitious target and one that is used as the basis for this work. In order to evaluate designs and technology against this target, this statement has to be converted into a specific measurable value.

Table 1-1 is taken from a World Health Organisation (WHO) report on guidelines for community noise (Berglund *et al.* 1999). A key value from this report is that noise outside a bedroom window at night should not exceed 60dBA. Perhaps more important for the silent aircraft initiative is what are typical background noise levels in built up areas from non-aircraft noise sources? It has long been recognised that in urban areas road traffic is the primary background noise source (UK Parliament 1963). A more recent study (UK Government 2004) looked at exposure to traffic noise in the Greater London Area (approximately 7 million people). Table 1-2, taken from this report, shows the proportion of the population in this area exposed to various noise levels. It should be noted that L_{den}, L_{day}, $L_{evening}$ and L_{night} are averaged values and not peak.

Using these results as a basis, a typical background noise level in an urban environment was taken as **60dBA** and in order to be 'virtually unnoticeable' the noise limit for a silent aircraft can be taken to match this. This value both accurately represents noise in urban environments and is within recommended WHO guidelines.

1.4. Approach

The fan designed and investigated in detail in this research is for a mixed flow ultra high bypass ratio turbofan which was identified as the most promising candidate for an ultra low noise design. For this type of engine the jet parameters, including noise, are closely coupled to the fan design and operation, specifically the pressure rise across the fan. Therefore, before looking at the detailed design of the fan the relationship between fan operation and jet noise needs to be understood.

As with the approach envisaged by ACARE to meet their 2020 goals, modification to operations have been used to reduce noise outside of the airport boundary during take-off. Following a literature review in chapter two, **chapter three** looks at the relationship between aircraft parameters and resulting jet noise outside of the airport with thrust and profile management used to minimise noise for a given configuration. This leads to a relationship between jet area and jet noise being developed that considers the aircraft operation from brakes off until well clear of the airport boundary.

With significant increases in jet area required relative to conventional designs in order to meet the noise limit, **chapter four** investigates the impact increasing jet area has on key fan parameters. By linking the resultant jet noise to fan pressure ratio and capacity, an approach is developed that enables fan pressure ratio and blade speed to be selected in order to both meet the jet noise target and minimise fan source noise. A variable area nozzle is a key enabler of this.

With principle fan parameters set in order to minimise fan source and jet noise, the detailed design of the fan rotor and outlet guide vanes (OGVs) is discussed in **chapter five**. For the rotor the detailed design must provide the required top of climb thrust, high cruise efficiency and, unique to the approach taken here, high capacity and low pressure rise during take-off. For the OGV, support of high incidence variation, introduced by utilising a variable area nozzle for jet noise reduction, is required.

With detailed aerodynamic design of the rotor and OGV completed, **chapter six** looks at the prediction of the various fan noise sources during take-off. Semi-empirical relationships used in guiding the selection of key fan parameters in chapter four are compared wirh results from higher fidelity models and the success of the design approach taken in that chapter evaluated. These noise models along with an airframe noise model are then incorporated into the optimised take-off departure profile developed in chapter three. This enables the take-off profile to be re-optimised considering all dominant noise sources, rather than just jet noise, minimising the overall noise footprint of the concept aircraft.

The overall success of the design against the noise target can then be judged and, in **chapter seven**, conclusions are drawn and future research discussed.

1.5. Context

As part of a wider silent aircraft project, the research presented in this thesis was based around the evolution and development of a 5000nm range, 250 passenger concept aircraft that made use of an all-lifting body airframe to reduce airframe noise and provide shielding of forward propagating engine noise (de la Rosa Blanco *et al.* 2007, Hileman *et al.* 2007b). The design choices that were made and are presented in this thesis are within this context. In particular, the utilisation of the airframe body for shielding led to rearward propagating fan source noise reduction being more critical than forward propagating source noise reduction.

Further, the focus of the research presented here is on the design of the fan and operation for low noise during take-off. Achieving low approach noise was covered as part of the wider Silent Aircraft project (Hileman *et al.* 2007a) with aircraft stability, go-around thrust requirements and flight speed being critical. Fan and turbine rearward propagating noise were some of the noise sources that made up the overall spectrum but a range of airframe noises including undercarriage and airfoil noise were also significant. Reducing approach noise did influence the design of the core and the overall architecture but did not influence the design of the fan. Therefore, approach noise is not discussed further here.

Finally, the aim of both the overall project and the work presented in this thesis was to look at the impact significant noise reduction as a primary design goal has on the design choices and trade-offs made. In this respect the detailed fan and OGV design, in particular in chapter five, are not intended to be optimum designs but are rather used to evaluate the success of some of the earlier design decisions that were made.

2. Literature Review

A complete review of the published literature relevant to the present research is beyond the scope of this thesis. Instead the present chapter, after a summary of each area, critically reviews the available literature with particular focus on areas that are utilised or influence the approach taken in later chapters.

Jet noise reduction, one of the critical aims of the research, is reviewed in the first section. The various noise sources from a subsonic jet are briefly discussed and prediction methods reviewed, including flight correction effects. Methods of reducing jet noise are then discussed in some detail. With fan noise sources often dominant for modern high bypass turbofans, especially at the cutback position, the next section looks at fan noise sources, prediction and reduction mechanisms. Modern compressor design is reviewed next with a focus on transonic single stage fans. This is by itself a sizeable field so the review focuses on a few specific areas with applicability to the level of design fidelity contained within this research. This includes the impact of reducing fan pressure ratio along with benefits and impacts of lean and sweep from an aerodynamic perspective. Finally, previous projects and publications with similar ambitions are reviewed.

2.1. Jet Noise

Throughout this section the emphasis is on subsonic jets as this is the regime required in order to meet the noise target of this research. Whilst noise sources such as shock, crackle and screech can dominate for higher speed jets, they will not be discussed further. Before discussing noise generation in a jet, an understanding of the jet structure is first required. With single jets the focus of the work in this thesis, coaxial jets are not discussed in any detail.

2.1.1. Structure of a circular subsonic jet

For subsonic, or ideally expanded supersonic, jets the structure consists of a potential core and a mixing region as shown in figure 2-1(a). The potential core, in which the jet velocity equals that at the nozzle exit plane, extends for approximately ten nozzle diameters downstream (Weinstein *et al.* 1956 for example). Around this core the mixing layer, in which the jet flow entrains and mixes with the atmosphere, grows as a circular ring. Downstream of the potential core the average velocity along the jet centreline starts to decrease and, after a transition region, the decrease is inversely proportional to the distance when the surrounding fluid is at rest (Schlichting 1968).

For the Reynolds numbers of full scale jets even at low velocities greater than 10^6 based on nozzle diameter, the mixing layer of the jet is highly turbulent. In such a flow there are structures that vary greatly in scale with the largest of the order of jet diameter. These structures draw energy from the flow with a cascade of smaller structures transferring energy down to the dissipative (smallest) scale.

Whilst the presence of small scale turbulence in jets has been recognised for a long time it was only in the 1970s, well after considerable progress has been made on jet noise (§2.1.2), that the existence of large scale coherent structures in the jet mixing layer was recognised (Crow and Champagne 1971, Brown and Roshko 1974, Winant and Broward 1974). These large structures form immediately downstream of the nozzle due to Kelvin-Helmholtz instabilities entraining ambient fluid as they progress downstream. Near the end of the potential core the structures have the ability to interact across the mixing layer and the large structures can then span the width of the jet. A convective Mach number $(V_j-V_\infty)/(a_j+a_\infty)$ first defined by Bogdanoff (1983) is used to categorise the behaviour of the convective structures. If the convective Mach number is less than 0.5 then the large structures will be similar to incompressible ones as observed by Brown and Roshko (1974).

2.1.2. Noise from circular subsonic jets

The earliest theoretical formulation for aerodynamic noise was the seminal work of Lighthill (1952, 1954). In his acoustic analogy, Lighthill combined equations for the conservation of mass and momentum for a bounded region of disturbed air in a form where one side resembled the wave equation and the other side contains second spatial derivatives of a term, T_{ij}, now referred to as the Lighthill stress tensor.

$$\frac{\partial^2 \rho'}{\partial t^2} - a_\infty^2 \nabla^2 \rho' = \frac{\partial^2 T_{ij}}{\partial x_i \partial x_j} \tag{2.1}$$

where primes indicate perturbation about a basic state and;

$$T_{ij} = \rho v_i v_j + \left(p - \rho' a_\infty^2 \right) \delta_{ij} - \tau_{ij} \tag{2.2}$$

Variations in T_{ij} vanish for linear inviscid flow but not for turbulent flow where the turbulence generates sound as a quadruple source distribution. In many cases (with small temperature variation and negligible viscous forces) Lighthill argued that only $\rho v_i v_j$, the unsteady Reynolds

stress, is important in determining T_{ij}. Then the sound field outside the source region can be written as an integral of T_{ij} over the source region. In the far field this reduces to;

$$\rho - \rho_\infty \sim \frac{1}{4\pi a_\infty^4} \int_V \frac{(x_i - y_i)(x_j - y_j)}{|\boldsymbol{x} - \boldsymbol{y}|^3} \frac{\partial^2 T_{ij}(\boldsymbol{y}, \tau)}{\partial t^2} d\boldsymbol{y} \tag{2.3}$$

where the integration is to range over all **y** in the volume V where T_{ij} is non zero and τ is the retarded time equal to $t-|\mathbf{x}-\mathbf{y}|/a_\infty$. If the strongest motions in the source containing eddies have velocity U, correlated over a length l, then the density field at a distance $|\mathbf{x}|$ using equation 2.2 in equation 2.3 scales as;

$$\rho - \rho_\infty \sim \frac{1}{a_\infty^4} \frac{1}{|\boldsymbol{x}|} \left(\frac{V_j}{l} \right)^2 . \rho_\infty V_j^2 l^3 \sim \rho_\infty M_j^4 \frac{l}{|\boldsymbol{x}|} \tag{2.4}$$

and for intensity;

$$I = \frac{a_\infty^3}{\rho_\infty} \overline{(\rho - \bar{\rho})^2} \sim \frac{\bar{\rho}^2}{\rho_\infty} \frac{V_j^8}{a_\infty^5} \left(\frac{l}{|\boldsymbol{x}|} \right)^2 \tag{2.5}$$

This is Lighthill's famous power law giving radiated sound intensity having an eighth power dependence on jet velocity.

Ffowcs-Williams' work on higher Mach number flow (1963) extended the analysis of Lighthill showing that convection of the sound producing turbulent eddies augment the quadrupole efficiency by a factor of $|1+M_c\cos\omega|^{-5}$ at low speed where M_c is the eddy convection Mach number, less than the jet Mach number, and ω the angular position of an observation point measured 180° from the direction of eddy motion. Ffowcs-Williams showed that at high supersonic speeds the augmentation factor has a limiting form of $|M_c\cos\omega|^{-5}$ leading to radiation intensity only increasing with the cube of the velocity. Harper-Bourne (2003) studied the convective amplification factor by making measurements of the same jet at two different polar angles and comparing the difference at the same Strouhal number. This approach removes the powerful eighth power law dependence and any changes of turbulence intensity with velocity. He found that the convective amplification factor was closer to three than five and put the discrepancy of previous theoretical work down to the frame of reference used when evaluating Lighthill's equation. This matches the value proposed by Goldstein and Howes (1973).

Early experimentation showed good agreement at high subsonic and supersonic Mach numbers with the V^8 and V^3 power laws respectively as illustrated by figure 2-2 reproduced from Bushell (1971) but also available in different forms from (Ahuja 1973), (Smith 1989), (Kobrynski 1968) and others. Between Mach numbers of 0.9 and 1.6 the eighth power law is seen to hold true with the gradient reducing to the third power at very high Mach numbers. At lower Mach numbers, though, an increasing departure was seen between the predictions from Lighthill's analogy and experimental results. Bushell (1971) and Ahuja (1973) through careful removal of other noise sources and use of large contraction ratios showed that an approximate eighth power law does continue down to low jet velocities, as predicted by Lighthill's analogy.

The excess noise, as it was termed at the time, came from a range of sources including the combustor (Bushell 1971), the turbine and upstream disturbances (Gordon and Maidanik 1967). In addition to these external sources, another potential source of sound from the jet as recognised by Lighthill (1954) could be created from unsteady flow at the nozzle exit. This was analysed in detail by Crighton (1972) when trying to find a solution that matched the characteristics of excess noise seen at the time. This included a relationship with velocity between the fourth and sixth power, a pronounced forward directivity and a peak frequency between four and ten times higher than jet mixing noise. Two different sources were identified, one from fluctuating mass flow and axial thrust interpreted in terms of monopole and dipole sources (equation 2.6) and the other from fluctuations in cross-steam thrust interpreted as a transverse dipole (equation 2.7).

$$I \sim V_j^6 \left(1+\cos\omega\right)^2 \tag{2.6}$$

$$I \sim V_j^6 \sin^2 \omega \tag{2.7}$$

The first of these sources, from fluctuating mass flow, peaks in the forward arc whilst the second, from fluctuations in cross-stream thrust, peaks in the perpendicular direction. With acoustic efficiency (total sound power divided by jet power) proportional to the square of the r.m.s. fluctuating thrust level, Crighton compared the sound power radiated through mixing with that through thrust fluctuations at the nozzle exit. Using the work of Crow and Champagne (1971), Crighton calculated a minimum acoustic efficiency (total sound power divided by jet power) of 10^{-6} M^3 under carefully controlled upstream conditions. This compares to an acoustic efficiency of 10^{-4} M^5 for the mixing noise of subsonic jets with clean exit conditions (Lighthill 1962) indicating that in a clean jet these new sources will only dominate over mixing noise for M ~ 0.1 or less. A 1% fluctuation in thrust level will lead to an acoustic efficiency of 10^{-4} M^3 overwhelming jet mixing noise in the forward arc. An additional effect of flow non-uniformity or fluctuation is the

possibility of exciting shear-layer instability waves that can lead to increases in jet mixing noise. Moore (1977) showed that only a small variation in jet dynamic head was required for this to occur. Fluctuating thrust from gas non-uniformities in the jet exhaust can also lead to increases in far-field noise (Marble and Candel 1977, Rienstra 1983).

Whilst jet velocity is the dominant parameter in determining jet mixing noise, jet density also plays a role. Hoch et al. (1973) reported experimental results from two research facilities that between them covered temperature effects for jets with velocity ranging from 150 to 800m/s. They found that at high jet velocities reducing density led to reduced noise as predicted by Lighthill's analogy (see equation 2.5) but at lower velocities reduced density led to increased noise. Similar results were obtained by Tanner *et al.* (1975) for Mach 1.4, 1.7 and 2.0 jets. Morfey (1973) rewrote Lighthill's acoustic analogy in a modified form to argue that another source was present that would be zero only when the flow is homogeneous. If this was not the case an additional dipole source would be present that scales as follows where T_s is the average and ΔT the variation in temperature in the source region:

$$I \sim V_j^6 \left(\Delta T / T_s\right)^2 \tag{2.8}$$

From this it follows that as jet velocity reduces, increases in jet temperature (leading to temperature and density variations in the source region) will tend to increase rather than decrease noise. Combined with Lighthill's analogy this dipole source explains the increasing noise seen at low speed and reducing noise at high speed seen from increasing jet temperature (Morfey *et al.* 1978). Experimental data places the cutover between a V^8 and a V^6 dependence being at a jet Mach number of roughly $1.6(h_j-h_\infty)/h_\infty$ where h is the specific enthalpy of the fluid (Lilley 1991). For a free stream temperature of 300K and a jet Mach number of 0.5 this would limit the jet temperature to no higher than approximately 394K in order to maintain a V^8 dependence.

Recently, drawing his conclusions from a series of detailed experiments, Viswanathan (2004) has suggested that this dipole source due to temperature effects is erroneous. Whilst a weak dependence of temperature on noise is seen, Viswanathan argues that the velocity exponent does not fall to a value of six even at high temperatures and low speeds. He puts the sixth power correlation seen by Hoch et al. (1973) and Tanner *et al.* (1975) to be the result of Reynolds number effects and rig contamination. Viswanathan concludes that Reynolds number effects cease to impact results only at values of 400,000 and above.

Models based on the theories of Lighthill (1952, 1954), Lilley (1974) and others have been extremely successful at predicting the spectral density normal to the jet axis, overall radiated power

and trends with changes in jet parameters. There has been less success in predicting noise closer to the jet axis. Fundamentally this is because a full understanding of the turbulent properties is first required to make predictions of the radiated noise and this still eludes research. It is generally agreed that the finer scale turbulence is a source of noise and that a noise source associated with large-scale turbulent structures is very important for high supersonic conditions. Critically, there is no general consensus, or even satisfactory model, for large scale structure noise for subsonic convective Mach number conditions (Morris and Boluriaan 2004).

Tam *et al.* (1996) divided the turbulent mixing noise into two distinct components for supersonic jets, one from fine scales (Tam and Auriault 1999) and one from large scales (Tam 1991). This is controversial as studies have shown a continuous cascade from the large to the smallest turbulent scales.

2.1.3. Flight effects

As flight Mach number approaches jet Mach number the relative velocity between the two mixing layers drops and jet mixing noise reduces. For low speed jets the impact of flight speed can be significant and therefore accurate prediction of far field changes in radiated noise is critical. In addition to modifying the overall sound power, the change in the shear layer tends to move peak noise directivity further away from the jet axis. Stone and Montegani (1980) split the impact of forward flight on jet noise into three effects; a kinematic effect due to the motion of the airplane with respect to the observer, a dynamic effect due to the motion of the sources with respect to the propagation medium and a source strength alteration due to the reduced shear. The kinematic effect, often referred to as Doppler amplification, provides a correction of $(1-M_\infty \cos\omega)^{-1}$ where M_∞ is the flight Mach number and ω is the polar angle from the aircraft direction to the observer (Ffowcs-Williams 1963, Crighton *et al.* 1977). The dynamic effect is a modification to the source convection correction discussed in §2.1.2 based on the work of Ffowcs-Williams (1963). Normal to the jet axis, where kinematic and dynamic effects are small, only the source strength modification is present. This is generally characterised as a relative velocity exponent, n, as in equation 2.9.

$$OASPL \sim 10\log_{10}\left(1-\frac{V_\infty}{V_j}\right)^n \tag{2.9}$$

In the available literature, n at 90° varies considerably in the range 1 to 5.5 with lower values from full scale testing such as the Bertin Arotrain experiments (Drevet *et al.* 1977) and larger values

from unheated wind tunnel tests (see Plumblee 1976 for examples). This issue was specifically looked at by Ahuja *et al.* (1978) who found that the discrepancy could be accounted for by the presence on non jet-mixing noise sources in the full scale tests. For jet mixing noise alone, literature places n at 90° in the range from 4.0 to 5.5 (Stone and Montegani 1980, Bryce 1984, Stone *et al.* 2003 amongst others).

There is a wide range of prediction methods for static jets, most of which are based on an acoustic analogy of some form. With differing approaches to temperature effects and the use of databases of static results to provide the empirical constants common, the relative velocity exponent, n, is often modified. For unheated jets this involves modifying n as a function of the polar angle and for heated jets also a function of temperature (ESDU 1990b). This replaces any corrections made to account for changes in source convection and/or Doppler amplification.

2.1.4. Noise reduction

Until now, the focus of this review has been on understanding noise generation in single circular subsonic jets. Here we look at modifications to the jet with a view to noise reduction. With jet mixing noise proportional to V^8 for subsonic jet speeds, the obvious way to reduce jet noise is to reduce jet velocity and this has had by far the most significant impact through the introduction of low and then high bypass ratio turbofans (McCune and Kerrebrock 1973). With this approach linked to the engine cycle and therefore subject to a whole host of other demands, not least minimising fuel burn, a range of other mechanisms has been studied. In general, with the detailed noise generating mechanism(s) in single circular jets not fully understood (§2.1.2), experimental campaigns have generally been used to advance understanding. This lack of fundamental understanding makes extrapolating results to different flow regimes, in particular for this thesis lower jet velocities, dangerous.

Coaxial Nozzles

Extracting core exhaust power to drive a fan, increasing propulsive efficiency, has led to significant reductions in jet noise. The flow patterns of the coaxial jet that results is influenced by the bypass ratio, the relative jet velocities and whether a plug is present in the core nozzle. Figure 2-1(b) shows an approximate flow pattern that results with three regions often defined; an initial region, an interaction region and a mixed flow region.

In general, the approach used in predicting the resulting noise is to modify single jet noise predictions for the core jet and/or the fully mixed out jet to take into account the impact of the

outer jet and/or modified mixing regions. Stone *et al.* (1983) using the results of Olsen and Friedman (1974) modified hot single jet predictions based on bypass to core temperature and velocity ratios. More recently, Fisher *et al.* (1998a, 1998b) have modelled the total jet noise as the superposition of noise from the mixed jet, the secondary shear layer and an effective jet which has primary jet velocity but reduced turbulence levels achieving good agreement with experimental data. In all regimes of interest, jet mixing noise from normal velocity profile coaxial jets is higher than fully mixed out equivalent jets.

Forced Mixing

In some engines, mixing of the core and bypass flow occurs upstream of a common nozzle. When the mixing of these two streams occurs near the exit nozzle, incomplete mixing occurs and the ability to estimate the increase in radiated noise, relative to a fully mixed flow, is required. Tester *et al.* (2004) modified the source model they developed for coaxial jets (Fisher *et al.* 1998a, 1998b) to predict the noise from both unforced and forced mixed jets. With unforced mixing there is, for the engine arrangements considered, little mixing prior to the exhaust nozzle and therefore the coaxial model predicts the noise well. For forced jets, significant mixing does occur and the noise can be modelled as that of a fully mixed jet plus an additional, high frequency, source from the mixer itself. As this source is the product of mixing between the two exhaust flows, rather than with the free stream, Tester and Fisher (2005) conclude that it is not reduced by flight effects. Pinker and Strange (1998) obtained reductions of up to 6 EPNdB in jet mixing noise when using a 12 lobed mixer design relative to an annular mixer. This compared well with the ideal noise reduction achievable, highlighting the potential benefit of a forced mixer and shared nozzle relative to a coaxial unmixed arrangement.

With the degree of mixing between secondary and primary flows critical in reducing jet noise, an understanding of lobed mixing is required. Waitz *et al.* (1997) developed a model of mixing streamwise vorticity that compares well with experiments. The enhanced mixing from lobes can be explained by two effects; (i) the increased length of the mixing interface and (ii) the streamwise vorticity created by the lobes. It was shown that close to 70% molecular mixing can be achieved five lobe wavelengths downstream when forced mixing is used. Abolfadl *et al.* (2001) performed detailed low speed tests on the mixing process using lobes and found typical values for mixedness 7.5 lobe heights downstream of between 0.7 and 0.5 for inlet velocity ratios of between 0.36 and 0.66. The mixing parameter was based on an integral of the velocity difference squared as a measure of momentum. The main area of impact of lobes on mixing enhancement is in the first two jet diameters downstream (Hu *et al.* 2002).

Lobes have also been used to mix a single jet with the free stream although the more successful noise reduction designs tend to result in significant thrust penalties. Zaman *et al.* (2003) have recently performed a detailed study of subsonic jet noise reduction using a rectangular lobed nozzle without vorticity added to the stream. This follows on from the work by Tam and Zaman (2000) covering a wider range of nozzle shapes. At the model scale a noise reduction in excess of 5dB OASPL was achieved for minimal thrust loss for a 6 lobed design. This was reduced to about 1.5dB when scaled up and A-weighted due to an increase in high frequency noise.

Tabs and Chevrons

Much of the recent work on jet noise reduction has been focused on the mixing of flows after exit from separate core and bypass nozzles using tabs and chevrons. Bridges *et al.* (2003) summarise the work done at the NASA Glenn Research centre in this area. This includes that by Saiyed *et al.* (2003) who estimated that a 2.7EPNdB noise reduction could be achieved for a 0.06% cruise thrust loss by adding chevrons to both the core and bypass nozzle. Included within this paper are plots showing EPNdB relative to a clean baseline nozzle for 12 designs as a function of the mixed out jet Mach number. The maximum noise benefit is obtained at high jet Mach numbers with the benefit reducing significantly as Mach number drops towards 0.8 (no data is presented for lower values). Indeed, several of the designs presented increase noise at the lower jet velocities.

In order to minimise thrust and enable increased noise reductions, adaptive chevrons are being developed and flight tested (Calkins *et al.* 2006). These use thermally activated shape memory alloys to make use of the temperature difference in the free stream between take-off and cruise, moving the chevron into the jet stream at take-off and out of the jet stream at cruise.

Ejection

An ejector is a device in which the kinetic energy of one fluid is used to pump a second fluid. It consists essentially of a duct through which is discharged a high velocity jet. The secondary fluid, ambient air in this case, is drawn into the ejector, mixes with the high velocity jet in the duct and is discharged. As such, the resultant flow is similar in some ways to that of a coaxial jet and therefore offers the opportunity of noise reduction relative to the primary, high velocity, jet.

Prior to the introduction of turbofans, the use of ejectors for noise reduction was researched extensively. North and Coles (1955) studied subsonic jets with ejector exit over inlet areas of 1.2 and 1.4 and ejector lengths up to a maximum of 1.5 engine exit diameters. With no forced mixing of the exhaust and ejected stream, 'an insignificant reduction in total sound power was realised'.

This can be explained by the work of Mikhail (1960) who investigated both experimentally and analytically the mixing of two coaxial streams inside a closed conduit. Whilst the velocity ratios used were higher than those that would be used in an ejector on any ultra low noise engine (2.5 and greater), extremely long mixing tube lengths were required in order to get a significant reduction in peak jet velocity.

Coles *et al.* (1958) used lobes between the primary and secondary streams to increase the mixing and entrain more secondary fluid. Reductions in the overall Sound Power Level of up to 8dB and the peak Sound Pressure Level of up to 12dB were achieved with an ejector length of twice the nozzle diameter and ejector diameter of 1.6 times the nozzle diameter. 3 to 5dB of the Sound Power Level reduction was attributed to the ejector and the rest to the forced mixing alone. Investigation of forced mixers with ejection was also performed by Rolls Royce according to an early review of jet noise suppression with up to 14dB reductions in OASPL achieved (Miller 1957). Over the next twenty years an extensive amount of research was conducted on using ejectors within aircraft engines with emphasis shifting from suppression of jet noise on early turbojet engines to other applications such as VSTOL over time (Fancher 1972). Comprehensive bibliographies on ejection and jet pumps covering literature from this period include those by Seddon and Dyke (1964) and Bonnington *et al.* (1976).

FitzSimmons *et al.* (1980) present data from a test programme that looked at the use of lobed nozzles and ejectors with up to 16 EPNdB reduction achieved for high supersonic Mach number jets. Brooks *et al.* (1980) present the flight test data from this work and also include Rolls Royce correlations on ejector performance based on lobe and ejector geometry parameters. A range of jet Mach numbers and flight speeds was tested for three nozzle configurations; one conical, one lobed and one lobed with a lined ejector. For a 140 knot flight speed and a Mach 2.0 jet, a significant reduction in noise is achieved both with and without the ejector relative to the conical baseline. As the jet velocity is reduced towards Mach 1.26 so is the reduction in noise. In fact, for the lower jet velocity Brooks *et al.* found an increase in peak noise occurs if just a lobed nozzle is used. Strange and Bryce (1992) used this work as a basis for an analytical model designed to predict jet noise reduction through the use of ejectors. The model shows reasonable correlation with test data once the constants are modified. They do state though that the model they present should be used with caution and obtaining ejector noise reduction performance still relies on experimental testing.

Tew *et al.* (1998) used the work of Waitz *et al.* (1997) discussed earlier to create a mixer-ejector noise-suppressor model primarily aimed at supersonic primary flow but also applicable to

subsonic cases. While this model showed good correlation with experimental data in terms of pumping and thrust, the actual impact on jet noise was not looked at. Presz *et al.* (2002) presented details of an ejector for use with the Spey 511-8 jet engine. Thrust was augmented at low speed with no loss in thrust at cruise speed due to nacelle boundary layer ingestion offsetting the increased wetted area. Unfortunately, again, no noise measurements were taken.

Nozzle Shaping

In a similar way to tabs or lobes, modifying the shape and dimensions of the jet can modify the relative length scales moving the sound produced to higher frequencies and reducing the overall noise level. Gutmark and Grinstein (1999) have presented a review of work in this area focusing on the fluid mechanical aspects and mixing process.

For rectangular jets, increasing the aspect ratio does lead to reductions in noise for a given thrust but sizeable reductions required extremely high aspect ratios. Munro and Ahuja (2003) have measured the noise of very high aspect ratio jets (>100) and found that noise was proportional to $h^{1.5}w^{0.5}$. For smaller aspect ratios though, any noise reductions are much less. For example Coles found less than a 0.5dB reduction in radiated sound power for a full scale 14:1 nozzle increasing to 3dB reduction for a 100:1 nozzle (Coles 1959). Experimental results from Tam and Zaman (2000) suggest shaping the nozzle into ellipses or rectangles of moderate aspect ratio is not an effective method of jet noise reduction with any directivity effects hard to measure. In terms of directivity, Massey *et al.* (2004) found distinct differences between noise at different azimuthal angles especially in terms of the frequency distribution. The influence on azimuthal angle changed significantly with polar angle though making conclusions hard to draw.

Gaeta and Ahuja have published work on splitting the jet up into a large number of very small nozzles (Gaeta *et al.* 2002) with around 5dB reduction in sound pressure levels but at the expense of thrust loss and an increase in engine back pressure.

Finally, bevelling the exit nozzle so that the face points away from noise sensitive areas has been shown to reduce noise, especially in the rear arc (Viswanathan 2005). As with most other noise reduction approaches though, the benefit reduces as jet velocity reduces, although a 2dB reduction was still seen at all frequencies for a Mach 0.7 jet in static conditions.

2.1.5. Summary

Research into understanding the structure of jets and predicting their noise levels has been continuing for over forty years. For a subsonic or ideally expanded supersonic jet, mixing noise

represents the noise floor of the jet. This is a quadrupole source scaling with eight powers of jet velocity. At lower speeds, fluctuations in the flow or flow inhomogeneity can lead to a range of possible dipole sources becoming significant. This reduces the noise scaling from eight down to six powers of velocity. Therefore, to maintain the eighth power scaling as velocity is reduced requires the jet to be close to ambient temperature and steady.

The core and bypass streams from a turbofan engine can either be unmixed leading to a coaxial jet or mixed out prior to the nozzle exit. Fully mixing out the core and bypass streams will lead to the lowest noise footprint although, unless well upstream of the nozzle, the mixer can add an additional source of high frequency noise. Fully mixing out the jet prior to nozzle exit is likely to be more important as jet velocity is reduced as otherwise dipole sources will become dominant.

Recent research into noise reduction for civil subsonic aircraft has focused on enhancing the mixing through the use of tabs, lobes or chevrons. Whilst flight tests have shown noise reductions can be achieved, this benefit reduces with jet velocity and, for the region of interest here, there is not enough evidence to merit their use. Ejection, whilst of more interest to researchers looking at noise from future supersonic aircraft, could be used to further reduce the noise of already quiet jets. Benefit would only come, though, if the exit jet was almost fully mixed out.

Finally, corrections used to account for flight effects lead to reductions in jet mixing noise. These reductions become more significant as the ratio of jet to free stream velocity approaches unity. With limited high quality experimental data available, uncertainties in the flight correction coefficient may lead to large uncertainties in the jet noise footprint.

2.2. Fan Noise

As low and then high bypass ratio turbofans were developed and jet noise reduced, internal engine noise sources started to contribute to the overall engine noise spectrum observed on the ground (Smith 1989). For most modern turbofan designs and concepts, fan noise is the dominant internal engine noise and is the dominant overall noise source at reduced thrust levels (Owens 1979, Smith 1989, Gliebe 2003). Whereas jet noise is, for subsonic conditions, dominated by mixing noise there is often no one dominant source with fan noise. Therefore, in this review the various sources that make up fan noise are discussed first. These include both tonal and broadband sources that propagate through the inlet and the exhaust. Next, the prediction of these sources is discussed with particular emphasis on the applicability of such predictions and limitations when

applied to unconventional low noise designs. Approaches to fan noise reduction are then reviewed before the area is summarised.

As with the section on jet noise, the aim in this section is to review previous work that has a bearing on how to design for low noise. For a more general review, the reader is directed to (Groeneweg *et al.* 1991) and (Huff 1998). Further, with fan noise reduction discussed within the text in §4.2.1 and §6.1, this section is kept brief.

2.2.1. Sources

Figures 2.3 and 2.4 show far field noise in the forward and rearward arc at a range of power levels with the range of sources that contribute to the overall spectrum highlighted. Whilst these spectrums are from a lower bypass ratio engine than is considered in this thesis they indicate well the complexity of the resulting noise field and range of fan noise sources present. For a higher bypass engine, fan broadband and tone noise would be more dominant especially in the rearward arc.

Tone Noise

Tone noise is coherent noise audible at discrete frequencies and, for modern single stage fans, can be split into two sources; rotor alone and rotor-stator interaction. Rotor-stator interaction tone noise is created by the periodic interaction of upstream blade wakes onto downstream blade rows or pylons and the periodic interaction of pressure fields from one blade row onto another. For modern single stage fans with an upstream rotor and downstream guide vane the blade spacing is often great enough for the first of these two mechanisms to dominate.

Whilst both swirling mean flow and changes in duct radius can significantly impact the resultant sound field, insight can be gained by treating the wakes as vortical gusts convected by a mean irrotational flow in a constant radius duct. These simplifications were used by Tyler and Sofrin (1962) to develop a discrete tone interaction noise theory in which the resulting sound in the duct was expressed as two different Fourier series; one considering rotor periodicity and one the stator periodicity. Equating the two lead to the following equation where B is the number of rotor blades, V is the number of stator blades, k is any integer and n is the blade passing frequency harmonic of interest.

$$m = nB + kV \tag{2.10}$$

This equation describes the modes that can exist in the vicinity of the stator where m is the number of lobes of the mode with a frequency of nBΩ rotating at nΩ/m radians per second where Ω is the rotor angular velocity. By considering duct acoustics Tyler and Sofrin showed that if the mode sweeps the outer wall of the annulus at supersonic speeds then it will propagate. If not it will decay exponentially. This leads to the cut-off condition;

$$\left|1+\frac{kV}{nB}\right| > \frac{M_{rot}}{\sqrt{1-M_x^2}} \tag{2.11}$$

In this equation M_{rot} is the absolute tip Mach number of the fan blade and M_x is the axial flow Mach number. When this condition exists the mode in question will not propagate. For a relative Mach number of one ($M_{rel}^2 = M_{rot}^2+M_x^2$) the right hand side of equation 2.11 equals unity leading to the often quoted relation;

$$\left|nB+kV\right| > nB \tag{2.12}$$

If this relation (and equally 2.11) is satisfied for k=-1 it is satisfied for all k. This approach is employed to 'cut-off' the 1st rotor-stator harmonic (n=1) in all modern engine designs by setting the number of stators V to be greater than twice the number of rotors B. Cutting off the 2nd harmonic would require more than four times the number of stators than rotors and, whilst this has been used in research fans, it has not been employed in production engines due to mechanical reasons and because increasing stator count leads to increases in broadband noise. When mean swirl between the rotor and stator is included in the analysis some upstream propagating counter-rotating modes are increased in amplitude but downstream propagating modes and co-rotating modes are more damped (Cooper and Peake 2001). For modes that are not cut-off the resulting far-field intensity and directivity are influenced by a range of factors. The noise is generated primarily at the leading edge with intensity dominated by the convected Mach number and gust strength (Huff 1998).

Using a similar argument to rotor-stator interaction noise, rotor-alone noise will be cut-off unless the relative tip Mach number is greater than one. Rotor alone tone noise at the BPF and higher harmonics is generated through inlet flow non-uniformities onto the rotor from nacelle separations or other upstream disturbances, all of which are generally small for modern designs. Another source of rotor-alone tone noise is from the shocks on the blade surfaces that propagate forward. This noise source can be significant and is worthy of further discussion.

Buzzsaw

As the relative tip Mach number of the flow onto the fan approaches unity, shocks start to form ahead of the rotor leading edge and on the rotor suction surface. These shocks propagate upstream and, due to variations from manufacturing and installation, coalesce into a range of multiple pure tones below the blade passing frequency referred to as MPT or buzzsaw noise. This noise propagates forward only but can be one of the dominant engine noise sources during take-off.

Morfey and Fisher (1970) were the first to develop a prediction of the intensity of the radiated sound through assuming identical blades and modelling the shock as being normal to the flow that would occur without the presence of the blades (i.e. M_{rel}). The theory agrees well with experiment and predicted peak noise for a relative Mach number of approximately 1.2. At higher Mach numbers the increased propagation distance more than offsets the increased shock strength leading to gradual reduction in sound power as Mach number is increased. A rapid reduction in sound power is predicted as relative Mach number drops below 1.05.

McAlpine and Fisher (2001, 2003) developed a model for investigating the propagation of the waveform that accounted for both a non uniform source (an irregular saw-tooth wave) and the presence of acoustic liners in the upstream nacelle. This model indicates that significant reductions in noise can be achieved through lining for relative tip Mach numbers below 1.2 but liners are much less effective at higher Mach numbers. Predictions using this model have been compared to experimental results obtained as part of the RESOUND programme (McAlpine *et al.* 2006). Whilst the agreement obtained at a range of relative tip Mach numbers for unlined ducts was good, there was less success for lined ducts. In particular the code significantly over-predicted the peak liner attenuation at lower tip Mach numbers. Suggested possible reasons for this were too high model decay rates in the code or scattered noise from splices in the real hardware masking the pure buzz-saw noise at frequencies in which the liners were particularly effective. Recent tests have shown splices used in current intake liners can increase propagated buzzsaw noise significantly (Yu *et al.* 2006).

With the take-off operating line on a fan map shallower than the cruise operating line, fans operate closer to stall during take-off than at cruise. This is especially so at cut-back power levels resulting in the shock being detached from the leading edge as illustrated by figure 2-5. This gives a propagating shock strength similar to that calculated by Morfey and Fisher. If the operating line is moved down (through changes in nozzle area or changes in flight conditions) the primary shock can become ingested into the blade passage with a weaker bow shock at the leading edge that is

attenuated by expansion waves emanating from the suction surface. Computational results by Xu (2004) backed by rig tests indicate that modification of the shock structure in this way can reduce the propagated SPL by up to 6dB.

Broadband Noise

There has been considerable success in reducing tone noise from modern high bypass engines through improved component design and lining. This has resulted in fan broadband noise becoming a major component in the overall radiated sound (Gliebe *et al.* 1995 for example).

Early rig tests led to correlations of broadband noise with rotor inlet relative tip Mach number and incidence (Ginder and Newby 1977, Gliebe 1979). From these tests, broadband noise was seen to vary with between five and six powers of Mach number and to increase by between 1.7dB and 2.5dB per additional degree of incidence. More recent results, based on FANPAC tests in Europe, have found similar trends (Lewy 2000). With multiple potential sources of broadband noise (see figure 2-4), recent work has focussed on trying to better understand and predict the individual sources.

Probably the most significant published research efforts in understanding broadband noise was the NASA sponsored Boeing 18" rig test (Ganz *et al.* 1998). Although only looking at the noise from a single fan design, several modifications were made to the rig to try and isolate the relative importance of the different broadband sources with both far-field and in-duct measurements made. Significant broadband noise was found to come from the fan alone even with clean inflow and no nacelle boundary layer. This noise was strongly effected by blade speed (approximately 6^{th} power indicating dipole source) and loading and weakly effected by tip clearance in both the forward and rearward direction. Rotor tip interaction with a boundary layer when present was also a significant source as was the interaction of the rotor with high order inlet non-uniformity at least under high loading. The effect of blade speed on this source was closer to 4^{th} than 6^{th} power and reducing tip clearance increased the far-field noise. The final significant source, dominant aft, was the interaction of the stator with the fan wake. This was strongly affected by blade speed (approximate 6^{th} power) and also by OGV count with increasing OGVs increasing the noise. Rotor tip clearance and loading had less of an impact on the resultant noise.

Similar results were seen by Woodward *et al.* (2002) who, while not solely looking at broadband noise, studied two rotors and thee stator combinations. For supersonic blade speeds the rotor alone noise field dominated in the forward arc but for lower speeds, rotor-stator interaction noise was dominant. In the rearward arc, rotor-stator noise remained dominant until higher speeds

when again rotor alone noise became significant. This relative dominance of sources is not always the case though with Gliebe *et. al.* (1995) finding nacelle boundary layer flow onto the rotor tip dominant.

The range of noise sources has also been looked at analytically. Glegg and Jochault (1998), who used the trailing edge noise of isolated airfoils as the starting point in the prediction of rotor only broadband noise, found sound power scaling to the fifth power of relative tip Mach number at lower speeds rising to the sixth power at high speeds along with a 2.4dB noise increase per degree of incidence. For rotor-stator interaction noise, Hanson and Horan (1998), building on the work of Glegg (1999), developed a cascade response model to inhomogeneous turbulence. Predictions from this include broadband noise being proportional to vane count but independent of chord indicating fewer wide chord blades would reduce broadband noise. Downstream noise was found to be proportional to the fifth power of mean flow Mach number onto the OGVs with upstream noise dependent on a slightly lower power. In terms of the turbulent parameters, noise was proportional to turbulent intensity and increases in length scale tended to increase noise at lower frequencies and reduce it at higher frequencies. Evers and Peake (2002) extended this work to account for non-zero thickness and camber finding that whilst blade geometry can have a significant effect on the noise generated from a single gust, for a full turbulent spectrum the impact is only of the order of 2dB. Coupling of the rotor into the analysis increases the downstream noise level (Hanson 2002).

2.2.2. Duct propagation, radiation and shielding

Fan source noise propagates upstream and downstream through acoustically lined ducts before radiating from either the inlet or nozzle lip. Acoustic modes are absorbed in different degrees by the liners and are also scattered by any discontinuities in the ducting making prediction of far field radiated noise complicated. A wide range of liner technologies exist that are in widespread use (Smith 1989) but for the results presented in this thesis liner attenuation and radiation based on the work completed as part of the Silent Aircraft Initiative will be used (Law and Dowling 2006, 2007). Far-field engine noise is estimated by solving appropriate eigenvalue problems for uniform axial inviscid flow in annular and cylindrical lined ducts. From the resulting modal amplitudes at the nozzle termination, the radiated sound pressure level is estimated using the Wiener-Hopf solutions from an unflanged duct.

For forward noise sources, shielding estimates are made based on the work of Agarwal and Dowling. For quick results, corrections as a function of polar angle, azimuthal angle and frequency were based on low frequency estimations extended conservatively to higher frequencies (Agarwal

and Dowling 2005). When higher fidelity estimations are required then more computationally intensive ray theory methods can be used (Agarwal *et al.* 2006).

2.2.3. Noise Prediction

The most widely used semi-empirical fan noise models are based on the work of Heidmann (1979). This includes the model used in the NASA ANOPP code (Zorumski 1982) and the ESDU code (ESDU 1998). These models only use basic design parameters and mass averaged flow quantities in their prediction, making them easy to apply. The main disadvantage is that they cannot take into account new or unconventional design features such as sweep and lean. Also, with the correlations based on tests from existing fans which have fixed nozzle areas, they may not properly reflect changes in the propagated noise if the fan is operating at an unconventional point. Finally, whilst tone, buzzsaw and broadband noise are predicted separately, there is no attempt to split the sources down further.

At the next level of complexity, noise prediction codes start to be specific to certain noise sources. The range and breadth of the different models developed is wide and well reviewed in a recent paper (Envia *et al.* 2004). For tonal sources, state of the art models are of high fidelity and able to predict the resultant noise with reasonable accuracy. The most common approach is to first obtain unsteady flow field data using a RANS code before using a linear code with a higher resolution grid to obtain noise predictions. For broadband noise on the other hand, much more significant prediction challenges remain. Whilst the same tools used in predicting tonal noise are applicable, the range of frequencies and scales involved make obtaining statistically meaningful data prohibitive. For interaction noise, state of the art broadband prediction codes use either experimental or computationally gained turbulence data as input to a simplified analytical model. These have generally been successful at predicting the spectral shape of the noise and trends with blade count and sweep but less successful at predicting absolute noise levels especially at higher Mach numbers. For self noise, most models are based on the work of Glegg and Jochault (1998). Here, the main limitation is knowledge on the turbulence at the trailing edge and, as with interaction noise, this leads to the trends being largely correct but the prediction of absolute levels less so.

2.2.4. Noise Reduction

Having looked at tonal and broadband fan noise sources, this sections aim is to discuss the possible ways such sources can be reduced for a given thrust level.

Blade count

The simplest way to reduce rotor-stator tone noise is to cut-off the lower order harmonics through reducing the rotor or increasing the OGV blade count (Tyler and Sofrin 1962). Whilst this approach is currently almost universally used for cutting off the 1st BPF, cutting off higher orders is not practical. Further, with rotor-stator broadband noise proportional to the number of OGVs (Ganz *et al.* 1998, Topol *et al.* 2004), a current research aim is to control tone noise through OGV sweep and lean thus allowing blade count to be reduced, reducing broadband noise whilst cutting on the 1st BPF.

Lean/Sweep

OGV sweep and lean has been successfully used to reduce tone noise. Analysis of potential tone noise reduction by Envia and Nallasamy (1998) indicated that both positive sweep (tip further downstream than hub) and positive lean (tip moved circumferentially in the direction of rotor rotation) will reduce noise with greater angles of sweep and lean leading to greater noise reduction. They argue that this is because such a design maximises the number of wake interactions per vane. Woodward et. al. (2001) tested this for a design in which OGV blade count has cut-off the 1st BPF and sideline noise reductions of the order of 3EPNdB were observed. Tone noise in particular was significantly reduced but small reductions in broadband noise of the order of 2dB were also observed at the lower fan speeds with reductions of up to 4dB at high frequencies. More recently, sweep alone has been shown to significantly reduce tonal noise when blade count is reduced and the 1st BPF cut-on (Heidelberg 2002). Hanson (2001) indicates that OGV sweep reduces broadband noise by reducing the chordwise component of Mach number and that lean has limited effect. Topol *et al.* (2004) suggested forward sweep at the tip (termed a tip boot) could reduce broadband noise if the broadband noise is primarily created in the tip region.

Whilst significant leaning of the rotor is not possible due to blade stressing, forward sweep of the rotor has been used to reduce multiple pure tone noise. This was the approach used by Xu (2004) to swallow the primary shock in the tip region as discussed in the subsection on buzzsaw noise.

Blade speed vs. Loading

With both tone and broadband noise scaling at between five and six powers of blade speed, an obvious way of reducing noise is to reduce the blade speed. For the same fan pressure ratio this leads to an increase in the loading;

$$\psi = \frac{c_p T_{01}}{U^2}\left(FPR^{\frac{\gamma-1}{\eta_p \gamma}} - 1 \right)$$

Several recent fan designs have used this approach with varying results. Bewick *et al.* (2001) reported the results of a low noise research fan (LNR1) designed and tested as part of the European RESOUND programme. This fan was designed to have the same design capacity and pressure rise but with a 15% reduction in speed. Large tonal noise reductions were achieved at speeds above 80% of design relative to the datum but no reductions were observed in broadband noise. The tonal noise reduction was put down to the rotor alone tone being cut off for the lower speed design when it was cut on for the datum.

A similar approach was undertaken as part of the NASA Advanced Subsonic Technology (AST) programme with the second fan designed as part of the programme (Neubert *et al.* 1997) having a 10% lower tip speed than the first (Hobbs *et al.* 1995). This fan was expected to be 2dB quieter based on scaling laws of 50 log (tip speed) and 7 log (vane number). In fact, on testing, the fan was found to be approximately 2dB noisier than the earlier design due to increased turbulence from the rotor tip interacting with the OGVs (Topol *et al.* 2004).

Whilst noise may scale with tip speed to the power five or six when moving along a working line or when loading does not change between designs, this is not the case if loading is increased to maintain pressure rise. Increases in noise due to increased loading from one design to the next can negate or even dominate changes due to tip speed.

Other

Other approaches that have been used to reduce or try to reduce fan noise include trailing edge blowing (Brookfield and Waitz 2000, Sutliff *et al.* 2002) and active noise control (Pla *et al.* 1996, Curtis 1999). Both of these have been successful at reducing tonal noise but lead to increasing design complexity and have not to date progressed beyond proof of concept testing.

2.2.5. Summary

With multiple sources and a complex propagation path, accurate prediction of fan noise on the ground is considerably harder than accurate prediction of jet noise. This is especially true for broadband noise due to the range of frequencies and scales that need to be considered. With tonal noise controlled through cutting of the 1st BPF and, more recently, the use of sweep and lean, for

modern high bypass ratio turbofans, broadband noise is of higher or similar magnitude to tone noise.

When operating with clean inflow, two broadband noise sources dominate; rotor alone and rotor-stator interaction. Rotor alone noise scales with between five and six powers of relative Mach number and is also linked to blade loading, usually characterised through incidence. Rotor-stator interaction scales with a similar power of Mach number, this time onto the OGV, but is less dependent on loading. Rotor alone noise appears to become increasingly significant as blade speed increases with rotor-stator noise dominant at lower speeds.

Buzzsaw noise can dominate forward propagating noise at supersonic inlet relative Mach numbers although recent analysis indicates that splice-free liners can significantly reduce propagating noise for relative Mach numbers below 1.2.

2.3. Fan Design

With this thesis looking at the design and operation of a fan for low noise, fan design itself is very briefly reviewed. As with previous sections, transonic fan design is a large subject and therefore here we limit discussion to a focus on aerodynamics. Whilst low jet noise and low fuel burn could be achieved through the use of a turboprop or contra-rotating propfan design (Peacock and Sadler 1989), the turbomachinery noise of these designs is currently unacceptable and they will not be discussed further. For a comprehensive discussion on compressor design in general the reader is referred to Cumpsty (1989), Gallimore (1999) and Wennerstrom (2000) as starting points.

Borradaile (1988) discusses the challenges of moving to increasing bypass ratios and lower pressure ratios. The introduction of either variable pitch or variable nozzle area is required below a FPR of approximately 1.4 so as to maintain sufficient stability margin at take-off and a gearbox is likely to be required between fan and LPT. Similar requirements were seen for the low FPR designs in the NASA ultra-efficient engine diameter study (Daggett *et al.* 2003).

Looking at the transonic rotor first, Calvert and Ginder (1999) discuss the overall design process including that of the blade sections. Highlighted in this work is the balance that needs to be achieved between all the various requirements including the control of shock strengths and peak Mach numbers in the uncovered section of the blade whilst at the same time minimising profile loss in the covered section. Precompression, whilst beneficial at design speed can lead to early choking and poor performance at part speed. Following an initial transonic fan design

documented by Wennerstrom (1984), a range of seven similar rotors were tested each of which has, as far as possible, one salient feature modified. Results are presented in a range of papers (Copenhaver *et al.* 1993, Law and Wadia 1993, Wadia and Law 1993, Wadia and Copenhaver 1996). For the 1.92 pressure rise design with rotor tip relative Mach number of 1.63, conclusions were that maximum thickness at the tip should be at approximately 55% to 60% chord, tight throat margin increases efficiency at design but leads to reduced part speed performance and reduced trailing edge camber is beneficial. Unfortunately, no similar studies are available for lower pressure rise, lower speed designs which obtain more of their pressure rise through turning. Recently, research has focused on three dimensional effects, specifically sweep and lean. For the rotor, forward sweep leads to slightly higher rotor alone efficiency and a significant increase in surge margin at design speed (Wadia *et al.* 1998, Denton and Xu 2002, Passrucker *et al.* 2003). Rearward sweep is less successful with surge margins generally reduced.

For the stator, inlet flows are generally subsonic at all operating conditions although supersonic patches are present on the suction surface near the hub. Following the introduction and refinement of controlled diffusion airfoils firstly for the core flow (Hobbs and Weingold 1984) and later in the end wall regions (Behlke 1986), recent research has looked at increasing incidence range (Koller *et al.* 2000, Kusters *et al.* 2000) and the use of sweep and lean (Denton and Xu 1999, Friedrichs *et al.* 2001, Gummer *et al.* 2001).

2.4. Holistic approaches to aircraft and engine noise reduction

As a precursor to the Silent Aircraft Initiative, Pilczer (2003) and Manneville (2004) looked at the use of an all-lifting body aircraft to achieve significant aircraft noise reduction. These works were at a conceptual level only but indicated significant noise reduction could be achieved especially if multiple engines were used embedded into the airframe suction surface.

In a series of papers, Antonie and Kroo (2002, 2004, 2005) have looked at optimisation of the aircraft, engines and operations for reduced environmental impact, including noise. Engine bypass ratio was seen to be the key driver to environmental change with only small improvements available through use of modified operational procedures including cutback. With only conventional designs considered, a key finding was that the minimum noise design required a much higher bypass ratio (and therefore lower fan pressure ratio) than minimum cost or fuel burn designs.

3. Required jet area for a 'silent' take-off

In this chapter, jet noise is identified as being fundamental to the preliminary design process due to its impact on cycle design. This leads to reduction of jet noise to a level considered silent being the first step in designing engines for a silent aircraft. To determine what jet area a silent aircraft requires, take-off needs to be considered. Regulatory and operational requirements relating to take-off are looked at so as to determine what constitutes a successful take-off. The departure profile is then optimised for low jet noise within these requirements giving, for specified aircraft parameters, the required jet area for a silent take-off. The impact of this on engine design is then discussed.

Modification of the departure profile for noise reduction is in use today. Current thrust cutback (or noise abatement) procedures are regulated (ICAO, FAA 1993) and in use at a large number of airports. They are relatively simple with operators currently only allowed to implement two variants across all airports for safety. Research into improving these procedures is linked to operation of the existing fleet and tends to focus on pilot acceptability (Elmer *et al.* 2002), modification of the ground track at specific airports for avoiding population centres (Visser and Wijnen 2001, Wijnen and Visser 2003) or use of navigation aids in order to more accurately fly specified departure profiles (Erkelens 2002). In this chapter optimisation of the departure profile for a baseline airport is used as the starting point in engine design, very different from existing research in this area

As jet noise will not be the only noise source at take-off, for this chapter the jet noise limit has been taken as 3dB below the overall noise limit of 60dBA specified in §1.3, i.e. 57dBA.

3.1. Jet noise reduction: Driving the engine cycle

Whilst a range of jet noise generation mechanisms exist that are, or have similar properties to, a dipole source distribution (§2.1.2), for a cold subsonic jet, mixing noise can be considered as the **noise floor** for the entire aircraft. This is because the noise is directly linked to thrust and is generated several diameters downstream of the jet making shielding hard. This thinking is not new (see Smith 1989 for example) but using this as the starting point for designing the entire engine and specifying how it is operated is new, as far as the author is aware. Equation 3.1 below, a copy of equation 2.5, shows how jet mixing noise scales for unheated subsonic jet speeds (Lighthill 1952).

$$I \sim \frac{\overline{\rho}^2}{\rho_\infty} \frac{V_j^8}{a_\infty^5} \left(\frac{l}{|x|} \right)^2 \tag{3.1}$$

With engine cycle design, which determines jet velocity, currently optimised for today's technology and installations, a considerable amount of research in recent years has focused on reducing the effective length scale of the jet. A wide range of concepts has been looked at including distributed nozzles, tabs, lobes and jet shaping. Moderate reductions in the order of a couple of dB have been achieved in this way but, as discussed in §2.1.4, as the driving jet velocity is reduced, the benefits of such technologies reduce.

To make a sizeable reduction in radiated jet noise the jet velocity must therefore be reduced which leads to an increase in jet area for a fixed thrust. This requirement, for conventional turbofan engines, directly leads to an increase in engine bypass ratio and a reduction in fan pressure ratio as core pressure rise and turbine exit temperature cannot be reduced due to the impact on thermal efficiency. This will lead to increased propulsive efficiency at the expense of additional weight and installation drag losses. As will be seen later in this chapter, in order to meet the target noise level, the required reduction in fan pressure ratio is to a value well below the optimum for today's technology and installations. Therefore, any increase in jet area needs to be minimised and optimisation of the departure profile is one way of achieving this.

With high temperature jet noise reducing in proportion to approximately V^6 rather than V^8 as speed is reduced (§2.1.2), avoiding a high temperature jet is critical. Therefore only single, fully mixed out jets are considered in this section. With these jets being formed from a hot core and a colder bypass, §3.3.2 discusses the most appropriate way of modelling the resulting noise.

3.2. What constitutes a successful take-off?

Not all take-offs have to be silent. Whilst any concept aircraft must be able to operate at the same airports and under the same conditions as conventional aircraft, not all operations need to meet the same noise goal. Extremes of altitude and temperature, in particular, place additional demands on the engines and designing for ultra low noise under these conditions does not make sense when most noise constrained airports are not subjected to such extremes.

3.2.1. Baseline Airport

The approach taken is to define a baseline airport that can be used to design the concept aircraft for which the airport can be designed and which can be used to evaluate performance. Table 3-1 lists the thirty busiest airports in the world by passenger number as of 2003, highlighting noise limitations in force at each. With London airports in particular subjected to significant noise constraints (see §1.2 also), the baseline airport was chosen to cover the most restrictive of London conditions (approximately at sea level). As such, runway length was set to 10,000 feet which is short by international 'hub' standards but is a common length for regional 'spoke' airports (Stansted for example). ICAO certification distances (ICAO 1993) of 2000m approach (from threshold), 450m sideline and 6500m flyover (from brakes off) do not match most airport boundaries with the flyover position in particular being well outside most airports. After examining a range of airport boundaries, the baseline values were set to 1000m from the start and end of the runway and 450m sideline as illustrated in figure 3-1. The hotter the conditions the lower the air density and the greater the jet velocity required for a given thrust. Therefore, as jet temperature, which is linked to atmospheric temperature, increases it becomes harder to meet a jet noise target for a given jet area. Baseline airport temperature therefore needs to be specified at a high value so as to cover the majority of airport operation hours. Table 3-2 and figure 3-2 show the number of hours above a specified temperature at London Heathrow for the period 1989 to 1999 inclusive. By allowing 1% of 0600 to 2300 operating time to be 'non-silent', the required maximum 'silent' operating temperature can be set to ISA+12°K. Finally, with higher humidity leading to less atmospheric attenuation (ESDU 1977), relative humidity was set to 70%. To summarise, the baseline airport has the following parameters;

- 10,000ft (3,048m) runway
- Distance from edge of runway to flyover/approach boundary of 1000m
- Distance from runway centreline to sideline boundary of 450m
- ISA+12K, sea level conditions, 70% relative humidity

Whilst this airport will be used to design against, a longer runway, 5,000ft (1,524m) elevation noise constrained airport is also considered briefly in §3.4 and chapter six. This airport is based on conditions at Denver and has a runway length of 12,000ft (3,658m). As noise constraints are less restrictive at Denver the low noise operations were set to cover 90% of operating hours rather

than 99% as for London. This leads to a maximum temperature of ISA+19.5K (based on data from NWS 1984-1992).

In terms of non-noise-constrained operation, any concept aircraft must be able to operate in the same range of conditions as conventional equivalent aircraft. Figure 3-3 shows a Weight-Altitude-Temperature (WAT) chart for the Boeing 767-300 which has similar range and payload requirements of the baseline silent aircraft. With the final engine concept having a low specific thrust and the aircraft having a high cruise altitude, the fan will be capable of delivering enough thrust. The limiting factor is likely to be the temperature either into or out of the combustion chamber and this is outside of the scope of this work.

3.2.2. Regulation and Operation

In Europe, section 25 of the JAA Joint Aviation Regulations (JAA) (and section 25 of the FAA Federal Aviation Regulations in the United States (FAA)) cover airworthiness standards for transport aircraft. Part V Volume 1 of ICAO PANS-OPS (ICAO) specifies recommended safe cutback procedures in Europe with Advisory Circular 91-53A (FAA 1993) the equivalent in the United States. The impact of this regulation, along with operational requirements from a range of airports, is considered in Appendix A.

To be considered a realistic option, any concept aircraft must comply with the regulatory and operational requirements currently in force. If any of these requirements cannot be met, an argument must be made as to why;

(a) the aircraft might be able to achieve an exemption or

(b) the regulations might change in the next 20 to 30 years.

The requirements, discussed in more detail in Appendix A, can be split into the following areas:

1. Engine-out safety requirements
2. Low noise cut-back requirements
3. Airport usage requirements
4. Passenger comfort requirements

Of these, (1) is the only area must be considered an essential requirement. For the others (3) and (4) will have economic impacts so should be met if possible. (2) is more complicated as the low noise operational procedures described in PANS-OPS and AC 91-53A are designed for very noisy aircraft relative to the target for this work. The critical requirement from these regulations is that no cut-back can occur until 800 feet which may significantly reduce the benefit of any take-off optimisation when the airport boundary is not far from the take-off point. Therefore, for this work, the 800 foot minimum cutback height limit will not be considered a requirement on the SAI Silent Aircraft. All other regulatory requirements will. As the engine-out condition will be met at all times and the take-off profile will be fully ATTCS managed, this does not impact the safe operation of the aircraft[*]. In summary, this leaves the following requirements that must be met as part of a low noise optimised take-off:

a) The following scenarios must be considered:

   - Normal take-off until an altitude of at least 1500 feet is reached.
   - Engine failure at V_{EF} followed by bringing the aircraft to a halt.
   - Engine failure at V_{EF} followed by continuing take-off up to an altitude of 400 feet.
   - Engine failure at V_{EF} followed by continuing take-off but with roll initiated at 5 knots less than the value of V_R specified.

b) For normal take-off, the aircraft must be at 35ft (10.7m) height and V_2 by 8,695ft (2650m) for the baseline 10,000ft (3048m) runway.

c) For aborted take-off after engine failure, wet take-off with 80% anti-lock braking efficiency is considered with 200psi tyre pressure. The tyre pressure corresponds to that of a B767-300 (Boeing 2003). Figure 3-4 shows the maximum available acceleration distance for different runway lengths in order for the aircraft to be able to stop within the runway length following engine failure at V_{EF}.

d) For take-off after engine failure, only the dry condition is evaluated. The aircraft must be at 35ft (10.7m) height and velocity V_2 by the time it passes the end of the runway following engine failure at V_{EF}. By the time an altitude of 400 feet is reached, the aircraft must be climbing at a rate of 1.7% (4 engine), 1.5% (3 engine) or 1.2% (2 engine).

[*] In any event, the eventual take-off profile presented in chapter 6 does meet this requirement.

Available thrust can be increased to 111% of that which would be used on a normal take-off profile (i.e. low noise optimised) at the point of engine failure (V_{EF}). If take off roll is initiated at 5 knots less than V_R then 35ft (10.7m) altitude must be achieved in the same or reduced distance.

e) For operational reasons, the average climb angle should be 4° from take-off until an altitude of 1000m and a minimum of 4° beyond this.

f) To comply with engine out requirements, a 111% allowance for ATTCS is assumed. Minimum climb angles as a function of L/D are shown in figure 3-5 for 2, 3 and 4 engine aircraft for the case where L/D in not impacted by engine failure. This figure is based on the following equation where θ^* is the mandated minimum climb angle after engine out (equal to 1.37° below 400ft (121.9m) and 0.69° above if 2 engines, 1.55° below and 0.86° above if three engines, 1.72° below and 0.97° above if 4 or more engines) and θ_{min} is the minimum climb angle required before engine out.

$$\theta_{\min} \approx \max\left[\begin{array}{l} \sin^{-1}\left(\dfrac{n_{eng}}{n_{eng}-1}\dfrac{1}{L/D}\Big|_{after} - \dfrac{1}{L/D}\Big|_{before}\right), \\ \sin^{-1}\left(\dfrac{1}{1.11}\dfrac{n_{eng}}{n_{eng}-1}\left(\dfrac{1}{L/D}\Big|_{after} + \sin\theta^*\right) - \dfrac{1}{L/D}\Big|_{before}\right) \end{array}\right] \tag{3.2}$$

g) Aircraft pitch should not exceed 20° for passenger comfort reasons.

Whilst the approach taken in this thesis, in line with the goal of the SAI, is to minimise noise outside of the airport boundary, it is worth briefly mentioning take-off requirements for noise certification (FAA FAR-36, JAA JAR-36). Subsections 160(a) and 160(b) define the reference certification take-off procedure including; sea level ISA+10K conditions, minimum cutback heights are 300m (two engines), 260m (three engines) and 210m (four or more engines) and a minimum climb gradient after cutback of either 4% (2.3°) or that required to sustain level flight after engine out, whichever is the greater.

3.3. Modelling

A time-stepping approach was used to model the take-off with thrust and climb angle limited so as not to exceed the jet mixing noise target anywhere outside of the airport boundary (see figure 3-1). This is illustrated in figure 3-6 with the take-off split into three regimes; acceleration, roll and

climb. When accelerating, along the runway only thrust is varied to meet the noise target, with increases in forward speed allowing gradual increases in gross thrust. Once the rotation speed V_R is reached the same approach continues but, in addition, aircraft angle of attack is increased at a specified rate. This continues until there is enough lift to get airborne. After a short initial period in which climb is established, flight speed is then fixed and the climb angle (which impacts thrust) modified in order to meet the noise target. Climb continues until the aircraft crosses the airport boundary which is a critical location in determining the success, or otherwise, of the take-off. If, for the given target noise level, not all requirements listed in §3.2.2 are met, jet area is increased and the take-off repeated.

This approach leads to the minimum, i.e. optimum, jet area required in order to meet the specified noise target.

3.3.1. Aircraft

Figure 3-7 shows the aircraft model used during the take-off modelling. For this chapter the thrust vector angle, β, was set to zero and pitching moment not considered. Resolving in and perpendicular to the direction of aircraft motion;

$$m\frac{dV_\infty}{dt} = n_{eng}T_G\cos(\alpha+\beta) - mg\sin\theta - D - n_{eng}D_{RAM} - \eta\mu W \tag{3.3}$$

$$L + T_G\sin(\alpha+\beta) + W = mg\cos\theta \tag{3.4}$$

where W is zero in the air and θ is zero on the ground. These equations were recast in terms of net thrust leading to the ram drag correction factor being small for small (α+β).

$$m\frac{dV_\infty}{dt} = n_{eng}T_N\cos(\alpha+\beta) - mg\sin\theta - D - n_{eng}D_{RAM}\left(1-\cos(\alpha+\beta)\right) - \eta\mu W \tag{3.5}$$

$$L + T_N\sin(\alpha+\beta) + D_{RAM}\sin(\alpha+\beta) + W = mg\cos\theta \tag{3.6}$$

With lift and drag a function of angle of attack, at each timestep the angle of attack has to be solved iteratively depending on the requirements. If net thrust and climb angle are known then equation 3.6 can be solved to find α. If a constant flight speed is requried then equations 3.5 and 3.6 have to be combined. For unknown net thrust;

$$\tan(\alpha+\beta)=\frac{mg\cos\theta-L}{mg\sin\theta+D+D_{RAM}}$$

and for unknown climb angle;

$$(mg)^2=\left(n_{eng}T_N\sin(\alpha+\beta)+n_{eng}D_{RAM}\sin(\alpha+\beta)+L\right)^2 +\left(n_{eng}T_N\cos(\alpha+\beta)-n_{eng}D_{RAM}\left(1-\cos(\alpha+\beta)\right)-D\right)^2$$

A simple Euler forward method was used when discritising equation 3.5. When modifying the thrust, T_N, to provide a specified climb angle and flight speed, the D_{RAM} correction in equation 3.5 was reduced to maintain stability. No other corrections were made for stability reasons except to the timestep during roll when it was reduced from 1.0 to 0.25 seconds. Whilst utilising a forward Euler approach does lead to second order errors for take-off these will lead to conservative results. This is because for $dV_\infty/dt\geq 0$, as is the case for the entire take-off, equation 3.7 will under predict V_∞ at time $t+\Delta t$ when using information at time t. This over predicts the runway length required to reach take-off speed. Similarly for $d\theta/dt\geq 0$, which is the case except for the period as the aircraft cuts back at the airport boundary, equations 3.8 and 3.9 will under predict the height and over predict the distance travelled at time $t+\Delta t$ when using information at time t. This leads to the aircraft being lower and thus noisier once airborne.

$$V_\infty^{t+\Delta t}=V_\infty^t+\frac{\Delta t}{m}\left[\begin{array}{l} n_{eng}T_N^t\cos\left(\alpha^t+\beta^t\right)-mg\sin\theta^t- \\ D^t-n_{eng}D_{RAM}^t\left(1-\cos\left(\alpha^t+\beta^t\right)\right)-\eta\mu W \end{array}\right]+O\left(\Delta t^2\right) \tag{3.7}$$

$$x^{t+\Delta t}=x^t+V_\infty^t\cos\theta^t+O\left(\Delta t^2\right) \tag{3.8}$$

$$h^{t+\Delta t}=h^t+V_\infty^t\sin\theta^t+O\left(\Delta t^2\right) \tag{3.9}$$

3.3.2. Jet

The jet noise model used for take-off optimisation needed to be computationally light as at each timestep multiple iterations of thrust and/or climb angle are required each of which requires the prediction of jet noise at several points on the ground. This limits the model to being semi-empirical. Three such models have been compared; the Stone Jet Noise Model (Stone *et al.* 1983), ESDU 88041 using ESDU 87011 for flight corrections (ESDU 1990a, b) and SAE ARP876 revision D (SAE 1994).

With the silent aircraft engines likely to be operating at ultra high bypass ratio with a very low specific thrust, when comparing the predictions of the three models the main area of interest is applicability to low jet Mach numbers and corrections made for flight conditions.

Stone Jet Noise Model

The version of the model discussed here (Stone *et al.* 1983) is based on earlier versions by the same author (Stone 1974, Stone and Montegani 1980) which are documented in the 1982 release of the NASA Aircraft Noise Prediction Program (Zorumski 1982) but with some corrections to the spectra. More recent work by the author that also documents single jet noise prediction but with a slightly modified Strouhal number calculation method (Stone *et al.* 1999) has not been used. This is because the modification is removed and the Strouhal number calculation method simplified in a later release looking at Chevron noise (Stone *et al.* 2003). In this version, though, numbers are not provided for single jet calculations.

The equations and correlations are designed to have no inherent limitation on the range of their applicability. In the original paper, predictions compared well with data on jet velocities down to 120m/s. The NASA ANOPP manual (Zorumski 1982) specifies the following ranges of key parameters for the model; jet area from $0.01m^2$ to $10m^2$, jet velocity relative to free stream sound speed from 0 to 2.5, flight Mach number from 0 to 0.9, jet total temperature to free stream static temperature ratio from 0.7 to 4, jet density to ambient density ratio from 0.2 to 1.2 and jet incidence angle with the free stream up to 30 degrees. This range of applicability will fully cover the silent aircraft key operating conditions.

ESDU Jet Noise Model

ESDU 98019 provides a noise prediction method that can be used with any database but for this comparison only the default database provided with the November 1998 release was available. The key limitation of this from the perspective of this work is that data is only provided down to a ratio of jet velocity to free stream sound speed of 0.5. Extrapolation is therefore required for a large portion of the silent aircraft take-off as both the start of roll and flyover conditions have jet velocities below this value (§3.4.1). In addition, sound propagation angles from only 60 to 150 degrees (relative to the aircraft direction) are provided although this does cover the peak noise area.

ESDU 87011 which provides the flight corrections is based on tests covering the following operating ranges; $0.1<V_\infty/V_j<0.3$, $0.5<V_j/a_\infty<1.5$, $1.0<T_j/T_\infty<2.5$ where V_∞ is the flight speed, V_j

the jet velocity, a_∞ the free stream sound speed, T_j the static jet temperature and T_∞ the static ambient temperature. The baseline aircraft (see §3.4.1) have V_∞/V_j up to 0.45 and V_j/a_∞ as low 0.42 therefore some caution is required especially in the applicability of the flight correction velocity component used in correcting the predicted SPL values as this has a larger impact on the overall result at high V_∞/V_j.

SAE Jet Noise Model

The range of applicability of the SAE model is listed by ANOPP as the same as the Stone model but the tabular correlations provided in both the version listed in ANOPP and revision D are more limited. Data is only provided down to jet velocities relative to free stream sound speed of 0.4 which just covers start of roll conditions of the baseline aircraft (§3.4.1). Data for polar angles from 20 to 160 degrees are provided and, for low temperature jets, the spectral distribution data is taken to be constant for values of jet velocity to free stream sound speed below 1.25. Relative velocity exponents provided with the SAE method, from the Bertin Aerotrain data (Drevet *et al.* 1977), are much lower than those provided in the Stone and ESDU models. Figure 5.13 of reference (SAE 1994) shows the uncertainty in predicted noise reduction through flight effects from the SAE model with increasing uncertainty for higher values of V_∞/V_j. At flyover, the baseline aircraft have free stream velocity to jet velocity up to 0.45 (§3.4.1) but the SAE data only goes up to a value of 0.31. Therefore the range of operation of the silent aircraft is well outside the range of data used in calculating the SAE flight correction exponents.

Flight correction exponents

As part of the NASA AST programme, Low compared the results obtained from Revision C of SAE ARP876 with test data obtained from a scale model of a Pratt and Whitney Advanced Ducted Propeller (Low 1994). Tests were performed in both static and free stream conditions up to a free stream Mach number of 0.35. Tests from 30% to 100% speed were included which cover jet velocities in the range applicable to the silent aircraft at take-off. The tests and predictions were for a coaxial nozzle but are still of interest here. Two key recommendations were made in using the SAE model for ultra high bypass engines:

- A six decibel reduction in predicted noise is applied at all frequencies and directions.

- New flight correction velocity exponents are used, increasing noise reduction for polar angles up to 130 degrees and reducing the reduction for higher angles.

Berton used this work when looking at the potential noise reduction from over-the-wing UHBR engines (Berton 2000). The six decibel difference between the SAE prediction and test data was linked to the secondary to primary nozzle area ratio of the test engine being twice the largest area ratio contained in the SAE database. With the Stone jet noise model based on area ratios as high as 43.5, Berton used this model but with the modified flight correction velocity components from Low. He then corrected the peak noise predictions from the Stone noise model to match the test data.

Based on this work the six decibel reduction can only be applied to coaxial nozzles but the new flight correction exponents from Low, which are specifically for high values of free stream to jet velocity, can be applied to single jets. To make further corrections to the single jet models will require test data from mixed exhaust UHBR engines not available at present.

When using these flight corrections with the Stone model, the following approach was taken. The Strouhal number corrections employed by Stone were unmodified as Low only provided overall sound pressure corrections from flight effects. The overall sound pressure calculation was modified to remove all flight effect modifications including corrections to the density exponent, the velocity exponent and the convection component. In their place the following flight correction was applied;

$$\Delta SPL = +10\log_{10}\left[\left(1-\frac{V_\infty}{V_j}\right)^{n(\omega)}\left(1-M_\infty\cos\omega_f\right)^{-1}\right] \tag{3.10}$$

where n(ω) is the flight correction power as specified by Low (1994), ω is the polar angle of the observer from the source reference direction and ω_f is the polar angle of the observer from the flight path.

Internal mixing correction

With the exhaust of the silent aircraft engine configuration utilising some form of mixing of the core and bypass jets (§3.1) the applicability of just using a single stream noise model requires consideration. In the literature review (§2.1.4) the work of Tester and Garrison on modelling jets with internal forced mixers was discussed (Garrison *et al.* 2004, Tester *et al.* 2004). This model added a high frequency, internal, source from the mixer to the fully mixed out prediction obtained using a single jet model such as those discussed above. The experimental noise data used by Tester and Garrison came from a BPR=4 engine where the nozzles tested were between

approximately three and six wavelengths downstream of the lobed mixers (Bridges and Wernet 2004). Figure 3-8 and figure 3-9 from Waitz *et al.* (1997) show the level of mixing downstream of a lobed mixer as a function of lobe wavelength λ where T is the velocity ratio. Whilst at this stage the final engine configuration creating the jet is not determined, if the jet exhaust is over ten wavelengths downstream of the lobed mixer the flow should be almost fully mixed out. Therefore, an additional noise source from forced mixing will not be included here and this decision used as an input into the design of the final concept engine (see §6.5.1).

Sensitivity to model choice

Appendix B presents the results of a brief study in which the three models discussed above are used to predict the noise at key flight conditions. For the Stone and SAE models, predictions are also made with the flight corrections from Low. There is fairly good agreement between the models under static conditions especially when just concerned with peak noise but the agreement is much worse when flight conditions are accounted for. This is because the silent aircraft has a very low specific thrust during take-off so flight correction has a large impact on the predicted noise relative to traditional turbofan designs. The unmodified SAE model has a very low flight correction exponent at and around a polar angle of 90° resulting in much higher noise predictions than the other models. Once the modified flight correction from Low is applied to both the SAE and Stone models they compare relatively well with the Stone model, predicting approximately 4dB higher noise at the peak noise point during flyover.

For three of these combinations; Stone, Stone + Low and SAE + Low, full take-off optimisation was performed for an early airframe and engine design (again, see Appendix B). In each case the jet area is modified in order to meet both the specified noise target and all take-off requirements. Relative to the Stone model, using the Stone + Low model results in an 8% reduction in the required jet area. If the SAE + Low model is used then the required jet area drops 24%.

Model Selection

The jet noise predictions by Stone with flight corrections by Low will be used for the remainder of this thesis. For the flight corrections, although based on results from a coaxial engine, the values of n calculated by Low were based on a similar range of flow regimes experienced during take-off in this work. This is not the case with the flight corrections contained in the unmodified noise models which were generally developed based on results from much higher jet velocities. For the jet noise model itself, this recommendation is based more on the fact that the other models looked at are less suitable than that the Stone model is ideal. The ESDU model is less suitable

because of the range of data extrapolation required. The SAE model is less suitable because the large change in predicted noise when moving to the Low corrections compared to the small change with the Stone model. It is recognised that the uncertainty in noise prediction has an impact on the accuracy of the results presented and future research to increase confidence is suggested in chapter seven.

3.3.3. Propagation

Atmospheric attenuation, lateral attenuation and ground reflection need to be included in order to predict the noise on the ground for a given polar, azimuthal and frequency distribution of source noise. Rather than predict noise at all points on the ground only locations on the airport boundary and, outside of the airport, on an extension of the runway centre-line are considered. With jet noise having no azimuthal directivity the peak noise location will occur along this line.

For a given point on the ground (x,s,0) and a given aircraft location (0,0,h), the propagation distance, r, polar angle, ω, and azimuthal angle, φ, are given in the following equations.

$$r = \sqrt{h^2 + x^2 + s^2} \tag{3.11}$$

$$\omega = 90 + \mathrm{sgn}\left(h\tan\Theta - x\right)\cos^{-1}\left(\frac{\sqrt{z^2 + s^2}}{r}\right) \tag{3.12}$$

$$\begin{aligned} \varphi &= \left(90 - \tan^{-1}\left(\frac{z}{|s|}\right)\right)\mathrm{sgn}\left(s\right) \\ &\text{if } \left(\varphi = 0 \,\&\left(\frac{h}{\tan\theta} + x\right) < 0\right), \varphi = 180 \end{aligned} \tag{3.13}$$

where $z = h\cos\Theta + x\sin\Theta$ and $\Theta = \theta + \alpha + \beta$ the sum of the climb angle, the angle of attack and any thrust vectoring angle. This is illustrated in figure 3-10.

Atmospheric and lateral attenuation corrections were calculated for a uniform atmosphere based on ground conditions and 70% relative humidity using ESDU databases (ESDU 1977, 1982). Lateral Attenuation is a function of the propagation distance, r, the elevation angle, ε (see figure 3-10) and the third octave frequency. Values from the ESDU database for fuselage mounted rather than under wing engines were used as this more closely matches the final configuration of the aircraft. For propagation distances in excess of 1200m, the value for 1200m was used as per ESDU recommendation. Similarly, for elevation angles less than 5 degrees the value of attenuation

for 5 degrees was used. A +3dB correction was applied to predicted noise to account for ground reflections. A more analytical analysis (ESDU 1994) was not deemed appropriate as for a broadband distributed noise source the interference patterns it predicts would not occur.

3.4. Results

3.4.1. Baseline aircraft

In looking at take-off optimisation, the following baseline parameters were used along with the jet noise target of 57dBA;

- MTOW = 160,000 kg
- L/D = 18
- V_{EF} = 60 m/s
- V_R = 65 m/s
- V_2 = 70 m/s
- T_{jet} = T_∞ + 25K
- A_{wing} = 700m^2
- c_L ≈ 0.057α - 0.033 for 0° ≤ α ≤ 20°
- μ = 0.02 when rolling freely
- Tyre pressure = 200 psi

For simplicity, the value of L/D is kept constant throughout and is unaffected by the landing gear or the loss of a critical engine. In practice, engine out will result in windmill drag from the engine and increased control surface drag needed to maintain yaw control. This will reduce L/D and impact the minimum climb angle requirement from equation 3.2. Estimating the increased drag requires knowledge of the engine and airframe design and therefore is left until the next chapter. Similarly, setting the jet temperature correctly requires knowledge of the engine cycle so, for this chapter, it was set to a low value that might be observed from a fully mixed UHBR engine. The coefficient of lift is from the final design presented in chapter six. This final design utilises a lightly loaded all-lifting body airframe giving the large wing area and low loading values. In this chapter the split between A_{wing} and c_L has no impact on the final results; what is important is that the product of the two results in reasonable values for angle of attack during take-off. For more accurate values of c_L please refer to figure 6-3.

Optimised take-off profiles for the baseline aircraft with two, three and four engines are presented in figure 3-11. For two engines the required total jet area is **10.56m^2**, for three engines **9.65m^2** and for four engines **9.58m^2**. With two engines take-off is 43 seconds after brakes off by which point the aircraft has travelled 1580m along the runway (see subplot A). Whilst still within the confines of the airport boundary the aircraft climbs steeply, briefly limited by maximum pitch up angle, before cutting back to a climb gradient of just below 4° as the airport boundary is crossed (B). This climb gradient is the minimum allowed above 400ft (121.9m) altitude so as to meet engine out requirements; see figure 3-5. Beyond the flyover point the climb angle increases slightly to 4°, required for operational reasons, and then remains constant. Because flight speed is restricted until 1500ft (457.2m) and climb angle is fixed the gross thrust also remains constant (D). This results in the peak noise on the ground reducing gradually as the altitude increases through radial spreading and atmospheric attenuation. Before the noise started to reduce the optimisation intent of meeting a specified noise level at all points was achieved with only small deviations observed at take-off and cutback where rapid changes in pitch angle occur.

To achieve the flight profile shown, engine gross thrust varies continuously until after the airport boundary is passed (D). Initially, with zero flight speed, gross thrust level is limited so as not to exceed the noise target. As flight speed increases then the jet noise is reduced for a given jet velocity allowing gross thrust to increase. This continues until the aircraft is airborne and climbing at maximum angle. As height is gained just after take-off lateral attenuation of the jet noise reduces requiring a reduction in thrust and climb angle (the reduction in lateral attenuation is much more significant than the small increase in propagation distance to the airport boundary). Variation in jet to free stream stagnation pressure ratio closely follows the variation in gross thrust (E). For a fully mixed UHBR engine this value is comparable to the fan pressure ratio showing that even at the sideline position a very low pressure ratio of 1.22 is required. Whilst gross thrust remains constant after the airport boundary is crossed the stagnation pressure ratio gradually increases. This can be explained by noting that for an unchoked fixed area nozzle gross thrust is a function of jet Mach number and free stream static pressure only. As altitude increases free stream static pressure drops and so jet Mach number must increase. This requires a higher stagnation pressure rise through the engine. Even with relatively low gross thrust at start of roll the aircraft accelerates rapidly up until V_R is reached (F). Once airborne, flight speed is approximately constant as required and critically does not drop below the specified V_2 speed of 70m/s. As is shown in §3.4.2, the results are relatively insensitive to small changes in flight speed.

To cover all the operational requirements listed in §3.2.2, take-off with engine failure at V_{EF} must be considered. Figure 3-12 presents take-off data for normal takeoff and for engine failure at V_{EF}.

Engine failure occurs 996m after brakes off at which point the aircraft is travelling 60m/s. At this point the gross thrust of the remaining engines is fixed. Two seconds later and at a distance of 1118m from brakes off the aircraft is travelling at 62.3m/s which can be taken as V_1 speed. From figure 3-4 is can be seen that for this V_1 speed the distance from brakes off when V_{EF} is reached is well within that required for accelerate-stop requirements. If take-off is to continue (referring back to figure 3-12), gross thrust from the remaining engines is increased 11% at this point. This pushes the peak jet to free stream stagnation pressure ratio encountered towards 1.24. The aircraft gets airborne 1760m after brakes off and has an altitude of over 200ft (61m) as the end of the runway is crossed; considerably higher than the 35ft (10.7m) required. At 400ft (121.9m) the climb angle is 3.1° or 5.4%, again well above that required by the regulations. Reducing the start of roll velocity, V_R, by 5 knots reduces the distance from brakes off at which 35ft (10.7m) altitude is reached as required.

To summarise, a two-engine variant of the baseline aircraft accelerates rapidly and climbs steeply before cutting back to a climb angle of approximately 4° as the airport boundary is crossed. This maintains a constant jet noise level of 57dBA outside of the airport boundary at all times. The critical operational requirement that drives the take-off profile to that seen is the minimum climb angle for engine out compliance at the flyover point.

Going from two to three engines makes a significant difference on the take-off profile. Again the critical operational requirement is the minimum climb angle for engine out compliance at flyover but this angle has been reduced considerably (see figure 3-5). With a reduced minimum climb angle, less thrust is required which, for the same noise level, allows the aircraft to fly lower with a reduced jet stagnation pressure ratio and leads to a 9% drop in required jet area. The reduction in thrust requirement is slightly offset by a shift in peak noise level to higher frequencies as the overall jet area is split into an increasing number of individual jets. This increases the annoyance weighting of the noise (see §1.1) leading to a higher A-weighted noise level with all other parameters unchanged. With the climb angle at flyover less than the average required for operational reasons the climb angle needs to be increased towards the 4° mark when possible. This occurs gradually as increased altitude allows increased thrust for the same noise level on the ground. Engine out results are plotted in figure 3-13. With a reduced engine diameter the three-engine aircraft takes longer to accelerate than the two-engine variant. V_{EF} is reached 1151m after brakes off, still well within the distance required for accelerate-stop. Similarly, following take-off after engine out, the 35ft (10.7m) height requirement is comfortably met.

For four engines the same trend continues with a reduction in the minimum climb angle required at flyover reducing the required thrust and jet area. The reduction in required thrust is relatively low and, when offset with the increasing annoyance of the noise, leads to the jet area reducing less than 1% relative to the three-engine variant. Again, all engine-out requirements are met with take-off performance plotted in figure 3-14.

3.4.2. Variation in noise target and aircraft parameters

To look at the sensitivity of the results to several key parameters, optimised take-off profiles were developed for a range of airframe and engine variants;

- MTOW = 100,000kg 200,000kg 300,000kg
- L/D = 16 22 28
- V_R = 50 m/s 60 m/s 70 m/s
- $T_j - T_\infty$ = 25K 50K 75K
- n_{eng} = 2 3 4
- Noise target = 54dBA 64dBA 74dBA

This leads to 729 possible combinations, all of which were analysed. Wing area was modified to keep MTOW * A_{wing} * V_R^2 constant so as to maintain similar angles of attack for all combinations. In determining the success of the take-off it was assumed that, as was the case for the baseline aircraft, the climb angle at the flyover position would be the critical parameter in determining whether operational requirements were met. To reduce required computation time the iteration on jet area was only performed to converge on this climb angle to within ±0.5°.

Multiple linear and non-linear regression was used to analyse the results with the purpose of creating a simple function that could be used to estimate the required jet area for given aircraft parameters, jet temperature and noise target. Initially a straightforward approach was taken with the jet noise set as a function of the logarithms of the input data;

$$\hat{N}_j = \beta_1 \log_{10}(m) + \beta_2 \log_{10}\left(\frac{L}{D}\right) + \beta_3 \log_{10}(\sin\theta_{\min}) + \beta_4 \log_{10}(A_j) + \beta_5 \log_{10}(T_j) + \beta_6 \log_{10}(V_R) + \beta_7 \tag{3.14}$$

where β_1 to β_7 are the parameters to be solved for, m is the aircraft mass and θ_{min} is the climb angle at flyover from equation 3.2. This equation takes the common form $y=X.\beta + \varepsilon$ where y is the observations (N_j), X is a matrix of regressors ($\log_{10}$(m), $\log_{10}$(L/D), etc.), β are the parameters to

be solved and ε are the errors to be minimised. This equation is linear and can be solved in the least squares sense giving;

$$\hat{N}_j = 45.57\log_{10}(m) - 19.20\log_{10}\left(\frac{L}{D}\right) + 6.88\log_{10}(\sin\theta_{\min}) - 39.84\log_{10}(A_j) + 44.06\log_{10}(T_j) + 5.18\log_{10}(V_R) - 227.0 \tag{3.15}$$

The resulting r.m.s. error was 0.38dB with a maximum error of 1.69dB. The coefficient of determination, R^2, is the fraction of the variation in the observations explained by the regression equation and is defined by equation 3.16 with overbar indicating mean and hat (circumflex) indicating the prediction. This metric is commonly used to indicate the success of the regression with a value of zero indicating no fit and a value of one indicating complete fit. For equation 3.15 above, R^2=0.9979. As more parameters are added to the equation the fit can become better without any statistical significance and so an adjusted R^2 value is used to correct for the number of predictors (equation 3.17, n is number of samples = 729, k is number of predictors = 7). R^2_{adjusted} is always less than R^2 but, because of the large number of samples used, is unchanged to four decimal places in this analysis.

$$R^2 = \frac{\Sigma(\hat{y}-\bar{y})^2}{\Sigma(y-\bar{y})^2} \tag{3.16}$$

$$R^2_{adjusted} = 1-(1-R^2)\frac{n-1}{n-k-1} \tag{3.17}$$

Whilst equation 3.15 provides a very good fit to the data there is a limited theoretical basis for it. Therefore an attempt was made, using jet noise modelling as a starting point, to create an equation of a more justifiable form. Starting from equation 2.5;

$$N_j \propto 10\log_{10}\left[\rho_j A_j V_j^8\left(1-\frac{V_\infty}{V_j}\right)^n\right]$$

where n is of the order 5 perpendicular to the jet axis. For zero angle of attack;

$$T_N = \rho_j A_j V_j^2\left(1-\frac{V_\infty}{V_j}\right) \approx mg\left(\frac{1}{L/D}+\sin\theta\right)$$

which when substituted into the equation for noise gives;

$$N_j \sim 40\log_{10}\left[mg\left(\frac{1}{L/D}+\sin\theta\right)\right]-30\log_{10}\left(\rho_j A_j\right)+10\left(n-4\right)\log_{10}\left(1-\frac{V_\infty}{V_j}\right)+C$$

Whilst this equation cannot be used directly as Vj and V_∞ are unknown it does provide a basis for combining m, L/D, θ_{min}, A_j and T_j in the regression ($T_j \propto \rho_j^{-1}$ as static pressure is equal to free stream pressure). The best solution was found using the following non-linear model with parameters both inside and outside of the log functions;

$$\hat{N}_j = \beta_1 \log_{10}\left[mg\left(\frac{1}{L/D}+\beta_2 \sin\theta_{\min}+\beta_3\right)\right]+\beta_4 \log_{10}\left(\frac{A_j}{T_j}\right)+\beta_5 \log_{10}\left(V_R\right)+\beta_6 \tag{3.18}$$

This equation was solved in the least squares sense to obtain the following equation for estimating jet noise for given airframe parameters;

$$\begin{aligned}\hat{N}_j = {} & 45.75\log_{10}\left[mg\left(\frac{1}{L/D}+0.4\sin\theta_{\min}+0.05\right)\right] \\ & -39.94\log_{10}\left(\frac{A_j}{T_j}\right)+5.00\log_{10}\left(V_R\right)-254.5\end{aligned} \tag{3.19}$$

The r.m.s. error was 0.34dB, a 0.04 improvement in that obtained from equation 3.15 with one less parameter used. Maximum error was slightly worse at 1.79dB but the values of both R^2 and $R^2_{adjusted}$ were improved to 0.9982 (again $R^2_{adjusted} = R^2$ to four decimal places). As a further judge of the suitability of this regression analysis in estimating the predicted jet noise from designs that were not part of the sample, the sample was randomly split into two. Non-linear regression was performed on one half using equation 3.18 giving an r.m.s. error of 0.35dB and a maximum error of 1.75dB. This equation was then used to estimate the jet noise from the other half of the sample giving an r.m.s. error of 0.34dB and a maximum error of 1.45dB. This clearly shows the suitability of the regression. Using two additional parameters to modify the A_j/T_j ratio reduced the corrected R^2 value to 0.9986 and the r.m.s error to 0.31dB but the simplicity and theoretical basis for equation 3.19 was preferred over small improvements in fit.

To use this equation as a basis for designing engines to meet a given noise goal, it must be rearranged to give jet area over temperature in terms of airframe parameters and the jet noise target;

$$\frac{A_j}{T_j} \approx \frac{\left[mg\left(\frac{1}{L/D}+0.4\sin\theta+0.05\right)\right]^{1.145} V_R^{0.125}}{10^{6.372}\times 10^{0.025 N_j}} \tag{3.20}$$

Figure 3-15 shows, relative to the baseline aircraft, how changes in mass, jet noise target, L/D and V_R impact the required jet area for two, three and four engine variant designs all with $T_j=T_\infty+25K$ ($T_\infty=300.15K$). The lines are from equation 3.20 whilst the points are for the optimised solutions from §3.4.1. Equation 3.20 only applies when climb angle at flyover is the critical condition in determining take-off and, when this is not the case, this has been indicated in the figure. As mass, noise target and aircraft L/D are changed there is not that significant a change in the departure profile. Therefore, whilst the required jet area does change significantly, the critical operational condition does not. This is not the case for changes in take-off velocity. Increases in V_R lead to increases in the used runway length and a range of other operational requirements start to become more important. With V_{EF} set to V_R-5m/s, as for the baseline case, accelerate-stop requirements can become critical. To alleviate this, the value of V_{EF} can be reduced so that the accelerate-stop distance matches the take-off distance following engine failure. For the baseline four-engine aircraft this leads to $V_{EF}\approx V_R$-15m/s when V_R=80m/s. Before this condition becomes limiting the all engine operating field length requirements becomes critical. This is because with all engines operating a 15% safety margin is required leading to the aircraft having to be 35ft (10.7m) high 2650m after brakes off. For the baseline four-engine case this requirement becomes critical at a value of V_R=77m/s and for the three-engine case at a value of V_R=80m/s. For the two-engine case this situation does not become critical until V_R is greater than 85m/s. Once all-engine operating runway length is the critical condition, further increases in V_R lead to a rapid increase in jet area in order to meet the noise target as the aircraft needs to accelerate quicker along the runway.

Whilst the baseline aircraft have subsonic jets for all of the take-off, this is not the case when the noise target is relaxed in the top right subplot of figure 3-15. The equation behind the lines in this plot (equation 3.20) only considers jet mixing noise but, for supersonic jet Mach numbers, shock noise will also be present unless the jet is ideally expanded through a converging diverging nozzle. The SAE method (1994), based on the work of Harper-Bourne and Fisher (1974), was used to estimate the impact shock noise has on the required jet area of the three-engine baseline aircraft as the noise target is relaxed. For a jet noise target of 80dBA the required jet area was calculated to be 2.54m^2 with shock noise not impacting this result. If the target is relaxed to 82.5dBA then ignoring shock noise leads to a jet area of 2.20m^2. Including shock noise in the optimisation run increases the required area 3.6% to 2.28m^2. Relaxing the target still further to 85dBA leads to areas of 1.87m^2 when shock noise is ignored and 2.05m^2 when shock noise is included (an increase in area of 9.6%).

3.4.3. Variation in airport parameters

Equations 3.19 and 3.20 only apply to aircraft operations at the baseline airport and under baseline atmospheric conditions as defined in §3.2.1. Whilst this is all that is needed to design against, it is worth looking briefly at how changes to some baseline airport parameters affect the result.

Whilst the sideline distance matches that used during noise certification, the flyover distance does not. The required jet area of the three baseline aircraft were re-optimised using a flyover distance of 6500m rather than 4048m to give an indication of the impact this has on the required area. For the two-engine design the required jet area is reduced 17% from 10.56m^2 down to 8.80m^2, for three engines the required jet area is reduced 16% from 9.65m^2 down to 8.10m^2 and for four engines the required jet area is reduced 16% from 9.58m^2 down to 8.04m^2.

In addition to the baseline airport a 5000ft (1524m) altitude noise constrained airport similar to Denver was discussed in §3.2.1. This airport had a 12,000ft (3,658m) runway with the same boundary as the baseline airport (450m sideline, 1000m flyover) and was under ISA+19.5K conditions. To operate from this airport the three baseline aircraft with two, three and four engines would meet jet noise levels of 60.0, 60.5 and 60.5 dBA respectively. This is an increase of 3 to 3.5 dB on the target set at the beginning of this chapter. With the noise target relaxed the aircraft accelerate to V_R in a similar distance but, because a higher angle of attack is required at take-off, leaves the ground later. Climb is not quite as steep as when operating at the baseline airport offsetting the extra 2000ft (609.6m) distance from brakes off to airport boundary.

3.5. Discussion

In this chapter, take-off optimisation has been used to estimate, for given aircraft and airport parameters, the smallest possible jet area that can be used when a specified noise level must not be exceeded during take-off. In general this work was based on low temperature, ideally expanded and fully mixed out jets. As such, any additional sources from the core and bypass not being fully mixed or higher temperatures will lead to even higher jet area requirements for the same noise level.

The use of optimised take-off procedures to minimise the required jet area is significantly more successful when the aircraft has three or more engines. This is because, at least for the baseline airport, the required climb angle at flyover is the critical operational requirement. This is determined by engine out conditions (equation 3.2) and a significantly higher climb angle is

required for a two-engine design. This is likely to be why previous optimisation which only looked at two-engine designs found limited benefits of thrust cutback (Antoine and Kroo 2002). The higher the number of engines the lower the climb angle with equation 3.20 indicating jet area for the baseline aircraft tends to $8.5m^2$ as the number of engines tends to infinity for an L/D of 18. Increasing the number of engines leads to increased maintenance costs and, if the core diameter becomes too small, reduced performance. Therefore, whilst increasing the number of engines from two to three is likely to be advantageous, further increase may not be.

The performance of the aircraft at take-off also has a significant impact on the required jet area. Both aircraft take-off mass and lift to drag ratio significantly impact the required jet area for a given noise target whilst take-off speed only has a significant impact once take-off distance starts to become critical. For a given aircraft mission (payload and range), any weight reduction possible positively impacts both take-off jet area and cruise fuel burn. A requirement to maximise take-off L/D has a more interesting impact. With the required lift at both cruise and take-off fixed and similar in magnitude, the selection of cruise altitude and flight speed leads to a required wing area and coefficient of lift. Increasing cruise altitude (thus reducing ρ_∞) and reducing flight speed leads to increased $c_L A_{wing}$.

$$L = \tfrac{1}{2} c_L A_{wing} \rho_\infty V_\infty^2$$

At take-off with $\rho_\infty V_\infty^2$ significantly lower c_L must be increased to compensate by increasing angle of attack or deploying high lift devices both of which increase drag. The higher cruise $c_L A_{wing}$ is then the less the required increase, leading to improved take-off L/D. Deploying high lift devices especially flaps at take-off needs to be avoided due to increased drag and noise. Therefore, with the maximum value of c_L limited, a large wing area is required. In summary, to increase take-off L/D a high cruise altitude, low cruise flight speed and large wing area are required.

Looking at the impact on the engine in more detail, let us compare the results from §3.4 with jet areas of current and next generation aircraft. Table 3-3 lists a small selection of existing aircraft, plus the Airbus A380 and Boeing 787-8, both of which are due to enter service in the near future. With only very limited data available, especially for the next generation aircraft, the values of jet area have been calculated from published thrust and mass flow rates along with an estimation of the jet temperature. Whilst only one of the listed aircraft has a fully mixed exhaust, the predicted areas and noise levels are based on fully mixed out values. This is to enable comparison with the results obtained in this chapter. No consideration has been made as to whether the aircraft could fly the required procedure or whether the engines could provide the range of thrust required

without encountering stability problems. To emphasise, the real aircraft do not have fully mixed core and bypass flows and for either airframe or engine reasons may not be able to fly the optimised procedures. Therefore the noise values in table 3-3 will be underestimates. When correcting the results to a MTOW equal to the baseline aircraft, the two-engine designs have jet areas ranging from 39% of that required to meet the noise target rising to 56% for the next generation design. For the four-engine designs the equivalent numbers are 39% rising to 51%. This indicates that any engines capable of powering the baseline aircraft must be significantly different from current and next generation designs.

For a three-spool, high bypass ratio engine with fixed cycle, top of climb thrust requirements can be used to see what engine parameters emerge when meeting the specified jet area. Using GasTurb (Kurzke 2004) to model the engine cycle, top of climb altitude was set to 35,000ft (10,668m) and net thrust estimated at 88.4kN to deliver a 300ft/min (1.52m/s) climb gradient under ISA conditions and Mach 0.8* with a lift over drag ratio of 20. Note that the jet areas calculated in §3.4.1 are the same as the nozzle areas used here as at take-off the nozzle is unchoked.

For the four-engine design:

- A_{noz} = 9.58m^2
- ToC FPR = 1.33
- ToC BPR = 19.6
- Fan diameter = 2.10m

For the three-engine design:

- A_{noz} = 9.65m^2
- ToC FPR = 1.33
- ToC BPR = 19.7
- Fan diameter = 2.43m

For the two-engine design:

- A_{noz} = 10.56m^2
- ToC FPR = 1.30
- ToC BPR = 21.4
- Fan diameter = 3.10m

Realistic input parameters were used in creating the engine cycles including a HPT stator exit temperature (T_{41}) of 1740°K, HPC exit temperature (T_3) of 900°K and mixer inlet stagnation pressure ratio $p_{0,bypass}/p_{0,core}$ of 1.0.

Figure 3-16 is adapted from a NASA report by Daggett, Brown and Kawai (2003) that looked at the optimum engine diameter for a 2015 B777-200ER equivalent aircraft. This study showed that whilst the engines with the highest BPR and lowest FPR exhibited the best specific fuel

* $\theta_{ToC} = \sin^{-1}\left(\frac{V_{vert}}{V_\infty}\right) = \sin^{-1}\left(\frac{0.3048(\,fpm/60)}{M_\infty\sqrt{\gamma R(216.16+\Delta T_{ISA})}}\right)$

consumption, when installation effects were accounted for, fan pressure ratio in the range 1.45 to 1.55 had the lowest operating costs. In the report operating costs were plotted against BPR giving optimum BPR in the range 11 to 15. Here FPR was used to plot operating costs against as it is much less sensitive to selection of core temperature limits and aircraft operating altitude than BPR. To obtain the required area for a silent aircraft whilst minimising operating costs therefore requires engines designed to give low pressure rise and high mass flow at take-off and more moderate pressure rise and mass flow at cruise. This suggests the need to introduce variable cycle concepts such as variable area nozzles, auxiliary fans or ejection.

3.5.1. Variable Area Nozzles

A variable area nozzle modifies the operating point of the fan and low pressure turbine. Opening the nozzle reduces the static pressure at mixer exit which reduces the static pressure at both the fan and LPT exit. For a high bypass ratio engine the reduction in fan back pressure dominates with fan mass flow increasing and fan pressure rise reducing, resulting in an increased jet area at reduced velocity. The low pressure turbine operating point then moves to deliver the required power at a matching shaft speed. Figure 3-17, modified from Hall et al. (2004), shows the impact on the fan with an increase in nozzle area giving a moderate cruise FPR and a low take-off FPR on an idealised fan map. The range of benefit of a variable area nozzle is limited by the capacity of the fan and other turbomachinery components before choking occurs. Such a system would need to be lightweight but, more importantly when operating with a high bypass ratio engine, have low leakage and a thrust coefficient close to one especially at the cruise position. Figure 3-18 presents two possible concepts that may meet such requirements one with a movable inner plug and one with overlapping nozzle sections that rotate circumferentially to modify the nozzle area. Research into nozzle area variation using shape memory alloy actuation technology is occurring (Rey *et al.* 2001, Song *et al.* 2004) and inflatable structures could also be utilised in this area. An additional benefit of a variable area nozzle is the capability to minimise fuel burn throughout cruise (Lopez-Diez *et al.* 1998)

3.5.2. Auxiliary Fans

Auxiliary fans that can be engaged for take-off and disengaged for cruise would allow for larger increases in jet area than variable area nozzles allow. The disadvantages are increased weight and mechanical complexity especially with the clutch mechanism. Whilst the auxiliary fans could be designed specifically for take-off, the cruise fan, which would likely also have to operate at take-off, would have to support a wide range of conditions. Matching fan power requirements with what the low pressure turbine can deliver would be a significant challenge and a variable area

nozzle to reduce the LPT exit static pressure would be required to move the operating line as is done on the Joint Strike Fighter (Bevilaqua 2005).

3.5.3. Ejection

The use of ejectors for jet noise suppression was briefly reviewed in §2.1.4. To achieve significant jet noise reduction the primary jet velocity must be reduced and this requires forced mixing between the primary and entrained jets. For realistic ejector lengths the primary and entrained flows will not be fully mixed out and therefore an ejector model that supports incomplete mixing is required. In order to allow estimates of possible jet noise reduction this model must be compatible with a semi-empirical jet noise code such as those for coaxial jets (Stone *et al.* 1981 for example). Appendix C summarises two models that were developed to fulfil this requirement, one incompressible and one compressible. Both model the mixing as a transfer of momentum from the primary to the entrained jet with no transfer of mass. This results in two streams at exit and so is compatible with coaxial jet noise prediction schemes.

Figure 3-19 presents the predicted performance of an ejector for three different mixing efficiencies, 30%, 60% and 100%. ISA sea level conditions were used with a stagnation pressure rise across the engine of 1.2, the aircraft velocity at 80m/s and $T_{jet}=T_{\infty}+22K$. Agreement between the two models is good and, for 60% efficiency, an ejector area ratio of two is estimated to reduce jet noise by about 7dB. This noise delta at 100m was predicted using the model from Stone *et al.* (1981) with corrections for atmospheric attenuation included*.

Referring back to Figure 3-15, a 7dB reduction in jet noise would enable the jet area of the baseline aircraft to be reduced to $6m^2$ which is approximately the same as the jet area of a fully mixed out Trent 1000 equivalent (table 3-3). Therefore, the use of ejection has potential in enabling the Silent Aircraft noise goals to be met. In order for such a potential reduction to be

---

* Whilst the Stone Jet Noise model as documented supports both single and coaxial jets, the correlations for the coaxial jets are only valid for area ratios of $0.67 < A_{entrained}/A_{core} < 43.5$. If the model is used for area ratios less than this, a discontinuity occurs as $A_{entrained}/A_{core} \rightarrow 0$. As this was an area of interest (i.e. small amounts of ejection), a correction was made to the model to smooth the correlations between a single jet and a coaxial jet.

$$G_C \xrightarrow{\text{modified to}} G_C^{\min\left(1, \frac{A_{entrained}/A_{core}}{0.67}\right)}$$

Another discontinuity occurs as the secondary jet velocity approaches that of the free stream with the presence of the secondary jet reducing the predicted noise levels. Therefore, in determining the peak noise, both coaxial and core only predictions were made and the maximum value used.

realised, though, several significant challenges would need to be overcome. The device would have to be stowable in order to maximise cruise performance and also light-weight.

Perhaps more critical is how uniform the exhausted flow would be in reality. Whilst the model assumed the primary jet velocity is reduced uniformly at all locations this is not the case for existing forced mixers where a complex velocity distribution is present (Hu *et al.* 2002, Zaman *et al.* 2003). Experimental data on ejectors driven by subsonic primary flows in which noise measurements were made is very limited. Coles *et al.* (1958) presented absolute noise data on an eight-lobed forced mixer with non-lined ejection where the driving jet was subsonic and these results have been compared with the estimations from the compressible ejector model discussed above. For no ejection, the model accurately predicts the noise measured, as would be expected. The addition of forced mixing is equivalent, from a noise reduction perspective, to a mixing efficiency of 27% on this model and the addition of forced mixing and ejection is equivalent to mixing efficiencies of between 34% and 44% depending on the ejector length. The ejector used by Coles *et al.* was not lined and they speculated that noise generated inside the ejector was one reason why more significant noise reductions were not seen. It is likely that as the primary jet velocity is reduced any noise sources internal to the ejector will become more important.

Therefore it is not unreasonable to speculate that internal noise sources, along with jet flow non-uniformity, could significantly reduce the noise benefit of ejection on an already quiet jet.

3.6. Chapter conclusions

To design an ultra low noise engine for an ultra low noise aircraft, jet noise needs to be looked at first as it drives the design of the engine cycle directly. A low jet noise optimised take-off profile has been developed in order to minimise the increase in jet area required to enable a jet noise level of 57dBA to be met. Except for aircraft requiring a high take-off speed, angle of climb after cutback is the critical condition in determining a successful take-off. For these conditions the required jet area can be estimated using equation 3.20. As the minimum climb angle, θ_{min}, is a function of the number of engines (equation 3.2), the fewer the engines the larger the required overall jet area for silent take-off.

To meet the noise target at the baseline airport, jet area needs to be significantly greater than the jet area of current and next generation turbofan powered aircraft. In order to deliver low cruise fuel burn whilst meeting the take-off jet noise target, variable cycle technologies are required. Possible technologies include variable area nozzles, auxiliary fans or ejection. A simple model of

an ejector that is compatible with coaxial jet noise models predicts significant reductions in jet noise if 60% of the ideal momentum transfer between the primary and entrained jets is achieved. Experimental data on noise reduction from ejectors driven by subsonic jets is very limited and significant doubts exist on whether this level of noise reduction could be met in practice. Complex deployment geometry further reduces the appeal of using such a system. A variable area nozzle is likely to be significantly lighter and less complex and as such requires further investigation. Of particular interest is how modification of the nozzle area effects fan operation, performance and noise. This places limits on what degree of nozzle variation can be achieved and what top of climb pressure ratio can be employed. This is the subject of the next chapter. With the aerothermal and acoustic implications of using a variable area nozzle worthy of detailed attention, the mechanical design of such a nozzle, whilst critical, has not been considered further.

4. Fan and nozzle operation for low noise

Modifying nozzle area has been identified as a promising approach for reducing take-off jet noise whilst delivering low cruise fuel burn. In this chapter, the impact of nozzle variation on fan performance and fan noise is discussed with the aim of minimising fan noise and ensuring the fan can provide the required mass flow rate and pressure rise.

Whilst previous work on quiet engine design has tended to be less far-reaching in terms of noise target and more constrained in that standard installation and flight operations were specified, several conclusions are applicable to this thesis. With lower fan pressure ratio (FPR) leading to lower jet noise and generally lower source noise, the trade-off between noise reduction and increasing fuel burn is critical. Gliebe and Janardan (2003) investigated direct drive and geared fans for large twin engine aircraft with the aim of achieving 5-10EPNdB reduction relative to FAR36 stage 3 at each measuring station. They concluded that top of climb FPR in the range 1.40 to 1.55 was optimal for low noise with acceptable weight and direct operating cost (DOC) penalties. More recent work by Daggett *et al.* (2003) with a 2015 timeframe aimed for ultra high efficiency with a noise level 20EPNdB cumulative below stage 3. It was found that a FPR of 1.45 to 1.55 was optimal in terms of DOC with lower FPR designs leading to increased weight and drag offsetting SFC improvements (figure 3-16). As an ultra low noise concept, Dittmar has proposed a two-stage fan of design overall pressure ratio 1.15 (Dittmar 1998, Dittmar *et al.* 2003). This gives low jet and fan noise but at the expense of a very large installation requirement leading to poor cruise performance. To meet the silent aircraft noise target and have competitive fuel burn, a turbofan engine concept needs to operate with a fan pressure ratio in the range proposed by Dittmar at take-off for low jet noise and in the range proposed by Gliebe and Daggett at top of climb for low fuel consumption.

To meet this aim, the first step is to calculate the top of climb FPR that would be achieved for a given jet noise target with a fixed nozzle. Then, in order to decide how much nozzle area variation is required an understanding is required of how modifying fan back pressure impacts fan noise and what limits the range of back pressures that can be supported. With the limitations of the fan understood, two approaches are presented to deliver both low noise and the required top of climb FPR: The first builds on equation 3.20 with the nozzle operating at two areas only; one at cruise and one at take-off. The second couples the full take-off optimisation procedure presented in chapter three with a realistic fan map and requires the variable area nozzle to vary continuously during take-off. This allows the fan to operate at an ideal position at all times but requires greater overall nozzle variation.

Rather than using the baseline aircraft presented in chapter three, the silent aircraft airframe is introduced in this chapter. This all-lifting body type airframe provides significant shielding of forward radiated fan noise and leads the focus of fan noise reduction to be primarily concerned with rearward propagating noise that will not be shielded.

4.1. Operation with a fixed nozzle area

For an ultra high bypass ratio engine the majority of the thrust comes from the bypass airflow. Modelling the impact of the core as a temperature and pressure correction applied to the flow all of which goes through the bypass (see figure 4-1), the following three equations can be solved to give required fan pressure ratio for specified net thrust, nozzle area and free-stream conditions. Equation 4.1 considers pressure rise from inlet to exhaust matching static pressure at the two conditions (after expansion the jet static pressure equals the free stream static pressure). Equation 4.2 looks at the net thrust produced by the engines per unit jet area and equation 4.3 covers nozzle choking:

$$FPR = \frac{1}{PR_{in}PR_{out}}\left(\frac{1+\frac{\gamma-1}{2}M_{jet}^2}{1+\frac{\gamma-1}{2}M_{\infty}^2}\right)^{\frac{\gamma}{\gamma-1}} \tag{4.1}$$

$$\frac{T_N}{A_{jet}} = \gamma p_{\infty} M_{jet}^2\left(C_{FG} - \frac{M_{\infty}}{M_{jet}}\left(\frac{1+\frac{\gamma-1}{2}M_{\infty}^2}{1+\frac{\gamma-1}{2}M_{jet}^2}\right)^{-\frac{1}{2}}\left(FPR^{\frac{\gamma-1}{\gamma\eta_p}} + \frac{\Delta T_0}{T_{0\infty}}\right)^{-\frac{1}{2}}\right) \tag{4.2}$$

$$\frac{A_{noz}}{A_{jet}} = \max\left[1, M_{jet}\right]\left(\frac{2}{\gamma+1}\left(1+\frac{\gamma-1}{2}\max\left[1, M_{jet}\right]^2\right)\right)^{-\frac{1}{2}\left(\frac{\gamma+1}{\gamma-1}\right)} \tag{4.3}$$

In these equations FPR is the mass averaged rise in stagnation pressure of the bypass flow across the fan stage, PR_{in} is the pressure recovery (ratio of stagnation pressures) from free stream to the fan face and PR_{out} is the pressure recovery from fan stator exit to jet. PR_{in} includes any losses from ingested boundary layers and losses in the inlet ducting. PR_{out} includes losses in the exhaust duct and mixer along with any change in stagnation pressure of the bypass flow due to mixing with the core flow. C_{FG} is the thrust coefficient, close to one, and is defined here as the ratio of gross thrust delivered to the sum of the mass flow and jet velocity. ΔT_0 is the temperature rise of the bypass flow across the mixer due to mixing with the core. The impact of the core on both ΔT_0 and PR_{out} is discussed in more detail in appendix D.

These three equations can be coupled with a modified form of equation 3.20 in which the jet static temperature is replaced with the free stream and jet Mach numbers and stagnation values. In addition, the jet area in equation 3.20 was for unchoked conditions at take-off and so is equal to the nozzle area in this section in which higher thrust conditions will also be considered.

$$A_{noz} \approx \frac{\left[mg\left(\frac{1}{L/D} + 0.4\sin\theta_{\min} + 0.05 \right) \right]^{1.15} V_R^{0.125}}{10^{6.61} \times 10^{0.025 N_j}} \frac{T_{0\infty} FPR^{\frac{\gamma-1}{\gamma\eta_p}} + \Delta T_0}{1 + \frac{\gamma-1}{2} M_{jet}^2} \tag{4.4}$$

These equations enable the fan pressure ratio as a function of jet noise outside the airport to be calculated and figure 4-2 presents this for three aircraft variants; a two-engine conventional aircraft similar to the baseline variant presented in §3.4.1 and two variants of a three-engine all-lifting body (see next paragraph). Nozzle area is fixed by the noise requirement during take-off leading to specified fan pressure ratios at top of climb and cruise. Values used in the creation of this and following figures can be found in table 4-1.

In calculating the flyover climb angle, θ_{min}, to enter into equation 4.4 the reduction in L/D following engine out is now considered in equation 3.2 (it was ignored in chapter three). The approach used is discussed in appendix E and it is this that leads to the two all-lifting body aircraft variants. On the loss of the critical engine the windmill drag and non axi-symmetric thrust will create a yawing moment. For a conventional aircraft, this is primarily corrected by the tail but for a tailless all-lifting body another approach needs to be found. The simplest is to use a drag creation device such as a split aileron on the outer wing. This needs to create a lot of drag to counteract the yawing moment and, as can be seen in figure 4-3, has a significant impact on the required minimum climb angle before engine out. For a jet noise level of 57dBA (the noise target), the required climb angle at flyover is increased from 2.1° to just over 3° using this method. As the top of climb fan pressure ratio is reduced the increase in required climb angle reduces slightly because the engines become smaller and therefore the windmill drag reduces. (This figure has top of climb FPR on the x-axis rather than jet noise so that it can be used when nozzle area is varied.) Calculating this drag required the fan face area and for a given fan face Mach number this can be found from equation 4.5 in which the jet and fan mass flow rates are matched. In this chapter, and in the creation of figure 4-3, the top of climb fan face Mach number has been set to 0.66 which is representative of high capacity modern designs.

$$\frac{A_{jet}}{A_{ff}} = \frac{\sqrt{FPR^{\frac{\gamma-1}{\gamma\eta_p}} + \Delta T_0 / T_{0\infty}}}{FPR.PR_{out}} \frac{M_{ff}}{M_{jet}} \left(\frac{1 + \frac{\gamma-1}{2} M_{ff}^2}{1 + \frac{\gamma-1}{2} M_{jet}^2} \right)^{-\frac{1}{2}\left(\frac{\gamma+1}{\gamma-1}\right)} \tag{4.5}$$

An alternative approach is to vector the remaining engines in the aircraft plane to counteract the yaw. This has much less of an impact on the required climb angle (from 2.1° to 2.3°, see figure 4-3) and, for the aircraft presented here, needs a thrust vector angle of 11.2° when meeting the noise target. For the two-engine conventional aircraft, the increase in drag leads to the required climb angle increasing from 3.7° to 4.1°.

Referring back to Figure 4-2, the first flight position to be calculated is the flyover position which determines the nozzle area used for the remaining positions. The flyover FPR has to be very low in order to meet the specified noise level when so close to the ground. The conventional design has a slightly higher flyover FPR than the others due to the increased flyover height for the two-engine design and increased climb angle. The thrust vectored all-lifting body has the lowest flyover FPR as the climb angle is lowest. Once the nozzle area is specified the remaining positions of sideline, top of climb and start of cruise are simply calculated by iterating jet Mach number until thrust meets the required value. Whilst the flyover thrust is different for each of the three designs, this is not the case for the other locations as the climb angles are the same. Therefore, the conventional design with the largest jet area has the lowest FPR, then the split aileron all-lifting body and then the thrust vectored all-lifting body.

Whilst the top of climb FPR is, as expected, the highest of the four positions considered it is still significantly lower than that likely to be optimum for future designs when fuel burn is considered (Daggett *et al.* 2003, Gliebe and Janardan 2003). This is especially true for the two-engine conventional design. Further, considering the position the fan would have to operate in during take-off reveals that in practice the optimised take-off could not occur with a fixed nozzle and at the specified noise level. Figure 4-4 plots the fan pressure ratio against fan face Mach number scaled to top of climb conditions. For the cruise position, as the noise level is reduced, and fan diameter increased, the fan face Mach number increases by a small amount. For the flyover and sideline positions the trend is reversed, with reducing noise level leading to reducing fan face Mach number and increasing pressure rise. This is because the take-off and cruise working lines diverge as design FPR reduces. Also plotted on figure 4-4 is a line of constant loading over flow coefficient squared that goes through the top of climb point. This is for a ToC FPR of 1.35 with only a small move anti-clockwise as FPR is increased. This line will approximately follow the locus of peak fan efficiency and so indicates where the fan can operate. Flow coefficient by itself is a better indication of this as it is directly linked to incidence, but this requires knowledge of blade speed. Operating above and to the left of this line is at higher incidence with reducing stall margin. Operating below and to the right is at lower incidence towards choke.

$$\frac{\psi}{\varphi^2} = \frac{\Delta h_0}{U^2}\left(\frac{U}{V_x}\right)^2 = \left(\frac{1}{(\gamma-1)M_{ff}^2} + \frac{1}{2}\right)\left(FPR^{\frac{\gamma-1}{\eta_p \gamma}} - 1\right) \tag{4.6}$$

Whilst the top of climb point does not need to operate at peak fan efficiency, the cruise point does. Therefore, as the noise target is reduced the locus of peak efficiency will need to move to the right in figure 4-4 and the take-off operating points will be at much higher values of ψ/φ^2 than peak efficiency. It will, therefore, be impossible to design a fixed pitch fan that can operate at the efficiency values required for cruise and support the optimised take-off with adequate stall margin. Variable pitch would make the task easier but introduces a range of mechanical problems.

To increase the achievable top of climb pressure ratio and enable the fan to operate with adequate stall margin requires an increase in nozzle area at take-off. Figure 4-5 shows the variation in nozzle area required for the three aircraft variants to meet top of climb pressure ratios of 1.45, 1.55 and 1.65 respectively. With the thrust vectored all-lifting body having the highest ToC FPR before the nozzle area change was introduced, it needs the smallest change in area to meet the specified FPR. Fan operability, which limits what can be achieved with a fixed nozzle area, also limits how much or little nozzle area can vary. If the nozzle is not opened enough at take-off the stall margin may not be adequate. If it is opened too much then the fan may choke and operate at very low efficiency. Therefore, before deciding how much nozzle variation can be achieved and what the top of climb FPR should be, a better understanding of fan operability is required. Further, fan noise is likely to be dominant once jet noise is removed. Therefore, the quieter the fan can operate the less need for liners and/or increased duct length.

4.2. Impact of fan operation on noise and stability

4.2.1. Noise

At a conceptual level, designing for low fan source noise is considerably more complicated than designing for low jet noise. Prediction of jet noise is relatively accurate, at least for static jets, and limited variables drive one towards low jet velocity. When designing for a specified noise level, as is the case with the silent aircraft, a specified jet noise requirement translates directly into a specified jet area during take-off. This is not the case with fan source noise. Multiple generation mechanisms exist, both tonal and broadband, including self noise, rotor-stator interaction and multiple pure tones (buzz-saw). A complex propagation path, the use of liners for attenuation and, for the current silent aircraft design, shielding of forward propagating noise from the airframe,

further complicate the problem. Publicly available noise prediction capabilities are less mature, especially in relation to broadband noise, which makes it difficult to design for an absolute noise level. This is especially true for an engine using a variable area nozzle as the fan operating line during take-off is markedly different from conventional civil engines on which most current correlations are based. For the preliminary fan design available results, predictions and correlations were therefore used to guide the process and there was no attempt to design for a specified noise level. The success of this is discussed in chapter six when liner attenuations and acoustic prediction tools are brought together to predict the overall noise level.

Previous research has shown that increased nozzle area can lead to reduced fan noise for a given thrust. Woodward and Lucas (1976) tested a 1.25 pressure ratio fan with area increases up to 20% of the design area. Reductions in noise level at all operating speeds were witnessed alongside increases in efficiency. Ginder and Newby (1977) developed a broadband noise prediction model based on this and other work that correlated fan noise to inflow incidence and relative tip Mach number. More recently, Hughes *et al.* (2005) have shown that small increases in nozzle area (up to 12.9%) can give thrust increases and reduced broadband noise with modern wide chord fan designs. Work on the same rig (Woodward *et al.* 2002) with two rotor designs had shown at subsonic fan tip speeds a link between noise generation and wake severity.

Correlations such as those based on the work of Heidmann (1979) provide a further insight into suitable approaches to noise reduction. The ESDU fan and compressor prediction code (ESDU 1998), based on the approach taken by Heidmann, present broadband and tonal noise sources in the form of equation 4.7 with some variation for the different sources. RSS is the rotor-stator spacing, BPF the blade passing frequency, T_{02}-T_{01} the temperature rise across the rotor, M_{rel} the relative Mach number onto the rotor tip, $\dot{m}$ the mass flow rate, ω the polar angle and f the frequency.

$$\begin{aligned} SPL(f) &= 20\log_{10}(T_{02}-T_{01}) + 10\log_{10}(\dot{m}) \\ &\quad + F_1(M_{rel}) + F_2(RSS) + F_3(\omega) + F_4(f/BPF) + C \end{aligned} \tag{4.7}$$

In terms of cycle and fan rotor preliminary design, the variables that can be targeted are the temperature rise across the fan, the mass flow rate and the relative Mach number onto the fan tip. With fan pressure ratio and mass flow rate set by the requirement for low jet noise, high fan efficiency is required to minimise temperature rise. This correlates well with the work of Ginder and Newby as efficiency is closely linked to incidence angle onto the rotor and, for a normal engine working line during take-off, reduced incidence equals increased efficiency.

As mentioned in §2.2.3, whilst a traditional 50log(tip speed) correlation, used in Ginder and Newby (1977) for example, suggest reducing fan tip speed to reduce noise, this is not always the case (Topol *et al.* 2004). The increased noise of the NASA AST fan was found to be primarily due to increased broadband noise from increased fan tip turbulence impacting the stator. Included within this work is a simple formulation covering rotor-stator broadband noise generation (equation 4.8) in which C is the absolute velocity onto the stator, V_0 is the turbulent velocity and N_V is the number of Outlet Guide Vanes (OGVs).

$$Sound\ Power \propto 10\log\left[C^3 V_0^2 N_V\right] \tag{4.8}$$

For a given pressure rise and mass flow rate, a reduction in blade speed leads to an increase in loading and swirl angle downstream of the rotor. This will increase the absolute velocity onto the OGV (C in equation 4.8 above). The increased swirl leads to the wakes travelling further before impinging on the OGV so the turbulent velocity should be lower, but this may not be the case if the rotor has been overloaded. Therefore, to minimise rotor-stator broadband noise, rotor efficiency should be high during take-off and there is likely to be an optimum loading value.

Whilst increasing the nozzle area will increase fan tip speed for the same thrust, the high cruise altitude and low design point fan pressure ratio lead to excess thrust at low flight speed (reducing the fan pressure ratio increases the cruise ram drag more than the take-off ram drag). In addition a three-engine design requires a reduced climb angle compared to a two-engine design. The fan can therefore operate at part speed during take-off resulting in low rotor loading at the tip and lower flow velocity onto the OGVs.

With the rapid onset of multiple pure tone noise at supersonic relative tip Mach numbers, maintaining subsonic tip velocity at all times during take-off is desirable. As discussed later, achieving this for the entire take-off leads to reduced cruise performance and therefore alternative mitigation strategies must be considered. As nozzle area is increased, fan back pressure is reduced and, for a fan operating with supersonic relative inlet flow, the primary shock structure is ingested into the blade passage, leading to choking. A weaker bow shock detached from the leading edge still propagates upstream but considerable reduction in MPT noise is predicted for this situation (Xu 2004). For fans working with a fixed nozzle area this effect is generally only seen at high fan speed where the shock is just ingested at the tip for peak efficiency.

To summarise, for low fan source noise whilst maintaining low jet noise, high efficiency and low tip loading is required during the entire take-off procedure. To minimise multiple pure tone

generation, when the relative flow onto the rotor tip is supersonic the primary shock structure should be ingested into the blade passage.

4.2.2. Stability

Several books provide in-depth discussion on compressor stability (Platzer and Carta 1988, Cumpsty 1989) and therefore only a brief discussion focussing on the limits of nozzle area variation is presented here.

At a specific speed a fan can only deliver a certain pressure rise before stalling or surging. For a fan operating with a variable area nozzle, this places a limit on how far the nozzle can be closed. For a given nozzle area the fan will operate at closer to stall during take-off than at cruise due to the reduced pressure rise from the ram effect. This leads to take-off stall margin being a critical requirement when designing a conventional fan. Here we want to operate with the nozzle as far open as possible during take-off. Therefore, stall and surge margin, if adequate at cruise, will not limit operation.

As nozzle area is increased, the static pressure at the back of the fan drops and mass flow rate increases. At a certain point the fan will choke, after which further reductions in back pressure will only impact flow downstream of the fan throat. To increase the mass flow further requires an increase in fan speed. Whilst a fan can operate choked, highly choked operation results in very poor fan efficiency and so should be avoided if possible.

Considering aeroelasticity, the fan must be designed and operated in such a way as to prevent high-cycle fatigue. Two regimes must be considered; forced vibration and flutter. Forced vibration is caused by periodic aerodynamic disturbances such as inlet asymmetry leading to harmonic excitation of the fan. Flutter is when the energy absorbed by negative aerodynamic damping exceeds the energy dissipated due to structural damping. Predicting and mitigating both regimes is out of the scope of this thesis (although natural frequencies of the fan are calculated in §5.3.1) but of the two, flutter is the more likely to limit the operating range of the fan. Figure 4-6, from Snyder and Burns (1988), shows the various types of flutter often encountered in compressors. From this is can be seen that, when operating at high mass flow and low pressure rise, choke flutter and classical unstalled supersonic flutter may occur. Choke flutter is thought to be linked to in-passage shocks with associated flow separation indicating that operating highly choked should be avoided, especially at high speed when in-passage shocks are present. Classical unstalled supersonic flutter, if present, effectively limits the maximum blade speed and, with the boundary

very steep with respect to speed, is unlikely to be a problem during take-off without also being a problem at top of climb.

Finally, increasing the nozzle area between top of climb and take-off increases the range of incidence that the OGVs must support. This can be seen by considering the Euler equation for turbomachinery across the rotor where the subscript 2 indicates rotor exit and α is the swirl angle.

$$\tan\alpha_2 = \frac{V_{x2} c_p T_{01}}{U_2}\left(FPR^{\frac{\gamma-1}{\eta_p \gamma}} - 1\right) \tag{4.9}$$

Whilst opening nozzle area increases the axial velocity, it also increases blade speed U and reduces fan pressure with the overall result being a reduction in exit swirl angle. Whilst separation of the flow on the OGVs due to high positive or negative incidence is not as severe as stall of the rotor, it increases loss and reduces thrust and therefore should be avoided.

To summarise, the degree the nozzle can open during take-off is limited by the following; fan choking (both from an efficiency and flutter perspective) and OGV incidence. Of the two, OGV incidence is likely to be limiting at low speed and fan choking at high speed.

4.3. Operation with two nozzle areas

With the nozzle setting impacting both fan and jet noise, the same nozzle position needs to meet the requirements of both sources. This requires the fan pressure ratio being at a specified level for low jet noise and the fan operating at an efficient position for low fan noise with sufficient stall margin. The aircraft is as close as it gets to ground outside the airport boundary at the flyover position and, as jet noise reduces more rapidly than fan noise when the engine is throttled back, this position is critical. As discussed later in this section, relative tip flow can be set to below unity Mach number at this position and therefore high fan efficiency is the main requirement. At the sideline position subsonic tip Mach number cannot be maintained and therefore whilst high efficiency is still important, any primary shock structures must be ingested to minimise MPT noise. This requires operating near the shoulder of the fan characteristic.

4.3.1. Approach

As briefly mentioned in §4.1, for a typical fan design, a locus of constant flow coefficient, φ, tracks peak rotor efficiency well, so ensuring both the cruise and flyover points are at the same flow coefficient will ensure they are both at, or close to, peak efficiency. If the nozzle is operated at a

fixed area during take-off, the sideline point on the fan characteristic is at a higher flow coefficient than flyover and on a higher thrust line. Setting the flyover flow coefficient to match cruise will also therefore place the sideline point near to the fan shoulder. Performing this calculation requires the use of a sample characteristic because the flow coefficient is a function of blade speed (equation 4.10). If a realistic fan map is not available, similar results can be obtained by fixing the stage loading divided by the flow coefficient squared, ψ/φ^2. This is independent of blade speed but diverges from peak efficiency at higher Mach numbers (equation 4.6).

$$\varphi = \frac{V_x}{U} \propto \frac{M_{ff}\left(1+\frac{\gamma-1}{2}M_{ff}^2\right)^{-\frac{1}{2}}}{U} \tag{4.10}$$

As in §4.1 the fan face Mach number at top of climb is set to 0.66. In choosing the top of climb fan pressure ratio the following procedure has therefore been followed;

a) set the top of climb fan face Mach number to meet specified capacity,

b) calculate the start of cruise fan face Mach number and pressure rise maintaining the same nozzle area as top of climb,

c) place the flyover operating point at the same flow coefficient, φ, as the start of cruise operating point for high efficiency at take-off and calculate the flyover FPR and nozzle area,

d) iterate top of climb FPR until the take-off nozzle area matches that required to meet the jet noise target.

This approach is illustrated on the fan characteristic in figure 4-7 and the resulting relationship between take-off jet noise and top of climb FPR can be seen in figure 4-8. For the conventional aircraft this approach indicates that a ToC FPR of 1.41 is required with a 20.5% increase in nozzle area between top of climb and take-off. For the all-lifting body with split aileron these values increase to a FPR of 1.44 and nozzle variation of 23.5% and for the thrust vectored version a FPR of 1.46 and nozzle variation of 23%. As efficiency plateaus near peak values, especially at part speed, the flyover flow coefficient can be increased slightly to enable a slightly higher ToC FPR to be achieved. Figure 4-9 shows the result of this with flyover flow coefficient set to cruise flow coefficient multiplied by 1.05. FPR values of the three variants are increased by approximately 0.03 and the required nozzle variation by an additional 6%. It is worth noting that a very small increase in ToC FPR requires a relatively large increase in nozzle area variation. The fan

characteristic used in the creation of these and subsequent plots in this chapter is a rotor only map from the fan developed in chapter five. This has only been used to match flow coefficients with fan efficiency fixed to the value in table 4-1.

As previously discussed, by ensuring subsonic relative flow onto the fan tip during take-off, multiple pure tone (buzz-saw) noise can be removed. The design point blade speed required for this can be calculated by first setting the flyover or sideline relative tip Mach number to one to get the corrected flyover/sideline blade speed (equation 4.11). A representative fan characteristic can then be used to find the design point tip speed.

$$U_{tip}\Big|_{take-off} = a_{ff}\sqrt{1-M_{ff}^2}$$

$$\left.\frac{U_{tip}}{\sqrt{\theta}}\right|_{take-off} = a_{0,ref}\sqrt{\frac{1-M_{ff}^2}{1+\frac{\gamma-1}{2}M_{ff}^2}} \tag{4.11}$$

Figure 4-10 shows the maximum corrected top of climb blade speed possible for $\varphi_{flyover} = \varphi_{cruise}$ and $\varphi_{flyover} = 1.05\ \varphi_{cruise}$ to meet subsonic relative flow for the whole take-off (where the sideline point is the limiting condition) or for just the flyover position. Depending on the aircraft, cutting off rotor alone tones at just flyover would require a corrected top of climb tip speed of around 375m/s and as low as 250m/s to cut-off rotor alone noise for the entire take-off.

In determining whether such speeds are realistic it is useful to look at what the top of climb stage loading would have to be. With loading a function of blade speed which changes from the hub to the tip the value of U used here is at a radius that gives equal duct area below and above;

$$r = r_{tip}\sqrt{\frac{1+htr^2}{2}}$$

This leads to the following definition of loading in which $U_{tip,corr}$ is corrected to the reference inlet stagnation temperature;

$$\psi = \frac{\Delta h_0}{U^2} = \frac{c_p T_{0,ref}\left(FPR^{\frac{\gamma-1}{\eta_p\gamma}}-1\right)}{\frac{1}{2}\left(1+htr^2\right)U_{tip,corr}^2} \tag{4.12}$$

Figure 4-11 is the equivalent of figure 4-10 but with lines of M_{rel}=1 plotted against top of climb stage loading rather than top of climb corrected blade speed. With modern fans having loading in

the range 0.44 to 0.50 a significant increase in loading would be required to cut-off rotor alone noise for the entire take-off.

Comparison can also be made with recent fan rig tests. Estimates of stage loading for the RESOUND datum and LNR1 fans are 0.49 and 0.68 respectively (based on data contained in Bewick *et al.* 2001, Xu 2004) for a hub-tip radius ratio of 0.31. Estimates of stage loading for the NASA AST fan designs are 0.60 (Hobbs *et al.* 1995) and 0.76 (Neubert *et al.* 1997) although the variable pitch design and high hub-tip radius ratio of 0.426 makes these values less comparable. The 2nd of the NASA AST fan designs experienced a noise increase over the 1st design that was attributed to the fan being overloaded.

4.3.2. Validation

To confirm the success or otherwise of the approach outlined above, a full take-off run was performed for the split aileron version of the all-lifting body. Design capacity was set to M_{ff}=0.66 and the top of climb FPR to 1.442 (taken from figure 4-8). Data from Table 4-1 was used and a nozzle area increase of 23.5% for take-off (figure 4-8) was expected to be required in order to meet the minimum flyover climb angle of just over 3.0° (figure 4-3). With the engine being modelled using equations 4.1 to 4.3 and 4.5, the jet temperature can now be calculated at every time step rather than specified in advance.

The resulting take-off profile and jet temperature variation are plotted in figure 4-12. To achieve this profile, and in particular the flyover climb angle, a nozzle area increase of 26% was required, slightly larger than the predicted 23.5%. One reason for this is that the prediction used purely flyover data in equation 4.4. In this equation (see also 3.20), the required take-off area is directly proportional to the jet temperature. The equation was developed for a fixed jet temperature at take-off (§3.4.2) and, as can be seen from figure 4-12, the jet temperature at flyover is the lowest temperature that occurs when a more realistic engine model is included. The mean temperature during take-off was 318.7K compared to 313.5K at flyover, indicating a 1.7% increase in nozzle area relative to the initial prediction would be required. With a ToC nozzle area of 2.46m^2, this correction increases the expected nozzle change at take-off up to 25.6%.

Whilst the jet temperature used in equation 4.4/3.20 could be modified to be the mean of the flyover and sideline values, using just the flyover condition gives a good result, accurate enough for estimating what ToC FPR can be achieved for a given take-off noise level.

Figure 4-13 plots the take-off fan capacity against pressure rise onto the scaled rotor only map that was used when matching cruise and flyover flow coefficients. The top of climb point is placed on the 100% speed line so that the start of cruise point, which is at the same nozzle area, is at peak efficiency. The thick line on this map joins up all the operating points (calculated for 1 second time steps) between the brakes off location and a point 5000m after brakes off. As intended, the flyover point is at peak efficiency with the start of roll point having lower stall margin due to the change in working line between zero and take-off flight speed. The fan is choked at the sideline point as required to minimise buzzsaw noise.

4.3.3. Sensitivity

Sensitivity of the split aileron version of the all-lifting body aircraft to key input parameters in table 4-1 was analysed. With cruise and flyover flow coefficients matched and the 57dBA jet noise target met, the following input parameters were modified; fan face Mach number, temperature rise due to core mixing, exit pressure recovery and top of climb/start of cruise flight level. The results can be seen in figure 4-14.

Before looking at each subplot in turn, it is worth making some general points about the flyover condition. From equation 3.20 it can be seen that flyover jet area divided by jet static temperature is a function of aircraft mass, rotation speed, jet noise level, L/D and flyover climb angle. With all these parameters constant, or almost constant*, in this analysis the ratio of jet area to temperature at flyover is also constant. Likewise, with flyover net thrust constant the flyover mass flow and jet velocity must also be constant;

$$T_N = \dot{m}\left(V_j - V_\infty\right) = \rho_j A_j V_j \left(V_j - V_\infty\right) = \frac{p_\infty}{R}\frac{A_j}{T_j} V_j \left(V_j - V_\infty\right)$$

With constant flyover jet velocity, increasing jet temperature will reduce the jet Mach number. From equation 4.1 it can be seen that this leads to a reduction in the sum of FPR, PR_{in} and PR_{out}. In summary:

a) The ratio of jet area to jet temperature remains constant at flyover

b) Flyover jet velocity and mass flow rate are fixed

* The flyover climb angle is a weak function of Top of Climb FPR which does change but for the range of interest only changes between approximately 3.0° and 3.1° (see figure 4-3). This does not influence the trends seen.

c) Increasing flyover jet temperature leads to a reduction in the sum of FPR, PR_{in} and PR_{out}.

Starting with the top left subplot, increasing ToC fan face Mach number leads to reducing fan face area as changes in top of climb mass flow rate are only a secondary effect and fan inlet conditions are unchanged. With equations 4.1 to 4.3 unaffected at flyover, mass flow rate and pressure rise remain constant and, with fan face area reduced, flyover fan face Mach number must increase. As flyover fan face Mach number increases, lines of constant flow coefficient become steeper and, to match flow coefficients, cruise mass flow rate must drop slightly and pressure rise increase. This also moves the top of climb point to slightly lower mass flow and higher pressure rise requiring greater nozzle variation between top of climb and flyover. As at flyover, fan face Mach number will increase at sideline and therefore sideline blade speed must reduce to maintain unity tip relative Mach number. With minimal change in relative positions on a fan map, reductions in sideline blade speed lead to reductions in top of climb blade speed.

Increasing the temperature correction due to core mixing (top right subplot) increases the jet temperature. From (a) and (b) above, this leads to increasing flyover jet area and reducing flyover FPR, with the reduction in temperature rise across the fan only having a secondary effect on the results. Increasing jet temperature moves lines of constant thrust down on a fan map and, with jet temperature increasing more at top of climb than at flyover, lines of constant thrust at ToC and flyover get closer together. This is because the temperature correction is proportional to the fan pressure rise minus one. As flyover and cruise flow coefficients remain matched, both mass flow rate and FPR will drop, more at the top of climb position than at the flyover position. Fan face area reduces due to the reduced top of climb mass flow rate and the change in required nozzle area also becomes less. Sideline fan face Mach number increases because the mass flow rate reduction is less than that at top of climb and this requires a lower blade speed to cut-off rotor alone noise. This translates to an even lower top of climb blade speed as the operating points are now closer together on a fan map. The impact of engine design parameters on stagnation temperature rise is discussed in appendix D.

Increasing exit pressure recovery (bottom left subplot) beyond one is feasible as bypass stagnation pressure could increase when mixed with the core flow. At flyover, increasing PR_{out} leads to a reduction in FPR and, with both ΔT_0 and temperature rise across the fan linked to FPR, a small reduction in jet temperature. From (c) this feeds back to the FPR reduction being slightly less than the PR_{out} rise and, from (a), flyover jet area will reduce slightly. At cruise the reduction in FPR due to increased PR_{out} is compounded by the reduced flyover FPR leading to increased cruise mass flow rate when flow coefficients are matched. The reduction in FPR at cruise is therefore more

than that at flyover and the same is true of the top of climb position, again with an increase in mass flow rate. This reduces the required nozzle area change between top of climb and take-off. With top of climb mass flow rate increasing and fan inlet conditions unchanged, fan face area increases. Flyover mass flow rate is unchanged so flyover fan face Mach number reduces and the same is true at the sideline position. A higher sideline blade speed can be utilised whilst maintaining unity relative Mach number enabling a higher top of climb blade speed. The impact of engine design parameters on pressure recovery due to mixing is discussed in appendix D.

If PR_{in} is increased rather than PR_{out}, except for fan face area, the same trends are seen. Whilst top of climb mass flow rate increases, it is offset by increases in fan inlet stagnation pressure and the fan face area remains constant. The trend in ToC blade speed remains the same as when changing PR_{out} due to flyover and sideline fan face Mach numbers still reducing. This is because the fan inlet stagnation pressure increases.

Increasing start of cruise altitude (bottom right subplot) has no impact on the flyover condition, so flyover jet area, temperature, mass flow rate and FPR are all unchanged. As top of climb/start of cruise altitude increases the free stream static pressure drops and, with net thrust fixed, A_{jet} and/or M_{jet} must increase (equation 4.2). Keeping cruise and flyover flow coefficients matched leads to both A_{jet} and M_{jet} increasing with a corresponding increase in top of climb FPR (equation 4.1). Take-off nozzle area is fixed so the change in area required between top of climb and take-off reduces. Whilst top of climb mass flow rate reduces, the reduction in inlet stagnation pressure is more significant and the fan face area must increase to maintain design capacity. This reduces fan face Mach number at both flyover and sideline and, as discussed above, allows higher blade speeds whilst cutting off rotor alone noise.

4.4. Operation with continuously varying nozzle area

In §4.3, operation with two distinct nozzle areas was analysed; one for take-off and one for top of climb and cruise. Whilst this approach is straightforward, works well with equation 3.20 and can show trends for different noise levels, it does have some limitations: Firstly, the ToC FPR achievable is only just in the target range. Secondly, whilst the approach placed the flyover position at what is thought to be an ideal location, start of roll is closer to stall and sideline more highly choked than would be desirable (figure 4-13). Therefore, a more advanced approach is developed in this section in which nozzle area varies continuously during take-off. Equation 3.20 can no longer be used and the take-off optimisation code needs to be linked directly into the fan operation as was done in §4.3.2 above.

To achieve a higher top of climb FPR whilst meeting the same jet noise target requires greater nozzle opening at take-off, with the fan operating at higher mass flow and lower pressure rise than before. For a fixed pitch fan and OGV there are limitations on how far the nozzle can be opened (§4.2.2):

- As nozzle area is increased the absolute flow angle onto the OGVs (α_2) reduces and can be taken as limiting nozzle opening at low speed.

- At higher speed the fan may choke before OGV incidence becomes a problem. Reducing the back pressure too much beyond that required to choke the rotor will lead to poor efficiency and flutter regions may be encountered. This can be taken as limiting nozzle opening at high speed.

This approach is illustrated on the sample fan map in figure 4-15. At low speed, fan operation is along a static working line with the position of this line determined by what incidence range the OGVs can support. When operating at higher speed during take-off the fan becomes choked and the line $d\varphi/dM_{ff} = 0$ can be used as the operating line in this region up until maximum design capacity is achieved. This is because once choked the relative flow angle at fan face, β_1, which is the inverse tan of one over the flow coefficient will remain fixed as back pressure is reduced further. Once the aircraft is sufficiently far from noise sensitive areas then the operating line can switch to match the cruise flow coefficient so that operation is at peak efficiency. In terms of setting blade speed, a similar approach to that taken with two nozzle areas is required and this is also indicated in figure 4-15. The take-off operating line should at all times remain outside the area in which strong detached shocks can propagate upstream.

The performance when nozzle area is continuously varied was compared to that when a fixed nozzle area was adapted during take-off. To do this, the lower working line in figure 4-15 was set so as to go over the flyover point from the validation exercise performed above (§4.3.2). Top of Climb FPR was then adjusted until the 57dBA jet noise level could be met with the required flyover climb angle (figure 4-3). It was found that a Top of Climb FPR of 1.446 could be achieved in this way when continuously varying the nozzle area compared to 1.442 when nozzle area was fixed. This difference is minor but what is more important is where the fan has to operate to achieve this. Figure 4-16 plots the take-off operating lines on the fan map for the two approaches (ignore the fixed nozzle operation for the time being as it is discussed below). Capacity is normalised against design capacity ($Q_{ff}/Q_{ff,ToC}$) and fan pressure ratio is normalised against design fan pressure ratio $(FPR-1)/(FPR_{ToC}-1)$. Referring to this figure, it can be seen that whilst flyover is

at the same position for the two approaches, start of roll and sideline are not. Start of roll surge margin and fan efficiency have been improved by moving the operating point down and to the right along a line of constant jet noise. At sideline, the reverse has occurred with the operating point moved up and to the left. This increases fan efficiency by 1.5% and reduces blade speed. Figure 4-17 shows how these modifications have occurred and the impact on the take-off profile (again ignore the fixed nozzle operation for the time being). During the initial phase of take-off the nozzle area is opened further than in the fixed case with a maximum of 38% opening relative to the ToC condition. This allows the aircraft to accelerate slightly quicker and take-off slightly earlier. The nozzle area is closed as sideline is approached to stop the fan going too far into choked operation. This limits the maximum thrust achievable and therefore maximum climb angle is slightly reduced. Increasing ToC FPR from 1.442 to 1.446 balances these two changes out and the required flyover climb angle is achieved.

In summary, whilst continuously varying the nozzle area may only deliver a small increase in ToC FPR it does ensure the fan is always operating at an ideal location.

4.5. Revisiting operation with a fixed nozzle area

At the start of this chapter, operation with a fixed nozzle area was discussed and figure 4-2 was created in order to predict what ToC FPR could be achieved for a given jet noise target. For the jet noise target of 57dBA the figure estimates that a ToC FPR of 1.36 can be achieved for the split aileron version of the all-lifting body, although stall margin was expected to be poor (figure 4-4). With the fan operation now linked into the take-off optimisation it is worth revisiting this estimate to see if it is achievable on the scaled fan characteristic used so far.

The result of this work is shown on figure 4-16 and figure 4-17. Whilst the flyover climb angle was met when operating with a ToC FPR of 1.36 and a jet noise limit of 57dBA, it is unlikely that a fan could operate in the required region. Whilst the stability line on the characteristic that was used is only indicative of what would occur in a real fan[*], the fact that the fan would have to operate along it does suggest stable operation would be unlikely. In addition, in order to achieve the results shown two modifications were required: First, the top of climb operating point was moved to a lower position on the scaled fan map (but with the results still normalised to the

[*] As already mentioned, the fan characteristic used is a rotor only characteristic for the fan designed in chapter five. It was created based on CFD solutions run at a range of speeds and back pressures with convergence of the solution being the only criterion used as to whether the fan operating point was valid. In addition, in order to be used in this chapter and when looking at engine cycle design in general, it was processed using a program called SmoothC, part of the GasTurb package (Kurtz, 2004).

original position on the figure). This makes it easier to operate during take-off but will move the start of cruise point away from peak efficiency. Second, although the aim was to operate with a fixed nozzle, in order to remain on the map small increases in nozzle area have had to occur at the start of roll and the flyover position (figure 4-17). Without increasing nozzle area the only way to increase the stall margin during take-off is to operate at higher thrust and therefore higher noise.

4.6. Discussion

With a desire to either increase top of climb fan pressure ratio or meet a specified fan pressure ratio with less nozzle variation, it is interesting to see what influences the result and how. Looking at airframe and operations first, anything that either enables lower take-off jet area or increases the distance between flyover and top of climb thrust lines on a fan map is of assistance. Jet area requirement is set by equation 3.10/4.4 with increasing take-off L/D, reducing takeoff MTOW and reducing take-off climb angle the best ways of reducing take-off jet area. This has all been discussed in chapter three, so will not be discussed further here. Enabling the fan to operate at lower percentage speed at take-off allows both a higher top of climb FPR and a higher top of climb corrected blade speed. This can be achieved in several ways. Firstly, as seen in §4.3.3, increasing start of cruise altitude helps because of the reduction in free stream pressure. An added benefit of cruising higher is that it leads to increased wing area and improved low speed performance. The disadvantage is longer climb to cruise, important for shorter flights, and a possible increase in radiative forcing through contrail formation at a higher altitude (Sausen *et al.* 1998, IPCC 1999, Williams *et al.* 2002).

For constant $M_\infty L/D$, which is approximately proportional to range for a given fuel load and therefore needs to be maximised, increasing the flight Mach number, M_∞, leads to reduced cruise L/D. Reducing cruise L/D leads to a small increase in ToC FPR as top of climb and cruise thrust requirements increase requiring jet Mach number to increase more than the free stream Mach number. This moves the ToC thrust line on the fan map away from the flyover point. This initial increase in ToC FPR is small, though, and any reduction in take-off L/D due to the aircraft being designed for a higher cruise Mach number is likely to be more significant. Therefore, cruising slower will enable higher ToC FPR for the same take-off jet noise level as improved low speed performance will have a greater impact than the increased ToC and cruise thrust requirements.

Looking now at changes that can be made to the engine, changes in top of climb fan face Mach number have minimal direct effect on the result. The sensitivity analysis in §4.3.3 did not look at secondary effects though. As design capacity increases the fan diameter will reduce, aircraft

structural mass and nacelle drag drop leading to reduced thrust requirement at all flight conditions. Conversely, fan efficiency will reduce, leading to a higher jet temperature and increased sfc. When considering these secondary effects, finding the optimum position for low noise is a sizable undertaking and has not been performed here. It is likely though that the result will be near to that for optimum fuel burn as increases in fuel burn will lead to increases in MTOW.

As discussed in more detail in appendix D, it is desirable from a fan operating perspective to minimise the pressure ratio correction and temperature increase due to mixing at both take-off and top of climb/cruise as long as the impact on cruise fuel burn is minimised. This is best achieved by increasing the design point bypass ratio with more energy extracted from the core to power the fan reducing LPT exit pressure and temperature. At cruise the ratio of bypass to core stagnation pressure ratio at mixer entry has to be near one to minimise losses. At part speed this ratio will increase reducing PR_{out} at flyover. This results in increased take-off fuel burn but does enable increased fan pressure ratio. In this chapter, PR_{out} has been kept constant for different flight conditions (see table 4-1); in chapter six it will be adjusted to take into account changing mixer conditions based on the results in appendix D. Whilst ΔT_0 is purely a function of core mixing, PR_{out} is also a function of the downstream duct design. Losses due to ducting have to be minimised during cruise and at top of climb when maximum thrust is required, but increased losses at take-off could be tolerated as this would increase flyover FPR enabling higher ToC FPR. One way to achieve this would be with deployable baffles in the exhaust. If lined these could reduce the duct length required to get fan noise to the required level. Finally, for a given duct and modelling the flow as a Fanno flow, increasing Mach number leads to increasing stagnation pressure loss which was not accounted for in this section. With the flow being accelerated through the inlet during take-off and diffused during cruise, calculation of inlet pressure recovery requires knowledge of free stream and fan face Mach numbers. For a podded design through, the loss is small and assuming a constant value, as was done in this chapter, is acceptable.

Matching cruise and flyover flow coefficients has been shown to deliver top of climb fan pressure ratio in the region required for low fuel burn when meeting the jet noise target of 57dBA. It is worth discussing how applicable this approach is when less significant noise reductions are required and in particular how useful a variable area nozzle is in these circumstances. From Figure 4-2 it can be seen that for the conventional two-engine aircraft with a ToC FPR of 1.55 a fixed nozzle area would be able to deliver a take-off jet noise level of approximately 66 dBA, an increase on 9 dBA from the target. If the nozzle area was adjusted so that the flyover flow coefficient matched the cruise flow coefficient then the noise level would drop to approximately 63.5 dBA, only 6.5 dBA from the target (figure 4-8). This would require flyover nozzle area to be

approximately 14% greater than top of climb nozzle area, only just outside the range of flight tested designs (Weir and Mendoza 2005). Whilst this only indicates a 2.5 dBA improvement through use of a variable area nozzle this is a significant reduction for an engine manufacturer. Further, as was seen in §4.5 and figure 4-16, operation with a fixed nozzle would require the top of climb point to be moved down the 100% speed line. Even then increased thrust at start of roll and flyover may be required so as to operate with sufficient stall margin, thus increasing noise.

4.7. Chapter conclusions

In this chapter, the optimised take-off approach developed in chapter three has been linked to the operation of the fan. For a fixed nozzle area it was found that a top of climb FPR of less than 1.35 was required for a conventional design in order to meet the jet noise target at take-off even before fan operability was considered. This is well below the 1.45 to 1.55 range that other studies have considered optimum for minimum cruise fuel burn. Utilising an all-lifting body similar to the SAI concept airframe can increase the achievable FPR slightly but significant fan stability problems would remain.

By considering the impact of nozzle area variation of fan noise and stability, two approaches were developed in order to deliver the required take-off jet noise level and the required top of climb FPR. The first involved operating at two distinct nozzle areas – one at top of climb and cruise and one at take-off with the nozzle variation determined by matching cruise and flyover fan flow coefficient. The equation developed in chapter three for estimating jet noise outside the baseline airport (3.20) could be used directly and the result was a top of climb FPR of 1.44, significantly higher than when operating with a fixed nozzle area. The second approach involved continuously modifying the nozzle area during take-off, with nozzle opening limited by OGV incidence at low fan speed and fan choking at high speed. This required fan operation to be directly linked into the take-off optimisation code and resulted in improved fan stability and a small increase in top of climb FPR to 1.45.

With the range of nozzle variation between take-off and top of climb thought to be limited by fan choking and OGV incidence, this is the subject of the next chapter. Specifically, can a fan stage (rotor, duct and OGV) be designed to work with a variable area nozzle to deliver high capacity and low pressure rise during take-off, the required top of climb thrust and efficient cruise?

5. Fan design for use with a variable area nozzle

In chapter four, fan operation was linked to take-off jet noise. In conjunction with trying to minimise fan source noise this determined the required nozzle variation and top of climb fan design parameters. In this chapter, a fan stage including rotor, duct and outlet guide vanes, is designed for use with a variable area nozzle operating as described in the previous chapter. Whilst meeting top of climb thrust requirements and operating at high efficiency during cruise remain the dominant design requirements, ensuring adequate stall margin at take-off, critical on conventional designs, is replaced by the need to maximise part speed fan capacity. This can be interpreted as moving the take-off operating line down and to the right in figure 4-15 without modifying the top of climb position. With forward noise shielded, the design of the engine section stator (ESS) was of secondary importance and therefore the downstream duct and OGV design was performed with a specified bleed mass flow used to remove core flow. The final design has rotor exit Mach number and swirl at the hub similar to the design by Kaplan *et al.* (2006) for which engine section stators were designed and, therefore, this approach is acceptable for the level of fidelity required here: The fan design is not intended to be the best possible to meet the design requirements, instead, it is intended to show that such requirements can be met and to enable more advanced noise predictions to be made (chapter six).

Whilst the results of chapter four indicate that a top of climb fan stage pressure of 1.45 is ideal, a value of 1.50 was selected as the design value for the fan here. This is because the work was performed within the Silent Aircraft Initiative project which has two final concept designs; a high risk embedded engine design (de la Rosa Blanco *et al.* 2007, Hileman *et al.* 2007b) and a lower risk podded design similar to the aircraft used as the baseline in this thesis. The higher risk design ingests some of the airframe suction surface boundary layer leading to reduced inlet pressure recovery. This, along with concerns over inlet distortion for the higher risk design, pushed the design pressure ratio up. Blade loading (equation 4.12) was set to 0.52; slightly higher than existing commercial designs but not as high as some research fans. With a hub to tip radius ratio of 0.29 (set to be similar to current designs) this gives a corrected top of climb blade speed of 371m/s if polytropic efficiency is 0.92. This is comfortably low enough to reduce tip relative Mach number to below one at flyover as required. Rotor-stator spacing was set to approximately three times rotor axial tip chord and the rotor tip radius to 1.0334m. This radius was set to give the required thrust for an earlier concept aircraft design and is very similar to the final radius used in chapter six.

5.1. Required traits from a fan

The design requirements that need to be met can be summarised as follows:

- Top of Climb capacity should be maximised without overly impacting efficiency. This is the same as for conventional designs and arises because as capacity increases fan diameter reduces for a given thrust requirement, leading to reductions in engine weight and nacelle drag. Trying to increase capacity too much leads to higher Mach numbers at the fan face and increased losses. This requirement primarily impacts the fan as this is where choking occurs.

- Cruise stage efficiency must be maximised as, for an ultra-high bypass ratio engine, fuel burn is very sensitive to fan performance. Increasing loading tends to increase performance but limits operating range

- The fan must be able to operate at high flow coefficient at low speed. Part speed operation usually occurs at low altitude during take-off and landing and, for a fixed nozzle area, this places the fan working line at a flow coefficient lower than the peak efficiency value. Here the opposite is required with the nozzle area increased to deliver high mass flow. For the fan, part speed choking must occur at as high a mass flow as possible. For the OGVs the challenge is to meet the required incidence range, significantly increased by opening the nozzle area, whilst minimising losses.

- The fan must operate at low source noise during take-off especially for rearward propagating noise. This is discussed in more detail in the following chapter but in this chapter can be translated into the following three requirements: Maximising fan rotor efficiency at take-off, reducing the mean flow velocity onto the OGVs and increasing the rotor-OGV spacing. This should all lead to reduced rearward propagating noise based on equation 4.8.

5.2. Tools and methods

5.2.1. Aerodynamic design and analysis

Fan aerodynamic design was performed using Multall, a highly developed 3D viscous solver widely used in industry and described in more detail by Denton and Xu (2002). The code,

specifically designed for turbomachinery applications, is computationally light enough to be used as a design tool.

Rotor

The fan rotor was designed for cold (0% speed) conditions at seven sections; 0%, 10%, 30%, 50%, 70%, 90% and 100% span with at each location the following parameters specified: Radius variation from inlet to exit; blade angle at eleven locations along the chord; leading and trailing edge thicknesses and shape; maximum thickness and location of maximum thickness. Finally, the stacking of the blade sections was specified in the axial and tangential directions. The program Stagen was used to translate the blade design into a Multall input file. At this time any deformation of the blade due to centrifugal and pressure forces was included. This was done by rotating each of the blade sections by an angle around a point in space calculated as discussed in §5.2.2. Whilst this does not fully reflect the blade deformation it does capture any twisting of the sections. The overall design was controlled using three data files; stagen.dat, chic.dat and twist.dat. The stagen file contained the blade design, the twist file contained the deformation to be applied to each section at each running speed and the chic file contained the operating points that the blade was to be run at, including rotational speed, initial conditions and fan back pressure. Inlet stagnation conditions were specified upstream of the fan bullet and simple radial equilibrium along with a specified static pressure was used at the downstream boundary. Grid density was set to 49 circumferential points, 49 spanwise points (two in the pinched tip) and 251 streamwise points (100 upstream, 101 in the blade passage and 50 downstream). The grid was extended past the bullet upstream so as to provide simple axial inlet conditions and capture detached shock structures at high rotational speeds. The bullet itself was not reduced to zero radius due to the limitations of the code and was instead restricted to a 50mm minimum radius. Downstream, the grid was kept axial. It was found that this grid density gave a good compromise between mesh dependency, numerical accuracy and run time. Reducing grid density, especially in the streamwise direction, led to convergence problems due to the highly sheared H-grid in the leading edge region.

Duct

When designing the duct between the rotor exit and OGV inlet, the rotor grid discussed above was extended downstream with an additional 100 points added in the streamwise direction. To simulate the core, a fixed mass flow was bled from the hub surface just downstream of the rotor.

OGVs

OGV section design away from the hub and casing boundary layers was performed using Mises, a viscous cascade analysis and design system (Drela and Youngren 1998). This tool has previously been successfully used in the design of OGVs that need to support a high incidence range (Koller *et al.* 2000, Kusters *et al.* 2000) which is the key design requirement here. Based on the work of Power (2006) and using a modified version of her code, each design section was described through the use of thirty parameters; seven to describe blade camber, twelve to describe the blade thickness, ten to describe the leading edge shape and one for the chord. For each of the design sections, blade profile optimisation was controlled through the Rolls Royce software SOFT (Shahpar 2002) utilising ARMOGA (Adaptive Range Multi-Objective Genetic Algorithm). Inlet Mach number, slope and Reynolds number were specified based on results from the upstream rotors with streamtube radius and thickness variation estimated based on results from SLEQ, a throughflow analysis code. For each of the design surfaces, the blade profile was optimised to minimise loss and downstream swirl at three conditions; cruise, top of climb and take-off. The top of climb and take-off conditions defined the maximum positive and maximum negative flow incidences respectively whilst the cruise condition defined the maximum required efficiency location. The weighting applied to this cruise condition was twice that of the top of climb and take-off conditions. Within Mises, the preferred isentropy and dissipation model was used with conservative entropy everywhere except at shock locations. The default transition model was used with an inlet turbulence level set to 1.6%.

Stage

Three dimensional analysis of the entire stage was then performed using Multall. The designed OGV sections were scaled slightly to give a smooth change in chord along the span, and additional sections at the hub and tip were specified based on the incoming boundary layer flow. The sections were then stacked with axial sweep and tangential lean specified. For the stage analysis, grid density was set to 55 circumferential points, 55 spanwise points (three in the pinched tip) and 432 streamwise points (100 upstream of the rotor, 101 in the rotor blade passage, 100 between rotor and OGV, 101 in the OGV blade passage and 30 downstream). Table 5-1 lists key control parameters that were used and figure 5-1 illustrates the grid with the location of the bleed marked.

5.2.2. Mechanical design and analysis

With rotor blade deformation due to centrifugal and pressure forces effecting the fan capacity and pressure rise, a means of estimating blade twist at running conditions was required. Figure 5-2 illustrates how deformation was included in the rotor blade design process: The finite element analysis suite Abaqus was used to calculate non-linear steady distortion of the rotor modelled as a solid titanium alloy (Ti6Al4V) and meshed using Patran. Both centrifugal and pressure forces (based on 40,000ft (12,192m), ISA+10, M_∞=0.8 inlet conditions) were included with the centrifugal force dominating the result. The Matlab CFD mesh was imported into Patran and used to create a solid object that could be meshed using 10-point tetrahedral elements for finite element analysis. An inertial force was applied and the pressure on the blade surfaces was translated onto the new mesh. Finally the model was constrained by fixing the blade root surface[*]. The resulting deformation to the tetrahedral grid was then translated back to the cfd grid and, for each design stream surface, the deformation simplified into a bulk rotation of the blade about a calculated point. This was performed for a range of rotational speeds to give twist for each section as a function of blade speed. Changes in blade deformation at different back pressures for the same rotational speed were not considered and nor were changes in twist for different flight conditions; everything was calculated at the top of climb.

In addition to steady deformation and stress analysis, preliminary dynamic analysis of the final fan design was performed. Again, Abaqus was used as the finite element solver to find the natural frequencies of the rotor at different rotational speeds.

5.3. Results

Figure 5-3 shows a cutaway of the final fan stage design and figure 5-4 the seven (approximate) streamlines used for both rotor and OGV design along with the location of the rotor and OGV. For the OGV, the stacking was modified slightly to improve aerodynamic performance after it had been used to estimate rotor-stator broadband noise (§6.1). The original stacking is therefore also shown in figure 5-4 for comparison. In the following subsections the design of the rotor, duct and outlet guide vanes are discussed and performance estimates presented.

[*] Earlier analysis included modelling of part of the bullet down to the axis of rotation so that more accurate boundary conditions could be applied. The error from just fixing the blade root was found to be minimal and automating the meshing and analysis process was much simpler with this approach.

5.3.1. Rotor

With an overall stage pressure rise of approximately 1.50 required, the fan rotor design pressure rise was set to 1.52. The tip gap was set to 0.25% of the span and the leading edge hub to tip radius ratio was set to 0.29, both similar to recent designs. Finally, blade count was set to 20, giving an adequate solidity and matching the Rolls Royce Trent 1000 fan. Limited time restricted any studies in the variation of these parameters. Leading edge, trailing edge and max thickness parameters were set to give similar values to that on a Trent variant fan as one of these blades was available for measuring. This was done as the mechanical analysis capabilities were limited to those discussed in §5.2.2 with blade off, bird strike and other important analysis being outside the scope of this work. Table 5-2 list the key input design values including thickness distribution and metal angles, Figure 5-5 sketches the variation in blade section from hub to tip, figure 5-6 plots the variation in chord, camber and solidity along the span and figure 5-7 plots the local camber along the chord for each design streamline.

For conventional fan designs the fan will twist as it accelerates from cold static conditions to "hot" full speed conditions. This leads to the blade tip metal angle (measured from the axial direction) being greater at part speed than at high speed. With a fixed nozzle area this can be beneficial as the take-off blade metal angle (at reduced fan speed) is greater than the ToC metal angle (at close to 100% speed). This moves the stall line to a higher pressure rise and lower mass flow rate for off-design blade speeds. Here we want to achieve the opposite – higher mass flow rate and lower pressure rise at part speed. Therefore, reducing or reversing the normal blade twist would be beneficial. This can be achieved through forward sweep (Wadia *et al.* 1998) and this concept was utilized in this design. Figure 5-8 presents the estimated blade stress and deflection under top of climb conditions. Whilst there is up to 6.5mm deflection of the blade at the tip, this is the same at both the leading and trailing edges, leading to no overall change in blade metal angle. This can be compared to an earlier design before forward sweep was introduced in which the blade twisted two degrees between cold and top of climb conditions (Crichton *et al.* 2007b). The rotor Campbell diagram, along with sketches of the various harmonic modes, is presented in figure 5-9 for reference. This, like the estimation of blade stress, is based on the blade being solid and fixed at the hub. A real blade would be hollow and therefore exhibit different harmonic modes, but designing and analysing such a blade was beyond the scope of this work.

The resulting fan rotor map is shown in figure 5-10, which plots pressure rise and polytropic efficiency versus capacity. The fan face area used in calculating the capacity is that at the fan leading edge, whilst pressure rise and efficiency calculations are mass averaged values calculated

across the entire domain. Choking capacity at 100% corrected speed is 1.149, equating to a fan face Mach number of 0.674, whilst the peak rotor only polytropic efficiency of 95.3% occurs at 90% corrected speed. This efficiency value is in line with trends and occurs at the correct speed for low cruise fuel burn. Figure 5-11 plots the radial variation in pressure rise, fan face Mach number and efficiency at 90% corrected speed, going from fully choked to near stall. Ideally, all radial locations would be at peak efficiency at the same time and this is almost the case in this design. As stall is approached efficiency drops at all radial locations with pressure rise increasing in the tip region. As choke is approached, efficiency again drops at all radial locations but much more rapidly in the tip region than in the hub region. This is linked to the rapid drop in tip pressure rise.

Figure 5-12 shows radial variation in fan rotor pressure rise, fan face Mach number and polytropic efficiency at four key operating locations; top of climb, cruise, sideline and flyover. The top of climb position, specified to enable 300ft/min (1.52m/s) climb rate at 40,000ft (12,192m) ISA+10K, is at 100% corrected speed providing a mass averaged pressure rise of 1.52. Pressure rise is evenly distributed across the span but the fan face Mach number is slightly higher nearer the hub than the tip. Efficiency peaks near the hub and drops off towards the tip due to shock losses. The cruise point shown here is at 90% speed close to the peak efficiency location. Pressure rise is again approximately constant across the span with tip efficiency improved due to reduced shock loss. At the take-off locations of sideline (max climb) and flyover (reduced thrust as airport boundary is crossed) the nozzle area is increased to minimize jet noise. This has the effect of reducing pressure rise at the tip in particular, which also reduces efficiency. The sideline position is at 90% corrected speed whilst the flyover position is at 70%. The reduced speed at flyover gives very low pressure rise across the span.

Pressure distributions on the blade profiles from 10% to 90% span are shown in figure 5-13 for these four key operating conditions. With a complicated shock structure at the three higher speed conditions, figure 5-14 to figure 5-16 presents 3D representations of the shock structure for top of climb, cruise and sideline respectively (no shocks exist on the blades at flyover). The shock structure shown in each blade passage is identical and just seen from a different angle to assist understanding of the three dimensional nature. Forward sweeping the blade pushes the primary shock structure back into the passage and, at the top of climb condition, a strong ingested shock exists above 60% span. Below 60% span the shock becomes detached and exists all the way down the span although weakening towards the hub. At cruise, an ingested shock exists in the top 20% of span with the primary shock detached at lower radii. The shock structure at the tip being just ingested is typical of the shock structure at peak efficiency (Wood *et al.* 1986). The cruise pressure

distribution is complicated with reflections leading to several weak shocks on the suction surface. Towards the hub the suction surface shock is stronger than would be ideal and future design iterations could focus on decelerating the flow without the presence of a shock. At sideline, with back pressure reduced further, the passage shock is strengthened and exists down to almost 50% span. No strong detached shocks propagate upstream, as required for low buzz-saw noise. Finally, at flyover the flow remains subsonic at all locations on both the suction and pressure surfaces with smooth acceleration and deceleration on the suction surface.

5.3.2. Duct

Opening the nozzle to deliver a high mass flow rate at a low pressure rise increases the range of incidence the OGVs must support. Maximum incidence is encountered at top of climb where the high pressure rise across the rotor leads to high downstream swirl, whilst the minimum incidence (or maximum negative incidence) is seen at take-off.

Outside of the boundary layers angular momentum is conserved along streamlines leading to the swirl velocity being inversely proportional to the streamline radius (Bailey and Carrotte 1996). Therefore, increasing the duct radius will reduce the exit swirl angle for given inlet conditions. For constant meridional velocity the inlet and exit swirl angles, δ, are related by the following equation:

$$\tan \delta_{out} = \frac{r_{in}}{r_{out}} \tan \delta_{in} \tag{5.1}$$

Considering top of climb (ToC) and take-off (T/O), the two extremes of swirl angle that need to be supported, leads to an equation for the incidence range at duct exit;

$$\Delta\delta_{out} = \tan^{-1}\left[\frac{\tan \delta_{ToC,in} - \tan \delta_{T/O,in}}{r_{ratio} + \tan \delta_{ToC,in} \tan \delta_{T/O,in}} \right], \quad r_{ratio} = \frac{r_{out}}{r_{in}} \tag{5.2}$$

For r_{ratio} equal to one then the exit incidence range matches the inlet incidence range, but for r_{ratio} greater than one the exit incidence range is reduced. For example, for inlet swirl at top of climb of 30° and at take-off of 10° a radius ratio of 1.1 will reduce the exit incidence range by over 1.5°.

This was utilised in the design of the duct with the casing radius increased by 8.3% between rotor trailing edge and OGV leading edge. Figure 5-17 shows sketches of the original and final duct designs, with streamlines at key conditions also marked. The change in swirl angle along the duct is shown in figure 5-18, where it can be seen that the increasing duct radius leads to reducing swirl at both top of climb and take-off conditions. This is especially so nearer the hub where the relative

change in radius is much greater. The final result (figure 5-19) is, from 30% span and up, a reduction in the incidence range that the OGV sees through the increase in duct radius. The change is minimal near the hub because even though the relative radius change is greatest, the difference in inlet swirl between the two extreme conditions is already small. Also shown in figure 5-19 is the absolute Mach number at duct exit for the two designs when operating at the cruise condition. Above mid-span the absolute Mach number is the same whilst closer to the hub the absolute Mach number has been reduced. This reduction in Mach number is from two effects: Firstly, the reduced swirl leads to reduced absolute Mach number for the same mass flow. Secondly, the mass flow rate at the hub has been reduced slightly. This is due to the streamtube curvature close to the rotor trailing edge increasing the hub back pressure. In addition to making OGV design easier, the lower Mach number should lead to reduced rotor-stator interaction broadband noise (equation 4.8).

In this and following calculations that include a bleed for the core flow, the bleed mass flow was set based on results from GasTurb for a range of thrust requirements. At 100% speed (based on top of climb inlet conditions), the mass flow was set to 12.41 kg/s giving a bypass ratio of about 14 at top of climb with a linear reduction in mass flow of 1.97kg/s for every 10% reduction in fan speed.

5.3.3. OGV

Table 5-3 lists the input design parameters for the five blade sections out of the boundary layers that were optimised using the approach described in §5.2.1, with the optimised blade sections, along with those at the hub and the casing, sketched in figure 5-5. The different operating requirements for each section (high Mach numbers at the hub, large incidence range at the tip) lead to the large variations in blade profile. The Mach number distributions on the blades are shown in figure 5-20. For the 30% to 90% area sections at cruise, the blade section Mach number profile has a smooth acceleration on the suction surface followed by a period at constant velocity before a gradual deceleration towards the trailing edge. Even for the 30% area section where the upstream Mach number is 0.76 the blade profile keeps the Mach number subsonic at all times. At the top of climb condition the incidence and therefore blade leading edge loading are increased, leading to the classical ski-jump pressure distribution. At take-off the blade sections are operating at negative incidence leading to rapid acceleration of the flow around the leading edge. The 10% area section, designed for a significantly higher upstream Mach number, is less successful than the other sections with strong shocks predicted on the suction surface at both cruise and top of climb and on the pressure surface at take-off.

Estimated loss versus inlet flow angle for the five blade sections are shown in figure 5-21 which also has the three design points marked. The program Polar, from the Mises package, was used in creating these plots and no modifications were applied to any of the smoothing or dissipation parameters. The limits of the lines are therefore where Mises encountered convergence problems, when either increasing or decreasing the inlet flow angle away from the design value. The gradient of the static pressure rise against inlet flow angle has also been looked at, as this dropping to zero indicates stall onset and all design points lie below stall incidence. The 10% area blade section is estimated to only just be able to meet the design incidence range with Mises failing to converge at lower flow angles than the take-off position, possibly indicating leading edge separation. At higher incidence the top of climb point is close to where the gradient of static pressure rise against flow angle drops to zero. The estimated performance of the 30% blade section is much improved with an achievable incidence range of 14°, 3° more than required. At 50% area, the positive incidence range is good, but again Mises failed to converge at flow angles less than the take-off condition. Finally, both the 70% and 90% area blade sections are predicted to have good performance and support operating ranges greater than required.

Initially the OGV sections were stacked as shown by the light grey line in figure 5-4 with the leading edge swept at a fixed angle and the duct designed in §5.3.2 unchanged. This was used in the creation of the noise estimates in chapter six with the fan stage map used in that chapter created as discussed in §6.4. This early design suffered from poor performance in the tip region, especially at top of climb where a large separation was predicted. Re-stacking and re-scaling the blade sections, along with a small modification to the casing line, significantly reduced this separation and a further benefit was achieved by leaning the blade tangentially to the suction surface by 30% of axial chord at the tip (see figure 5-3). This tangential (i.e. circumferential) lean, opposite from convention, unloaded the leading edge, helping to support the large incidence range required.

5.3.4. Stage

A fan map for the final design is shown in figure 5-22 showing both rotor alone and whole stage performance. In this figure, bypass flow pressure rise and polytropic efficiency are plotted against fan leading edge capacity (core and bypass flow). Also shown in figure 5-22 are the stage performance values used in chapter six, based on earlier results.

The stage pressure rise at 100% speed meets the initial target of 1.50 although this pressure rise at choking is slightly less than this. For this point, stage polytropic efficiency is estimated at 90.9%, duct pressure recovery at 0.996 and OGV pressure recovery at 0.991. With a small separation still

present at the tip, mass averaged downstream swirl is 1.2°. Peak stage efficiency estimated at 92.5% occurs at 90% speed as required with an exit mass averaged swirl angle of 0.6°. For this location, pressure recovery in the duct is estimated at 0.997 and pressure recovery across the OGV at 0.993. At sideline, the efficiency drops to 86.8% although downstream swirl is predicted to remain the same as at cruise. The drop in efficiency is primarily due to the loss in OGV pressure recovery which drops to 0.986. Finally, at flyover the stage efficiency is estimated at 90.2% with duct pressure recovery of 0.998 and OGV pressure recovery of 0.994. Mass averaged exit swirl is only 0.2°.

For the four locations discussed above, rotor and OGV isentropic Mach number contours are plotted in figure 5-23 and figure 5-24 along with surface streamlines. For the OGVs, with upstream stagnation conditions a function of radius, the isentropic Mach number contours are only estimates based on conditions just ahead of the leading edge on the same meridional gridline.

5.4. Discussion

Referring back to §5.1, the required fan rotor trait unique to this design was the ability to operate at high mass flow rate at part speed. This was thought to be limited by fan choking at higher part speed and OGV incidence at lower part speed.

5.4.1. High fan capacity at part speed

To judge the success or failure of the fan design in relation to part speed capacity let us first compare results with modern single-stage high bypass ratio fan designs[*]. Figure 5-25 compares the bypass map for the fan designed here with three available (Freeman and Cumpsty 1992, Xu 2004, Kaplan *et al.* 2006). By normalising mass flow rate to the 100% speed choking mass flow rate clear differences can be seen as fan speed is reduced. The fan designed here, and possibly that by Kaplan (although not enough data is available), have significantly higher relative capacity at part speed than the fans presented by Freemen and Cumpsty or Xu. Whilst the use of forward sweep to minimise twist is partly responsible for this, its impact is relatively small. The main reason is that the design tip Mach number is much lower for the fan designed here and the benefit of this can be explained by the use of a 1D model.

[*] Unfortunately, very limited data has been published, especially off design, making this comparison difficult.

For the fan designed here, the upper 64% of the span has a relative inlet Mach number greater than unity at the design point, accounting for approximately 78% of the mass flow rate and therefore the transonic region is the most critical.

Transonic blade profiles have a relatively sharp leading edges and little turning with a large portion of the pressure rise achieved through the shock structure between and in front of the blades. At the inlet to the rotor, three basic flow regimes are witnessed; subsonic inlet flow when at part-speed, supersonic inlet flow with a detached shock and supersonic inlet flow with a weak attached shock, prandtl-meyer expansion and a stronger passage shock. The third of these regimes is known as unique incidence.

Figure 5-26 shows the flow through the rotor for the first and second of these conditions (for the subsonic case the shock is not present). By conserving mass, relative specific enthalpy and considering momentum, Freeman and Cumpsty (1992) developed the following equation for the flow from rotor inlet to the position of max blade thickness assuming no camber on the suction surface between these positions. Whilst the approximation of no camber can only really be applied at the tip here, choking models for subsonic blade designs give similar trends in off-design performance.

$$\left(1+\tfrac{\gamma-1}{2}M_{12.rel}^2\right)^{-½}\frac{1+\gamma M_{12.rel}^2\left(1-t/g\right)}{M_{12.rel}\left(1-t/g\right)}=\frac{\left(\cos\chi_1/\cos\beta_1\right)+\gamma M_{1.rel}^2\cos\left(\beta_1-\chi_1\right)}{M_{1,rel}}\left(1+\tfrac{\gamma-1}{2}M_{1.rel}^2\right)^{-½} \tag{5.3}$$

This equation holds for both subsonic and supersonic inlet flow. As β_1 is reduced from a high angle of attack to X_1 and then to below X_1, $M_{12,rel}$ increases until choking occurs. Therefore, in these regimes there is a minimum incidence angle for given blade parameters and relative inlet Mach number.

The third flow regime that can exist when there is supersonic relative inlet flow has the main shock ingested into the blade passage with a weak bow shock attached to the leading edge as shown in figure 5-27. This condition is well described in several books, including Cumpsty (1989). In summary, as the leading edge shock is attached, the leading edge sufficiently sharp and the inlet Mach number not too high, the entropy rise in the bow shock is negligible and can be treated as an expansion wave of opposite sign. The flow from entry to the expansion wave a-b that just intersects the leading edge of the next blade can be linked through the Prandtl-Meyer relation;

$$\nu\left(M_{1,rel}\right)+\beta_1=\nu\left(M_e\right)+\beta_e \tag{5.4}$$

where ν is a function of Mach number only, calculated from the Prandtl-Meyer function and β_e is the flow angle at position 'a' which can be taken as X_1 if there is minimal camber in the suction surface up to this point. Conserving mass between inlet and the line a-b leads to a second equation;

$$F\left(M_{1,rel}\right)s\cos\beta_1 = F\left(M_e\right)\left(s\cos\beta_e - \left(t_e + \delta_e^*\right)\right) \tag{5.5}$$

where F is the capacity, t_e is the blade thickness at 'a' and δ_e^* is the displacement thickness at 'a'. β_e can again be approximated to X_1. The above two equations uniquely determine β_1 for given $M_{1,rel}$ and blade geometry resulting in the flow condition being specified as 'unique incidence'.

Using these equations, the minimum incidence can be found before mass flow rate is limited either through choking or unique incidence. Figure 5-28 presents this for a zero thickness blade of varying metal angles and figure 5-29 the same, but for a non-zero thickness blade. Discussing the results from a zero thickness blade first, the left hand subplot shows the changeover between choking limiting mass flow and unique incidence limiting mass flow occurs at a relative Mach number of unity. Above unity Mach number the minimum incidence is fixed, below the minimum incidence achievable reduces as Mach number reduces. The gradient of this line determines how quickly the limiting mass flow rate reduces with blade speed – the steeper the line the slower the reduction in mass flow rate. This leads to the maximum mass flow rate of higher blade speed designs reducing quicker than lower speed designs as blade speed is reduced.

This can be seen clearly in the right hand subplot. Fan design capacity has remained approximately constant over recent years and therefore in this subplot, non-dimensional mass flow rate at the mass flow limiting conditions has been normalised to a value of Q=1.14, approximately equal to a fan face Mach number of 0.665. Non-dimensional blade speed at which the mass flow rate limit is reached is then plotted for the different metal angles relative to the blade speed at the design capacity. As metal angle increases, corresponding to an increasing design point blade speed, the mass flow rate at part speed decreases. For example, at 65% speed the mass flow rate is limited to 87% of design point mass flow rate for X_1=45° reducing to 69% of design point mass flow rate for X_1=66°.

When the blade thickness is made non-zero, the picture becomes more complicated but similar trends exist. For a given thickness of blade, the rate of reduction in choking angle versus inlet relative Mach number is greater the lower the inlet metal angle. The main difference compared to zero thickness blades is in the unique incidence condition with the choking angle now a function

of blade metal angle and inlet relative Mach number. The thicker the leading edge, the higher the choking incidence angle and the more rapidly it increases with inlet relative Mach number. Achieving the design capacity becomes harder as leading edge thickness is increased but, if it can be achieved, the higher the part speed capacity will be. Overall, the best way to maximise relative part speed capacity is to maximise the value of $di_{choke}/dM_{1,rel}$ where i is the incidence angle. This is achieved (see left hand subplot) by maximising $(t_e+\delta_e^*)/s$ and minimising t/g within the limits of the incidence range the blade can support. This will remove the dip seen in figure 5-29 where the mass limiting condition transitions from unique incidence to choking. To demonstrate, figure 5-30 plots the maximum mass flow at part speed and 80% span for a fan with the same basic parameters as the one designed here (Q_{ff}=1.14, 371m/s corrected tip speed, hub to tip radius ratio of 0.29). As blade speed is reduced from the design point, mass flow rate drops slowest for the designs which are constrained by unique incidence due to higher values of $(t_e+\delta_e^*)/s$. Delaying the mass limiting transition to choking as long as possible gives the best performance and this is done by minimising the value of t/g.

Also plotted in Figure 5-30 is the maximum capacity of the fan designed here at 80% span. Estimates for the blade thickness are $(t_e+\delta_e^*)/s$=0.04 and g/t=0.08, which is desirable based on the above analysis. (Although it should be noted that from the simple 1D analysis such a high value of $(t_e+\delta_e^*)/s$ should not be capable of delivering the required mass flow rate.) The part speed capacity is near the maximum indicated from the 1D calculation and, by analysing the blade to blade flow for the fan, the mass limiting condition can be seen to switch from unique incidence to choking at approximately 85% speed when the upstream Mach number is approximately one.

Finally, at subsonic conditions as the relative tip Mach number reduces, the incidence onto the blade at choking becomes negative and leading edge separation may occur before choking limits operation. This cannot be avoided at very low blade speeds but to avoid it at higher speeds the blade profiles should support operating at negative incidence if possible. This is especially the case closer to the hub where the design relative Mach number is less. Designing for negative incidence onto the fan was not looked at in detail here but could be an area of future research.

5.4.2. OGV Incidence Range

From Figure 5-10, it can be seen that the choking capacity of the fan is approximately equal to 1.0 at 70% speed, 1.05 at 80% speed, 1.1 at 90% speed and 1.15 at 100% speed. In figure 5-22, converged solutions at these capacities are shown at 90% and 100% speed with a significant difference between choking and achieved capacity seen only at 70% speed. This indicates that

OGV incidence range starts to become the factor limiting nozzle opening below 80% speed whereas choking is the limiting factor at 80% speed and above.

As discussed in §4.2, reducing the loading will reduce the swirl angle and velocities onto the OGVs making their design easier by placing less restriction on nozzle opening. This may well reduce rotor-stator broadband noise but would increase other noise sources and, as discussed above, reduce rotor part speed capacity.

If a suitable balance between these competing requirements cannot be achieved with a fixed geometry OGV then the use of variable geometry could be considered. This may preclude the use of lean but would enable a large flow angle range to be supported. Further, if some downstream swirl could be tolerated at take-off, the entire OGV could be rotated rather than just a leading edge section. This would be simpler mechanically and would not constrain the blade geometry as much as a variable leading edge would.

5.5. Chapter conclusions

Even though the fan stage performance estimations from Multall represent the start rather than the end of a fan design process, initial indications are encouraging. Design pressure rise was met, capacity is estimated to be in line with trends, and a high peak stage efficiency of 92.5% was estimated at the cruise condition.

For the fan, maximum part speed capacity relative to design speed capacity can be achieved by, firstly, minimising blade speed. This reduces the inlet metal angle for a given capacity and leads to the mass flow limiting condition occurring at a lower incidence angle relative to the design point mass flow limiting angle. Secondly, the fan should be mass limited by the unique incidence condition rather than choking whenever the relative Mach number is greater than unity. A simple 1D model indicates that this can be achieved by moving blade mass forwards as much as possible and ensures that there is no region in which mass limiting incidence increases as blade speed reduces. Finally, forward sweep was introduced to stiffen the blade and reduce untwist. This kept part speed metal angles as close as possible to design speed metal angles and maximised part speed capacity.

For the OGV, Mises was used to optimise blade sections that could support the required incidence range. Once 3D tools had been used to introduce sweep and lean, the overall performance of the OGVs was good, with a mass averaged stagnation pressure recovery of 99.3%

at cruise. The design of the tip section was the most challenging due to the large boundary layer present and this required some modification to the casing geometry.

Reducing fan speed increases inlet swirl and Mach number onto the OGV and makes designing the OGV to support the required operating range more challenging. Therefore, a balance needs to be achieved when selecting blade speed between part speed fan capacity, OGV operating range, cruise stage efficiency and noise. Increasing duct radius between the rotor trailing edge and OGV leading edge can help but, at least for the design requirements here, a trade-off is still required.

As stated in the introduction to this chapter, the primary aim was not to design the best possible fan. Instead, within time constraints, it was to see if a fan and OGV could be designed that delivered the top of climb thrust, cruise performance and take-off capacity. Future iterations of the design should focus on improving the tip performance of the OGV and increasing the supported incidence range of the hub sections of the fan. Performance at approach and idle power settings should also be investigated along with the mechanical design and in particular, flutter tolerance. In addition, the engine section stator (ESS), not included in the work here, needs to be designed.

6. Minimising take-off noise

With a fan stage that can operate with the required nozzle area variation designed, we can now return to the optimisation of the take-off profile. Initial noise estimates indicated that fan noise (particularly rearward propagating broadband noise) and airfoil noise from the airframe contribute to the overall noise level during take-off. Therefore, in this chapter, fan and airfoil noise sources are included when modifying the take-off profile, with estimations of liner attenuation and airframe shielding included. Then, for the key locations of sideline and flyover, higher fidelity estimations with further noise sources (core, compressor and turbine) are made to judge the success or failure of the optimisation. Overall, the aim of this chapter is to answer the question: 'What is the minimum take-off noise achievable for the SAI concept aircraft?'

First, we need to fully define the SAI concept aircraft used in this chapter. Two final concept aircraft were created as part of the overall project, both designed for 250 passengers and a 5000nm mission;

- a low-noise, high-risk design illustrated in figure 6-1, with an all-lifting body airframe whose suction surface boundary layer was ingested into nine fans driven by three core engines,

- a reduced-risk design illustrated in figure 6-2, still utilising an all-lifting body but with three podded engines ingesting clean airflow.

Results from the reduced-risk design will be the focus of this chapter for two reasons: Firstly, the higher-risk design requires a range of corrections associated with the ingestion of airframe boundary layer that reduce the fidelity of the approximations. Secondly, the fan presented in chapter five has not been specifically designed to tolerate the large levels of inlet distortion present at cruise in the higher-risk design. This inlet distortion presents significant challenges to the design of the fan.

The work presented in this chapter was completed before the 3D viscous analysis of the fan OGVs could be completed. Therefore, the operating range and pressure losses through the OGV used in the creation of the fan stage map are based on mass averaged results from the Mises calculations discussed in §5.3.3. The resulting map is very similar to the final fan stage map especially in relation to pressure rise and capacity. The final efficiency calculations are slightly better than those used here, but this will only weakly affect the results.

6.1. Fan Source Noise Estimation

As with jet noise estimation, in order to predict fan noise when optimising the take-off profile, a fast semi-empirical model is required. Three such models were available, all based on the work of Heidmann (1979) and documented in the ESDU fan source noise model (ESDU 1998).

With the rotor and OGV blade count set to cut-off the 1st blade passing frequency and significant shielding of forward noise, early indications were that rearward propagating broadband noise would be the dominant fan noise source. Therefore an attempt was made to estimate fan rearward broadband noise in more detail. This was accomplished with the assistance of Ed Envia of the NASA Glenn Research Centre. Details of the Envia code, as it will be referred to in this thesis, can be found in the paper by Nallasamy and Envia (2005). It predicts both forward and rearward propagating broadband noise from the interaction of rotor wake turbulence onto the OGVs. Experiments have suggested that this is the dominant fan rearward broadband noise source (Ganz *et al.* 1998) although rotor alone noise is of similar magnitude. Turbulent intensity and length scale along with mean flow data, all from CFD rotor calculations, are used to estimate narrow band spectrum data. The OGVs are modelled as twisted flat plates and noise calculated using a 2D strip-wise aerodynamic model with a 3D duct acoustic model:

$$\left\langle \left| p_{mn}(f) \right|^2 \right\rangle = \int_{r_{hub}}^{r_{tip}} \left| C_{mn}(r,f) \right|^2 \psi_m^2(\kappa_{mn} r) \Phi(r,f)\, dr \tag{6.1}$$

In equation 6.1, C_{mn} is integral along the chord at the radius in question of the stator unsteady pressure, ψ_m is the annular duct shape and Φ is the spectral density function of the incident, locally isotropic, turbulence.

With Multall using a mixing length turbulence model, the Rolls Royce code Hydra was used to provide CFD data that included turbulence intensity and length scale data. The k-epsilon turbulence model was used with 0.5% inlet turbulent intensity and inlet turbulent viscosity of ten times laminar. Reference inlet conditions for calculating k and ε were Mach 0.8, 40,000ft (12,192m) ISA+10K and an inlet Mach number of 0.675 was used when calculating the reference velocity into the domain.

$$k = \tfrac{3}{2}\left(v_{ref} I\right)^2 \qquad \varepsilon = 0.09 \rho k^2 \mu_t^{-1}$$

A rotor alone grid that extended to the OGV leading edge was used in this calculation with Padram (Shahpar and Lapworth 2003) used in the creation of the mesh. A high-resolution grid

from Multall was used as the starting point in the creation of the blade definition file with the pinched tip removed and replaced by a tip gap and a circular trailing edge created. The grid itself is consists of H meshes upstream, downstream and between the rotor, an O-mesh around the blade and a further H mesh in the tip gap. The final grid density was 4.5 million cells and details of the grid are presented in figure 6-4. Increasing grid density further was impractical due to the available computing resources, although a test did show that increasing grid density led to small changes in the turbulence data at the domain exit but there was no affect on the non-turbulence parameters.

Figure 6-5 compares the mass averaged estimations of fan and duct performance between Multall and Hydra. Only speeds between 70% and 90% are included as this is the regime of interest during take-off. The most noticeable difference in the results is in the pressure rise at the higher speeds with Hydra predicting reduced pressure rise and capacity across the entire span. This was attributed to two things: First, the y+ values on the blade in the Hydra results had to be greater than 20 as wall functions were being used. This caused a small amount of fish-tailing and is a known problem with the version of code that was used. To see the impact of this, a modified grid with y+ values closer to 3 was created and point eight re-run with the Spalart Allmaras rather than the k-epsilon turbulence model. The result of this is shown as point X on the figure and a small difference can be seen. Fish tailing did not account for most of the discrepancy though and closer analysis showed that, whilst the downstream conditions were closely matched to the Multall result, upstream conditions were not and this is the second reason for the discrepancy. This was because when the hydra grid was created the inlet duct length was shortened to try and reduce computation time. When this was done a design point Multall result was used to calculate the inlet conditions at the new boundary. In particular, there was predicted to be some swirl and a small rise in stagnation conditions. When calculating the pressure and temperature rise across the rotor, this increase was not taken as being part of the rotor pressure rise giving reduced performance. To look at the impact this error had, the code was re-run but with no inlet swirl and fixed values of inlet stagnation temperature and pressure. The result is shown as point Y on the figures indicating that this was the reason for most of the discrepancy. Unfortunately, this error was not realised until after the results had been sent off to NASA for noise prediction. Figure 6-6 shows the radial variation in rotor only pressure rise and efficiency between the Multall and Hydra results at 90% speed.

Figure 6-7 plots the in-duct spectral power density estimations from Envia for each of the nine Hydra operating points shown in figure 6-5. Overlaid on the raw data, created at a frequency resolution of BPF/10, is a 5^{th} order polynomial fitted in the least squares sense. This curve should be considered the prediction as it removes certain unnatural resonances that occur due to 2D

cascade model (Nallasamy and Envia 2005). As expected, as blade speed increases the predicted peak noise increases and, comparing plots 3 and 8, which are at peak efficiency, gives a 5^{th} to 6^{th} power relationship in the peak noise level. The variation with fan back pressure is perhaps more surprising. At both 70% and 90% blade speeds a clear reduction in the estimated noise is seen as back pressure is increased – the opposite of what would be expected from equation 4.7 used by the Heidmann based fan noise methods. This can be explained by equation 4.8 from Topol *et al.* (2004). In this equation rotor-stator broadband sound power is proportional to the mean flow velocity onto the OGVs cubed and the turbulent velocity onto the OGVs squared. As back pressure is reduced the Hydra results show a reduction in the turbulent velocity at the exit of the domain but, with an increase in the mass flow rate, also an increase in the mean velocity onto the OGVs. Using equation 4.7 with results area averaged across the radius gives the estimated reduction in noise between point 1 and point 3 of 2.2 dB, between point 4 and point 6 of 2.9 dB and between point 7 and point 9 of 2.6 dB, similar to the reductions seen in the figure.

Also shown in Figure 6-7 are predictions for the overall fan rearward broadband noise based on the Heidmann method. Free stream impedance was used when integrating the SPL predictions to give in-duct acoustic power and corrections were made to account for the bandwidth of the $1/3^{rd}$ octave predictions. Overall, the peak noise estimates compare surprisingly well, especially at the lower back pressures and the trends with blade speed are similar. The trend with back pressure is reversed through with increasing back pressure indicating small increases in noise. It is thought that the likely reason for this is that the Heidmann based methods include all broadband noise sources and not just rotor-stator interaction noise. Rotor alone noise, from the interaction of the turbulent boundary layer with the trailing edge, was found to be only just less than rotor-stator interaction noise in the Boeing 18" rig test (Ganz *et al.* 1998) and this increases as stall is approached. With a mean incidence increase of 2.1° between points 1 and 3 when going up the 70% speed line, a 2.4dB increase per degree (Glegg and Jochault 1998) would suggest a 5dB noise increase in fan alone broadband noise, more than the reduction in rotor-stator interaction noise.

Rotor-stator interaction noise has been seen to dominate at higher frequencies, with rotor alone and possibly other sources, such as rotor boundary layer interaction, being more significant at the lower frequencies (Ganz *et al.* 1998). This may explain the Heidmann predictions containing more low frequency noise than the Envia prediction. At higher frequencies, though, Nallasamay and Envia found good agreement between their code and overall fan broadband exhaust results, especially when significant reductions in sound power per Hz start to occur. With this in mind, of the three Heidmann based models available for use in the optimisation code, the Small Engine variant was deemed the most appropriate. This variant has the same peak values and gives exactly

the same predictions as the ESDU variant at low frequencies. At higher frequencies the drop off in noise is more rapid and closely matches the Envia results. Modifying this method to match the Envia low frequency drop-off, or to match the trend in noise and back pressure, was rejected. This is because the Envia code only includes rotor-stator interaction whilst a method that includes all fan broadband noise sources is required.

6.2. Liners, shielding and propagation

Liners in the inlet and exhaust duct were used to attenuate the noise and the design of these liners along with calculations of their effectiveness can be found in (Law and Dowling 2007). Calculation of far-field noise when properly accounting for liner attenuation is computationally intensive and could not be integrated into the take-off optimisation code. Instead, blanket corrections were applied to the source SPL values based on higher fidelity results at a few key points. For these higher fidelity predictions, and when estimating the applicable bulk correction, the rearward propagating engine noise is modelled by solving appropriate eigenvalue problems for uniform axial inviscid flow in annular and cylindrical lined ducts. From the resulting modal amplitudes at the nozzle termination, the radiated sound pressure level is estimated using the Wiener-Hopf solutions from an unflanged duct (Munt 1977, Gabard and Astley 2006). Similar methods are applied for forward propagating noise with details available from Law and Dowling (2007).

Refraction, fourth power amplification and Doppler frequency shift corrections were then applied to the fan source noise hemispheres to account for flight effects. To account for refraction and the different source directivity (airframe, inlet and exhaust axis are all different), the polar and azimuthal source angles calculated using equations 3.12 and 3.13 are modified: Firstly, the polar and azimuthal angles to the measuring locations relative to the direction of flight are calculated. These are then translated by the aircraft angle of attack to give angles relative to the aircraft. These source angles are used when estimating airframe noise at the specified locations. These angles are then translated again by the thrust vectoring angle to give angles relative to the jet. These angles are used when estimating jet noise at the specified locations.

When calculating fan noise radiated through the inlet, the polar angles relative to the flight path are first corrected for refraction (as done by Rolls Royce, based on the work of Amiet 1975) so that the source polar angle gives the required flight polar angle on the ground (equation 6.2). Then these new source polar angles and the original azimuthal angles are translated by the angle of

attack to get the fan inlet noise source angles. The same approach is used for nozzle propagating out of the exhaust but with a modified refraction equation (6.3).

$$\omega_{source} = \tan^{-1}\left[\frac{\sin(\omega_{reciever})}{\cos(\omega_{reciever}) - M_{\infty}}\right] \text{ for inlet radiated sources} \tag{6.2}$$

$$\omega_{source} = \cos^{-1}\left[\frac{\cos(\omega_{reciever})}{1 - M_{\infty}\cos(\omega_{reciever})}\right] \text{ for exhaust radiated sources} \tag{6.3}$$

Finally, for forward propagating fan noise, shielding corrections were applied. These corrections, a function of polar angle, azimuthal angle and frequency, were based on low frequency estimations by Agarwal and Dowling (2005), extended conservatively to higher frequencies.

6.3. Airframe Noise

Airframe noise emanates from the scattering of the boundary layer off of the airfoil trailing edge. This airfoil self-noise is the noise floor for a given configuration and is appropriate for analysis here because the aircraft uses a deployable drooped leading edge for lift augmentation, which has negligible direct noise emission (Andreou *et al.* 2006), and the undercarriage will be stowed shortly after rotation. The airframe noise was estimated using empirical relationships based on the average chord and the area of the entire airframe (Fink 1977, ESDU 2003).

6.4. Modifications to the take-off optimisation

The following modifications have been made to the take-off optimisation in this chapter as compared to chapter four:

Fan Map

In chapter four, fan stage efficiency was assumed and a rotor only fan map used in the determination of take-off and cruise operating lines. In this chapter, a fan stage map is used directly with efficiency varying as operation moves to different points of the map. As stated in the introduction to this chapter, the work performed here was completed prior to the three dimensional viscous analysis of the OGVs being completed. Therefore, the fan stage characteristic has been created through the combination of the three dimensional viscous results for the rotor and intermediate duct along with the two dimensional results for the OGVs. This was achieved by

estimating the loss at a range of radii for each point on the fan map based on the swirl and Mach number calculations at duct exit along with the loss buckets presented in Figure 5-21. For swirl outside of the calculated range, loss was capped to 10% of inlet dynamic head and the results were mass averaged to give overall OGV loss for each operating point on the fan map. This is presented in figure 6-8 alongside the results across only the rotor. It should be noted that the rotor only results are in the presence of the downstream duct and therefore differ from the rotor only map presented in figure 5-10 which had no downstream duct curvature.

With a fan stage map available, the take-off operating line can be directly linked to what the stage can deliver rather than limiting nozzle opening by specifying a static working line at low fan speed as was done in §4.4. The fan stage 85% polytropic efficiency contour goes through the notional 75% speed take-off operating point used to mark the point of minimum swirl seen by the OGVs in chapter five and therefore this contour has been used for specifying the take-off operating line here. Using the line of 85% stage efficiency is suitable up till 95% fan speed (see figure 6-8) after which the operating line must move towards the top of climb point. This, along with the cruise operating point, is illustrated in figure 6-11, which includes results from the following section.

Corrections for core mixing

In chapter four, the top of climb FPR was varied and therefore any corrections to account for core mixing had to support such changes (see table 4-1 and appendix D). In this chapter top of climb FPR is fixed and therefore more accurate corrections for core mixing can be applied. Using GasTurb (Kurzke 2004) to look at the change in the bypass flow for take-off and top of climb conditions lead to the following approximate relationships giving a correction for core mixing as a function of fan operation. $PR_{out,ToC}$, $PR_{out,zero}$, $\Delta T_{0,ToC}$ and $\Delta T_{0,zero}$ are specified in table 6-1.

$$PR_{out} = PR_{out,zero} + \left(PR_{out,ToC} - PR_{out,zero}\right)\frac{FPR}{FPR_{ToC}}\frac{Q_{ff,ToC}}{Q_{ff}} \tag{6.4}$$

$$\Delta T_0 = \Delta T_{0,zero} + \left(\Delta T_{0,ToC} - \Delta T_{0,zero}\right)\frac{FPR-1}{FPR_{ToC}-1} \tag{6.5}$$

6.5. Results

6.5.1. Concept Aircraft

The final podded engine concept aircraft design is an evolution of the split aileron version of the all-lifting body baseline aircraft used in chapter four. Key aircraft parameters are listed in table 6-1 with coefficients of lift, drag and moment during take-off shown in figure 6-3 (when the undercarriage is deployed, the coefficient of drag is increased by 0.0045).

The airframe design is very similar to that used for the higher-risk embedded design with details available from Hileman *et al.* (2007b). A carved leading edge is used to move lift forward on the centre body enabling the outer wings to have an ideal elliptical lift distribution. This is predicted to give a very high lift to drag ratio. The start of cruise altitude is set to 40,000ft (12,192m) giving a large wing and improving low-speed performance as discussed in §3.5.

The aircraft is powered by three podded engines located at the rear on the upper surface of the centre body which significantly shields the forward propagating noise. The fan has a speed reduction gearbox between it and the LPT and a leading edge radius set to 1.10m, slightly larger than the 1.0334m radius of the fan designed in chapter five. This was done to match the excess thrust of the higher-risk embedded engine design discussed earlier and so enable like for like comparisons. In this thesis the top of climb FPR has been reduced from the initial design intent of 1.50 to a value of 1.467 reducing this thrust margin slightly. This FPR value is closer to what was deemed ideal for the podded design in chapter four and was set without any scaling of the fan map; just by moving the top of climb point along the 100% speed line. Engine out yaw corrections is achieved through a split aileron on the outer wing.

The downstream duct length is a compromise between increasing losses and reducing noise. For the engine presented here, the duct length was set to ensure the core and bypass flows were fully mixed out by nozzle exit. For complete mixing to occur, the distance from mixer to exhaust should be 10 wavelengths of the lobe mixer. Although detailed mixer design was not performed, it was estimated that a twenty-lobed plugged mixer could be used giving a lobe wavelength of approximately 200mm and a required duct length between mixer exit and nozzle of at least 2m. The length of the annular bypass section was set to match the length of the mixer section purely to give an engine arrangement of reasonable size and a scale drawing is shown in figure 6-9. Liner calculations estimated that this design could reduce rearward propagating noise by approximately 12.5dB at the critical polar angles and for the frequency range of interest. Doubling the annular

duct length would provide a further ~5dB fan noise reduction but this would have weight and drag consequences.

6.5.2. Optimisation for just jet noise

Initially, the take-off was optimised just for jet noise with the results shown in figure 6-10, figure 6-11 and figure 6-12. With the aircraft similar to the split aileron version used in chapter four, figure 4-9 indicates that, for a ToC FPR of 1.467, the jet noise target of 57dBA should be met. This is the case with a jet noise value of 56.7dBA achievable when operating the fan shown in figure 6-11.

In figure 6-12, the x-axis refers to the distance of the aircraft from brakes-off rather than the distance of the noise receiving location. The noise for each source is the estimate after liners, shielding and atmospheric effects have been taken into account. Further, the noise plotted is the maximum estimated for the source in question when the aircraft is at the specified location. With different directivity for each source the total aircraft noise shown is not the sum of the noise sources in the plot rather it is the sum of the noise sources at the maximum overall noise location.

Whilst jet noise is well below the overall SAI noise target throughout the take-off, other noise sources are dominant especially at the flyover position, giving an overall maximum noise level of just over 70dBA. This is because, as the flyover position is approached, the distance from aircraft to ground outside of the airport boundary drops rapidly from the square root of aircraft height and the sideline distance to just the aircraft height. With jet noise proportional to the eighth power of velocity, cutting back climb angle and thrust keeps jet noise at the required level. Fan noise sources scale with lower powers of velocity and therefore, relative to jet noise, increase. For the forward propagating fan noise this relative increase in noise is offset by the airframe shielding being much more effective when the receiver location is directly below the aircraft rather than along a sideline. For the rearward propagating fan noise, there is no shielding and therefore significant noise increases on the ground are observed. Airframe noise, a function of aircraft velocity rather than engine operating condition, is not reduced by the cutback and so on-ground values increase rapidly. Shielding of forward propagating sources is much more effective than was initially envisaged leading to buzz-saw noise being significantly below overall noise even when cut on.

Figure 6-11 shows the operation of the fan during take-off both for low jet and low overall noise (see next section). When operating for low jet noise, the start of roll position is at 73% fan speed increasing to 87% fan speed at sideline with nozzle area reduced to stop the fan operating at poor

efficiency before cutting back to 71% at flyover. Figure 6-10 shows the variation in airframe and engine parameters in more detail from brakes off until 6km out, beyond the flyover location of 4048m. Take-off is approximately 2km after brakes off (subplot A) with climb angle rapidly increasing to 7.5° (subplot B). As height is gained lateral attenuation decreases and the climb angle has to reduce gradually to keep within the noise target. As the end of the airport boundary is approached the climb angle reduces rapidly to 3.0°, the minimum required to satisfy engine out safety conditions. Beyond the flyover point, with aircraft height continuing to increase, the climb angle can increase gradually.

With angle of attack increasing at the start of roll, aircraft L/D (subplot C) increases before reducing slightly as angle of attack increases beyond optimum. 50ft (15.2m) above ground the undercarriage is stowed and L/D increases to approximately 21.5. With flight speed during take-off constant beyond this point (subplot D), angle of attack remains approximately constant and L/D remains at this level for the remainder of the noise constrained portion of the take-off. The rotational velocity of 65m/s leads to a climb speed of 74m/s. Looking at engine performance, the nozzle area is initially 47% greater than the top of climb value (subplot E) with overall net thrust of around 280kN (subplot F). As roll is approached the net thrust remains approximately constant with nozzle increase reduced to 28% as the fan moves up the operating line. Once climb starts, the thrust reduces to maintain a constant flight speed at reducing climb angle and this is accompanied by a gradual increase in nozzle area. At flyover the rapid reduction in thrust requires an increase in nozzle area to a value 34% higher than ToC. Finally it should be noted that whilst this departure satisfies accelerate-stop, field length and engine out requirements (FAA, JAA), the main thrust cutback occurs just below the regulated cutback height of 800ft (243.8m) (ICAO, FAA 1993).

6.5.3. Optimisation for jet, fan and airfoil noise

To reduce the flyover noise level, the take-off profile was optimised for all of the included noise sources; jet, fan and airframe. The resulting aircraft and fan operation are overlaid onto the results for jet noise only optimisation in figure 6-10 and figure 6-11. With airframe noise insensitive to aircraft thrust and fan noise less sensitive than jet noise, the easiest way to reduce the overall flyover noise level is to increase the aircraft altitude at this point. This requires more rapid acceleration and earlier take-off as shown in figure 6-10 leading to increased start of roll and sideline noise. Roll velocity, V_R, is reduced from 65m/s to 57m/s which both enables earlier take-off and reduces airframe source noise. The downside of a reduced flight speed is an increase in the required angle of attack so as to maintain lift and a resulting reduction in the lift to drag ratio. The

aircraft takes off approximately 500m earlier and is 1200ft (366m) rather than 780ft (238m) above the ground when cutback occurs, above the minimum regulated cutback height. Initial climb angle is nine degrees, limited by the maximum aircraft pitch angle of 20 degrees, whilst the critical flyover climb angle is increased from 3.0° to 3.1°. This increase is required because the reduced L/D impacts the result of equation 3.2. With the aircraft accelerating quicker and climbing steeper the thrust provided by the engines is increased at all time steps. To maintain fan operation along the prescribed working line, this reduces the required increase in nozzle area. From figure 6-11 it can be seen that start of roll fan speed has been increased to 81% and sideline to almost 92%. With only a small thrust increase at flyover, this point is approximately unchanged at just over 71%.

Figure 6-12 shows the resulting peak noise outside the airport boundary as the aircraft goes from brakes-off to 6km out. Overall, the start of roll and sideline noise levels have increased from around 63dBA to 65.5dBA and the flyover noise level reduced from just over 70dBA to 65.5dBA. The reduced flight speed and increased aircraft height at flyover reduce airframe noise by 6dB and the increased height reduces fan rearward broadband noise by almost 5dB.

6.5.4. Comparison with higher fidelity predictions

In the above results, the correction made for liner attenuation was a single value set to match the result from more computationally intensive code. To validate this, alternative predictions of engine source noise levels were made for the take-off, optimised for low overall noise at the key sideline and flyover locations. For sideline noise, the position was set at 2km after brakes off whilst for flyover noise the position was set just after the airport boundary.

Jet and airfoil modelling was unaffected but, instead of ESDU predictions, a version of Rolls Royce code was used in the estimation of engine source noise before liner attenuation and propagation. This code was also used in the prediction of core, turbine and compressor noise. Rearward propagating engine noise is modelled as specified in §6.2 with the acoustic fan power in the duct assumed to be evenly distributed across the appropriate cut-on modes. For forward noise sources, shielding estimates are unchanged as the ray theory methods (Agarwal *et al.* 2006) used when looking at the higher risk design in more detail (Crichton *et al.* 2007a) could not be used in the timeframe available. The GasTurb model, used in creating the temperature and pressure corrections from the core flow, was used directly here. This gave more accurate temperature and pressures downstream of the mixer at the flyover and sideline operating points.

Results are presented in figure 6-13 for the sideline and flyover locations with the x-axis origin in both of these plots corresponding to the location of the aircraft. Fan forward, turbine and compressor noise sources are all predicted to be minimal with compressor noise so low that it does not appear on the figures. The turbine tones are highly attenuated due to their very high frequency (see de la Rosa Blanco et. al. (2007) for details of the turbine design), which is one reason for the sharp peak seen for this source. Core noise, not included in the optimisation, is less than fan rearward noise but is estimated to be the second strongest source at the flyover location and should therefore perhaps be included in future optimisations.

Overall noise is predicted to be about 0.5dB higher than the estimate in figure 6-12 due to small differences in the fan rearward noise propagation code and the more accurate liner predictions. This is small, especially in relation to the overall accuracy of fan broadband noise prediction.

6.5.5. Aircraft and airport variants

A range of optimisations was carried out to see how modifications to the baseline aircraft or airport impacted the achievable noise level.

ICAO certification flyover distance

If the airport boundary is modified to match the ICAO flyover certification distance of 6.5km from brakes off and the temperature set to ISA+10K, significant noise reductions are possible[*]. The increased time between brakes-off and cutback enables the aircraft to climb to an increased altitude before the airport boundary is crossed and an estimated noise reduction of 3 dB relative to the baseline airport is possible, giving an overall noise level of 62.5 dBA. Climb angles and noise estimates can be found in figure 6-14[†].

The dominant noise sources remain jet and fan rearward broadband but, with noise level reduced, the ratio is changed. The reduced thrust levels lead to lower jet noise and fan noise, therefore, has a bigger influence on the take-off profile prior to cutback. During the initial climb, the pitch angle limit of 20° no longer restricts climb and a maximum climb angle of just over 8° occurs. Reducing lateral attenuation with altitude leads to climb angle having to reduce as with the baseline case but,

[*] The flyover climb angle was set to meet the requirements of part 25 of the JAA/FAA regulations here. This gives a climb angle of 3.2° or 5.6% when ATTCS allowance is included. The noise certification requirements (part 36) only require a climb angle of 4% or enough to maintain level flight on loss of the critical engine. The second of these is just the most critical and leads to a required climb angle of 2.5° or 4.4% at flyover. If flyover climb angle was lowered to this value then noise would reduce by a further 0.5dBA (see section on no ATTCS allowance below for impact of flyover climb angle change).

[†] The reason that jet noise continues to increase in this figure even when a 4° climb angle has been reached 7km after brakes off is that, with altitude greater than 1500ft, acceleration is allowed.

with the increased distance to the airport boundary allowing the aircraft to reach a higher altitude, climb angle can start to increase again.

With ICAO certification values being based on EPNdB rather than dBA values, EPNdB calculations were made for the sideline and flyover locations. The chapter three certification values are 99.6 EPNdB at sideline and 98.9 EPNdB at flyover for this aircraft based on the maximum take-off weight and number of engines (ICAO 1993). Chapter four, which came into force on the 1st January 2006, only specifies a reduction of 10dB in the sum of sideline, flyover and approach noise relative to chapter three. If this noise reduction is evenly distributed across the three measuring locations then chapter four limits for this aircraft can be taken as 96.3 EPNdB at sideline and 95.6 EPNdB at flyover.

With the optimised procedure flown here, along the sideline the maximum noise was 72 EPNdB and at flyover the noise value was 73 EPNdB. These are approximately 24dB and 23dB below the ICAO limits respectively. To put this into context, if each new chapter that is introduced is 10dB cumulative lower than the last, this aircraft would be chapter 11 compliant (i.e. 7 chapters more stringent than is currently required by ICAO) based on sideline and flyover results. For comparison, very quiet recently certified civil aircraft with modern high bypass ratio fans (Trent 892 powered Airbus 340, GE 90 powered Boeing 777) are up to about 25dB cumulative below chapter three, i.e. notionally chapter six compliant (NoisedB 2007).

As mentioned in the introduction, the Quota Count system in operation at Heathrow is more stringent than the ICAO certification requirements and is a *de facto* worldwide standard for large civil aircraft. In this system, each aircraft is assigned a quota count value based on their certified noise value with a 3dB noise reduction equivalent to the halving of the quota count. A quota count of one is for aircraft with a noise value between 90.0 and 92.9 EPNdB. Therefore, the concept aircraft developed here would have a notional QC value of one over sixty-four (i.e. if this was the only restriction on movements, sixty four 'silent aircraft' movements could occur instead of one QC1 movement). At present, the current minimum QC level is 0.5.

90% MTOW, ISA Conditions

Whilst the aircraft has been designed to operate 'silently' from the baseline airport at MTOW during 99% of operating hours, this is not typical. A more typical operation of the aircraft would be under ISA conditions at 90% of maximum weight (80% payload, 71% fuel for example). When operating under these conditions the achievable noise level is reduced to 63.8 dBA, 1.7 dB less

than when at MTOW, ISA+12K as can be seen in figure 6-15. (Operating at MTOW, ISA only reduces noise by 0.3 dB.)

Reducing rearward propagating fan noise

The baseline aircraft has a duct length downstream of the OGVs equal to twice the fan diameter (see figure 6-9), half of which is before and half after the mixer. It was estimated that a further reduction in fan broadband noise of approximately 5dB could be achieved through a doubling of the annular duct proportion of the duct, and the impact of this can be seen in figure 6-16. The 5dB reduction in fan rearward noise leads to an overall noise level reduction of 3.1 dB to 62.4 dBA. Fan noise, whilst still dominant at flyover, is well below jet noise before this point. This reduction assumes core noise does not modify the result.

No ATTCS Allowance

When the minimum climb angle of the baseline aircraft was calculated, an 11% thrust increase following engine-out was included to account for the presence of an ATTCS (Automatic Take-off Thrust Control System). If no thrust increase on engine out is allowed, the noise outside the airport increases by approximately 0.4 dB as compared to when a thrust increase was allowed. This is due to the minimum flyover climb angle increasing from 3.1° to 3.7°.

High altitude noise constrained airport

In §3.2.1, in which the baseline airport was specified, a second higher altitude noise constrained airport was also mentioned. This was at 5,000ft (1,524m) altitude, had a 12,000ft (3,658m) runway and, based on Denver conditions, had a maximum temperature for low noise operation of ISA+19.5K. When optimising the take-off at this airport, a minimum overall noise level outside of the airport boundary of 67.2 dBA was achieved, a 1.7 dB increase relative to the baseline airport. This is about half the increase in noise that was seen when looking at jet noise only in §3.4.3.

6.6. Discussion

The concept podded engine aircraft (figure 6-2) presented in this chapter is estimated to be significantly quieter than current aircraft that are in service. In this discussion, two questions are looked at; where do the noise reductions come from and how could further noise reductions be achieved?

How is the ultra-low noise level achieved?

Figure 6-17, copied from Schwartz (2006), created using some of the tools presented in this thesis, illustrates well where the noise reductions come from. This figure was created for an earlier design but illustrates the relative importance of the various technologies. Peak take-off noise and cruise fuel burn are plotted relative to the estimated values for a Boeing 787 operating without any cutback from the baseline airport. The design presented in this chapter is similar to design step 11 and the significant changes that occur to reach this point can be split into four areas; reducing thrust requirement, reducing specific thrust, acoustic treatment and improving operations.

Concentrating on the noise reduction, reducing thrust comes about through improving technology (step 3) and the use of an all-lifting body which has improved take-off lift to drag ratio (step 10). Increasing mass flow and reducing pressure rise across the fan lowers both jet and fan noise as the fan tip speed reduces to maintain loading (step 4) and opening the nozzle area at take-off (step 6). In terms of acoustic treatment, moving to a mixed exhaust gives room for additional liners (step 5). Finally, utilising a noise managed take-off has a significant benefit (step 9), especially when the number of engines is increased from two to three (step 8).

Figure 6-18 shows how the optimised take-off profile reduces noise for the final podded design when both fan and jet noise are considered. Firstly, with no cutback and the engine operating at fixed corrected speed after the initial acceleration, noise peaks at over 8dB higher than the final solution as the flyover boundary is crossed. For this departure, the climb angle was set to the minimum initial climb angle required below 400 foot. Increasing take-off fan speed does reduce the flyover noise level slightly but only by a couple of dB and the sideline noise level increases more than the flyover noise level drops. Introducing a simple cutback as the airport boundary is approached allows a balance between sideline and flyover noise to be achieved and gives most of the achievable operational benefit. This simple cutback is similar to the ICAO cutback procedure but further benefits accrue from nozzle area changing at the same time. Finally, by continuously modifying the fan speed, an additional 1dB cumulative reduction can be achieved at the flyover and sideline locations. Whilst this is not a major reduction, it is still beneficial.

Achieving further noise reduction

Turning now to how to achieve further noise reductions, the obvious first problem that needs to be tackled is fan noise. The low tip speed design, operating at part speed during take-off does give a significant noise reduction but, even with the liners, fan rearward noise is the main reason for the design being 5.5dB above the SAI target of 60dBA when operating at the baseline airport.

Doubling the length of the annular section of the duct (figure 6-16) can bring overall noise down to 62.4dBA but further reductions become harder and increasing duct lengths will only increase fuel burn. Therefore, alternative means of reducing rearward noise should be looked at. The use of deployable lined baffles in the exhaust is one solution that was briefly mentioned in §4.6 but this still leads to increased weight and reduced cruise performance. Another possibility is to look at a more radical design altogether and this is what the higher-risk SAI aircraft mentioned at the start of this chapter represents (see figure 6-1).

In this aircraft, each engine powers three fans, all with the same rotational speed as the low pressure turbine but with two off-set from the axis of rotation. This increases the blade passing frequency of the fan, increasing the frequency of the noise. Liners become more effective and atmospheric attenuation increases. Another benefit is that for the same overall length of ducting, the reduction in radius of each fan leads to higher duct length to diameter ratios and further lining improvements. Finally, to reduce the cruise thrust requirement and fuel burn the suction surface boundary layer is ingested into the engine. This final step is of significant risk as designing a fan to support continuous distortion during cruise will be challenging. With these changes, the take-off noise is estimated to be below 62dBA, almost at the SAI target (Crichton *et al.* 2007a). Further reductions become increasingly hard as multiple noise sources start to become important and the liners have already removed all the easy to attenuate modes.

6.7. Chapter Conclusions

A 250 passenger, 5000nm range all-lifting body aircraft with three podded engines designed for low noise is estimated to not exceed a 65.5 dBA noise level outside of the SAI baseline airport during take-off. For the ICAO certification distances this falls to 62.5 dBA with EPNdB values of 72 at sideline and 73 at flyover. To put these numbers into context if just take-off is considered, the aircraft would notionally be ICAO chapter eleven compliant and have a Quota Count of one sixty fourth. This is on the basis that each new ICAO chapter introduced in the future will be the same as when chapter four superseded chapter three (i.e. requiring a cumulative 10dB noise reduction) and that QC levels extend below 0.5 in the same was as they currently operate between values of 0.5 and 16.

Whilst the estimated noise level is much lower than quiet aircraft in the existing fleet, it is still 5.5dB above the initial target of 60dBA. To reduce noise further requires fan rearward noise in particular to be targeted and this was done in the higher-risk concept aircraft design shown in

figure 6-1. Even then, initial indications are that the final noise level will be approximately 2dB above target.

7. Conclusions and Future Work

7.1. Conclusions

The aim of the Silent Aircraft Initiative was to design a concept civil aircraft that was inaudible outside of the airport boundary in an urban environment. Achieving such a design would, if realised commercially, remove one of the key constraints on the expansion of aviation and allow the placement of airports closer to centres of population. In this thesis, this aim was translated into a target noise level of 60dBA outside of a baseline airport, itself specified by analysing existing noise constrained airports.

Initial indications are that through the use of a high performance all-lifting body aircraft, ultra high bypass ratio podded engines with variable area nozzles and optimised departure profiles, take-off noise can be reduced to within 5.5dBA of this target whilst maintaining good cruise performance. This translates to a value of 73EPNdB for the ICAO certification distances, approximately 23dB below the current ICAO chapter four requirements at each take-off point. Embedding the engines and linking each core to three fans may reduce this to within 2dBA of the target but further reductions become increasingly hard.

In addition to the development of the concept aircraft fan, this thesis has presented an approach to design, especially the selection of key engine parameters, in which noise is as critical as fuel burn. With jet mixing noise hard to shield and, for low-speed jets only limited noise reduction through enhanced mixing possible, jet noise reduction was identified as key to the approach. Nozzle area at take-off needs to be increased significantly in order to reduce jet noise to the required level, well beyond that optimum for low cruise fuel burn. To reduce the area increase, the airframe should have excellent low-speed performance and a high cruise altitude all-lifting body is ideally suited. Optimisation of the departure profile can then be used to reduce the required take-off jet area further with most of the benefit coming from the introduction of a thrust cutback as the airport boundary is crossed. A three or four-engine design benefits from this cutback significantly more than a two-engine design as engine out climb angle is the critical safety requirement that must be met. Even with performance optimised, a fixed cycle design cannot deliver both the take-off noise level and low cruise fuel burn and therefore the introduction of variable cycle technology into the engine is required.

A variable area nozzle was identified as the most promising of the options considered and the operation of this was linked to a simplified model of the engine. This allowed the trade between take-off jet noise and top of climb fan design parameters to be clearly seen. At take-off, nozzle area increase is limited by incidence onto the outlet guide vanes at lower fan speed and rotor capacity at higher fan speed. This links the achievable top of climb fan pressure ratio to take-off jet noise and, for the aircraft designed here, a top of climb FPR of 1.45, in the range required for minimum fuel burn, was estimated as the maximum achievable when also limiting take-off jet noise to 57dBA.

A forward swept fan rotor and outlet guide vane was designed to work specifically with the variable area nozzle. Critical design requirements, unchanged from conventional designs, were delivering the top of climb thrust at high capacity, and delivering peak efficiency at cruise. Unique to the design presented here were the maximisation of part speed capacity and the support of a high incidence range onto the OGVs so as to minimise take-off jet noise. This replaced achieving take-off surge margin, critical for conventional designs. The selection of design blade speed is key to this process, especially so as it also impacts fan source noise. Reducing blade speed increases part speed capacity and, in general, reduces fan source noise. As blade speed reduces fan loading increases, and designing the OGVs becomes increasingly challenging. In addition, with the velocity onto the OGVs increasing for a given mass flow rate and pressure rise as loading is increased, some designs with very high loading have seen increases in fan noise and therefore a balance needs to be made. Here, the fan loading at top of climb was set to 0.52 giving a corrected blade tip speed of 371m/s and cutting off rotor alone tones at flyover. More work is required to see if this loading value is optimum.

A simple model of the fan blade indicates that additional part speed capacity increases can be made by ensuring that when the relative flow Mach number onto the fan is supersonic the fan should operate at unique incidence with only a weak shock ahead of the fan. From the model, achieving this requires blade mass to be moved forward and, for the fan designed here, the maximum thickness is never further back than 57% of axial chord. Further work is required to see if the trends seen from this simple model translate into results from a fully 3D viscous analysis. With OGV design still very challenging, an increase in the duct radius between rotor trailing edge and OGV leading edge was successfully introduced to reduce both the maximum flow Mach number onto the OGVs and to reduce the incidence range that needed to be supported. Initial indications are that the fan stage performs well with a high cruise bypass stage efficiency of 92.5% and operation at 85% efficiency or higher throughout take-off.

Looking at the work in a wider context, whilst an eye on fuel burn has been maintained throughout, minimising fuel consumption and the wider environmental impact have not been the subject of this thesis. These would need to be considered much more seriously if the concept aircraft developed here or ideas from it were carried forward. Whilst cruising higher or increase liner lengths, both of which assist in noise reduction, increase the wider environmental impact, certain technologies may benefit it. In particular, the use of a variable area nozzle adds an additional degree of freedom to engine operation allowing cruise fuel burn to be minimised at all times. The significant noise reductions possible through its introduction, especially when the fan is designed to work with it, make solving the mechanical challenges it poses imperative.

7.2. Suggested Future Work

Looking at the fan design first, as discussed at the end of chapter five the design work to date is only the start of the process. Particular areas requiring additional work are in the mechanical analysis of the blade, especially in terms of flutter resistance and, with forward sweep increasing leading edge stresses, foreign object damage tolerance. In terms of rotor aerodynamic design, the midspan section has a leading edge shock present (see figure 5-23) that could be reduced in strength with improved design. Also, the outer section of the fan performs best at a slightly higher back pressure than the inner section (see figure 5-11) and peak efficiency could be improved through better matching. With bypass performance and noise of prime interest, the core flow was modelled as a bleed in this thesis. The design of the hub section needs to be looked at in more detail, including the design of the engine section stator (ESS).

In chapter five, a simple model was used to look at part speed capacity indicating that moving blade mass forward would assist. This should be investigated in more detail with 3D viscous analysis of a range of designs, all with the same design capacity. Coupled with this, more research is required on the impact blade speed has on where the fan can operate during take-off: As blade speed is reduced part speed fan capacity will increase, but OGV incidence will become more limiting. This will allow increased nozzle opening at high fan speed (i.e. sideline) but reduced nozzle opening at low fan speed (i.e. flyover). Is the currently selected speed optimum?

Turning now to noise, designing for ultra-low noise requires models that accurately capture the correct trends with design parameters and also the correct noise levels. For jet mixing noise, the largest uncertainty comes about through the corrections applied to account for flight effects as discussed in §3.3.2. This is because as jet velocity reduces the flight corrections have a much greater impact on the final noise footprint. The work of Low (1994) was used in this thesis but

this was for coaxial nozzles and no similar work is available for fully mixed nozzles in which the focus is on very low jet velocities. Ideally, a test campaign should be performed for a representative geometry which includes a mixer well upstream of the nozzle exit (see figure 6-9) so as to also account for any forced mixing noise that may be present.

The increased fidelity noise calculations presented in §6.5.4, whilst helping to validate the code used during the optimisation process, do not represent the current state of the art. To increase the confidence in the overall noise predictions, the range of fan noise sources should ideally be predicted using more advanced tools. Of particular importance is improved prediction of rotor alone and rotor-nacelle boundary layer interaction noise as these could then be combined with the Envia results for rotor-stator broadband noise. Linked to this is a need to better understand the change in fan broadband noise as operation is moved along a line of constant fan speed. For rotor alone noise, both rig tests (Ganz *et al.* 1998) and analysis (Glegg and Jochault 1998) indicate a reduction in noise as incidence is reduced. Does this continue down beyond peak efficiency incidence and what about when the flow is choked? For rotor-stator interaction noise, the Envia results indicate that rotor-stator interaction noise will tend to increase as the increase in Mach number onto the OGVs is more significant than the reduction in wake turbulent intensity. Rig tests (Ganz *et al.* 1998) have shown almost no change in rotor-stator interaction noise with loading but this may be because the range of variation was not large enough. Answers to these questions are unlikely to be straightforward and therefore continuing research on the prediction of broadband noise is required which is itself inextricably linked to the accurate prediction of turbulence. Finally in terms of noise, no estimate has been made in this thesis of noise from any other components in the bypass duct, in particular support struts. This should be performed in the future if the design is developed to a point in which the location of any such struts is known.

This thesis has shown that a variable area nozzle is critical to delivering low noise at take-off whilst also operating with an optimum fan pressure ratio at cruise. The mechanical design of such a nozzle is required as if the weight is too high or the losses too big, cruise fuel burn will be increased. The right hand sketch in figure 3-18 is promising as, in addition to increasing nozzle area, it would bevel the nozzle which could lead to further jet noise reductions directly below the longer lip (Viswanathan 2005).

Finally, as discussed in chapter six, one possible way to reduce noise and fuel burn is to embed the engines into the airframe and ingest boundary layer flow. This reduces the thrust required and introduces the possibility of extending ducting without increasing losses. For such a concept to work, the fan will have to support a degree of distortion throughout cruise, impacting efficiency,

operability and life. The potential benefits are significant and therefore research in this area is recommended looking at performance and life at cruise, and noise at take-off.

References

Abolfadl, M. A., Metwally, M. A., El-Messiry, A. M., and Ali, M. A., "Experimental Investigation of Lobed Mixer Performance," *Journal of Propulsion and Power*, Vol. 17, No. 5, 2001, pp. 1109-16.

ACARE, "European Aeronautics: A vision for 2020," Advisory Council for Aeronautics Research in Europe, 2000

Agarwal, A. and Dowling, A. P., "Low Frequency Acoustic Shielding of Engine Noise by the Silent Aircraft Airframe," *11th AIAA/CEAS Aeroacoustics Conference*, Monteray, California, 2005. AIAA-2005-2996.

Agarwal, A., Dowling, A. P., Shin, H-C., Graham, W., and Sefi, S., "A Ray Tracing Approach to Calculate Acoustic Shielding by the Silent Aircraft Airframe," *12th AIAA/CEAS Aeroacoustics Conference*, Cambridge, Massachusetts, 2006. AIAA-2006-2618.

Ahuja, K. K., "Correlation and prediction of Jet Noise," *Journal of Sound and Vibration*, Vol. 29, No. 2, 1973, pp. 155-68.

Ahuja, K. K., Tester, B. J., and Tanna, H. K., "The Free Jet as a Simulator of Forward Velocity Effects on Jet Noise," NASA CR-3056, 1978

Amiet, R. K., "Correction of open-jet wind-tunnel measurements for shear layer refraction," *2nd AIAA Aeroacoustics Conference*, Hamtpon, Virginia, 1975. AIAA-75-532.

Andreou, C., Graham, W., and Shin, H-C., "Aeroacoustic Study of Airfoil Leading Edge High-Lift Devices," *12th AIAA/CEAS Aeroacoustics Conference*, Cambridge, Massachusetts, 2006. AIAA-2006-2515.

Antoine, N. E. and Kroo, I. M., "Optimizing Aircraft and Operations for Minimum Noise," *AIAA's Aircraft Technology, Integration, and Operations (ATIO) 2002 Technical Forum*, Los Angeles, California, 2002. AIAA-2002-5868.

Antoine, N. E. and Kroo, I. M., "Aircraft Optimization for Minimal Environmental Impact," *Journal of Aircraft*, Vol. 41, No. 4, 2004, pp. 790-6.

Antoine, N. E. and Kroo, I. M., "Framework for Aircraft Conceptual Design and Environmental Performance Studies," *AIAA Journal*, Vol. 43, No. 10, 2005, pp. 2100-9.

Bailey, D. W. and Carrotte, J. F., "The Influence of Inlet Swirl on the Flow within an Annular S-Shaped Duct," *International Gas Turbine and Aeroengine Congress and Exhibition*, Birmingham, UK, 1996. ASME 96-GT-60.

Behlke, R. F., "The Deveopment of a Second Generation of Controlled Diffusion Airfoils for Multistage Compressors," *Journal of Turbomachinery*, Vol. 108, 1986, pp. 32-41.

Berglund, B., Lindvall, T., and Schwela, D. H., "Guidelines for Community Noise," World Health Organization, 1999

Berton, Jeffery J., "Noise Reduction Potential of Large, Over-the-Wing Mounted, Advanced Turbofan Engines," NASA TM-2000-210025, 2000

Bevilaqua, P. M., "Joint Strike Fighter Dual-Cycle Propulsion System," *Journal of Propulsion and Power*, Vol. 21, No. 5, 2005, pp. 778-83.

Bewick, C. L., Adams, M. J., Schwaller, P. J. G., and Xu, L., "Noise and Aerodynamic Design and Test of a Low Tip Speed Fan," *7th AIAA/CEAS Aeroacoustics Conference*, Maastricht, The Netherlands, 2001. AIAA-2001-2268.

Birch, N., "Future Challenges," *Rolls Royce Noise Appreciation Course*, 2002

Boeing, "767-200/200ER 767-300/300ER/300 FREIGHTER Airplane Characteristics for Airport Planning," Boeing Commercial Airplanes, 2003

Bogdanoff, D. W., "Compressibility Effects in Turbulent Shear Layers," *AIAA Journal*, Vol. 21, No. 6, 1983, pp. 926-7.

Bonnington, S. T., King, A. L., and Hemmings, J. A. G., "Jet pumps and ejectors: a state of the art review and bibliography." 2nd ed. BHRA Fluid Engineering. 1976

Borradaile, J. A., "Towards the optimum ducted UHBR engine," *24th ASME, SAE, and ASEE Joint Propulsion Conference*, Boston, Massachusetts, 1988. AIAA-88-2954.

Bridges, J. and Wernet, M., "Cross-Stream PIV Measurements of Jets With Internal Lobed Mixers," *10th AIAA/CEAS Aeroacoustics Conference*, Manchester, United Kingdom, 2004. AIAA-2004-2896.

Bridges, J., Wernet, M., and Brown, C., "Control of Jet Noise Through Mixing Enhancement," NASA TM-2003-212335, 2003

Brookfield, J. M. and Waitz, I. A., "Trailing-edge blowing for reduction of turbomachinery fan noise," *Journal of Propulsion and Power*, Vol. 16, No. 1, 2000, pp. 57-64.

Brooks, J. R., McKinnon, R. A., and Johnson, E. S., "Results from Flight Noise Tests on a Viper Turbojet Fitted with Ejector/Suppressor Nozzle Systems," *6th AIAA Aeroacoustics Conference*, Hartford, Connecticut, 1980. AIAA-1980-1028.

Brown, G. L. and Roshko, A., "On Density Effects and Large Structure in Turbulent Mixing Layers," *Journal of Fluid Mechanics*, Vol. 64, 1974, pp. 775-816.

Bryce, W.D., "The prediction of static-to-flight changes in jet noise," *9th AIAA Aeroacoustics Conference*, Williamsburg, Virginia, 1984. AIAA-84-2358.

Bushell, K. W., "A survey of Low Velocity and Coaxial Jet Noise with application to prediction," *Journal of Sound and Vibration*, Vol. 17, No. 2, 1971, pp. 271-82.

Calkins, F. T., Butler, G. W., and Mabe, J. H., "Variable Geometry Chevrons for Jet Noise Reduction," *12th AIAA/CEAS Aeroacoustics Conference*, Cambridge, Massachusetts, 2006. AIAA-2006-2546.

Calvert, W. J. and Ginder, R. B., "Transonic fan and compressor design," *Proceedings of the Institution of Mechanical Engineers, Part C:Journal of Mechanical Engineering Science*, Vol. 213, 1999, pp. 419-36.

Coles, W. D., "Jet-Engine Exhaust Noise from Slot Nozzles," NASA TN D-60, 1959

Coles, W. D., Mihaloew, J. A., and Callaghan, E. E., "Turbojet engine nozzle reduction with mixing nozzle-ejector combinations," NACA TN 4317, 1958

Cooper, A. J. and Peake, N., "Propagation of unsteady disturbances in a slowly varying duct with mean swirling flow," *Journal of Fluid Mechanics*, Vol. 445, 2001, pp. 207-34.

Copenhaver, W. W., Hah, C., and Puterbaugh, S. L., "Three-Dimensional Flow Phenomena in a Transonic, High Throughflow, Axial-Flow Compressor Stage," *Journal of Turbomachinery*, Vol. 115, 1993, pp. 240-8.

Crichton, D., Hileman, J., de la Rosa Blanco, E., and Law, T. R., "Design and operation for ultra low noise take-off," *45th AIAA Aerospace Sciences Meeting and Exhibit*, Reno, Nevada, 2007a. AIAA-2007-456.

Crichton, D., Xu, L., and Hall, C. A., "Preliminary Fan Design for a Silent Aircraft," *Journal of Turbomachinery*, Vol. 129, 2007b, pp. 184-91.

Crighton, D. G., "The excess noise field of subsonic jets," *Journal of Fluid Mechanics*, Vol. 56, No. 4, 1972, pp. 683-94.

Crighton, D. G., Ffowcs-Williams, J.E., and Cheeseman, I. C., "The Outlook for Simulation of Forward Flight Effects on Aircraft Noise," *Journal of Aircraft*, Vol. 14, No. 11, 1977, pp. 1117-25.

Crow, S. C. and Champagne, F. H., "Orderly structure in jet turbulence," *Journal of Fluid Mechanics*, Vol. 48, No. 3, 1971, pp. 547-91.

Cumpsty, N., "Compressor Aerodynamics." 1989: Longman Scientific and Technical. ISBN 0-582-12364-X.

Cumpsty, N., "Jet Propulsion." 2 ed. 2003: Cambridge University Press. ISBN 0-521-54144-1.

Curtis, A.R.D., "Active Control of Fan Noise by Vane Actuators," NASA CR-1999-209156, 1999

Daggett, D. L., Brown, S. T., and Kawai, R. T., "Ultra-Efficient Engine Diameter Study," NASA CR-2003-212309, 2003

de la Rosa Blanco, E., Hall, C. A., and Crichton, D., "Challenges in the Silent Aircraft Engine Design," *45th AIAA Aerospace Sciences Meeting and Exhibit*, Reno, Nevada, 2007. AIAA-2007-0454.

Denton, J.D., "The Calculation of Three Dimensional Viscous Flow Through Multistage Turbomachines," *Journal of Turbomachinery*, Vol. 114, No. 1, 1990, pp. 18-26.

Denton, J.D. and Xu, L., "The exploitation of three-dimensional flow in turbomachinery design," *Proceedings of the Institution of Mechanical Engineers, Part C:Journal of Mechanical Engineering Science*, Vol. 213, 1999, pp. 125-37.

Denton, J.D. and Xu, L., "The effects of Lean and Sweep on Transonic Fan Performance," *ASME Turbo Expo*, Amsterdam, The Netherlands, 2002. GT-2002-30327.

Dittmar, J. H., "A Fan Concept to Meet the 2017 Noise Goals," NASA TM-1998-208663, 1998

Dittmar, J. H., Tweedt, D., Jeracki, R., Envia, E., Bartos, K., and Slater, J., "A Fan Design That Meets the NASA Aeronautics Noise Goals," NASA TM-2003-212322, 2003

Donoghue, J. A., "The fan is the thing," *Air Transport World*, November 2004. http://www.atwonline.com/magazine/article.html?articleID=1086

Drela, M. and Youngren, H., "A User's Guide to MISES 2.53," MIT Computational Aerospace Sciences Laboratory, 1998

Drevet, P., Duponchel, J. P., and Jacques, J. R., "The effect of flight on jet noise as observed on the Bertin Aérotrain," *Journal of Sound and Vibration*, Vol. 54, No. 2, 1977, pp. 173-210.

Elmer, K., Wat, J., Gershzohn, G., Shivashankara, B. N., Clarke, J-P., and Ho, N., "A study of Noise Abatement Procedures Using Ames B747-400 Flight Simulator," *8th AIAA/CEAS Aeroacoustics Conference and Exhibit*, Breckenridge, Colorado, 2002. AIAA-2002-2540.

Envia, E. and Nallasamy, M., "Design Selection and Analysis of a Swept and Leaned Stator Concept," NASA TM-1998-208662, 1998

Envia, E., Wilson, A. G., and Huff, D. L., "Fan Noise: A Challenge to CAA," *International Journal of Computational Fluid Dynamics*, Vol. 18, No. 6, 2004, pp. 471-80.

Erkelens, L. J. J., "Advanced Noise Abatement Procedures for Approach and Departure," *AIAA Guidance, Navigation and Control Conference and Exhibit*, Monterey, California, 2002. AIAA-2002-4858.

ESDU, "Evaluation of the Attenuation of Sound by a Uniform Atmosphere,"Item 78002, 1977

ESDU, "Estimation of Lateral Attenuation of Air-to-Ground Jet or Turbofan Aircraft Noise in one-third octave bands,"Item 82027, 1982

ESDU, "Estimation of subsonic far-field jet-mixing noise from single-stream circular nozzles,"Item 89041, 1990a

ESDU, "Prediction of single-stream jet noise in flight from static circular-nozzle data,"Item 87011, 1990b

ESDU, "The correction of measured noise spectra for the effects of ground reflection,"Item 94035, 1994

ESDU, "Prediction of noise generated by fans and compressors in turbojet and turbofan engines,"Item 98008, 1998

ESDU, "Airframe Noise Prediction,"Item 90023 Amendment C, 2003

Evers, I. and Peake, N., "On sound generation by the interaction between turbulence and a cascade of airfoils with non-uniform mean flow," *Journal of Fluid Mechanics*, Vol. 463, 2002, pp. 25-52.

FAA, "Federal Aviation Regulations section 25: Airworthiness Standards: Transport Category Airplanes," Federal Aviation Administration

FAA, "Federal Aviation Regulations section 36: Noise Standards: Aircraft Type and Airworthiness Certification," Federal Aviation Administration

FAA, "Noise Abatement Departure Profiles," Federal Aviation Administration AC 91-53A, 1993

Fancher, R. B., "Low-Area Ratio, Thrust-Augmenting Ejectors," *Journal of Aircraft*, Vol. 9, No. 3, 1972, pp. 243-8.

Ffowcs-Williams, J.E., "The Noise from Turbulence convected at High Speed," *Philisophical Transactions of the Royal Society of London. Series A, Mathematical and Physical Sciences*, Vol. 255, No. 1061, 1963, pp. 469-503.

Fink, M. R., "Airframe Noise Prediction Method,"FAA-RD-77-29 (available from DTIC as AD A039 664), 1977

Fisher, M. J., Preston, G. A., and Bryce, W.D., "Modelling of the Noise from simple Coaxial Jets, Part I: With unheated primary flow," *Journal of Sound and Vibration*, Vol. 209, No. 3, 1998a, pp. 385-403.

Fisher, M. J., Preston, G. A., and Mead, C. J., "Modelling of the Noise from Simple Coaxial Jets, Part II: With heated primary flow," *Journal of Sound and Vibration*, Vol. 209, No. 3, 1998b, pp. 405-17.

FitzSimmons, R. D., McKinnon, R. A., Johnson, E. S., and Brooks, J. R., "Flight and Wind Tunnel Test Results of a Mechanical Jet Noise Suppressor Nozzle," *Journal of Aircraft*, Vol. 18, No. 9, 1980, pp. 725-30.

Freeman, C. and Cumpsty, N., "Method for the Prediction of Supersonic Compressor Blade Performance," *Journal of Propulsion and Power*, Vol. 8, No. 1, 1992, pp. 199-208.

Friedrichs, J., Baumgarten, S., Kosyna, G., and Stark, U., "Effect of Stator Design on Stator Boundary Layer Flow in a Highly Loaded Single-Stage Axial-Flow Low-Speed Compressor," *Journal of Turbomachinery*, Vol. 123, 2001, pp. 483-9.

Gabard, G. and Astley, R. J., "Theoretical Model for Sound Radiation from Annular Jet Pipes: Farfield and Nearfield Predictions," *Journal of Fluid Mechanics*, Vol. 549, 2006, pp. 315-41.

Gaeta, R. J., Ahuja, K. K., Schein, D. B., and Solomon, W. D., "Large Jet-Noise Reductions Through Distributed Nozzles," *8th AIAA/CEAS Aeroacoustics Conference*, Breckenridge, Colorado, 2002. AIAA-2002-2456.

Gallimore, S. J., "Axial flow compressor design," *Proceedings of the Institution of Mechanical Engineers, Part C:Journal of Mechanical Engineering Science*, Vol. 213, No. 5, 1999, pp. 437-49.

Ganz, U.W, Joppa, P.D., Patten, T.J., and Scharpf, D.F., "Boeing 18-Inch Fan Rig Broadband Noise Test," NASA CR-1998-208704, 1998

Garrison, L. A., Dalton, W.N., Lyrintzis, A. S., and Blaisdell, G. A., "On the Development of Semi-Empirical Noise Models for the Prediction of the Noise from Jets with Forced Mixers," *10th AIAA/CEAS Aeroacoustics Conference*, Manchester, UK, 2004. AIAA-2004-2898.

Ginder, R. B. and Newby, D. R., "An improved correlation for the broadband noise of high speed fans," *Journal of Aircraft*, Vol. 14, No. 9, 1977, pp. 844-9.

Glegg, S. A. L., "The response of a swept blade row to a three-dimensional gust," *Journal of Sound and Vibration*, Vol. 227, No. 1, 1999, pp. 29-64.

Glegg, S. A. L. and Jochault, C., "Broadband Self-Noise from a Ducted Fan," *AIAA Journal*, Vol. 36, No. 8, 1998, pp. 1387-95.

Gliebe, P. R., "The Effect of Throttling of Forward Radiated Fan Noise," *5th AIAA Aeroacoustics Conference*, Seattle, Washington, 1979. AIAA-1979-0640.

Gliebe, P. R., "The GE90: Quiet by Design. Quieter Aircraft Engines through leveraging New Technologies," *Berkeley Airport Noise Symposium*, 2003

Gliebe, P. R., Ho, P. Y., and Mani, R., "UHB Engine Fan Broadband Noise Reduction Study," GE Aircraft Engines NASA Contract NAS3 26617, 1995

Gliebe, P. R. and Janardan, B. A., "Ultra-High Bypass Engine Aeroacoustic Study," NASA-2003-212525, 2003

Goldstein, M. E. and Howes, W. L., "New Aspects of Subsonic Jet Noise Theory," NASA TN D-7158, 1973

Gordon, C. G. and Maidanik, G., "Influence of Upstream Flow Discontinuities on the Accoustic Power radiated by a Model Air Jet," NASA CR-679, 1967

Government, UK, "The Future of Air Transport," Department for Transport, 2003a

Government, UK, "Review of the quota count (QC) system," Department for Transport, 2003b

Government, UK, "Noise Mapping England : The London Road Traffic Noise Map," Department for the Environment, Food and Rural Affairs (Defra), 2004

Green, J. E., Cottington, R. V, Davies, M., Dawes, W. N., Fielding, J. P., Hume, C. J., Lee, J., McClarty, J., Mans, K. D. R., Mitchell, K., and Newton, P. J., "Air Travel - Greener by Design: The Technology Challenge," Greener by Design, 2001

Groeneweg, J. F., Sofrin, T. G., and Rice, E. J., "Turbomachinery Noise," in *Aeroacoustics of Flight Vehicles: Theory and Practice, Volume 1: Noise Sources*, H.H. Hubbard, Editor. 1991, published by NASA. RP-1258, WRDC Technical Report 90-3052.

Gummer, V., Wenger, U., and Kau, H. P., "Using Sweep and Dihedral to Control Three-Dimensional Flow in Transonic Stators of Axial Compressors," *Journal of Turbomachinery*, Vol. 123, No. 1, 2001, pp. 40-8.

Gutmark, E. J. and Grinstein, F. F., "Flow Control with non-circular jets," *Annual Review of Fluid Mechanics*, Vol. 31, 1999, pp. 239-72.

Hall, C. A., Crichton, D., Freuler, P., and Agarwal, A., "Engine configurations for the Silent Aircraft," *148th ASA Meeting*, San Diego, 2004

Hanson, D. B., "Theory for Broadband Noise of Rotor and Stator Cascades With Inhomogeneous Inflow Turbulence Including Effects of Lean and Sweep," NASA NASA/CR-2001-210762, 2001

Hanson, D. B., "Broadband theory for coupled fan stages including blade row reflection/transmission effects," *8th AIAA/CEAS Aeroacoustics Conference*, Breckenridge, Colorado, 2002. AIAA-2002-2488.

Hanson, D. B. and Horan, K. P., "Turbulence/Cascade Interaction: Spectra of inflow, cascade response and noise," *4th AIAA/CEAS Aeroacoustics Conference*, Toulouse, France, 1998. AIAA-1998-2319.

Harper-Bourne, M., "Jet Noise Turbulence Measurements," *9th AIAA/CEAS Aeroacoustics Conference and Exhibit*, Hilton Head, South Carolina, 2003. AIAA-2003-3214.

Harper-Bourne, M. and Fisher, M. J., "The noise from shock waves in supersonic jets," *Noise Mechanisms*, Brussels, Belgium, 1974. AGARD CP-131 (11.1-11.13).

Heidelberg, L. J., "Fan Noise Source Diagnostic Test - Tone Modal Structure Results," *8th AIAA/CEAS Aeroacoustics Conference*, Breckenridge, Colorado, 2002. AIAA-2002-2428, NASA/TM-2002-211594.

Heidmann, M. F., "Interim Prediction Method for Fan and Compressor Source Noises," NASA TM X-71763, 1979

Hileman, J. I., Reynolds, T.G., de la Rosa Blanco, E., and Law, T. R., "Development of Approach Procedures for the Silent Aircraft," *45th AIAA Aerospace Sciences Meeting and Exhibit*, Reno, Nevada, 2007a. AIAA-2007-0451.

Hileman, J. I., Spakovszky, Z. S., Drela, M., and Sargeant, M. A., "Airframe Design for 'Silent Aircraft'," *45th AIAA Aerospace Sciences Meeting and Exhibit*, Reno, Nevada, 2007b. AIAA-2007-0453.

Hill, P. G., "Turbulent jets in ducted streams," *Journal of Fluid Mechanics*, Vol. 22, 1965, pp. 161-86.

Hobbs, D. E., Neubert, R. J., Malmborg, E. W., Philbrick, D. H., and Spear, D. A., "Low Noise Research Fan Stage Design," NASA CR-195382, 1995

Hobbs, D. E. and Weingold, H. D., "Development of Controlled Diffusion Airfoils for Multistage Compressor Application," *ASME Journal of Engineering for Gas Turbines and Power*, Vol. 106, 1984, pp. 271-8.

Hoch, R. G., Duponchel, J. P., Cocking, B. J., and Bryce, W.D., "Studies on the influcence of density on jet noise," *Journal of Sound and Vibration*, Vol. 28, No. 4, 1973, pp. 649-68.

Hu, H., Saga, T., Kobayashi, T., and Taniguchi, N., "Mixing Process in a Lobed Jet Flow," *AIAA Journal*, Vol. 40, No. 7, 2002, pp. 1339-46.

Huff, D. L., "Fan Noise Prediction: Status and Needs," *36th AIAA Aerospace Sciences Meeting and Exhibit*, Reno, Nevada, 1998. AIAA-1988-177.

Hughes, C. E., Woodward, R. P., Podboy, G. G., and Jeracki, R. J., "The effect of bypass nozzle exit area on fan aerodynamic performance and noise in a model turbofan simulator," *ASME Turbo Expo: Power for Land, Sea and Air*, Reno, Nevada, 2005. GT2005-68573.

ICAO, "PANS-OPS Volume 1 Part V : Noise Abatement Procedures," International Civil Aviation Organization

ICAO, "Convention on International Civil Aviation - Annexe 16, Volume 1, Third Edition," 1993

IPCC, Intergovernmental Panel on Climate Change, "Aviation and the Global Atmosphere." 1999: Cambridge University Press. ISBN 0521664047.

JAA, "Joint Aviation Regulations section 25: Airworthiness Standards: Transport Category Airplanes," Joint Aviation Authorities

JAA, "Joint Aviation Regulations section 36: Noise Standards: Aircraft Type and Airworthiness Certification," Joint Aviation Authorities

Jenkinson, L.R., Simpkin, P., and Rhodes, D., "Civil Jet Aircraft Design." 1999: Elsevier. ISBN 0-340-74152-X.

Kaplan, B., Nicke, E., and Voss, C., "Design of a Highly Efficient Low-Noise Fan for Ultra-High Bypass Engines," *ASME Turbo Expo 2006: Power for Land, Sea and Air*, Barcelona, Spain, 2006. GT2006-90363.

Kobrynski, M., "On the calculation of the maximum sound pressure spectrum from stationary and mobile jets," *Journal of Sound and Vibration*, Vol. 7, 1968, pp. 263-86.

Koller, U., Monig, R., Kusters, B., and Schreiber, H-A., "Development of Advanced Compressor Airfoils for Heavy-Duty Gas Turbines - Part I: Design and Optimization," *Journal of Turbomachinery*, Vol. 122, 2000, pp. 397-405.

Kroo, I. M. and Shevell, R. S., "Aircraft Design: Synthesis and Analysis," Desktop Aeronautics Inc., 2006

Kurzke, J., "GasTurb," 2004: Gas Turbine Cycle Analysis Programme. www.gasturb.de

Kusters, B., Schreiber, H-A., Koller, U., and Monig, R., "Development of Advanced Compressor Airfoils for Heavy-Duty Gas Turbines - `Part II: Experimental and Theoretical Analysis," *Journal of Turbomachinery*, Vol. 122, 2000, pp. 406-15.

Law, C. H. and Wadia, A. R., "Low Aspect Ratio Transonic Rotors: Part 1 - Baseline Design and Performance," *Journal of Turbomachinery*, Vol. 115, 1993, pp. 218-25.

Law, T. R. and Dowling, A. P., "Optimization of Traditional and Blown Liners for a Silent Aircraft," *12th AIAA/CEAS Aeroacoustics Conference*, Cambridge, Massachusetts, 2006. AIAA-2006-2525.

Law, T. R. and Dowling, A. P., "Optimisation of Annular and Cylindrical Liners for Mixed Exhaust Aeroengines," *13th AIAA/CEAS Aeroacoustics Conference*, Rome, Italy, 2007 (to be published)

Lewy, S., "Experimental Study of Fan Broadband Noise on a Turbofan model," *7th Ineternational Congress on Sound and Vibration*, Garmish-Partenkirchen, Germany, 2000

Lighthill, M. J., "On sound generated aerodynamically (Part I: General theory)," *Proceedings of the Royal Society of London. Series A: Mathmatical and Physical Sciences*, Vol. 211, No. 1107, 1952, pp. 564-87.

Lighthill, M. J., "On Sound Generated Aerodynamically (Part II: Turbulence as a Source of Sound)," *Proceedings of the Royal Society of London. Series A: Mathmatical and Physical Sciences*, Vol. 222, No. 1148, 1954, pp. 1-32.

Lighthill, M. J., "The Bakerian Lecture: Sound Generated Aerodynamically," *Proceedings of the Royal Society of London. Series A: Mathmatical and Physical Sciences*, Vol. 267, No. 1329, 1962, pp. 147-82.

Lilley, G. M., "On the Noise from Jets," *Noise Mechanisms*, Brussels, Belgium, 1974. AGARD-CP-131 (13.1-13.12).

Lilley, G. M., "Jet Noise Classical Theory and Experiments," in *Aeroacoustics of Flight Vehicles: Theory and Practice, Volume 1: Noise Sources*, H.H. Hubbard, Editor. 1991, published by NASA. RP-1258, WRDC Technical Report 90-3052.

Lopez-Diez, A., Rodriguez, M., San Segundo, M. P., and Minguez, B., "Applications of Variable Area Nozzles for Civil Airplanes," *34th AIAA/ASME/SAE/ASEE Joint Propulsion Conference & Exhibit*, Cleveland, Ohio, 1998

Low, J.K.C., "Ultra-High Bypass Ratio Jet Noise," NASA CR-195394, 1994

Manneville, A., "Propulsion System Concepts for Silent Aircraft," Master of Science Dissertation, Massachusetts Institute of Technology, Cambridge, MA, 2004.

Marble, F. E. and Candel, S. M., "Acoustic disturbance from gas non-uniformities covected through a nozzle," *Journal of Sound and Vibration*, Vol. 55, No. 2, 1977, pp. 225-43.

Massey, K. C., Ahuja, K. K., and Gaeta, R., "Noise Scaling for Unheated Low Aspect Ratio Rectangular Jets," *10th AIAA/CEAS Aeroacoustics Conference*, Manchester, England, 2004. AIAA-2004-2946.

McAlpine, A. and Fisher, M. J., "On the prediction of "buzz-saw" noise in aero-engine inlets," *Journal of Sound and Vibration*, Vol. 248, No. 1, 2001, pp. 123-49.

McAlpine, A. and Fisher, M. J., "On the prediction of "buzz-saw" noise in acoustically lined aero-engine inlet ducts," *Journal of Sound and Vibration*, Vol. 265, 2003, pp. 175-200.

McAlpine, A., Fisher, M. J., and Tester, B. J., ""Buzz-saw" noise: A comparison of measurement with prediction," *Journal of Sound and Vibration*, Vol. 290, 2006, pp. 1202-33.

McCune, J. E. and Kerrebrock, J. L., "Noise from Aircraft Turbomachinery," *Annual Review of Fluid Mechanics*, Vol. 5, 1973, pp. 281-300.

MetOffice, "Land Surface Observation Stations Data," British Atmospheric Data Centre. http://badc.nerc.ac.uk/data/surface/

Mikhail, S., "Mixing of coaxial streams inside a closed conduit," *Journal of Mechanical Engineering Science*, Vol. 2, No. 1, 1960, pp. 59-68.

Miller, M. M., "Sound and Furor: The Jet Noise Suppression Age," *SAE Transactions*, Vol. 65, 1957, pp. 595-607.

Moore, C. J., "The role of shear-layer instability waves in jet exhaust noise," *Journal of Fluid Mechanics*, Vol. 80, No. 2, 1977, pp. 321-67.

Morfey, C. L., "Amplification of aerodynamic noise by convected flow inhomogeneities," *Journal of Sound and Vibration*, Vol. 31, No. 4, 1973, pp. 391-7.

Morfey, C. L. and Fisher, M. J., "Shock-Wave Radiation from a Supersonic Ducted Rotor," *The Aeronautical Journal of the Royal Aeronautical Society*, Vol. 74, 1970, pp. 579-85.

Morfey, C. L., Szewczyk, V. M., and Tester, B. J., "New scaling laws for hot and cold jet mixing noise based on a geometric acoustics model," *Journal of Sound and Vibration*, Vol. 61, No. 2, 1978, pp. 255-92.

Morris, P. J. and Boluriaan, S., "The Prediction of Jet Noise From CFD Data," *10th AIAA/CEAS Aeroacoustics Conference*, Manchester, UK, 2004. AIAA-2004-2977.

Munro, S. E. and Ahuja, K. K., "Aeroacoustics of a high aspect ratio jet," *9th AIAA/CEAS Aeroacoustics Conference*, Hilton Head, South Carolina, 2003. AIAA-2003-3323.

Munt, R. M., "The Interaction of Sound with a Subsonic Jet Issuing from a Semi Infinite Cylindrical Pipe," *Journal of Fluid Mechanics*, Vol. 83, 1977, pp. 609-40.

Nallasamy, M. and Envia, E., "Computation of rotor wake turbulence noise," *Journal of Sound and Vibration*, Vol. 282, 2005, pp. 649-78.

Neubert, R. J., Bock, L., Malmborg, E. W., and Owen-Peer, W., "Advanced Low-Noise Research Fan Stage Design," NASA CR-97-206308, 1997

NoisedB, "Noise Certification Database," 2007, International Civil Aviation Organization. http://noisedb.stac.aviation-civile.gouv.fr/find.php

North, W. J. and Coles, W. D., "Effect of exhaust nozzle ejectors on turbojet noise generation," NACA TN-3573, 1955

NWS, "SCRAM Surface Meteorological Archived Data," 1984-1992, National Weather Service

Olsen, W. A. and Friedman, R., "Jet Noise from Coaxial Nozzles over a wide range of Geometric and Flow Parameters," *12th Aerospace Sciences Meeting*, Washington, D.C., 1974. AIAA-1974-43.

Owens, R. E., "Energy Efficient Engine Propulsion System-Aircraft Integration Evaluation," NASA CR-159488, 1979

Parliament, UK, "Noise: Final Report," Committee on the Problem of Noise, UK Parliament, 1963

Passrucker, H., Engber, M., Kablitz, S., and Hennecke, D. K., "Effects of forward sweep in a transonic compressor rotor," *Proceedings of the Institution of Mechanical Engineers, Part A:Journal of Power and Energy*, Vol. 217, No. 4, 2003, pp. 357-65.

Peacock, N. J. and Sadler, J. H. R., "Advanced Propulsion Systems for Large Subsonic Transports," *25th ASME, SAE and ASEE Joint Propulsion Conference*, Monterey, California, 1989. AIAA-89-2477.

Pilczer, Deborah, "Noise Reduction Assessments and Preliminary Design Implications for a Functionally-Silent Aircraft," Master of Science Dissertation, Massacusetts Institute of Technology, Cambridge, MA, 2003.

Pinker, R. A. and Strange, P.J.R., "The Noise Benefits of Forced Mixing," *4th AIAA/CEAS Aeroacoustics Conference*, Toulouse, France, 1998. AIAA-1998-2256.

Pla, F. G., Hu, Z., and Sutliff, D. L., "Active Fan Noise Cancellation in the NASA Lewis Active Noise Control Fan Facility,"NASA/CR-1985111, 1996

Platzer, M. F. and Carta, F. O., eds. "Aeroelasticity in Axial-Flow Turbomachines." 1988. AGARD-AG-298.

Plumblee, H. E., "Effects of forward velocity on turbulent jet mixing noise," NASA CR-2702, 1976

Power, B., "Aspirated Compressor Design," Cambridge University, 2006, *personal communication*

Presz, W., Reynolds, G., and Hunter, C., "Thrust Augmentation with Mixer/Ejector Systems," *40th AIAA Aerospace Sciences Meeting & Exhibit*, Reno, Nevada, 2002. AIAA-2002-0230.

Rey, N. M., Tillman, G., Miller, R. M., Wynosky, T., Larkin, M. J., Flamm, J. D., and Bangert, L. S., "Shape memory alloy actuation for a variable area fan nozzle," *Proceedings of SPIE*, Vol. 4332, 2001, pp. 371-82.

Rienstra, S. W., "A small strouhal number analysis for acoustic wave-jet flow-pipe interaction," *Journal of Sound and Vibration*, Vol. 86, No. 4, 1983, pp. 539-56.

SAE, "Gas Turbine Jet Exhaust Noise Prediction,"ARP876 revision D, 1994

Saiyed, N. H., Mikkelsen, K. L., and Bridges, J. E., "Acoustics and Thrust of Quiet Separate-Flow High-Bypass-Ratio Nozzles," *AIAA Journal*, Vol. 41, No. 3, 2003, pp. 372-8.

Sausen, R., Gierens, K., Ponater, M., and Schumann, U., "A Diagnostic Study of the Global Distribution of Contrails Part I: Present Day Climate," *Theoretical and Applied Climatology*, Vol. 61, No. 3-4, 1998, pp. 127-41.

Schlichting, H., "Boundary-Layer Theory." 1968, New York: McGraw-Hill

Schwartz, E., "Environmental Assessment of Silent Aircraft Technologies," MPhil Dissertation, Department of Engineering, Cambridge University, 2006.

Seddon, J. and Dyke, M., "Ejectors and mixing streams, Royal Aircraft Establishment Library Bibliography No. 252." 1964: Ministry of Aviation

Shahpar, S., "SOFT: A New Design and Optimisation Tool for Turbomachinery," *Evolutionary Methods for Design, Optimisation and Control*, Barcelona, 2002

Shahpar, S. and Lapworth, L., "PADRAM: Parametric Design and Rapid Meshing System for Turbomachinery Optimisation," *Proceedings of ASME Turbo Expo 2003*, Atlanta, Georgia, 2003. GT-2003-38698.

Smith, C. P., "The Environmental Challenge - Bringing Technology to Market," *International Symposium on Air Breathing Engines*, Munich, Germany, 2005. ISABE-2005-1008.

Smith, M. J. T., "Aircraft Noise." 1 ed. Cambridge Aerospace Series. 1989: Cambridge University Press. ISBN 0-521-33186-2.

Snyder, L. E. and Burns, D. W., "Forced Vibration and Flutter Design Methadology," in *Aeroelasticity in Axial Flow Turbomachines*, M.F. Platzer and F.O. Carta, Editors. 1988. AGARD-AG-298.

Song, G., Ma, N., Lee, H., and Arnold, S., "Design and control of a proof-of-concept variable area exhaust nozzle using shape-memory alloy actuators," *Proceedings of SPIE*, Vol. 5388, 2004, pp. 78-86.

Stone, J. R., "Interim prediction method for Jet Noise," NASA X-71618, 1974

Stone, J. R., Groesbeck, D. E., and Zola, C. L., "An improved prediction method for noise generated by conventional profile coaxial jets," NASA TM-82712, 1981

Stone, J. R., Groesbeck, D. E., and Zola, C. L., "Conventional Profile Coaxial Jet Noise Prediction," *AIAA Journal*, Vol. 21, No. 3, 1983, pp. 336-42.

Stone, J. R., Krejsa, E. A., and Clark, B. J., "Jet Noise Modeling for Coannular Nozzles Including the Effects of Chevrons," NASA CR-2003-212522, 2003

Stone, J. R. and Montegani, F.J., "An Improved Prediction Method for the Noise Generated in Flight by Circular Jets," NASA TM-81470, 1980

Stone, J. R., Zola, C. L., and Clark, B. J., "An Improved Model for Conventional and Inverted-Velocity-Profile Coannular Jet Noise," *37th AIAA Aerospace Sciences Meeting and Exhibit*, Reno, Nevada, 1999. AIAA-99-0078.

Strange, P.J.R. and Bryce, W.D., "The Conceptual Design of Nozzle/Ejector Configurations for Large Jet Noise Reductions," *14th DGLR/AIAA Aeroacoustics Conference*, Aachen, Germany, 1992

Sutliff, D. L., Tweedt, D. L., Fite, E. B., and Envia, E., "Low-Speed Fan Noise Reduction with Trailing Edge Blowing," NASA TM-2002-211559, 2002

Tam, C.K.W., "Jet Noise Generated by Large-Scale Coherent Motion," in *Aeroacoustics of Flight Vehicles: Theory and Practice*, H. Hubbard, Editor. 1991, published by NASA, Reference Publication 1258

Tam, C.K.W. and Auriault, L., "Jet Mixing Noise from Fine-Scale Turbulence," *AIAA Journal*, Vol. 37, No. 2, 1999, pp. 145-53.

Tam, C.K.W., Golebiowski, M., and Seiner, J. M., "On the two components of turbulent mixing noise from supersonic jets," *2nd AIAA/CEAS Conference*, State College, Pennsylvania, 1996. AIAA-1996-1716.

Tam, C.K.W. and Zaman, K.B.M.Q., "Subsonic Jet Noise from Nonaxisymetric and Tabbed Nozzles," *AIAA Journal*, Vol. 38, No. 4, 2000, pp. 592-9.

Tanna, H. K., Dean, P. D., and Fisher, M. J., "The influence of temperature on shock free supersonic jet noise," *Journal of Sound and Vibration*, Vol. 39, No. 4, 1975, pp. 429-60.

Tester, B. J. and Fisher, M. J., "A contribution to the understanding and prediction of jet noise generation in forced mixers: Part II Flight Effects," *11th AIAA/CEAS Aeroacoustics Conference*, Monterey, California, 2005. AIAA-2005-3094.

Tester, B. J., Fisher, M. J., and Dalton, W.N., "A contribution to the understanding and prediction of jet noise generation in forced mixers," *10th AIAA/CEAS Aeroacoustics Conference*, Manchester, UK, 2004. AIAA-2004-2897.

Tew, D. E., Teeple, B. S., and Waitz, I. A., "Mixer-Ejector Noise-Suppressor Model," *Journal of Propulsion and Power*, Vol. 14, No. 6, 1998, pp. 941-50.

Topol, D. A., Ingram, C. L., Larkin, M. J., Roche, C. H., and Thulin, R. D., "Advanced Subsonic Technology (AST) 22-Inch Low Noise Research Fan Rig Preliminary Design of ADP-Type Fan 3," NASA CR-2004-212718, 2004

Tyler, J. M. and Sofrin, T. G., "Axial Flow Compressor Noise Studies," *Transactions of the Society of Automotive Engineers*, Vol. 70, 1962, pp. 309-32.

Visser, H. G. and Wijnen, R. A. A., "Optimization of Noise Abatement Departure Trajectories," *Journal of Aircraft*, Vol. 38, No. 4, 2001, pp. 620-6.

Viswanathan, K., "Aeroacoustics of hot jets," *Journal of Fluid Mechanics*, Vol. 516, 2004, pp. 39-82.

Viswanathan, K., "Nozzle Shaping for Reduction of Jet Noise from Single Jets," *AIAA Journal*, Vol. 43, No. 5, 2005, pp. 1008-22.

Wadia, A. R. and Copenhaver, W. W., "An Investigation of the Effects of Cascade Area Ratios on Transonic Compressor Performance," *Journal of Turbomachinery*, Vol. 118, 1996, pp. 760-70.

Wadia, A. R. and Law, C. H., "Low Aspect Ratio Transonic Rotors: Part 2 - Influence of Location of Maximum Thickness on Transonic Compressor Performance," *Journal of Turbomachinery*, Vol. 115, 1993, pp. 226-39.

Wadia, A. R., Szucs, P. N., and Crall, D. W., "Inner Workings of Aerodynamic Sweep," *Journal of Turbomachinery*, Vol. 120, 1998, pp. 671-82.

Waitz, I. A., Qiu, Y. J., Manning, T. A., Fung, A. K. S., Elliot, J. K., Kerwin, J. M., Krasnodebski, J. K., O'Sullivan, M. N., Tew, D. E., Greitzer, E. M., Marble, F. E., Tan, C. S., and Tillman, T. G., "Enhanced Mixing with Streamwise Vorticity," *Progress in Aerospace Science*, Vol. 33, 1997, pp. 323-51.

Weinstein, A. S., Osterle, J. F., and Forstall, W., "Momentum Diffusion from a Slot Jet into a moving secondary," *Journal of Applied Mechanics*, 1956, pp. 437-43.

Weir, D. S. and Mendoza, J.M., "Static and Flight Aeroacoustic Evaluations of a Variable Exhaust Nozzle," *11th AIAA/CEAS Aeroacoustics Conference*, Monterey, California, 2005. AIAA-2005-3049.

Wennerstrom, A. J., "Experimental Study of a High-Through-Flow Transonic Axial Compressor Stage," *ASME Journal of Engineering for Gas Turbines and Power*, Vol. 106, 1984, pp. 552-60.

Wennerstrom, A. J., "Design of highly loaded axial-flow fans and compressors." 2000. ISBN 0-933283-11-3.

Whurr, J. R., "Variable Area Nozzle" Patent Number US 2005/0229586 A1 United States, 2005, assigned to Rolls Royce plc.

Wijnen, R. A. A. and Visser, H. G., "Optimal departure trajectories with respect to sleep disturbance," *Aerospace Science and Technology*, Vol. 7, 2003, pp. 81-91.

Williams, V., Noland, R. B., and Toumi, R., "Reducing the climate change impacts of aviation by restricting cruise altitudes," *Transportation Research Part D*, Vol. 7, 2002, pp. 451-64.

Winant, C. D. and Broward, F. K., "Vortex Pairing: The Mechanism of Turbulent Mixing Layer Growth at Moderate Reynolds Number," *Journal of Fluid Mechanics*, Vol. 63, 1974, pp. 237-55.

Wood, J. R., Strazisar, A. J., and Simonyi, P. S., "Shock structure measured in a transonic fan using laser anemometry," *AGARD Conference : Transonic and Supersonic Phenomena in Turbomachines*, Munich, 1986. CP401.

Woodward, R. P., Elliot, D. B., Hughes, C. E., and Berton, J. J., "Benefits of Swept and Leanded Stators for Fan Noise Reduction," *Journal of Aircraft*, Vol. 38, No. 6, 2001, pp. 1130-8.

Woodward, R. P., Hughes, C. E., Jeracki, R., and Miller, C. J., "Fan Noise Source Diagnostic Test - Far Field Acoustic Results," *8th AIAA/CEAS Aeroacoustics Conference & Exhibit*, Breckenridge, Colorado, 2002. AIAA-2002-2427.

Woodward, R. P. and Lucas, J. G., "Acoustic and Aerodynamic Performance of a 1.83 meter diameter 1.25 pressure ratio fan (QF-8)," NASA TN D-8130, 1976

Xu, L., "Shockwave and noise abatement of transonic fans," *ASME Turbo Expo: Power for Land, Sea and Air*, Vienna, Austria, 2004. GT2004-53545.

Yu, J., Kwan, H., Chien, E., Ruiz, M., Nesbitt, E., Uellenberg, S., Premo, J., and Czech, M., "Quiet Technology Demonstrator 2 - Intake Liner Design and Validation," *12th AIAA/CEAS Aeroacoustics Conference*, Cambridge, Massachusetts, 2006. AIAA-2006-2458.

Zaman, K.B.M.Q., Wang, F.Y., and Georgiadis, N.J., "Noise, Turbulence, and Thrust of Subsonic Freejets from Lobed Nozzles," *AIAA Journal*, Vol. 41, No. 3, 2003, pp. 398-406.

Zorumski, W., "Aircraft Noise Prediction Program Theoretical Manual," NASA TM-83100, 1982

Appendices

Appendix A: Take-off regulations and operational requirements

REGULATION

A range of regulation exists in the area of take-off covering both safe and quiet take-off.

Joint Aviation Regulation and Federal Aviation Regulations

Section 25 of the JAA Joint Aviation Regulations (JAA) covers airworthiness standards for transport aircraft. Sections 105 to 121 and Appendix I cover take-off with the following key requirements relating to engine design:

Section 25.107

- V_{EF} is the calibrated airspeed at which the critical engine is assumed to fail.
- V_1 may not be less than V_{EF} plus the speed gained with the critical engine inoperative for 2 seconds.
- V_R may not be less then V_1 and a single value of V_R must be used to show compliance both with all engines operating and one engine inoperative.
- It must be shown that using a rotation speed of V_R – 5 knots (2.57m/s) with one engine inoperative does not exceed the one engine inoperative take-off distance based on a rotation speed of V_R.
- V_2 may not be less than V_R and must have been reached by the time a height of 35ft is attained.
- V_{LOF} is the airspeed at which the plane first becomes airborne.
- V_{FTO} is a speed selected by the applicant at which engine out climb can occur and the aircraft manoeuvre.

Section 25.109

- The accelerate stop distance on a dry runway is the greater of:
    - The distance to accelerate to V_1 with engine failure at V_{EF}, stay at V_1 for 2 seconds and then come to a complete stop on a dry runway without the use of thrust reversers.

  - The distance to accelerate to V_1 without engine failure, stay at V_1 for 2 seconds and then come to a complete stop on a dry runway without the use of thrust reversers.

- The accelerate stop distance on a wet runway is calculated in the same way except thrust reversers may be used and the maximum allowable braking coefficients are specified in the regulations.

Section 25.111

- Climb gradients above 400 feet must be at or above 1.7% for 4 or more engines (1.5% if 3 and 1.2% if 2) with one engine inoperative.
- May not make any change in power or thrust that requires action by the pilot until 400 feet except for gear retraction or automatic propeller feathering

Section 25.123

- The take-off distance on a dry runway is the greater of:
  - The distance required to reach an altitude of 35ft with engine failure occurring at V_{EF}.
  - 115% of the distance required to reach an altitude of 35ft with all engines operating.
- The take-off distance on a wet runway is the greater of:
  - The take-off distance on a dry runway
  - The distance required to reach an altitude of 15ft with engine failure occurring at V_{EF} assuming V_2 is reached by 35ft.

Section 25.121

- With one engine out and landing gear extended, must be able to climb at 0.5% at V_{LOF} if 4 or more engines (0.3% if 3 and level flight if 2)
- With one engine out and landing gear retracted, must be able to climb at 3.0% at V_{LOF} if 4 or more engines (2.7% if 3 and 2.4% if 2) up to 400 feet.

- With one engine out in the en-route configuration up to 1500 feet, must be able to climb at 1.7% at V_{FTO} if 4 or more engines (1.5% if 3 and 1.2% if 2) at maximum available power.

Appendix I

- For aircraft with ATTCS (Automatic Takeoff Thrust Control System), the thrust available on engine out for the remaining engines can be increased to 111% of the thrust used before engine out. This 111% limit in the regulation is to limit the degradation in the event of ATTCS failure.

The FAA Federal Aviation Regulations closely match those of the JAA. Section 25 (FAA) covers airworthiness standards for transport aircraft.

ICAO PANS-OPS Volume 1 Part V

Part V Volume 1 of ICAO PANS-OPS (Procedures for Air Navigation Services – Aircraft Operations) (ICAO) specifies recommended safe cutback procedures based on the following:

- Cut-back cannot be initiated at a height of less than 800 feet.
- Thrust after cutback must be no less than that to maintain engine out required levels of climb (1.7% for 4 or more engines,1.5% if 3 engines and 1.2% if 2 engines).
- Flight speed after cutback must be no less than V_2.
- These requirements remain until the aircraft has reached 3000 feet or is fully transitioned to en route climb configuration.

No allowance is explicitly made for ATTCS equipped aircraft.

FAA Advisory Circular 91-53A

The FAA Noise Abatement Departure Profiles (FAA 1993) specify safe cutback procedures for use in the US. This AC is mandated in the US and is very similar to ICAO PANS-OPS Volume 1 Part V. One difference though is that for aircraft with ATTCS, the thrust available after cutback on engine-out only needs to be that required to maintain level flight (provided that the ATTCS will increase thrust to meet the minimum climb gradients).

OPERATIONS

In addition to regulations in relation to take-off, several non-technical operational constrains must be considered.

Typical airport requirements

A range of airports SIDs (Standard Instrument Departures) were looked at to see whether additional constraints are placed on the aircraft take-off requirement that may impact the Silent Aircraft:

- Heathrow (RWYS 27R/L, BPK 6F to 6G)
    - Designed for low noise routing
    - Minimum climb gradient of 4% (2.3°) until 4000'
- Birmingham (RWYS 33 and 15, CPT 3D and 1E and COWLEY 2D and 1E)
    - Designed for low noise routing
    - Minimum climb gradient of 4.8% (2.75°) up to FL50
    - Minimum climb gradient of 5% (2.86°) from there up to FL60
- Liverpool (RWYS 27 and 09, POL 4T and 5V)
    - Designed for low noise routing
    - Minimum climb gradient of 6.1% (3.5°) up to 4000'
- Madrid Barajas (RWY 15, PINAR1B)
    - Minimum climb gradient of 7% (4.0°) up to 14500'
- Madrid Barajas (RWY 36LNVS3E)
    - Minimum climb gradient of 7.5% (4.3°) up to 4500'
    - Only authorized aircraft

Based on this, an average climb angle of 4° for the first 1000m altitude and a minimum climb angle of 4° after this will meet operational requirements at the majority of airports. To meet remaining requirements a 6° climb angle should be supported in 'non-silent' mode.

Passenger Comfort

Whilst a maximum pitch up angle during take-off tends not to be imposed by airframe manufacturers, a 20° pitch up angle is often imposed by operators for passenger comfort. This will be imposed in this thesis.

REQUIRED CLIMB ANGLES FOR ENGINE-OUT CONDITION

Taking the angle of thrust as equal to the angle of flight, the required minimum angle of climb prior to an engine out can be calculated as follows assuming thrust can be increased 11% using ATTCS:

$$\theta_{\min} \approx \max\left[\sin^{-1}\left(\frac{n_{eng}}{n_{eng}-1}\frac{1}{L/D}\Big|_{after} - \frac{1}{L/D}\Big|_{before}\right), \sin^{-1}\left(\frac{1}{1.11}\frac{n_{eng}}{n_{eng}-1}\left(\frac{1}{L/D}\Big|_{after} + \sin\theta^*\right) - \frac{1}{L/D}\Big|_{before}\right)\right]$$

where n_{eng} is the number of engines and θ^* is the mandated minimum climb angle after engine out. The first of these two equations ensures that even if thrust is not increased the aircraft can maintain level flight. If there is no credit for ATTCS, then the equation becomes.

$$\theta_{\min} \approx \sin^{-1}\left(\frac{n_{eng}}{n_{eng}-1}\left(\frac{1}{L/D}\Big|_{after} + \sin\theta^*\right) - \frac{1}{L/D}\Big|_{before}\right)$$

AVAILABLE RUNWAY LENGTH FOR TAKE-OFF

The critical condition on take off is the greater of the accelerate stop distance and the take-off distance. To enable calculation of required thrust and engine size, these requirements can be translated into required distances to reach specified speeds for a given runway length. Figure A1 shows a simplified view of the forces on the aircraft while on the runway:

- L = $\frac{1}{2}\rho A_{wing} c_L V_\infty^2$ is the lift
- D = $\frac{1}{2}\rho A_{wing} c_D V_\infty^2$ is the aerodynamic drag

- $\eta\mu$(mg-L) is the force through the tyres with η the efficiency of the anti-lock braking system (max of 0.8 when wet under braking, 1 otherwise) and μ the braking coefficient (it is assumed that braking occurs on all wheels)
- T_N is the thrust produced by the aircraft engines
- mg is the aircraft weight

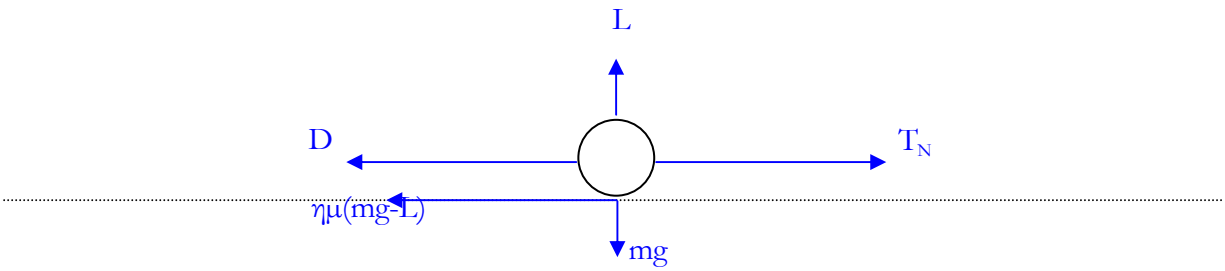

Figure A1: Forces on aircraft when on runway

Resolving horizontally;

$$T_N - \tfrac{1}{2}\rho A_{wing} c_D V_\infty^2 - \eta\mu\left(mg - \tfrac{1}{2}\rho A_{wing} c_L V_\infty^2\right) = m\frac{dV_\infty}{dt}$$

Integrating between two velocities;

$$s = \int_{V_\infty=V_a}^{V_\infty=V_b} V_\infty dt = \int_{V_\infty=V_a}^{V_\infty=V_b} \frac{V_\infty}{dV_\infty/dt} dV_\infty = \int_{V_\infty=V_a}^{V_\infty=V_b} \frac{mV_\infty}{\left(T_N - \tfrac{1}{2}\rho A_{wing} c_D V_\infty^2 - \eta\mu\left(mg - \tfrac{1}{2}\rho A_{wing} c_L V_\infty^2\right)\right)} dV_\infty$$

Accelerate stop distance

The accelerate stop distance can be split into four phases:

- s_a = distance to accelerate to V_{EF}.
- s_b = distance to accelerate from V_{EF} to V_1 after engine failure at V_{EF}.
- s_c = 2 seconds whilst travelling at V_1.
- s_d = distance to brake to a halt from V_1.

The acceleration distances s_a and s_b are determined by normal operating conditions as reaction to engine out does not occur until V1 is reached. Therefore the available runway length will determine what s_a+s_b can be.

With maximum stopping distance on a wet runway, and with maximum braking coefficients specified by the JAA and FAA for wet conditions as a function of V_∞, estimates of maximum required stopping distance can be specified.

$$s_d = \frac{1}{\eta g}\int_{V_\infty=V_1}^{V_\infty=0} \frac{V_\infty}{c_1 V_\infty^3 + (c_2+c_0)V_\infty^2 + c_3 V_\infty + c_4} dV_\infty,$$

$$c_0 = \frac{\rho A_{wing} c_D}{2mg\eta},\ c_1 \text{ to } c_4 \text{ speciefied in JAR 25.109}$$

It is assumed here that the aircraft is providing no lift (or down force) and no thrust (forwards or reverse) during braking:

Take-off distance

The take-off distance can be split into four phases:

- s_a = distance to accelerate to V_{EF}.
- s_b = distance to accelerate from V_{EF} to V_1 possibly after engine failure at V_{EF}.
- s_c = distance to accelerate from V_1 to V_R
- s_d = distance to rotate and climb to 35 feet whilst accelerating to V_2 (15 feet in wet conditions)

The critical take-off distance is the maximum of:

(a) 115% of $s_a+s_b+s_c+s_d$ with no engine failure in dry conditions

(b) $s_a+s_b+s_c+s_d$ with engine failure in dry conditions

(c) $s_a+s_b+s_c+s_d$ with engine failure in wet conditions

Which of these distances is determined by a range of factors including the number of engines. For the level of design detail of the silent aircraft, (b) and (c) will be the same therefore two conditions need to be looked at when evaluating the required runway length for take-off.

Appendix B: Comparison of different jet noise models

With the engines designed from the ground up to deliver the required jet noise level, the selection of jet noise model is critical. In this appendix two comparisons are made using different noise models. Firstly, for a pre-determined flight path created with the nozzle area varying as discussed in chapter four, noise on the ground is compared. Secondly, for a fixed nozzle area, take-off is optimised using different noise models with the goal of meeting the same jet noise target.

COMPARING PREDICTED NOISE AT SPECIFIED FLIGHT POINTS

To produce the low jet noise required during take-off whilst maintaining thrust requires low jet velocity and low specific thrust. Specific points where comparisons can be made are at the start of roll, sideline and flyover conditions. Start of roll removes any flight effects corrections in the models, sideline is at maximum absolute jet velocity and flyover has high V_∞/V_{jet}. The values of thrust, flight velocity etc used for these points are based on the use of the Stone model with modified flight effects from Low using an early airframe design under a jet noise limit of 54dBA outside the airport boundary.

Table B1 lists all of the relevant data for these three points.

For the start of roll and sideline conditions, jet noise is predicted along the airport boundary parallel and 450m away from the runway centreline. For the flyover condition, jet noise is predicted directly below the aircraft. Angle of attack and climb angle are considered when linking polar angles to location on the ground and atmospheric and lateral attenuation are taken into account using ESDU models (ESDU 1977, 1982). A 3dB correction is made for ground reflection and, as the airframe configuration has three engines, a $10\log_{10}(3)$ correction is made to the single engine predictions. Figure B1 presents the result of this work with noise on the ground outside the airport in dBA predicted using the three different noise models. The modified flight correction exponent proposed by Low has been used to modify the SAE and Stone models and the predictions from this are shown alongside the unmodified predictions. Figure B2 shows the predicted frequency distribution of the noise for the different models at a point perpendicular to the aircraft.

COMPARING TAKE-OFF PROFILE FOR GIVEN JET NOISE LIMIT

In determining which model to use as a basis for silent aircraft noise predictions it is worth looking at how the noise model selected impacts the take-off profile and required jet area for a specific noise level during take-off. With the ESDU model requiring a large degree of extrapolation and the unmodified SAE ARP model predicting much higher noise during flight than all the other models only the following three models have been used:

- Original Stone model
- Stone model with modified flight correction
- SAE ARP876 model with modified flight correction

Figure B3 shows the result of this work for the three models under test. Whilst for the data in table B1 the nozzle is changed to keep on a specified fan operating line, here the nozzle area is fixed for the noise critical portion of the take-off. This is to ensure fan operation and choking does not complicated any comparisons.

To meet the noise level and successfully take-off when using the unmodified Stone jet noise model required a nozzle area per engine of 4.67m^2. With the required thrust levels the same for all three models at the flyover position (same velocity, no acceleration and same angle of climb) the models that predict lower acoustic power at flyover do not require the aircraft to be as high above the ground. Therefore the equivalent nozzle area when using the modified Stone model is 8 % less at 4.29m^2 and when using the modified SAE model it is 24% less at 3.54m^2. To be at a higher altitude at the flyover position requires the aircraft to accelerate quicker and take-off earlier and this can be seen in the top two sub plots of figure B3. The lower two subplots show how the two parameters most critical in the prediction of jet noise, V_j/a_0 and V_a/V_j, vary during take-off.

		Start of roll	**Sideline**	**Flyover**
Aircraft Parameters	Height	0m	44m	206m
	Sideline Distance	450m	450m	0m
	Flight Velocity	0m/s	82m/s	82m/s
	Angle of climb	0°	7.0°	2.4°
	Angle of attack	4.5°	15.0°	15.5°
Engine Parameters	Net Thrust per engine	96.7kN	95.8kN	55.6kN
	Jet Velocity	132.4m/s	196.1m/s	155.3m/s
	Nozzle area	5.06m^2	3.97m^2	4.52m^2
	Fan Pressure Ratio	1.178	1.280	1.183
	Jet temperature	307.5K	309.3K	306.9K
	Jet stagnation temperature	316.3K	328.4K	318.9K
	Jet density	1.148 kgm^{-3}	1.135 kgm^{-3}	1.122 kgm^{-3}
Free Stream Parameters	Atmospheric conditions	ISA + 12K sea level		
	Temperature	300.15K	299.9K	298.8K
	Stagnation Temperature	300.15K	303.2K	302.2K
	Density	1.176 kgm^{-3}	1.171 kgm^{-3}	1.153 kgm^{-3}

Table B1: Parameters used for jet noise comparison

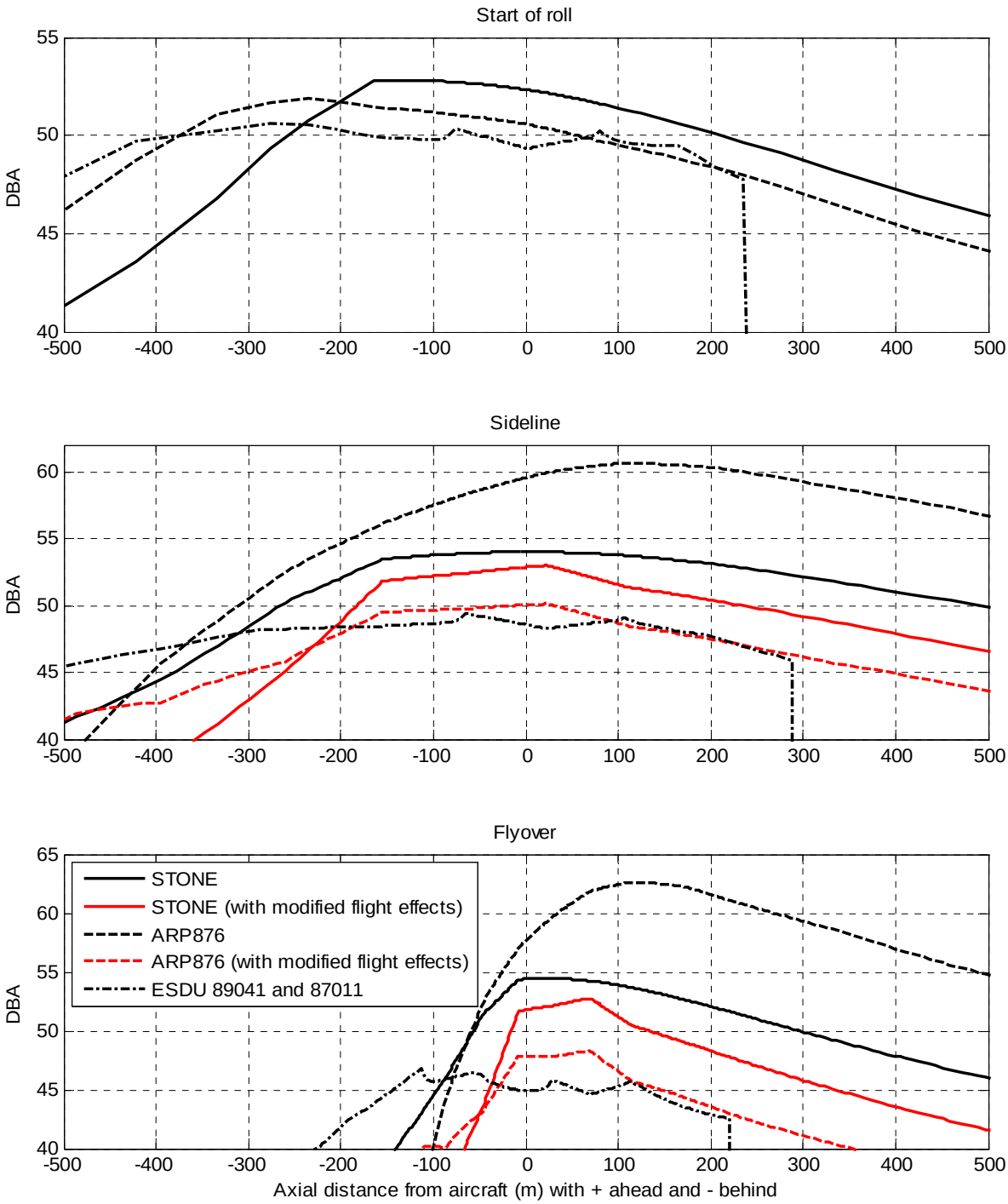

Figure B1: Comparison of predicted jet noise outside the airport boundary in dBA at start of roll, sideline and approach positions based on a take-off profile optimised using the Stone model with Low flight corrections.

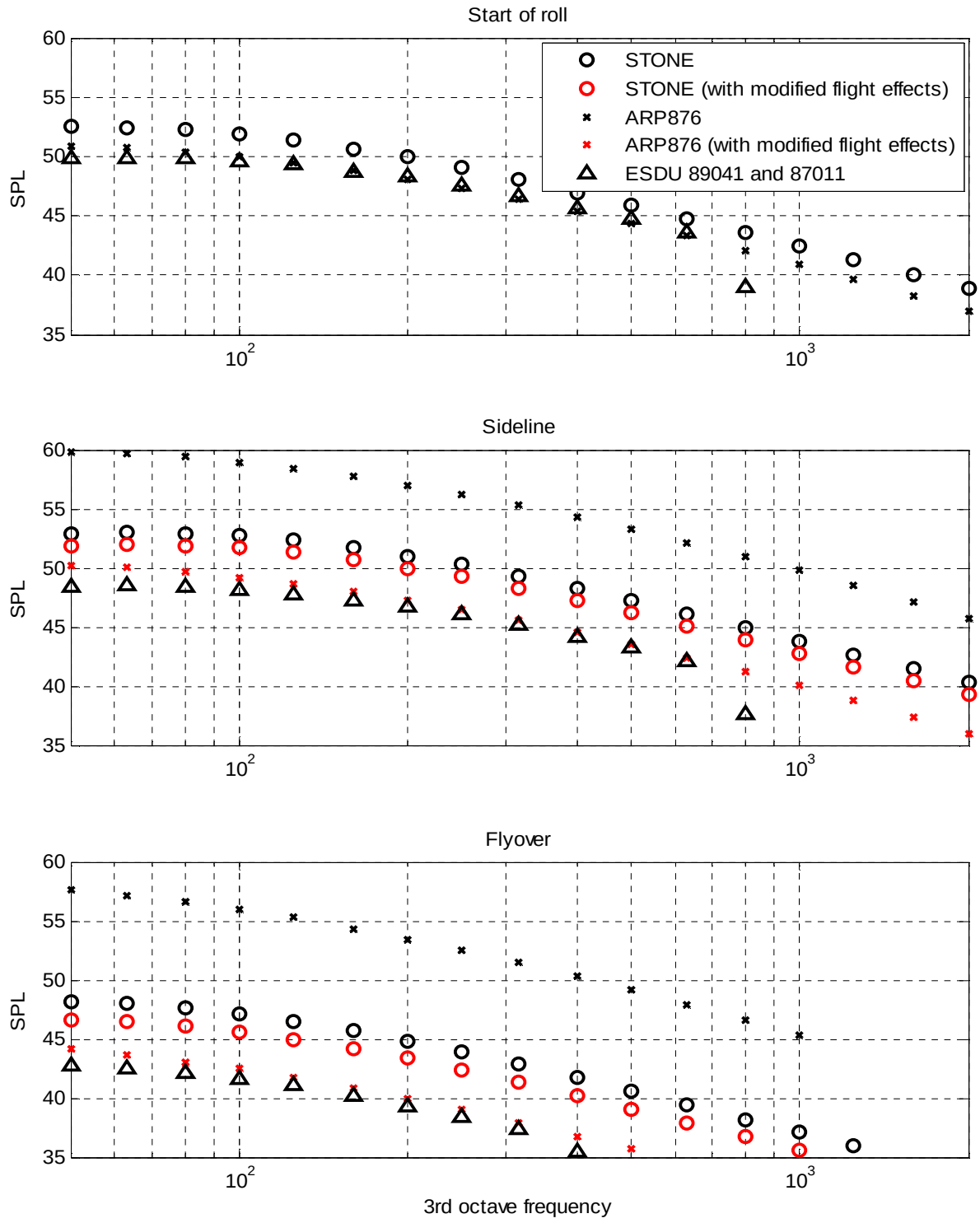

Figure B2: Comparison of predicted jet noise outside the airport boundary in SPL perpendicular to the aircraft at start of roll, sideline and approach positions. (Atmospheric attenuation not included and no correction for number of engines)

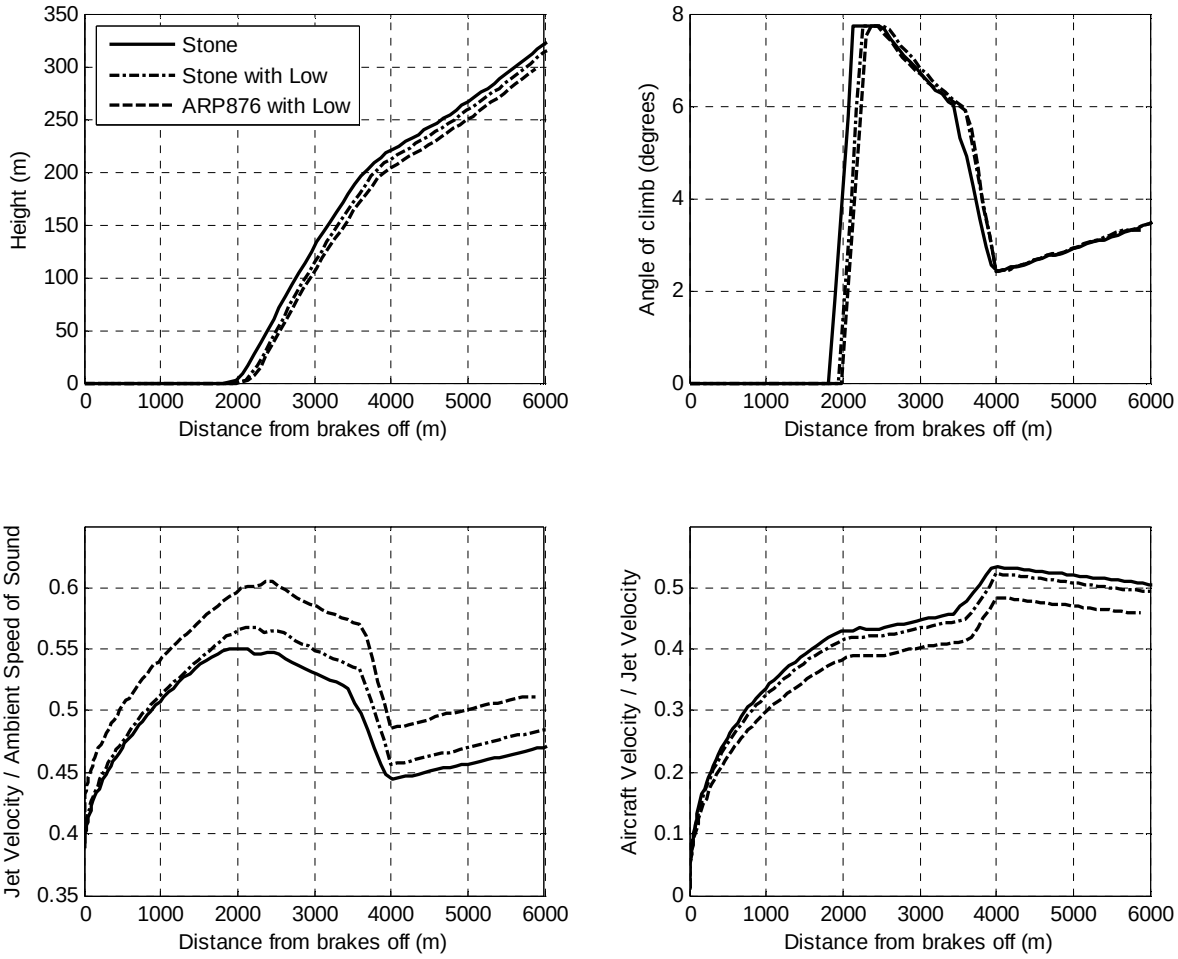

Figure B3: Variation in take-off profile for 3-engine aircraft whilst not exceeding 54dBA jet noise outside airport boundary using three different jet noise models.

Appendix C: Modelling of non-ideal ejection to predict jet noise reduction

To maximise noise reduction through ejection the primary jet from the engine should be completely mixed with the entrained airflow giving a uniform exit jet velocity. Limitations on ejection length and weight mean that this ideal is not met in reality and any model used at predicting possible noise reductions must account for this. Unforced mixing between a primary and secondary stream results in a bell shaped velocity profile (Weinstein *et al.* 1956, Mikhail 1960, Hill 1965, Fancher 1972) whilst for forced mixing using lobes, more complicated velocity profiles are found (Hu *et al.* 2002, Zaman *et al.* 2003). With the aim of the model to predict noise reduction the output parameters need to be compatible with a semi-empirical jet noise model such as those by Stone (Stone and Montegani 1980, Stone *et al.* 1981). This requires the exit flow to consist of two coaxial streams each of constant velocity.

INCOMPRESSIBLE MODELLING

With the use of ejection only occurring at low flight speeds, incompressible modelling can be used to give an indication of ejector effectiveness. This approach is similar to that of Presz but with extensions to include flight effects and non-ideal mixing (Presz *et al.* 2002). In addition, rather than quantify performance based on the primary jet velocity, performance is based on engine exit total pressure.

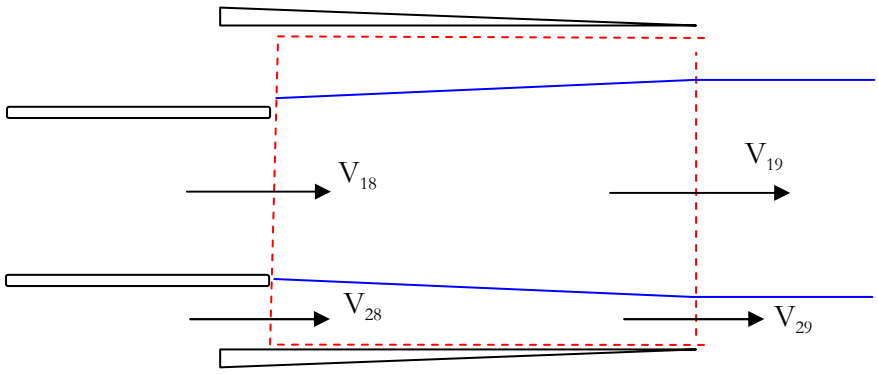

Figure C1: Control volume analysis of ejector with non-ideal mixing

The following assumptions are made in this analysis:

- All velocities are constant across their respective areas
- The ejector is of constant area
- Density is constant
- The static pressure across the inlet is constant

- The ejector exhausts at ambient pressure
- The secondary flow into the ejector is from ambient and Bernoulli's equation holds for this flow.
- Skin friction can be ignored.

Let us define the following parameters;

- Ejector exit to engine exit area ratio; $\alpha = \dfrac{A_9}{A_{18}}$
- Engine exit to free stream total pressure; $\Delta = \dfrac{p_{18} + \frac{1}{2}\rho V_{18}^2}{p_\infty + \frac{1}{2}\rho V_\infty^2}$
- Density to free stream static pressure ratio; $C = \dfrac{\rho}{p_\infty}$

For the ideal case where V_9=V_{19}=V_{29} applying conservation of mass and momentum in the control volume leads to the following quadratic in V_9 squared;

$$V_9^4\left[C^2\alpha^2\left(\alpha^2-8\alpha+8\right)\right]+\left[2(\Delta-1)(2\alpha-3)+CV_\infty^2\left(\alpha^2+2\Delta\alpha-3\Delta-4\alpha+3\right)\right]^2$$
$$-V_9^2\left[2C\alpha\left(2(\Delta-1)\left(2\alpha^2-9\alpha+8\right)+CV_\infty^2\left(8(\Delta-1)+\alpha\left(\alpha^2+2\Delta\alpha-9\Delta-8\alpha+15\right)\right)\right)\right]=0$$

From which the ideal exit velocity can be calculated. For the non ideal case let us conserve momentum overall whilst modelling the flow of momentum between the two streams:

$$\dot{m}_{19}V_{19} + p_{19}A_{19} = \dot{m}_{18}V_{18} + p_{18}A_{18} - \eta_{ejector}\left[\Delta\dot{m}V\right]_{ideal}$$

$$\dot{m}_{29}V_{29} + p_{29}A_{29} = \dot{m}_{28}V_{28} + p_{28}A_{28} + \eta_{ejector}\left[\Delta\dot{m}V\right]_{ideal}$$

where; $\left[\Delta\dot{m}V\right]_{ideal} = \left(A_{19}+A_{29}\right)V_\infty X$

and;
$$X^2\left[\alpha^2V_9^2\left(3-2\alpha\right)^2\right]+X\left[2\alpha V_9^2(\alpha-1)\left(3-2\alpha+CV_\infty^2\left(2\alpha^2-7\alpha+6\right)-CV_9^2\left(2\alpha^2-7\alpha+5\right)\right)\right]$$
$$+\left[\left(V_\infty^2-V_9^2\right)(\alpha-1)^2\left(2\alpha-3+CV_9^2\left(CV_\infty^2(\alpha-2)^2-(\alpha-1)\left(2+CV_9^2(\alpha-3)\right)\right)\right)\right]=0$$

In this equation V_9 is the ideal exit velocity calculated above.

This leads to the following set of simultaneous equations which can be solved to give exit velocities as a function on input parameters only.

$$p_\infty + \tfrac{1}{2}\rho V_\infty^2 = p_{28} + \tfrac{1}{2}\rho V_{28}^2$$
$$\rho A_{19}V_{19}^2 - \rho A_{18}V_{18}^2 = p_{28}A_{18} - p_\infty A_{19} - p_\infty A_9\eta X$$
$$\rho A_{29}V_{29}^2 - \rho A_{28}V_{28}^2 = p_{28}A_{28} - p_\infty A_{29} + p_\infty A_9\eta X$$
$$A_{18}V_{18} = A_{19}V_{19}$$
$$A_{28}V_{28} = A_{29}V_{29}$$
$$A_9 = A_{18} + A_{28} = A_{19} + A_{29}$$

Substituting in α, Δ and C leads to the following cubic equation for the static pressure ratio p_{28}/p_∞:

$$c_1\left(\frac{p_{28}}{p_\infty}\right)^3 + c_2\left(\frac{p_{28}}{p_\infty}\right)^2 + c_3\left(\frac{p_{28}}{p_\infty}\right) - c_4 = 0 \text{ where;}$$

$$c_1 = \alpha^2(\alpha - 1)$$

$$c_2 = \alpha^2\left(2\Delta - 5 + \alpha\left(5 - \alpha - 2\Delta + \eta X(\alpha - 2)\right) - CV_\infty^2(\alpha - 1)(1 + \Delta)\right)$$

$$c_3 = 4(1 - 2\alpha)(\Delta - 1)^2 + \alpha^4(\eta X - 2)(\eta X - 1) + 2\alpha^2\left(7 - 5\Delta + 2\Delta^2 + 3\eta X(\Delta - 1)\right) - 2\alpha^3\left(5 - \Delta + \eta X(2\Delta - 5)\right)$$
$$+CV_\infty^2\left((\alpha - 1)\left(4(\alpha - 1)(\Delta - 1)^2 + \alpha^2(3\Delta - 1)\right) - \eta X\alpha^2\left(3 - 3\Delta + 2\Delta\alpha + \alpha^2 - 4\alpha\right) + CV_\infty^2(\alpha - 1)(\alpha + \Delta - 1)(1 - \Delta + \alpha\Delta)\right)$$

$$c_4 = 4(\eta X\alpha - 2\alpha + 1)(\Delta - 1)^2 + \alpha^4(\eta X - 1)^2 + 2\alpha^3(\eta X - 1)\left(\eta X(\Delta - 1) + 2\right) + 4\alpha^2\left(2 - 2\Delta + \Delta^2 - \eta X(\Delta - 1)(\Delta - 2)\right)$$
$$+CV_\infty^2\Big[2(\alpha - 1)(\Delta - 1)\left(2 - 2\Delta - 2\alpha + 2\alpha\Delta + \alpha^2\right) - \eta X\alpha\left((\alpha - 2)^2(\alpha - 1) + \Delta\left(8 + 3\alpha(\alpha - 4)\right) + 4\Delta^2(\alpha - 1)\right)$$
$$+(\eta X)^2\alpha^3(\alpha + \Delta - 1) - CV_\infty^2(\alpha - 1)(\alpha + \Delta - 1)\left(\Delta - 1 - \alpha\Delta + \eta X\alpha(\Delta - 1)\right)\Big]$$

And with p_{28} known the inlet and exit velocities can easily be obtained;

$$V_{18} = \sqrt{\frac{\Delta\left(2 + CV_\infty^2\right) - 2\frac{p_{28}}{p_\infty}}{C}}$$

$$V_{28} = \sqrt{\frac{2 + CV_\infty^2 - 2\frac{p_{28}}{p_\infty}}{C}}$$

$$V_{19}^2\left[C\alpha V_{18}\right] + V_{19}\left[\alpha^2\left(1 - \tfrac{p_{28}}{p_\infty}\right) + C\left(V_{28}^2(1 - \alpha) - V_{18}^2(1 + \alpha)\right)\right] + V_{18}\left[\alpha\left(\tfrac{p_{28}}{p_\infty} - 1\right) + C\left(V_{18}^2 + V_{28}^2(\alpha - 1)\right)\right] = 0$$

$$V_{29} = V_{28}\frac{\alpha - 1}{\alpha - V_{18}/V_{19}}$$

COMPRESSIBLE MODELLING

To further investigate the possible benefit of ejection and investigate the validity of applying incompressible equations to flows with jet velocities above Mach 0.5 compressibility effects are now considered. The approach taken, as with the incompressible case, is to use a mixing efficiency parameter to determine the proportion of specific enthalpy and momentum transferred between the two flows with no mass being transferred.

For mass;

- $\dot{m}_{19} = \dot{m}_{18}$
- $\dot{m}_{29} = \dot{m}_{28}$

For specific enthalpy;

- $h_{019} = \left(1 - \eta_{ejector}\right)h_{018} + \eta_{ejector}h_{019,ideal}$

- $h_{029} = \left(1-\eta_{ejector}\right) h_{028} + \eta_{ejector} h_{029,ideal}$

  where $h_{019,ideal} \equiv h_{029,ideal} = \left(\dot{m}_{18} h_{018} + \dot{m}_{28} h_{028}\right) / \left(\dot{m}_{19} + \dot{m}_{29}\right)$

For momentum;

- $\dot{m}_{19} V_{19} + p_{\infty} A_{19} = \dot{m}_{18} V_{18} + p_{18} A_{18} - \eta_{ejector} \left[\Delta \dot{m} V\right]_{ideal}$
- $\dot{m}_{29} V_{29} + p_{\infty} A_{29} = \dot{m}_{28} V_{28} + p_{28} A_{28} + \eta_{ejector} \left[\Delta \dot{m} V\right]_{ideal}$

  where $\begin{aligned} \left[\Delta \dot{m} V\right]_{ideal} &= \dot{m}_{19} \left(V_{19} - V_{19,ideal}\right) + A_{18} p_{18} - A_{19,ideal} p_{\infty} \\ &= \dot{m}_{29} \left(V_{29,ideal} - V_{29}\right) - A_{28} p_{28} + A_{29,ideal} p_{\infty} \end{aligned}$

The equations need to be solved through iterating p_{18}, first for the ideal case and then for the non-ideal case.

Appendix D: Impact of core engine parameters on exhaust

Core parameter values at the design point are generally selected for component life and fuel burn but, for the silent aircraft, off-design performance during take-off is of especially high importance. To achieve low jet noise requires a low jet pressure ratio which whilst dominated by the fan pressure ratio in a UHBR engine is also impacted by the core. If the LPT exit stagnation pressure is less than that of the bypass then the mixed out stagnation pressure will be reduced and vice versa. In addition, the mixing of high temperature core fluid with that from the bypass stream increases the jet stagnation temperature. This reduces the density providing an increase in both thrust and jet noise. This appendix looks at how selection of design point values impact off design performance and makes recommendations on the selection of key parameter values.

The work presented here was based on an intermediate iteration of the concept silent aircraft that had three boundary layer ingesting engines.

Impact of core/bypass mixing on fan design

It is desirable to minimise the change in FPR and nozzle area between top of climb and take-off to minimise the variation of incidence onto the fan OGVs, avoid diffusion in the exhaust duct and simplify nozzle design. Equations 4.1 to 4.3 and 4.5 can be used to look at how values of ΔT_0 and PR_{out} at the two conditions impact the required fan pressure ratio, fan face Mach number and nozzle area change required to meet a specified flyover noise value for a given top of climb FPR. Table D1 lists the parameters used for these two locations. Inlet pressure recovery is in the range expected for a boundary layer ingesting design. Exit pressure recovery and stagnation temperature rise have been selected iteratively and match the recommended values from discussions in the following section. The jet noise modelling and atmospheric corrections used in chapter three were also used here but for the aircraft at a fixed location in space rather than for the entire take-off run.

	Top of Climb	Flyover
Key parameter	FPR = 1.5	Peak Jet Noise = 54dBA
M_{ff}	0.66	varies
PR_{IN}	0.96	0.98
PR_{OUT}	0.966	0.959
ΔT_0	36.3K	17.3K

Atmospheric Conditions	ISA+10K	ISA+12K
Altitude	12192m	205m
Net Thrust per engine	25.71kN	55.44kN
M_∞	0.8	0.237
Fan polytropic efficiency	92%	92%

Table D1: Primary parameters used for top of climb and flyover conditions with ToC FPR=1.5

Figure D1 presents the variation in flyover FPR, M_{ff} and nozzle area increase for changes in exit pressure recovery and figure D2 presents the same data for changes in flow stagnation temperature increase due to mixing. Points marked on these figures are discussed in the next section.

With jet noise being dominated by jet velocity, flyover jet velocity in the entire range of the two plots varies between only 159.0m/s and 158.6m/s with an average of 158.8m/s. (Nozzle area at flyover varies between 4.0m^2 and 4.2m^2.) With jet velocity and therefore stagnation pressure barely changing, increases in PR_{OUT} at flyover reduce the required FPR. Increases in flyover jet stagnation temperature (figure D2) also reduce the required FPR. This is because as the temperature is increased the density is reduced and FPR must be lowered to maintain the same jet velocity. Flyover FPR is independent of changes in top of climb pressure recovery and temperature change as the change in nozzle and fan areas have no impact on the nozzle area required at flyover.

Flyover fan face Mach number has opposite sensitivity to flyover FPR; it is sensitive to changes in top of climb values but relatively insensitive to changes in flyover values. Considering changes in flyover values first, changes in pressure recovery (figure D1) are offset by changes in FPR. This results in a slight reduction in jet stagnation temperature and increase in density leading to a very small increase in mass flow rate and fan face Mach number to meet the same thrust requirement. Changes in flyover jet stagnation temperature (figure D2) have an opposite effect as reduction in density reduces the required mass flow rate through the fan for the same thrust. The effect is much more pronounced when changing design point conditions. This is because increases in PR_{OUT} and jet stagnation temperature at top of climb reduce the required fan face area resulting in higher fan face Mach number for the same mass flow off-design.

The percentage change in nozzle area from top of climb to flyover is sensitive to changes in pressure recovery and stagnation temperature rise at both conditions. For changes in pressure recovery (figure D1), increasing PR_{OUT} at top of climb reduces the top of climb nozzle area but does not impact flyover nozzle area. Increasing PR_{OUT} at flyover has no impact in top of climb nozzle area but does lead to a slight reduction in flyover nozzle area. This is because the fan has to do less work resulting in a lower jet stagnation temperature so the same thrust and noise can be achieved with a small reduction in jet area. The overall result of this is as pressure recovery is increased at top of climb and reduced at flyover the required change in nozzle area between these two conditions increases.

For changes in stagnation temperature (figure D2), increasing ΔT_0 at top of climb reduces the required nozzle area at this condition but has no impact on flyover. Likewise increasing ΔT_0 at flyover has no impact on top of climb but does impact flyover. The reduction in jet density requires an increased jet area to meet the thrust requirement with the same noise level. Overall this results in increases in stagnation temperature at both top of climb and flyover leading to larger nozzle variation between the two conditions.

As stated at the beginning of this section it is desirable to minimise changes in FPR and nozzle area between top of climb and flyover for the silent aircraft. It is also desirable to minimise fan face Mach number at flyover relative to the top of climb value to avoid operating with highly ingested shocks in the fan. Reducing exit pressure recovery through core mixing at both top of climb and flyover will therefore assist fan operation although this cannot be at the expense of reductions to cruise efficiency. The same is true of stagnation temperature rises; reductions at both top of climb and flyover will assist in fan design. As the achievable values of PR_{OUT} and ΔT_0 are linked to the design and off-design performance of the core, this must now be looked at in more detail.

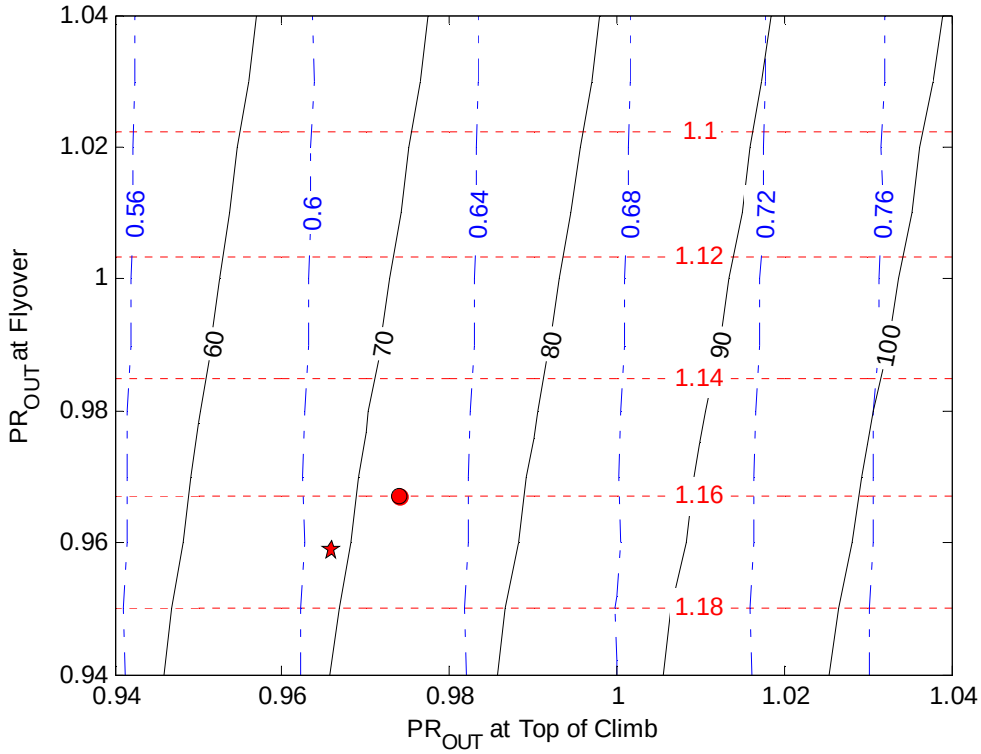

Figure D1: Variation of FPR (dotted red), M_{ff} (dashed blue) and percentage nozzle opening (solid black) at flyover with exit pressure recovery variation for three engine 1.5 ToC FPR BLI aircraft. Circle = optimum SFC point, star = compromise point.

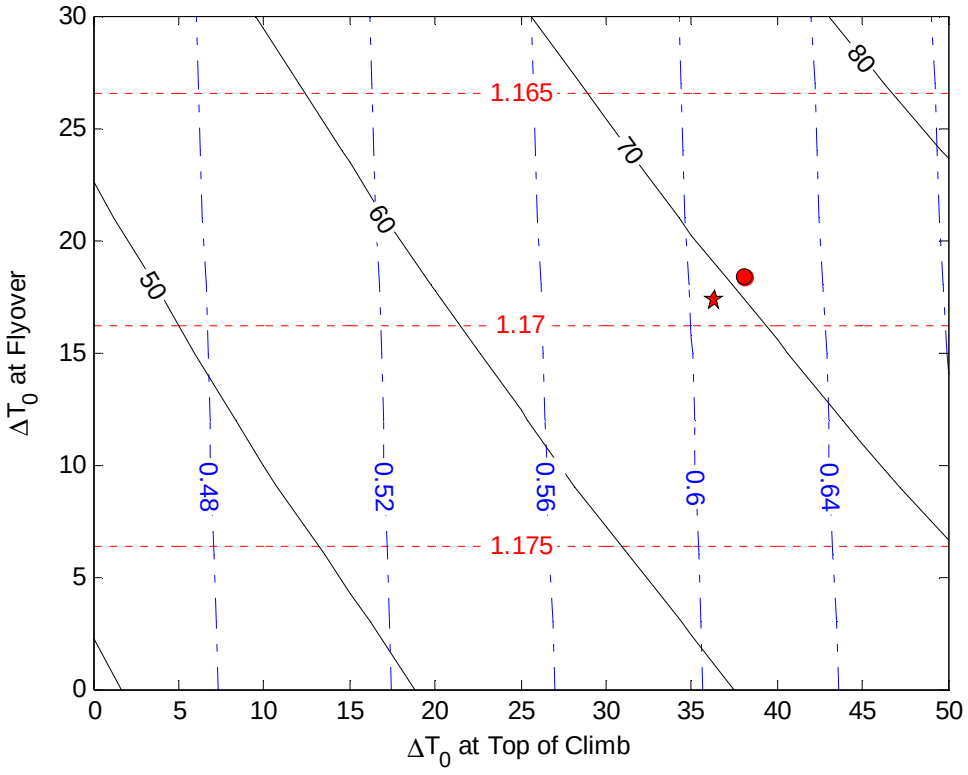

Figure D2: Variation of FPR (dotted red), M_{ff} (dashed blue) and percentage nozzle opening (solid black) at flyover with exhaust stagnation pressure increase from mixing for three engine 1.5 ToC FPR BLI aircraft. Circle = optimum SFC point, star = compromise point.

Varying design bypass ratio and mixer Mach number

To assist in fan design for low jet noise it is desirable to minimise PR_{OUT} and ΔT_0 at both top of climb and flyover conditions without adversely impacting cruise fuel burn. GasTurb (Kurzke 2004) was used to perform a range of parametric analysis starting from a default engine design and looking at how modifications to various parameters impact these values.

The approach taken was as follows*:

1. Use top of climb values as the design point to preliminarily size the engine with parameters taken from table D1.

2. Using a scaled fan characteristic and default GasTurb characteristics for other components to create two off-design mission points for cruise and flyover conditions.

    a. For cruise, thrust requirement was set to 20kN under ISA conditions and nozzle area was varied to give a FPR of 1.4.

    b. For flyover, as GasTurb cannot predict jet noise, the nozzle area was varied to give a flyover jet velocity of 158.8m/s and parameters from table D1 used. (The variation in jet velocity in figures D1 and D2 is only 0.4m/s around this value.)

3. A design point parametric study was carried out varying a range of parameters and resulting off-design values found including SFC, PR_{OUT} (from just mixing) and ΔT_0,

The design values that have the largest influence on the core's impact on the fan and jet are the mixer design values. Two parameters are required to specify the mixer design in GasTurb; firstly the design bypass ratio or the bypass to core stagnation pressure ratio and secondly the mixer Mach number or the mixer area. With forced mixing and a long exhaust the mixing efficiency is set to 100%.

In the creation of the following plots the design bypass ratio was varied from 12.25 to 14.0 in 0.25 steps and the mixer Mach number was varied from 0.33 to 0.57 in 0.03 steps.

* For low pressure ratio fans, lines of constant thrust can become very flat and, depending on how fan and other component efficiency varies even rise with increasing Mach number in places. This makes off-design iteration to meet certain criteria complicated and it was found that GasTurb often struggled to find a solution even when one exits. The most successful method for finding off-design flyover positions (defined by a thrust requirement and jet velocity) was to (i) set a Limiter to be the negative jet velocity within 'composed values' and (ii) set an off design iteration to vary nozzle area to meet the thrust requirement. This was considerably more successful than trying to iterate to meet a jet velocity whilst using thrust as a limiter.

Figure D3 shows contours of cruise SFC (g/(kN*s)) for variation in top of climb (design point) mixer pressure ratio and Mach number. Minimum cruise SFC occurs for a design bypass ratio of about 13.2 and the lower the mixer Mach number the lower the SFC. This bypass ratio equates to a bypass to core stagnation pressure ratio of about 1.01. Figure D4 shows how fan diameter varies for the same parameters. To avoid the mixer taking up more cross sectional area than the fan, it makes sense to limit the mixer area to πr_{tip}^2 where r_{tip} is the fan tip radius. On the figures this corresponds to not going below a mixer Mach number of about 0.42. It should be noted that the SFC stated here is for the bare engine and does not take into account increases in nacelle drag as fan diameter increases.

Figures D5 and D6 show the variation in PR_{OUT} at top of climb and flyover respectively for different design point values of BPR and mixer Mach number. As would be expected the higher the bypass to core design point pressure ratio the lower PR_{OUT} is. Also increasing the design point mixer Mach number reduces PR_{OUT} especially at flyover. As a large nozzle exit area is required during take-off (between $4m^2$ and $4.2m^2$ is required at flyover and possibly greater at other stages) the mixer area cannot be reduced too far or a large amount of diffusion would be required in the exit duct.

Figures D7 and D8 show the variation in ΔT_0 at top of climb and flyover respectively for different design point values of BPR and mixer Mach number. At top of climb ΔT_0 is independent of the mixer Mach number and only a function of bypass ratio with higher bypass ratios leading to lower jet temperatures. At flyover a minimum in jet temperature seems to occur between a BPR of 13.75 and 14 with higher mixer Mach numbers leading to lower temperatures.

Based on the above analysis, to assist fan operation during take-off both design point BPR and design point mixer Mach number want to be set as high as possible. The limiting factor on setting BPR is cruise SFC and the limiting factors on setting mixer Mach number are cruise SFC and exit duct diffusion during take-off.

For the design analysed here with a top of climb FPR of 1.5 compromise values of design point BPR and mixer Mach number are 13.5 and 0.45 respectively. This equates to a stagnation pressure ratio between bypass and core of 1.08 at the design point and a mixer area of $3.7m^2$. This point is marked with a white star on the figures D3 through D8. The point with minimum cruise SFC (without mixer diameter exceeding fan diameter) is also marked on these figures with a white circle. The resulting values of PR_{OUT} and ΔT_0 for both minimum SFC and compromise points at top of climb and flyover are marked on figures D1 and D2 (with an additional 0.02 reduction in

PR_{OUT} included to account for duct losses). This design point sacrifices less than 0.05 (0.3%) of SFC at cruise in order to assist fan operation during take-off.

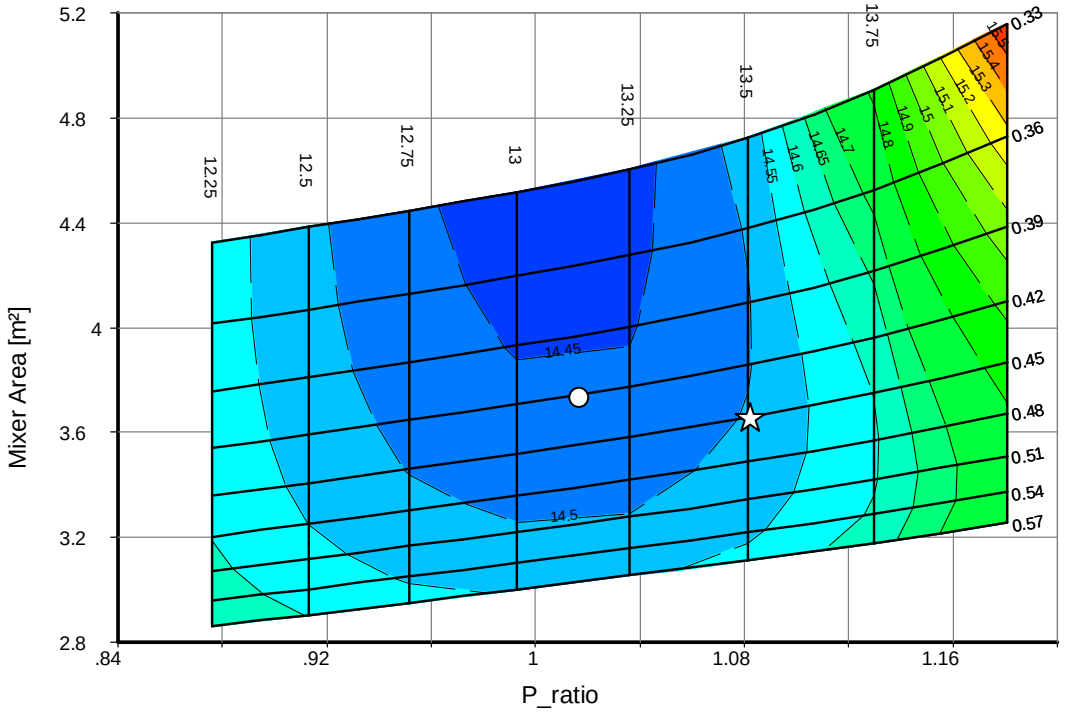

Figure D3: Contours of SFC at cruise with mixer design parameters (ToC FPR = 1.5). Circle = optimum SFC point, star = compromise point.

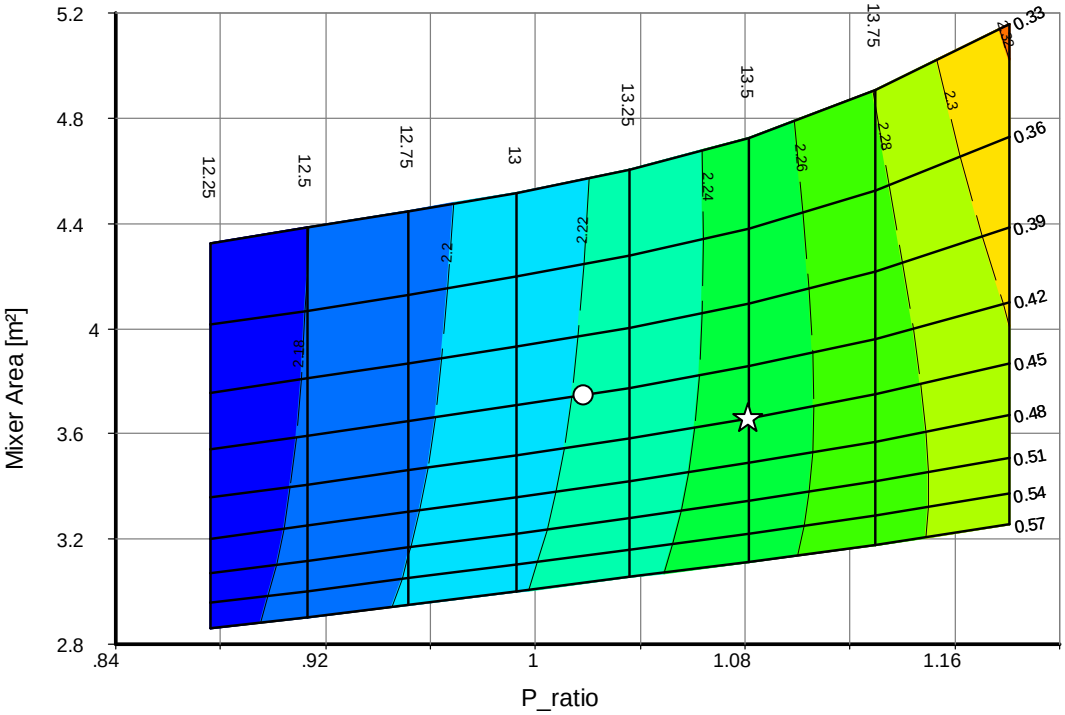

Figure D4: Contours of fan diameter with mixer design parameters. Circle = optimum SFC point, star = compromise point.

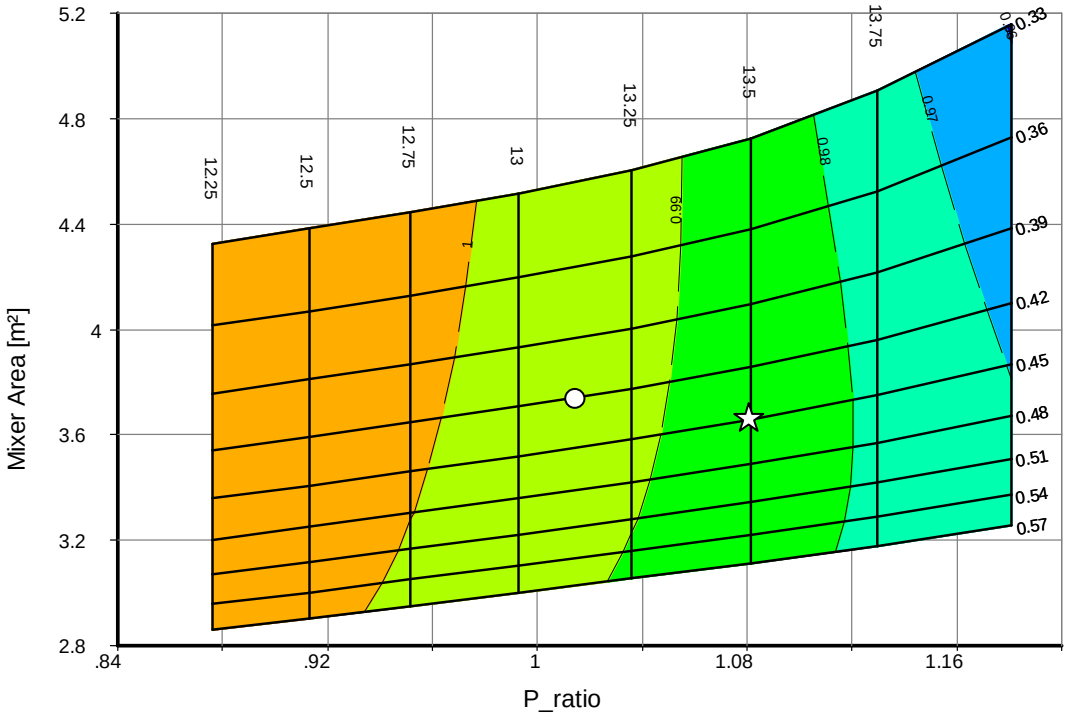

Figure D5: Contours of PR_{OUT} at top of climb with mixer design parameters. Circle = optimum SFC point, star = compromise point.

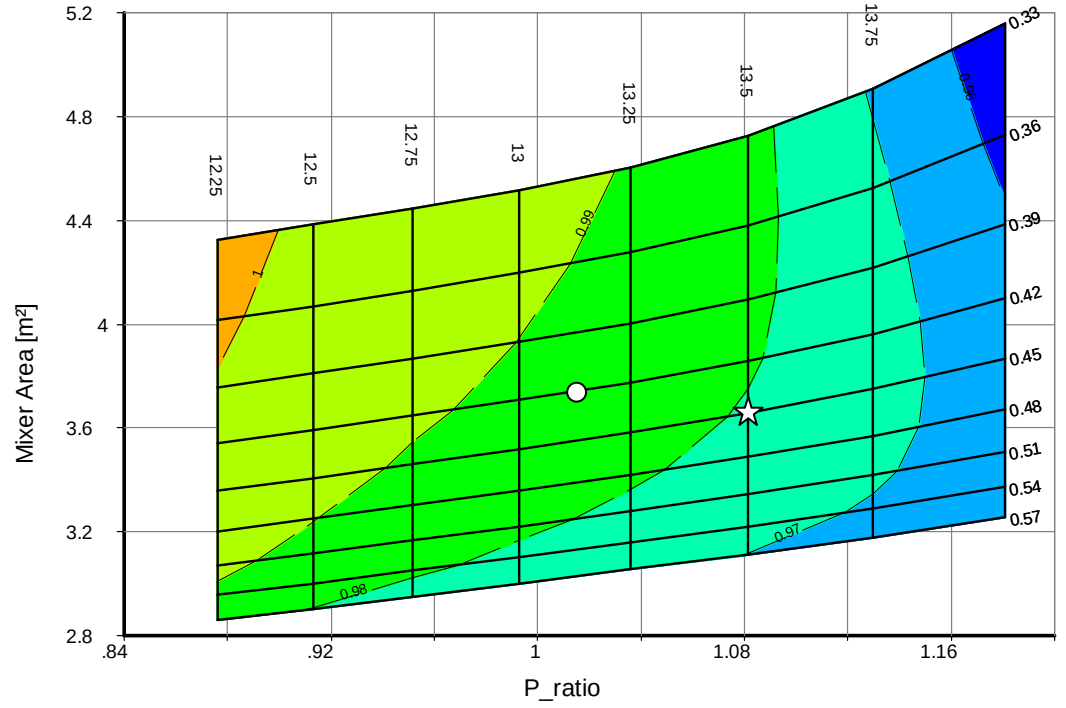

Figure D6: Contours of PR_{OUT} at flyover with mixer design parameters. Circle = optimum SFC point, star = compromise point.

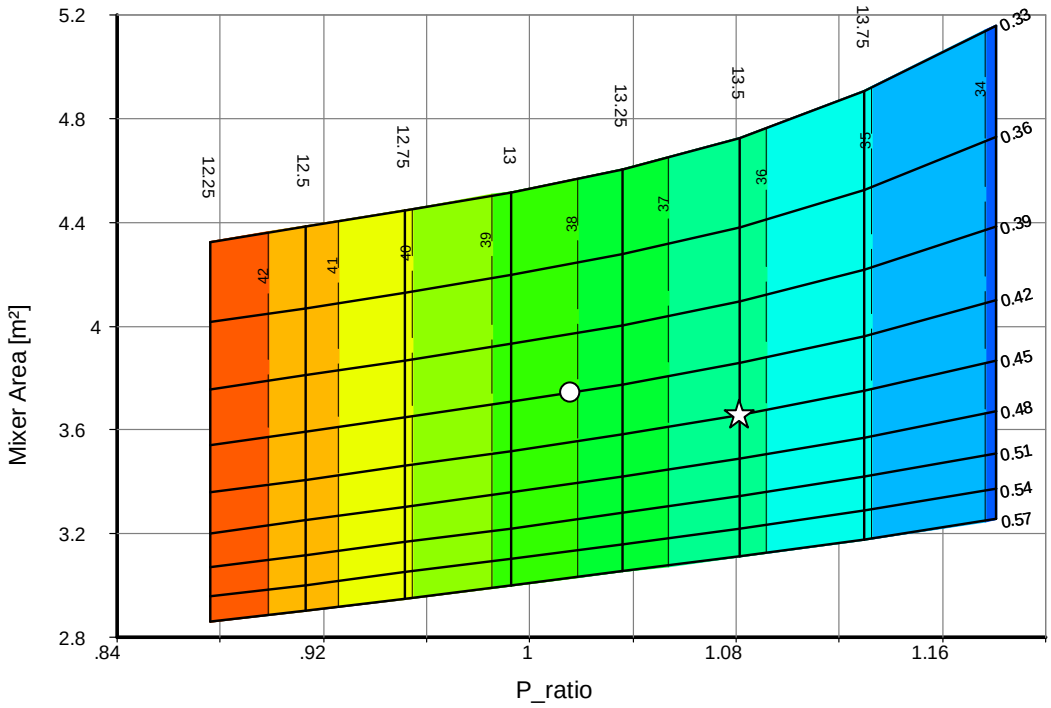

Figure D7: Variation in ΔT_0 at top of climb with mixer design parameters. Circle = optimum SFC point, star = compromise point.

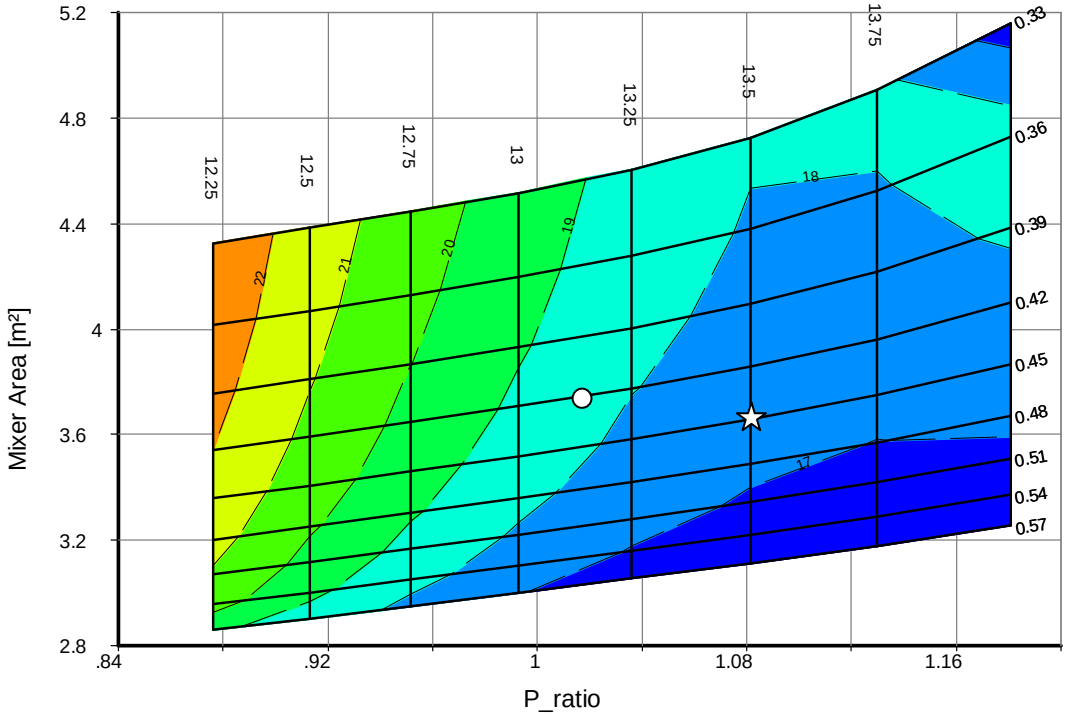

Figure D8: Variation in ΔT_0 at flyover with mixer design parameters. Circle = optimum SFC point, star = compromise point.

Varying compressor exit and turbine entry temperatures

The impact on PR_{OUT} and ΔT_0 of changing design point compressor exit and turbine inlet temperatures was briefly investigated. As combustor inlet and exit temperatures are increased thermal efficiency increases and SFC reduces. It was found that to reduce pressure recovery requires a move to lower temperature limits whilst to reduce the temperature rise requires a rise of temperature limits. This is because as the temperature limit is increased the bypass ratio increases and less core gas is mixed with the bypass flow.

If 0.05 of SFC could be sacrificed to reduce pressure recovery to assist off-design fan operation (as was done above) this was found to be equivalent to a reduction in turbine entry temperature from 1740K to 1710K or a reduction in compressor exit temperatue from 900K to 887K. Reducing turbine entry temperature has the most benefit but still only reduces PR_{OUT} through mixing by less than 0.0003 at top of climb and by less than 0.0009 at flyover. This is 26 times less effective at top of climb and 9 times less effective at flyover than the changes made to mixing parameters above for the same SFC penalty.

Therefore temperature limits into and out of the combustion chamber should be set as high as possible to improve SFC. Any changes in exit pressure recovery or stagnation temperature required to assist off-design fan operation can be achieved with less SFC penalty through changes in mixer design parameters.

Sensitivity of results to top of climb FPR : Selection of mixer design conditions

To investigate the impact top of climb FPR has on these results the study was repeated but this time with ToC FPR of 1.45 rather than 1.5. To account for this the cruise point was modified to have a FPR of 1.36 rather than 1.40 but with thrust remaining at 20kN per engine. Flyover jet noise / velocity and thrust were unchanged.

Minimum cruise SFC was found to occur for a design bypass ratio of about 14.65 and the lower the mixer Mach number the lower the SFC. This bypass ratio equates to a bypass to core stagnation pressure ratio of about 1.0, very similar to the case with FPR=1.5. To avoid the mixer taking up more cross sectional area than the fan, it again makes sense to limit the mixer area to πr_{tip}^2 where r_{tip} is the fan tip radius. This corresponds to not going below a mixer Mach number of about 0.42, again similar to that found with the higher FPR.

The summary of this work was that optimum pressure ratio and Mach number for cruise SFC are relatively unaffected by the reduction in top of climb FPR. As would be expected the optimum SFC is reduced by lowering the FPR but this may be offset by increases in nacelle drag and engine weight.

With the FPR=1.5 design, whilst limiting the mixer area to less than or equal πr_{tip}^2 where r_{tip} is the fan tip radius, less than a 0.05 increase in cruise SFC was sacrificed in positioning the design point to assist fan operation during take-off. If the same approach is adopted here then compromise values of design point BPR and mixer Mach number are 14.95 and 0.45 respectively. This equates to a stagnation pressure ratio between bypass and core of 1.07 at the design point and a mixer area of $4.1m^2$.

The resulting compromise flyover fan parameters are a FPR of 1.16 and a fan face Mach number of 0.52 requiring a nozzle opening of 50% leading to the pressure ratio and temperature corrections in table D2. Achieving these values will be considerably easier than those obtained with a 1.5 ToC FPR.

	Top of Climb	Flyover
PR_{OUT}	0.968	0.967
ΔT_0	32.9K	17.5K

Table D2: Parameters for top of climb and flyover conditions with ToC FPR=1.45

Sensitivity of results to top of climb FPR : Impact on PR_{out} and ΔT_0

Whilst the previous section looked at how reducing the design point FPR by 0.05 impacted the selection of mixer design conditions, a better idea of how PR_{out} and ΔT_0 vary as FPR is modified is required in order to create the plots in chapter four. A parametric study was performed in GasTurb to analyse this with the outer fan pressure ratio varied from 1.8 down to 1.175. Core exit (LPT inlet) conditions were kept constant as was fan capacity, net thrust and the mixer core to bypass stagnation pressure ratio.

With these constraints increases in FPR should lead to increases in ΔT_0 primarily due to the reduction in bypass mass flow. This was seen in the study with ΔT_0 varying almost exactly proportional to the FPR minus one as illustrated in figure D9. A similar trend would be expected with the change in exit pressure recovery due to mixing being more significant at higher FPR

again due to reduced bypass mass flow. Whilst such a trend was seen there was no simple relationship to FPR.

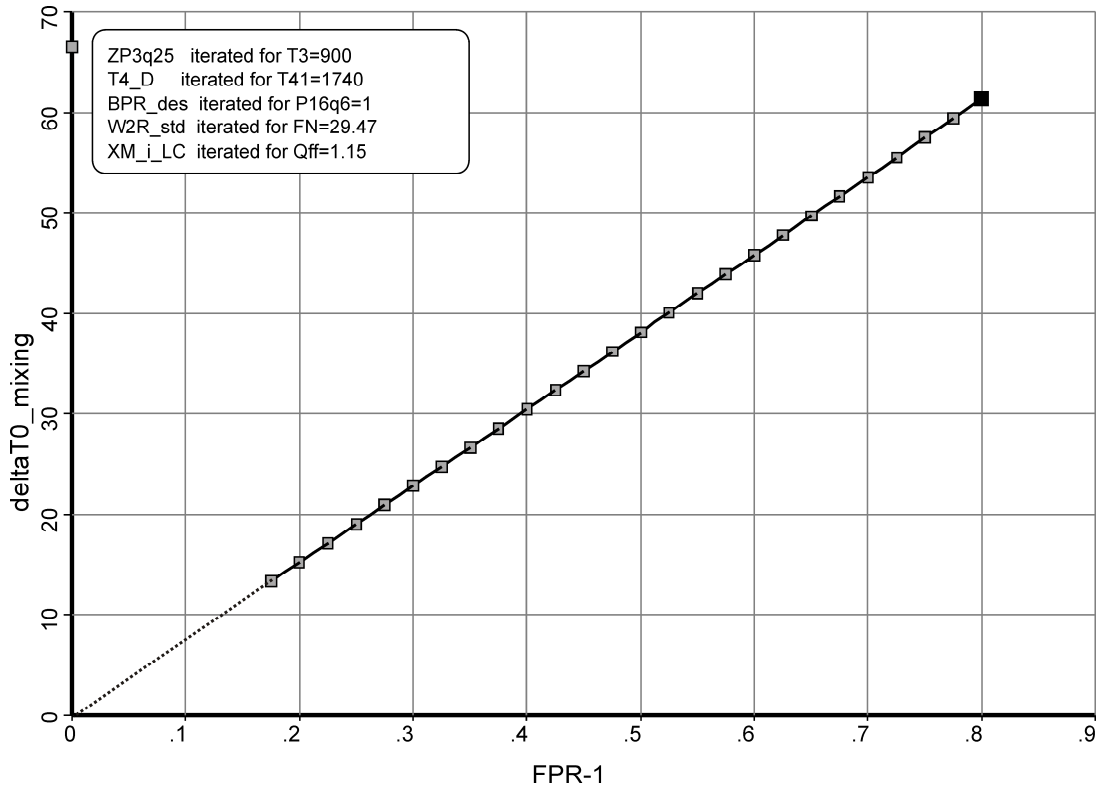

Figure D9: Variation in design point mixer temperature rise when changing fan outer pressure ratio

Appendix E: Change in L/D following engine out

When the critical engine fails not only does the available thrust reduce but the overall drag also increases. In this appendix approximations of this drag increase are used to calculate the change in L/D following engine out during take-off for use in equation 3.2. With lift remaining approximately constant during engine out (L≈mg);

$$\left.\frac{1}{L/D}\right|_{after} = \left.\frac{1}{L/D}\right|_{before} + \frac{D_{wm} + D_{trim}}{L} \qquad \text{E.1}$$

where D_{wm} is the additional drag from the now windmilling engine and D_{trim} the additional control surface drag required to correct the resulting yaw. The control surface drag is a function of the remaining thrust which, for a small angle of attack can be estimated as;

$$T_N \approx D + D_{wm} + D_{trim} + mg\sin\theta^* \qquad \text{E.2}$$

where θ* is the climb angle after engine out and D is the drag before engine out. Figure E1 shows simplified force vectors for the two airframe configurations considered in this thesis; a conventional tube and wing and an all-lifting body.

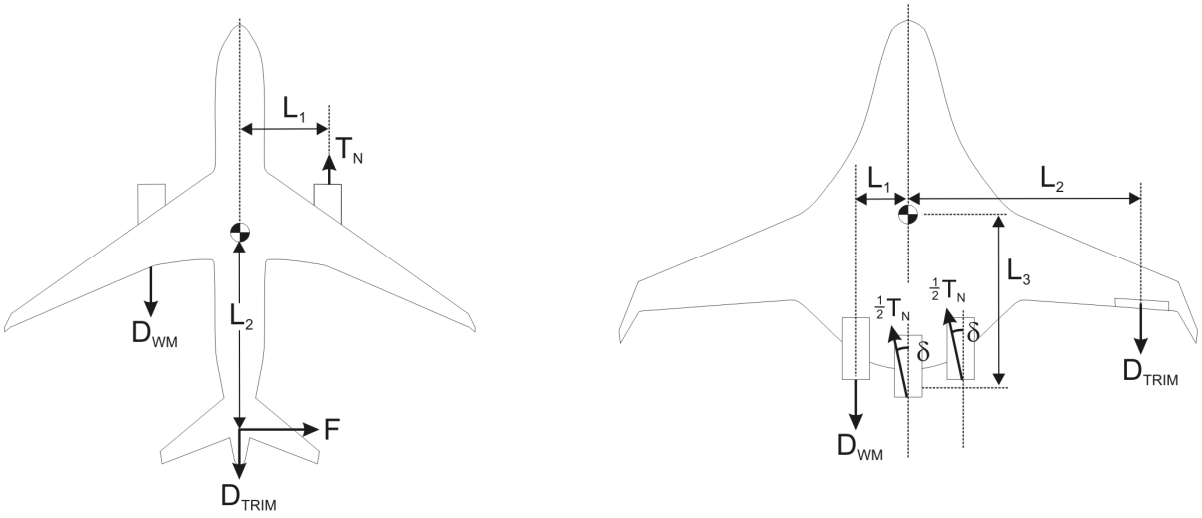

Figure E1: Engine out thrust and drag vectors in aircraft plane for two-engine conventional and three-engine all-lifting body configurations

(L_1 is the distance to the outboard (critical) engine and L_3 is the average distance from the centre of gravity to the exhaust of the remaining engines.)

Conventional

For a conventional tube and wing as a first level approximation the tail only is used to counteract any yawing moment. Using the approach of Kroo and Shevell (2006) where the correction in trim drag is the induced drag from the tail force;

$$D_{wm} \approx 0.0044 p_{\infty} A_{inlet} \approx 0.0044 p_{\infty} A_{ff} \tag{E.3}$$

$$D_{trim} \approx \frac{F^2}{\frac{1}{2}\rho_{\infty} V_{\infty}^2 h^2 \pi e} = \frac{\left(\frac{L_1}{L_2}\left(\frac{T_N}{n_{eng}-1} + D_{wm}\right)\right)^2}{\frac{1}{2}\rho_{\infty} V_{\infty}^2 h^2 \pi e} \tag{E.4}$$

The equation for windmill drag is empirical and suitable for high bypass ratio engines whilst in the equation for trim drag, h is the height of the rudder and e is a correction of the order 0.8 for non-elliptical loading (Oswold Factor). With T_N a function of D_{trim} this results in a quadratic equation which can be solved to give trim drag;

$$D_{trim} \approx \frac{1}{2}\left(X - 2Y + \sqrt{X\left(X - 4Y\right)}\right)$$
$$\text{where } X = \frac{1}{2}\left(n_{eng} - 1\right)^2 \rho_{\infty} V_{\infty}^2 h^2 \pi e \left(\frac{L_2}{L_1}\right)^2,\ Y = D + n_{eng} D_{wm} + mg \sin\theta^* \tag{E.5}$$

Using these equations the change in L/D with engine out is now only a function of pre-engine out conditions, engine out climb angle θ*, fan face area and airframe geometry.

3 engine all-lifting body

For a three-engine all-lifting body there is no tail and therefore the yaw correction must be achieved through alternative means. Two solutions are considered here; a split aileron (drag creation device) on the outer wing and through the use of thrust vectoring. Whilst the windmill drag is unchanged the trim drag is modified to account for both a different number of engines and the alternative yaw correction approach.

If a split aileron is used;

$$D_{trim} \approx \frac{L_1}{L_2}\left(\frac{T_N}{n_{eng} - 1} + D_{WM}\right) \approx \frac{D + n_{eng} D_{wm} + mg \sin\theta^*}{\left(n_{eng} - 1\right)\frac{L_2}{L_1} - 1} \tag{E.6}$$

If thrust vectoring is used, splitting the thrust into components in line with and perpendicular to the aircraft and taking moments about the centre of gravity;

$$T_N \sin\delta \approx \frac{L_1}{L_3}\left(\frac{T_N \cos\delta}{n_{eng}-1} + D_{wm}\right) \qquad \text{E.7}$$

This can be solved to find the thrust vector angle δ where T_N in equation E.2 is now $T_N \cos\delta$;

$$\tan\delta \approx \frac{L_1}{L_3}\left(\frac{1}{n_{eng}-1} + \frac{D_{wm}}{D + D_{wm} + mg\sin\theta^*}\right) \qquad \text{E.8}$$

in which the right hand side is dominated by the first term. Finally, in order to calculate the change in L/D caused by engine out, the loss in axial thrust through the use of thrust vectoring can be thought of as a trim drag;

$$D_{trim} \approx T_N\left(1-\cos\delta\right) \approx \left(D + D_{wm} + mg\sin\theta^*\right)\left(1-\cos\delta\right) \qquad \text{E.9}$$

Tables and Figures

Specific environment	Critical health effect(s)	LAeq [dB(A)]	Time base [hours]	LAmax [dB(A)]
Outdoor living area	Serious annoyance, daytime and evening	55	16	-
	Moderate annoyance, daytime and evening	50	16	-
Dwelling, indoors	Speech intelligibility & moderate annoyance, daytime & evening	35	16	
Inside bedrooms	Sleep disturbance, night-time	30	8	45
Outside bedrooms	Sleep disturbance, window open (outdoor values)	45	8	60
School class rooms & pre-schools, indoors	Speech intelligibility, disturbance of information extraction, message communication	35	during class	-
Pre-school bedrooms, indoor	Sleep disturbance	30	sleeping-time	45
School, playground outdoor	Annoyance (external source)	55	during play	-
Hospital, ward rooms, indoors	Sleep disturbance, night-time	30	8	40
	Sleep disturbance, daytime and evenings	30	16	-
Hospitals, treatment rooms, indoors	Interference with rest and recovery	#1		
Industrial, commercial shopping and traffic areas, indoors and outdoors	Hearing impairment	70	24	110
Ceremonies, festivals and entertainment events	Hearing impairment (patrons:<5 times/year)	100	4	110
Public addresses, indoors and outdoors	Hearing impairment	85	1	110
Music and other sounds through headphones/ earphones	Hearing impairment (free-field value)	85 #4	1	110
Impulse sounds from toys, fireworks and firearms	Hearing impairment (adults)	-	-	140 #2
	Hearing impairment (children)	-	-	120 #2
Outdoors in parkland and conservations areas	Disruption of tranquillity	#3		
#1: As low as possible. #2: Peak sound pressure measured 100 mm from the ear. #3: Existing quiet outdoor areas should be preserved and the ratio of intruding noise to natural background sound should be kept low. #4: Under headphones, adapted to free-field values.				

Table 1-1: Guideline values for community noise in specific environments (Berglund *et al.* 1999)

Noise Level (dB(A))	L_{den}	L_{day}	$L_{evening}$	L_{night}
<55	67%	73%	77%	84%
>55	33%	27%	23%	16%
>60	22%	20%	16%	6%
>65	14%	12%	6%	0%
>70	4%	3%	1%	0%
>75	0%	0%	0%	0%

Table 1-2: Proportion of population exposed to various noise levels in Greater London Area (Government 2004)

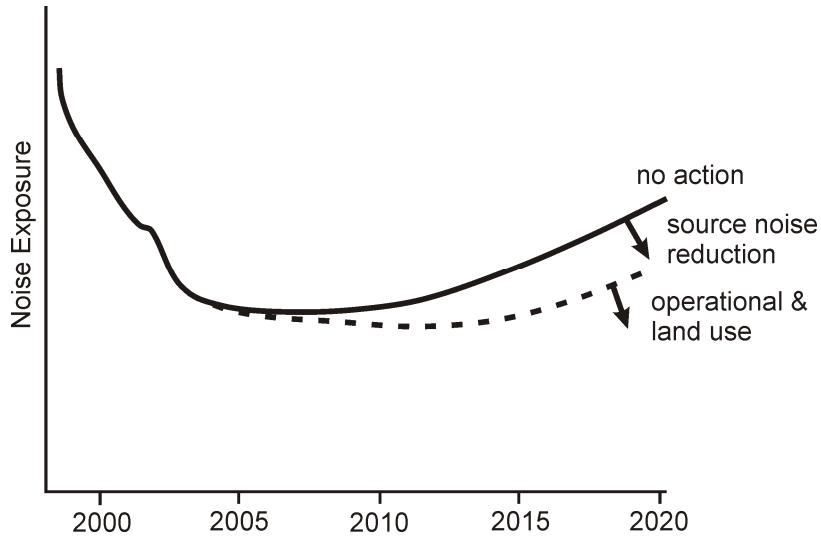

Figure 1-1: Illustration of aircraft noise trends (Green *et al.* 2001)

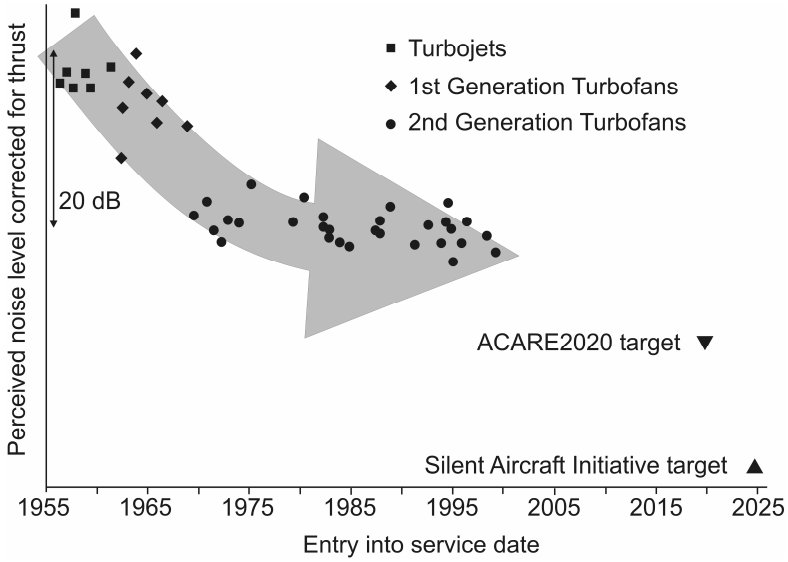

Figure 1-2: Reduction in thrust corrected aircraft noise level over time for new aircraft entering into service (adapted from Birch 2002)

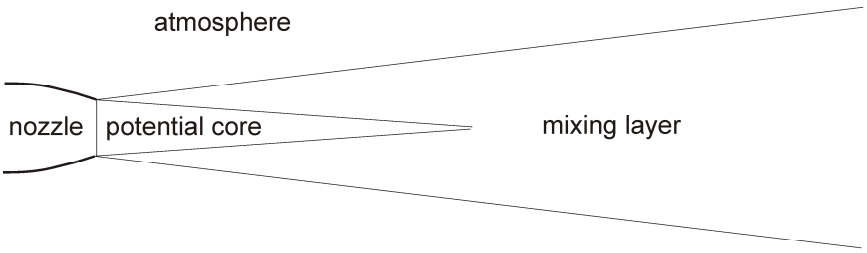

(a) single circular jet model

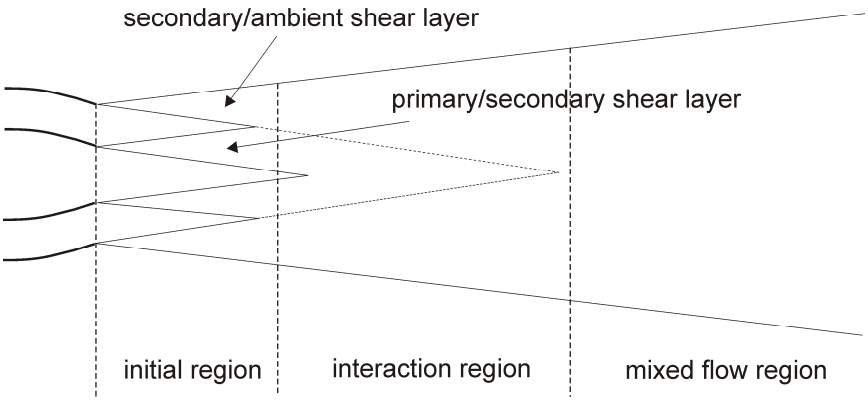

(b) coaxial jet model

Figure 2-1: Schematic of jet mixing

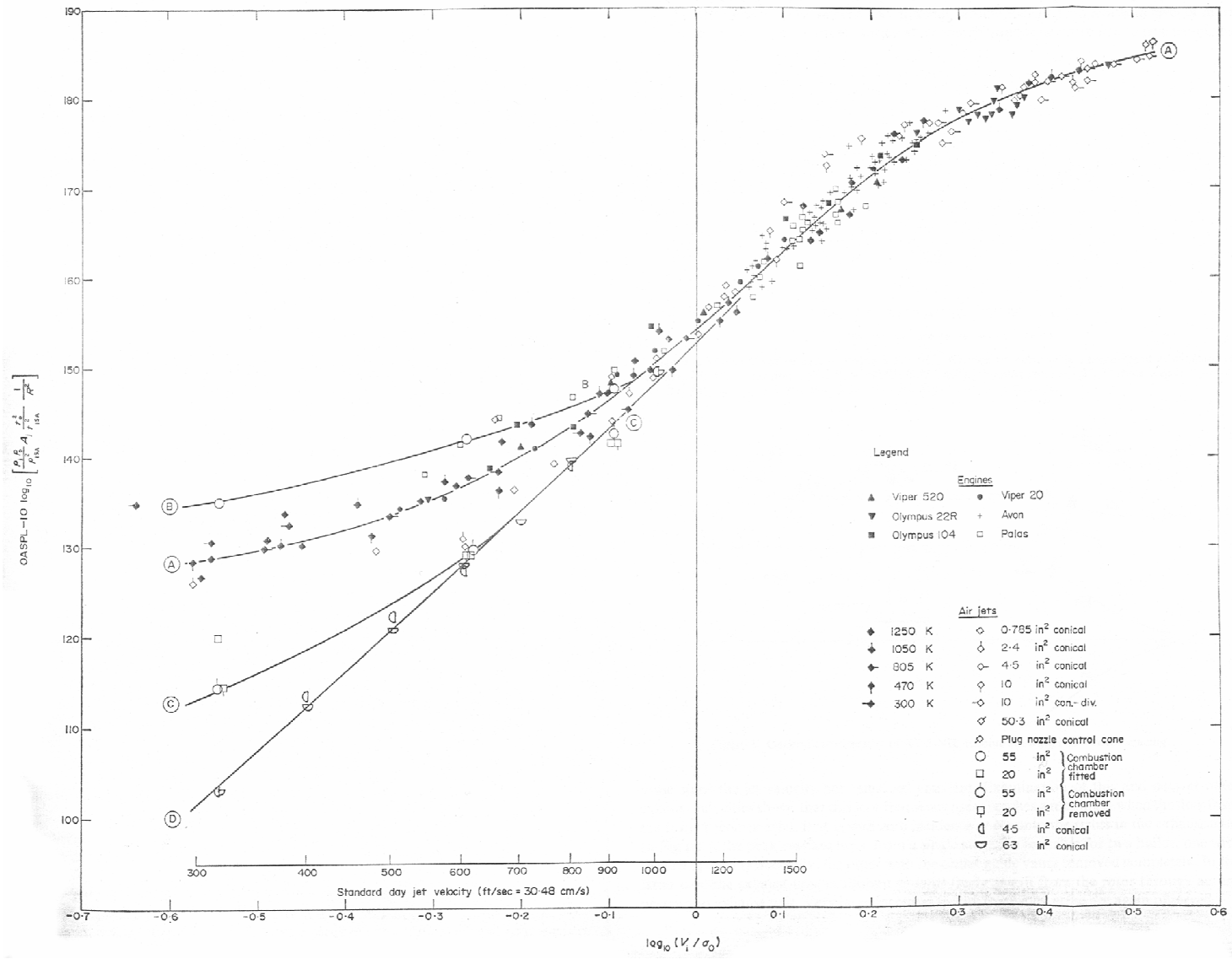

Figure 2-2: Jet noise versus jet velocity (Bushell 1971)

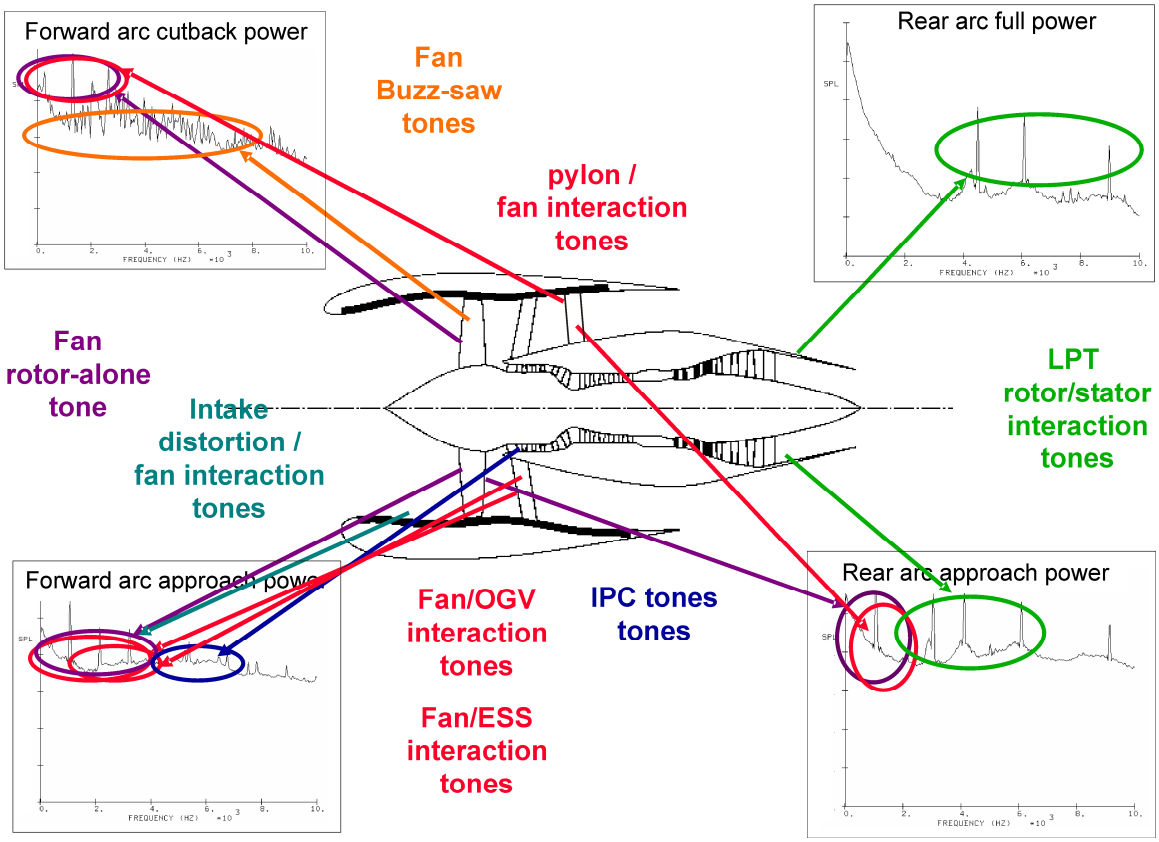

Figure 2-3: Engine tone noise sources (adapted from Rolls Royce with permission)

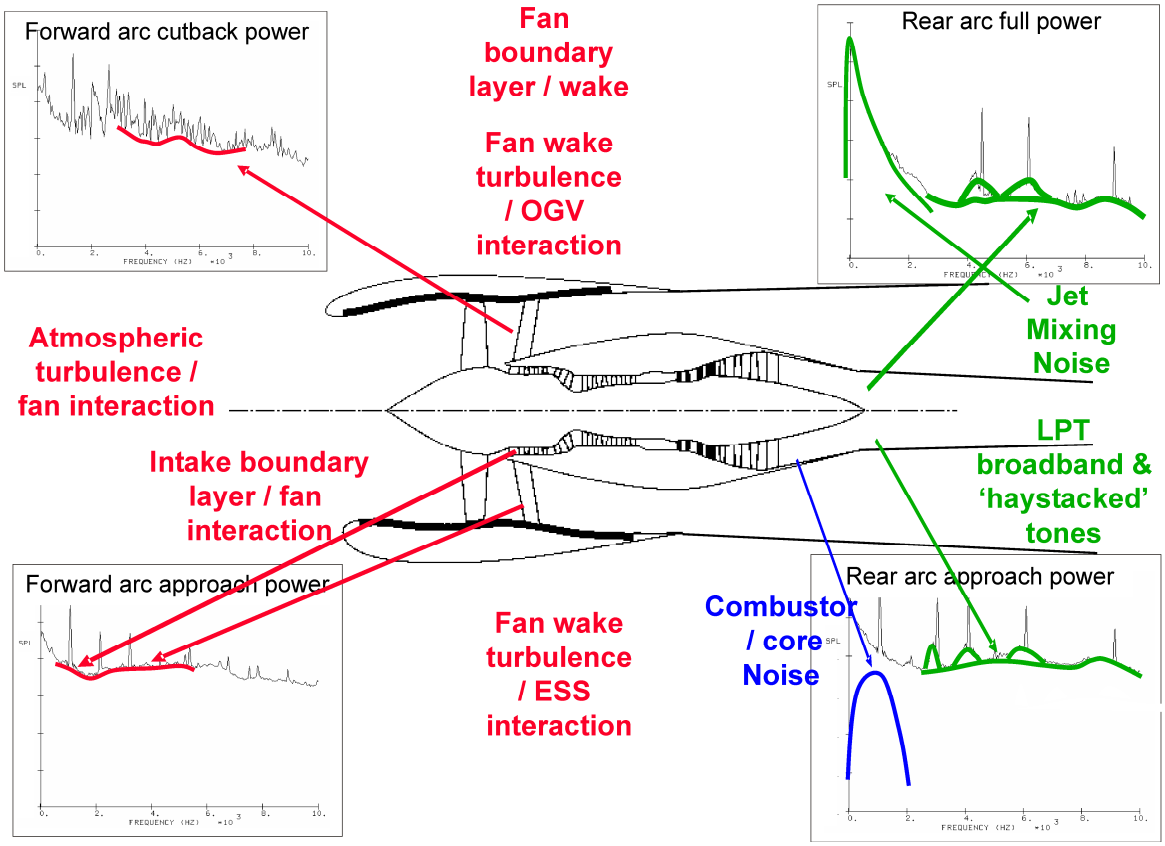

Figure 2-4: Engine broadband noise sources (adapted from Rolls Royce with permission)

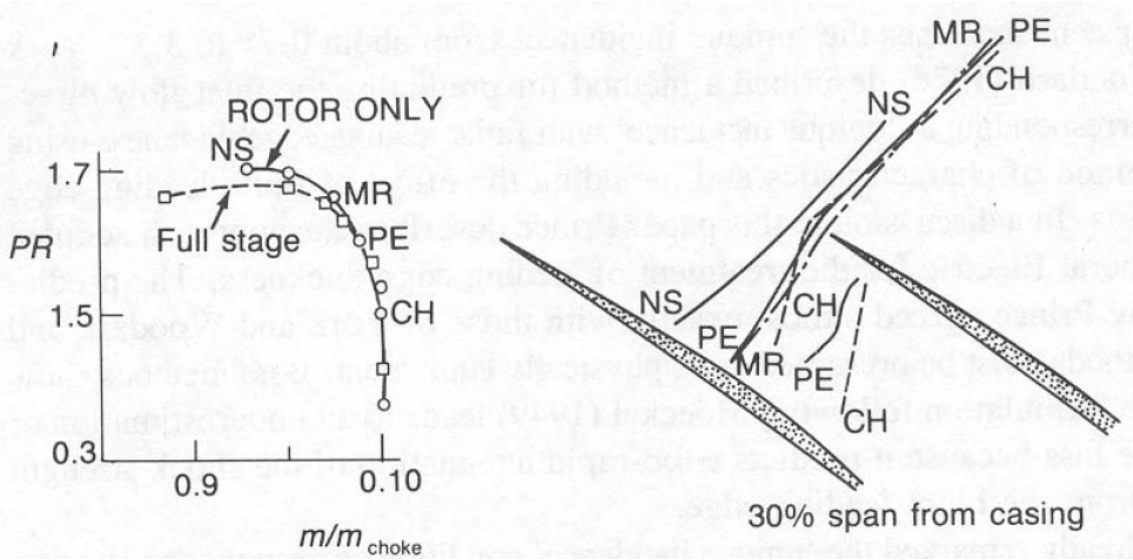

Figure 2-5: Fan operating characteristic and measured leading edge shock structure at design point (PE = peak efficiency, CH= choke, MR = mid range, NS = near stall). (From Cumpsty 1989.)

Rank	Airport	Total Passengers	Runway length (ft)	Elevation (ft)	Noise Limitations
1	ATLANTA (ATL)	79 086 792	11889	1026	(a)
2	CHICAGO (ORD)	69 508 672	13000	667	(a)
3	LONDON (LHR)	63 487 136	12802	80	(a) (b) (c) (d) (e)
4	TOKYO (HND)	62 876 269	10335	15	(a) (d)
5	LOS ANGELES (LAX)	54 982 838	12090	126	(a)
6	DALLAS/FT WORTH AIRPORT (DFW)	53 253 607	13400	603	(a)
7	FRANKFURT/MAIN (FRA)	48 351 664	13123	365	(a) (b) (c) (d)
8	PARIS (CDG)	48 220 436	11860	387	(a) (b) (d) (e)
9	AMSTERDAM (AMS)	39 960 400	11330	-11	(a) (b) (c) (d) (e)
10	DENVER (DEN)	37 505 138	12000	5431	(a) (b)*
11	PHOENIX (PHX)	37 412 165	11001	1132	(a)
12	LAS VEGAS (LAS)	36 285 932	12635	2174	(a) (b)*
13	MADRID (MAD)	35 854 293	13450	1999	(a) (b)
14	HOUSTON (IAH)	34 154 574	12000	98	
15	MINNEAPOLIS/ST PAUL (MSP)	33 201 860	10000	841	(a) (b) (d)
16	DETROIT (DTW)	32 664 620	12000	639	(a)
17	NEW YORK (JFK)	31 732 371	14572	12	(a) (d)**
18	BANGKOK (BKK)	30 175 379	12139	9	
19	LONDON (LGW)	30 007 021	10364	202	(a) (b) (c) (d) (e)
20	MIAMI (MIA)	29 595 618	13000	10	(a)
21	NEWARK (EWR)	29 431 061	9300	18	(a) (e)**
22	SAN FRANCISCO (SFO)	29 313 271	11870	11	(a)
23	ORLANDO (MCO)	27 319 223	12004	96	(a)
24	HONG KONG (HKG)	27 092 290	11130	15	(a)
25	SEATTLE (SEA)	26 755 888	11900	429	(a)
26	TOKYO (NRT)	26 537 406	13123	135	(a) (b) (d)
27	ROME (FCO)	26 284 478	12795	14	(a) (b)* (d)
28	SYDNEY (SYD)	25 333 508	13000	21	(a) (b) (c) (d)
29	TORONTO (YYZ)	24 739 312	11050	569	(a) (c)
30	PHILADELPHIA (PHL)	24 671 075	10500	21	(a)

* Certain runways only, **Only in excess of 112PNdB

Table 3-1: Busiest airports in the world by passenger number 2003 (www.airports.org) with runway lengths and elevations (Jenkinson *et al.* 1999) and noise limitations in place as of 2004 (http://www.boeing.com/commercial/noise/flash.html)

Noise Limitations

(a) Noise abatement procedures in place
(b) Curfews in operation
(c) Noise / traffic quotas or budgets used
(d) Noise surcharge applied
(e) Noise level limits in force

Limitations on aircraft not meeting ICAO stage 3 (ICAO 1993) are not shown

Temperature (ISA @ sea level = 15°C)	24 hour operations			0600 to 2300 operations		
	Av. hours per year > Temp	% hours above temp	% hours at or below temp	Av. hours per year > Temp	% hours above temp	% hours at or below temp
ISA	2399.3	27.40%	72.60%	2117.3	32.23%	67.77%
ISA+1°C	1965.5	22.45%	77.55%	1786.4	27.19%	72.81%
ISA+2°C	1572.5	17.96%	82.04%	1469.2	22.36%	77.64%
ISA+3°C	1240.2	14.17%	85.83%	1184.9	18.04%	81.96%
ISA+4°C	967.5	11.05%	88.95%	940.8	14.32%	85.68%
ISA+5°C	749.7	8.56%	91.44%	736.5	11.21%	88.79%
ISA+6°C	575.2	6.57%	93.43%	569.4	8.67%	91.33%
ISA+7°C	433	4.95%	95.05%	431.3	6.56%	93.44%
ISA+8°C	318.9	3.64%	96.36%	318.2	4.84%	95.16%
ISA+9°C	229.8	2.62%	97.38%	229.6	3.49%	96.51%
ISA+10°C	161.2	1.84%	98.16%	161.1	2.45%	97.55%
ISA+11°C	107.2	1.22%	98.78%	107.2	1.63%	98.37%
ISA+12°C	67.3	0.77%	99.23%	67.3	1.02%	98.98%
ISA+13°C	43.8	0.50%	99.50%	43.8	0.67%	99.33%
ISA+14°C	28.7	0.33%	99.67%	28.7	0.44%	99.56%
ISA+15°C	15.2	0.17%	99.83%	15.2	0.23%	99.77%
ISA+16°C	8.4	0.10%	99.90%	8.4	0.13%	99.87%
ISA+17°C	3.9	0.04%	99.96%	3.9	0.06%	99.94%
ISA+18°C	1.9	0.02%	99.98%	1.9	0.03%	99.97%
ISA+19°C	0.6	0.01%	99.99%	0.6	0.01%	99.99%
ISA+20°C	0.3	0.00%	100.00%	0.3	0.00%	100.00%

Table 3-2: Hours exceeding specified temperature at London Heathrow for period 1989 to 1999 inclusive (raw data from MetOffice)

[1997 excluded as no data available for several months]

Aircraft		B737-900ER	B747-400	B777-200	A340-300	A380	B787-8
Engine		CFM56-7B27	PW4062	PW4077	CFM56-5C4P	Trent 900	Trent 1000
Number of engines		2	4	2	4	4	2
MTOW	Tonnes	85.1	396.8	247.2	274.8	560.0	215.9
Gross Thrust per engine	kN	121.4	281.6	342.5	151.2	311.4	333.6
Mass flow per engine	kgs^{-1}	355	795[#1]	1040[#1]	483	1200	1211
L/D		16				18	
V_R	ms^{-1}	70					
T_j [#2]	K	T_∞+90	T_∞+100	T_∞+73	T_∞+70	T_∞+40	T_∞+35
ρ_j	kgm^{-3}	0.93	0.91	0.98	0.99	1.08	1.09
V_j [#3]	ms^{-1}	342	354	329	313	260	276
A_j [#4]	m^2	1.1	2.5	3.2	1.6	4.3	4.0
$A_{j,TOT}$	m^2	2.2	10.0	6.4	6.4	17.2	8.0
N_j	dB(A)	76.6	79.0	78.5	77.7	72.4	68.7
Following data normalised for MTOW = 160,000kg							
$A_{j,TOT}$	m^2	4.1	4.0	4.1	3.7	4.9	5.9
N_j	dB(A)	78.2	76.7	77.4	76.4	69.3	67.9

[#1] Estimated from other parameters as mass flow rate not listed

[#2] GasTurb model used to estimate fully mixed out jet temperature (Kurzke 2004)

[#3] Gross thrust per engine divided by mass flow per engine

[#4] Mass flow per engine divided by (jet velocity * jet density)

Table 3-3: Estimation of take-off jet mixing noise of existing and next generation aircraft from baseline airport utilising optimised take-off procedures

(Estimates of MTOW, mass flow rate and thrust sourced from www.boeing.com, www.cfm56.com, www.pratt-whitney.com, www.airbus.com and www.rolls-royce.com. All engines modelled as fully mixed out for simplicity and to give noise floor. Noise estimated using equation 3.19. Capability of engines providing take-off thrust levels with adequate stall/surge margin not considered.)

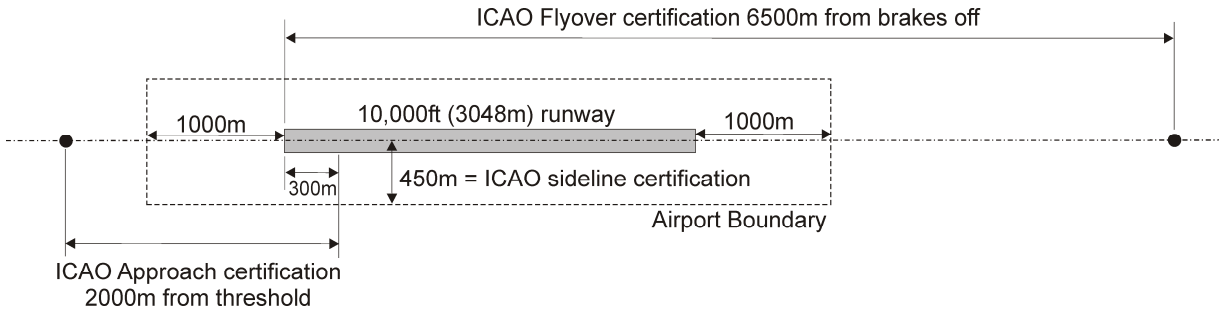

Figure 3-1: Baseline airport runway and boundary relative to ICAO certification distances

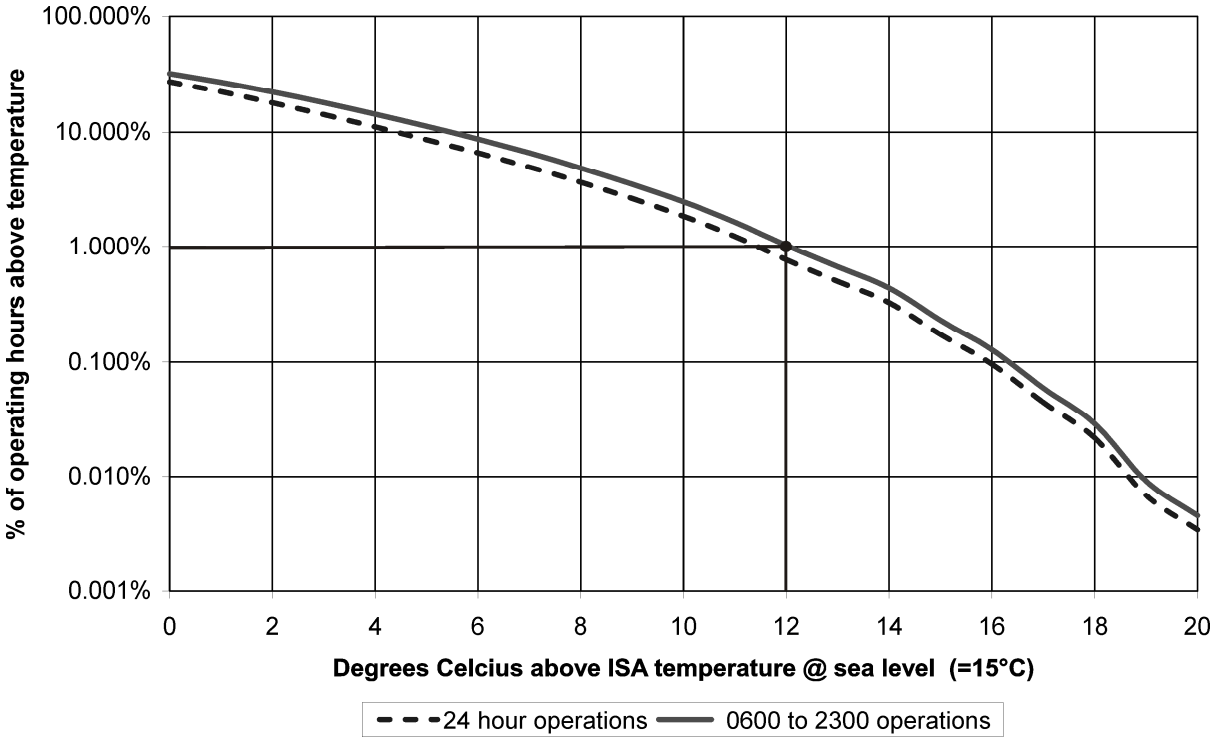

Figure 3-2: Percentage of operating hours exceeding specified temperature at London Heathrow for period 1989 to 1999 inclusive (raw data from MetOffice)

[1997 excluded as no data available for several months]

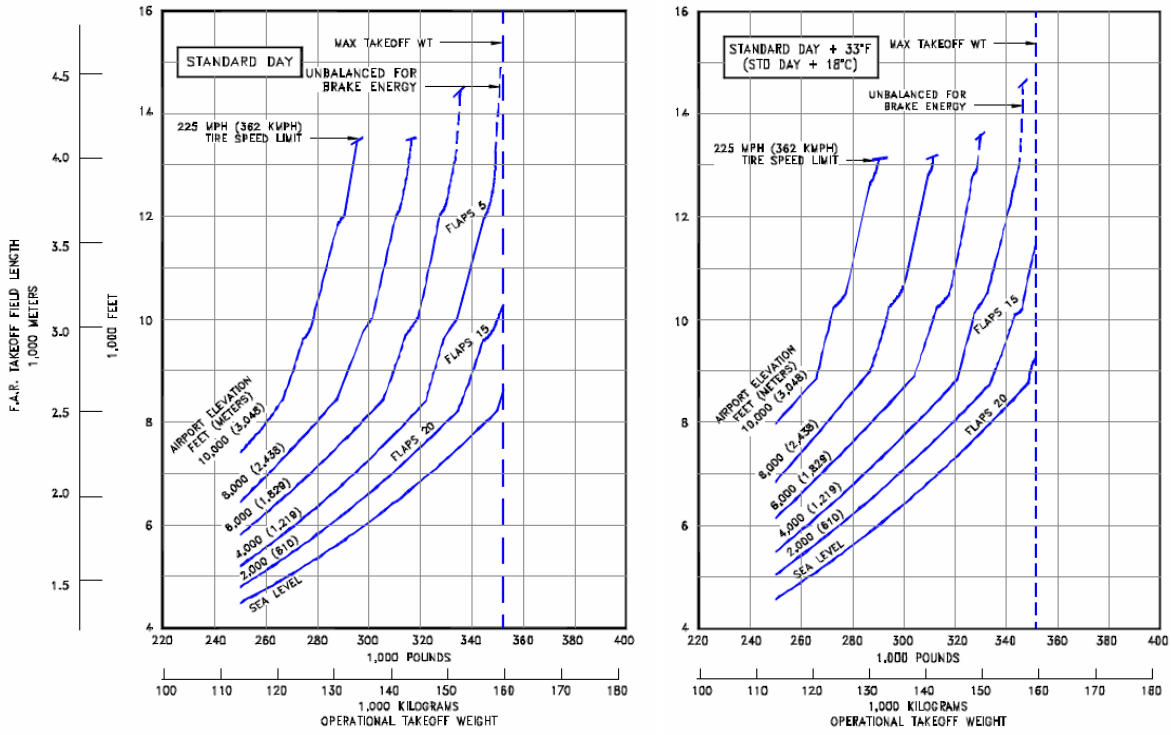

Figure 3-3: Runway length requirements for B767-300 with CF6-80A engines (Boeing 2003)

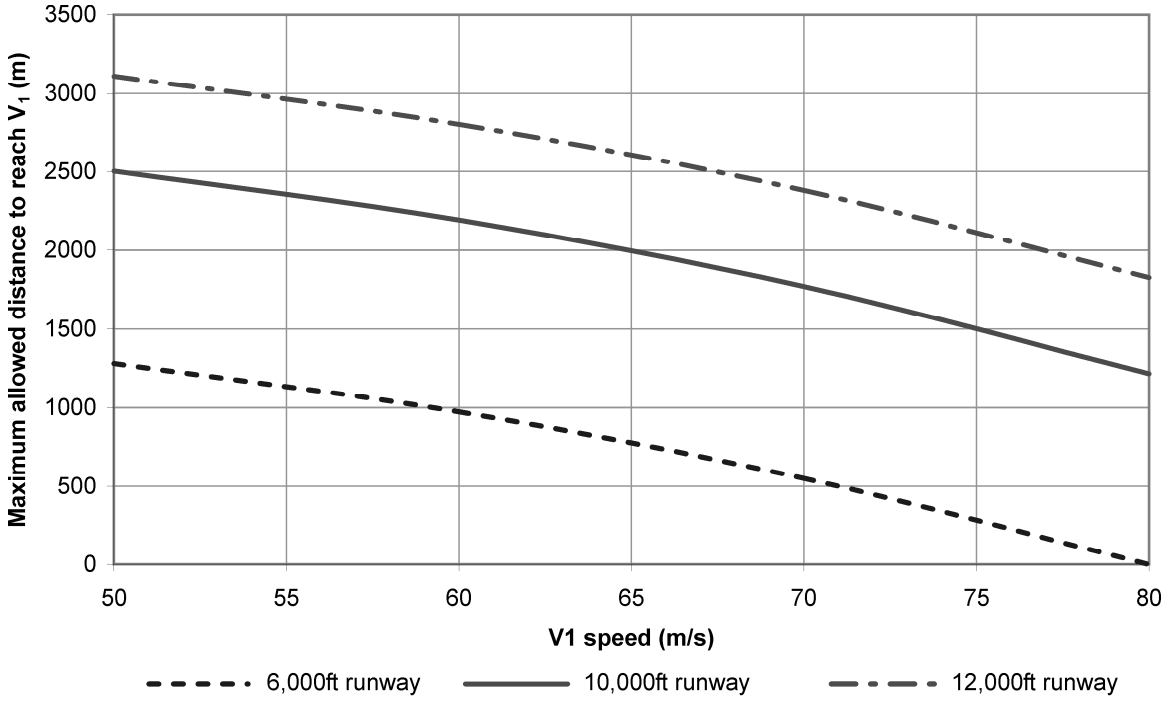

Figure 3-4: Available runway length to reach V_1 so as to satisfy accelerate-stop regulations for different runway lengths.

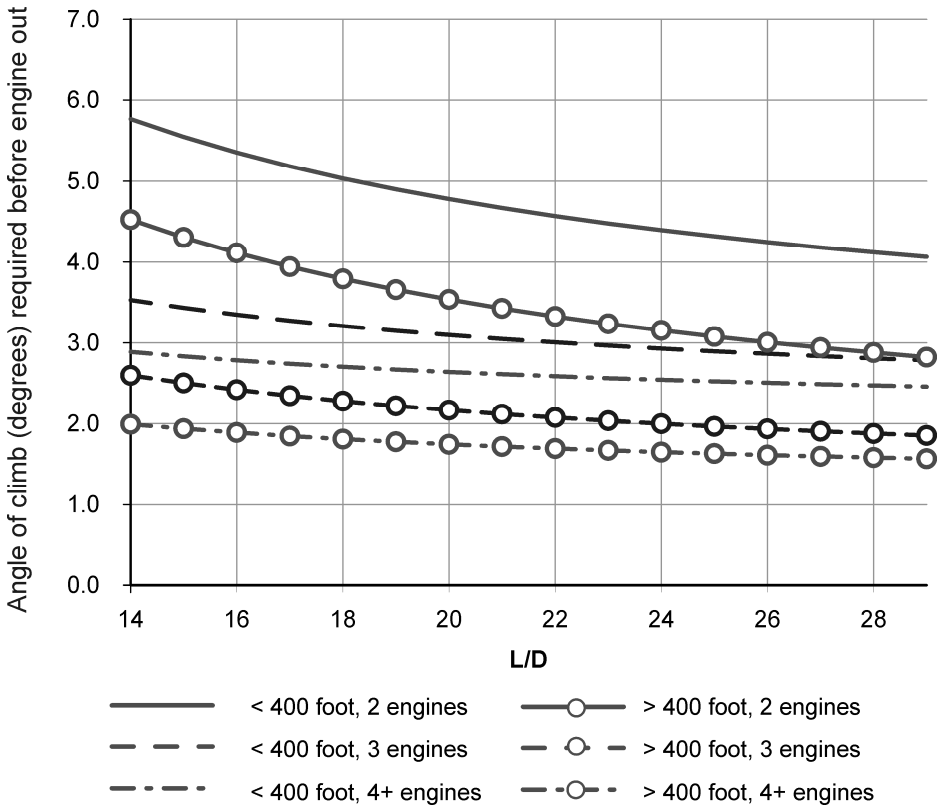

Figure 3-5: Minimum climb angle required to satisfy engine-out regulations (no change in L/D due to engine out, gear retracted)

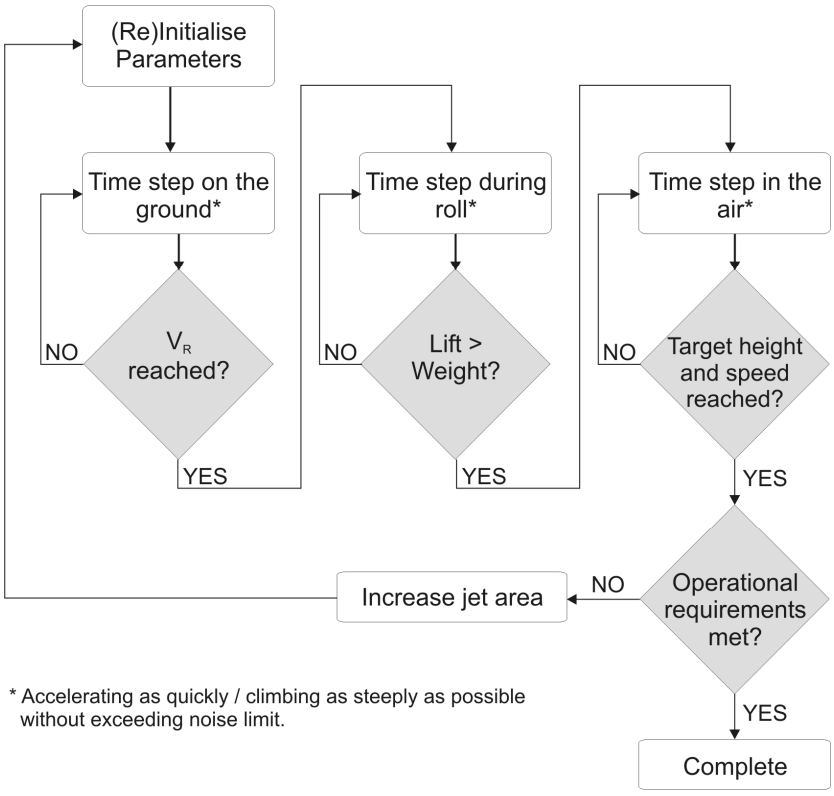

Figure 3-6: Time-stepping flow chart used during take-off optimisation

Whilst on the ground:

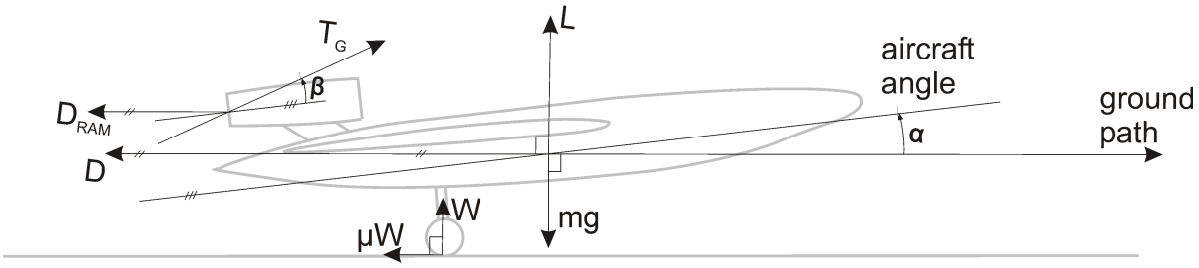

In the air:

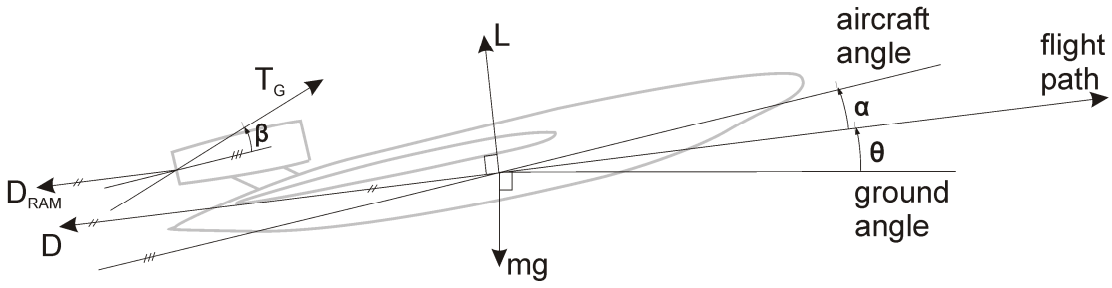

Figure 3-7: Aircraft model used during take-off optimisation

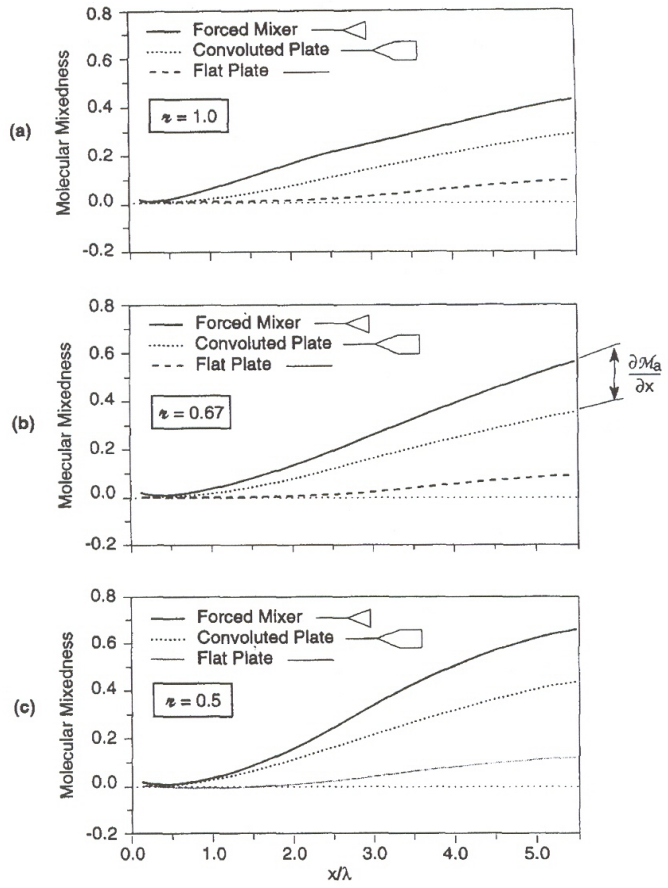

Figure 3-8: Mixing enhancement through forced mixing (Waitz *et al.* 1997)

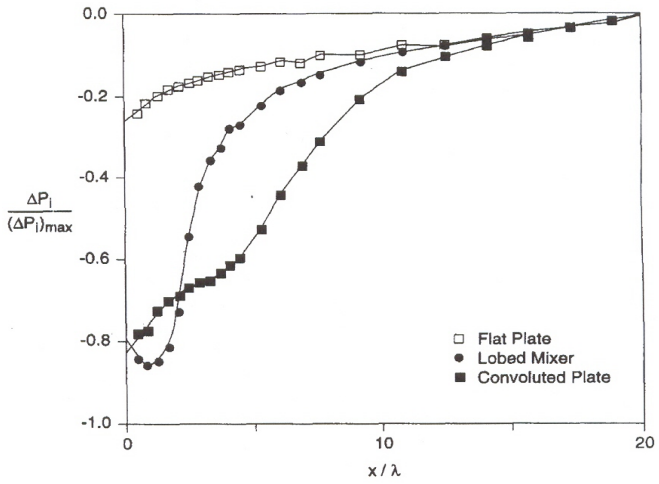

Figure 3-9: Static pressure rise across mixing section through forced mixing with a velocity ratio of 0.31 (Waitz *et al.* 1997)

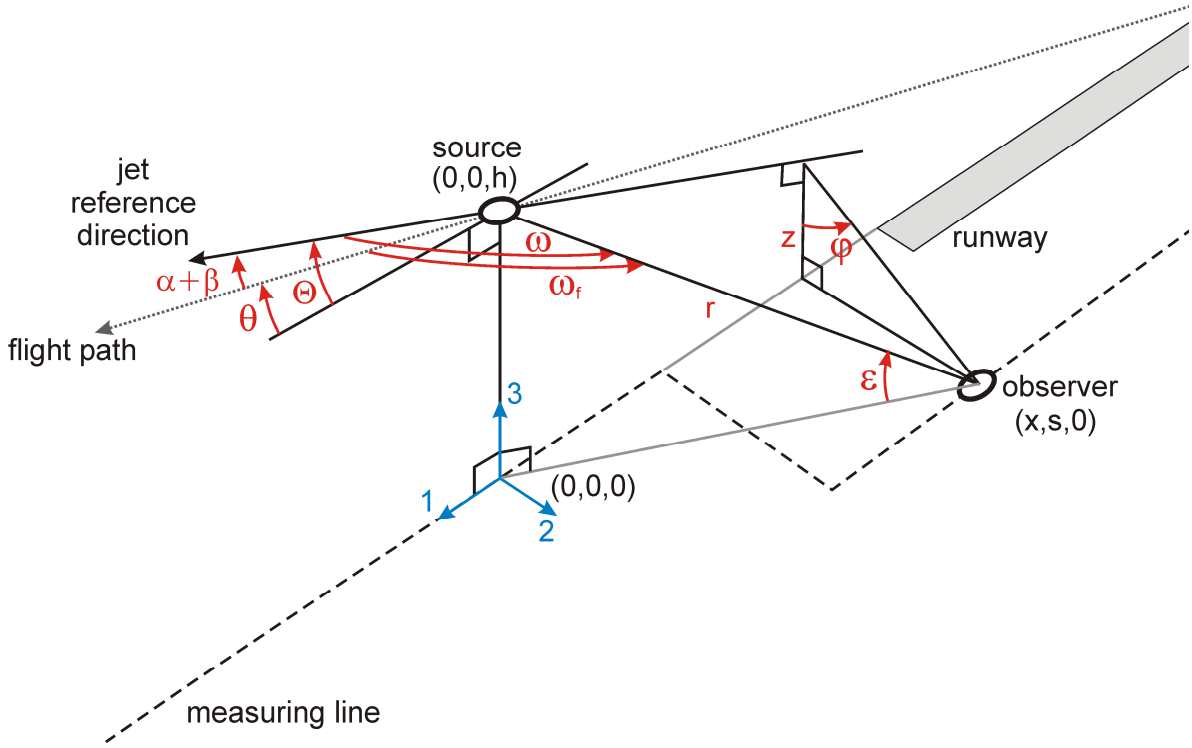

Figure 3-10: Polar and azimuthal angle definition

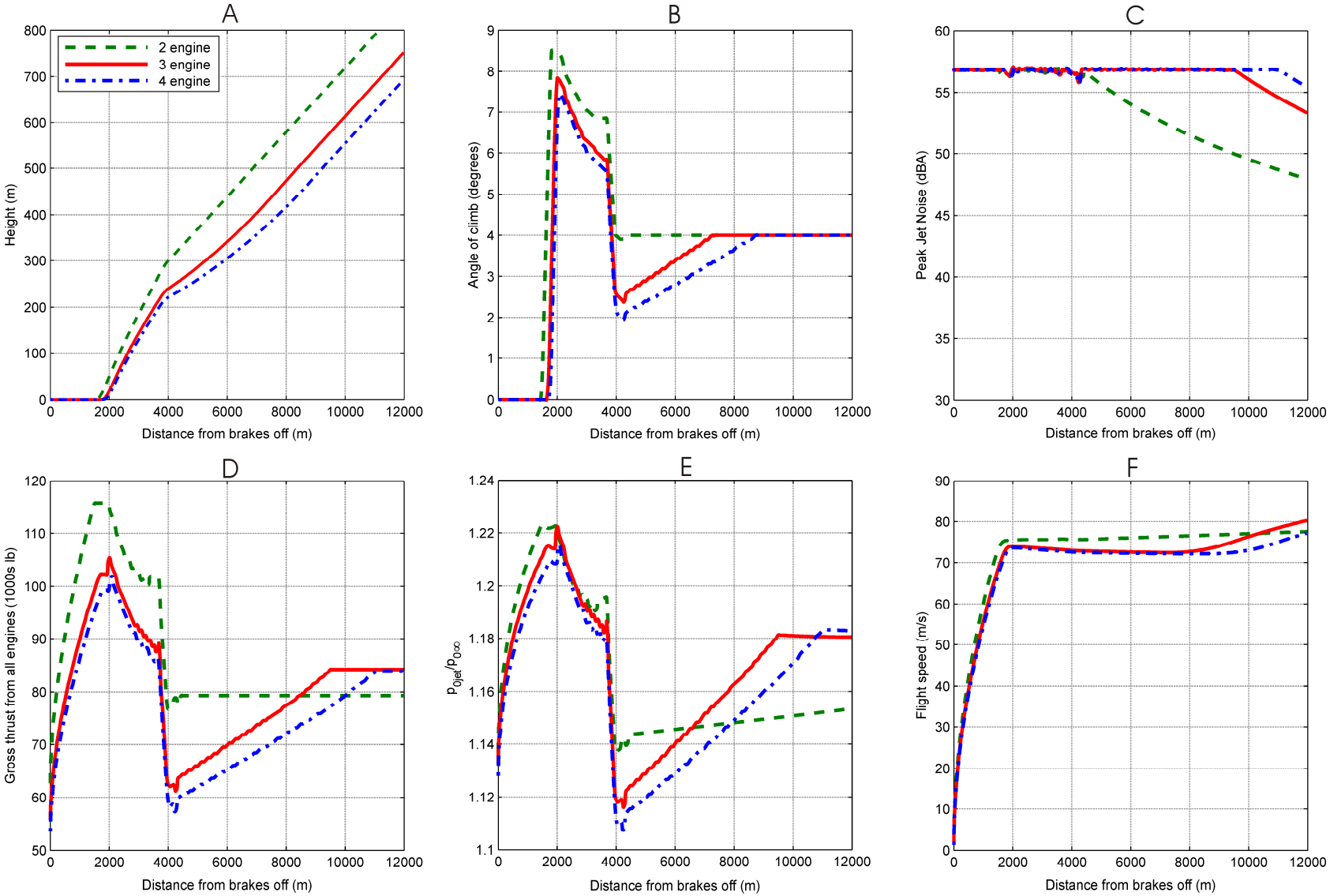

Figure 3-11: Optimised take-off performance for baseline aircraft and airport with fixed jet area set for noise target of 57dBA

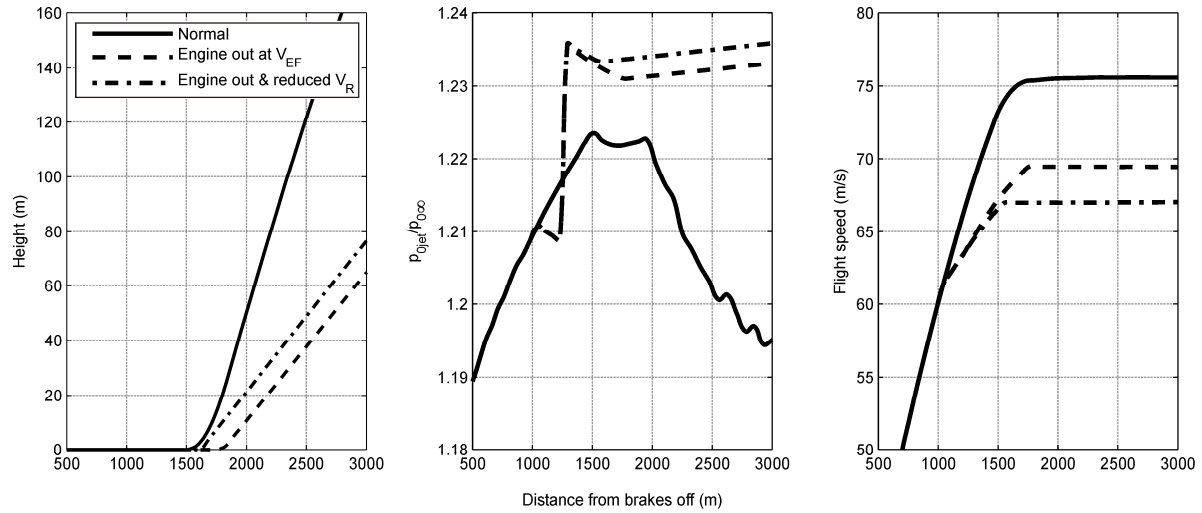

Figure 3-12: Engine out performance of 2-engine baseline aircraft (V_{EF}=60m/s, 996m after brakes off)

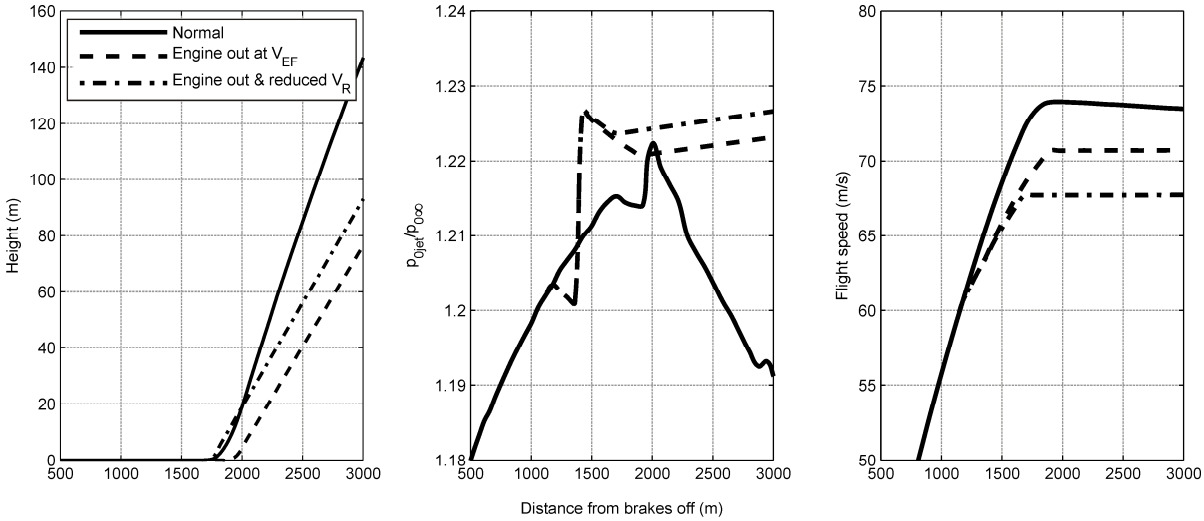

Figure 3-13: Engine out performance of 3-engine baseline aircraft (V_{EF}=60m/s, 1151m after brakes off)

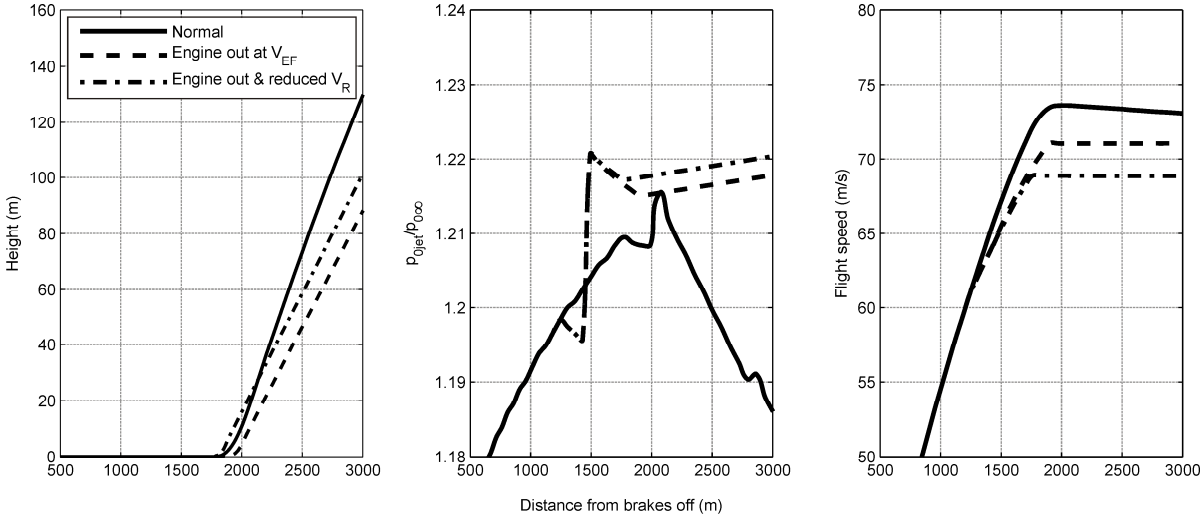

Figure 3-14: Engine out performance of 4-engine baseline aircraft (V_{EF}=60m/s, 1204m after brakes off)

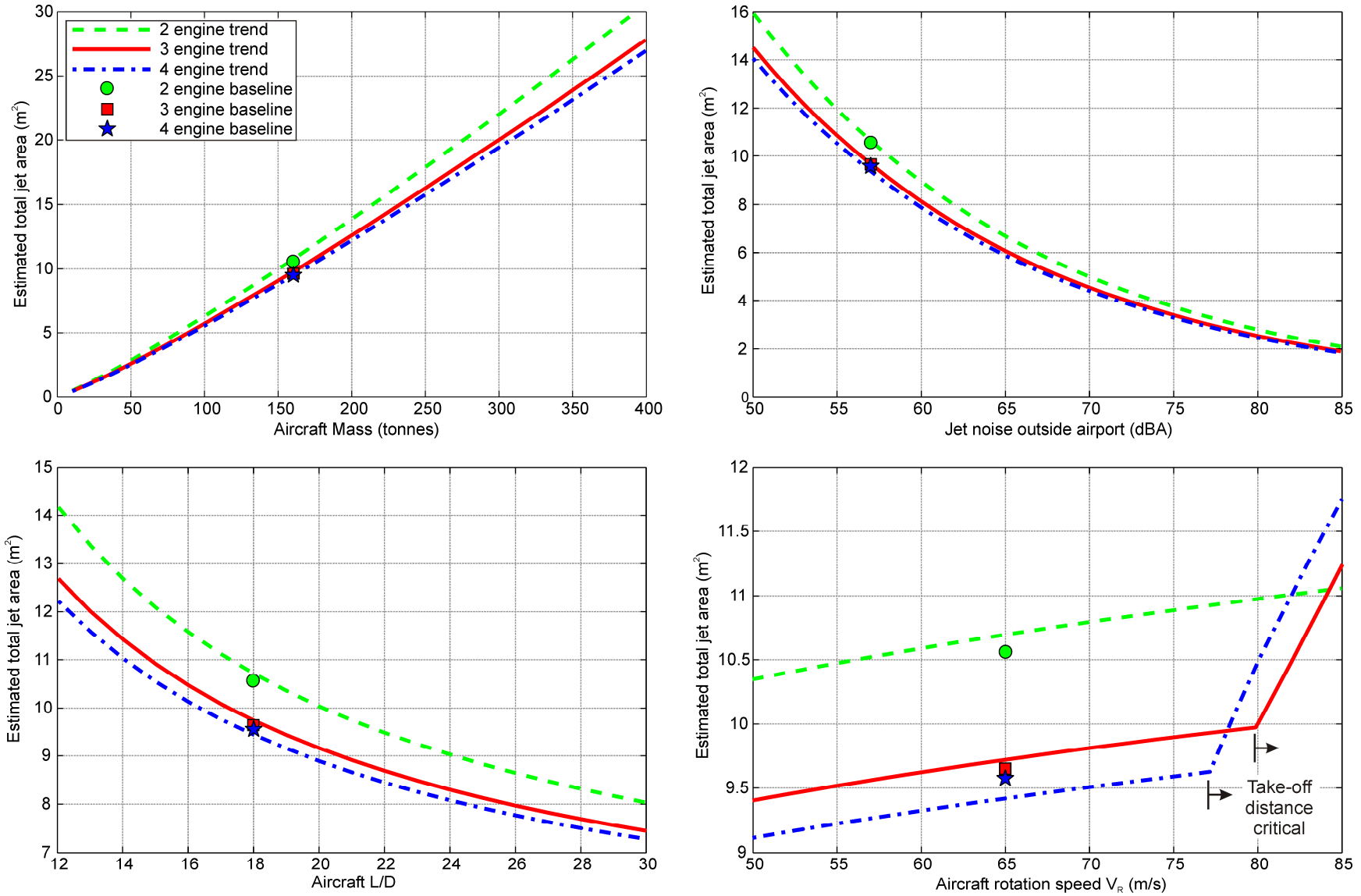

Figure 3-15: Impact of modifying key parameters on required jet area of baseline aircraft for specified jet mixing noise target

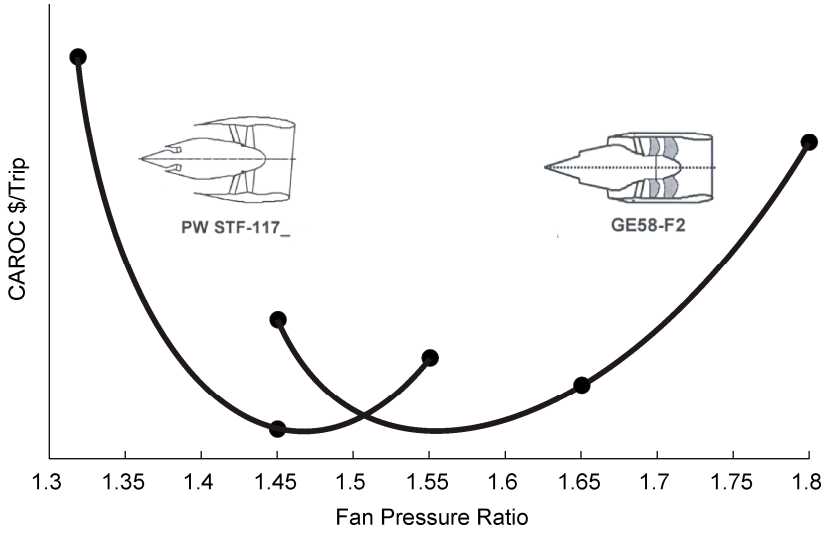

Figure 3-16: Estimations of optimum FPR for 2015 technology (adapted from Daggett *et al.* 2003)

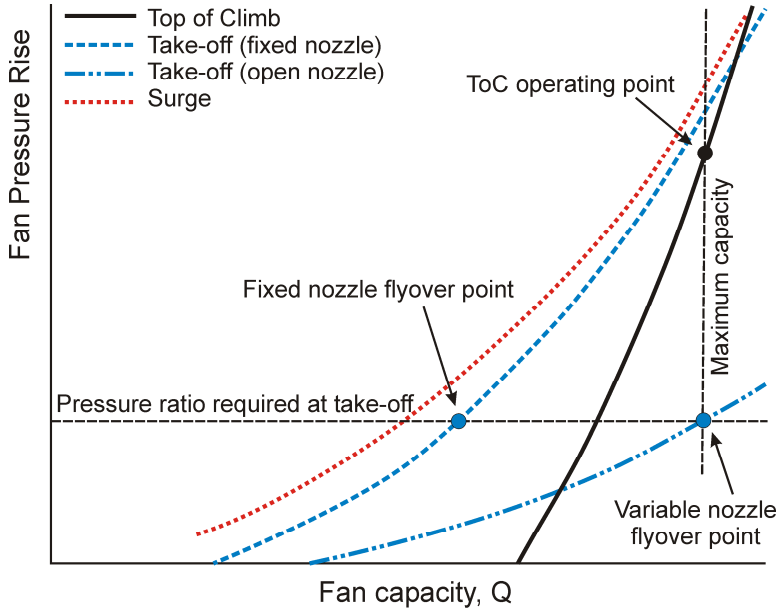

Figure 3-17: Operating lines on fan map showing ideal impact of increasing nozzle area at take-off to deliver high mass flow and low pressure rise (Hall *et al.* 2004)

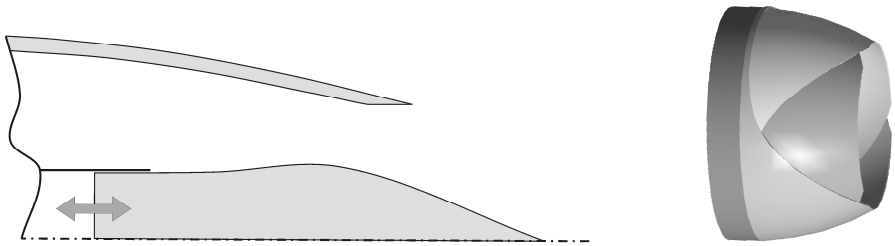

Figure 3-18: Two low loss variable area nozzle concepts

Concept on left (Whurr 2005) is plug that moves axially downstream to reduce nozzle area and upstream to increase it. Concept on right (author's own) is three or more overlapping nozzle sections that can rotate independently. If they lie on top of each other then effective nozzle area is increased.

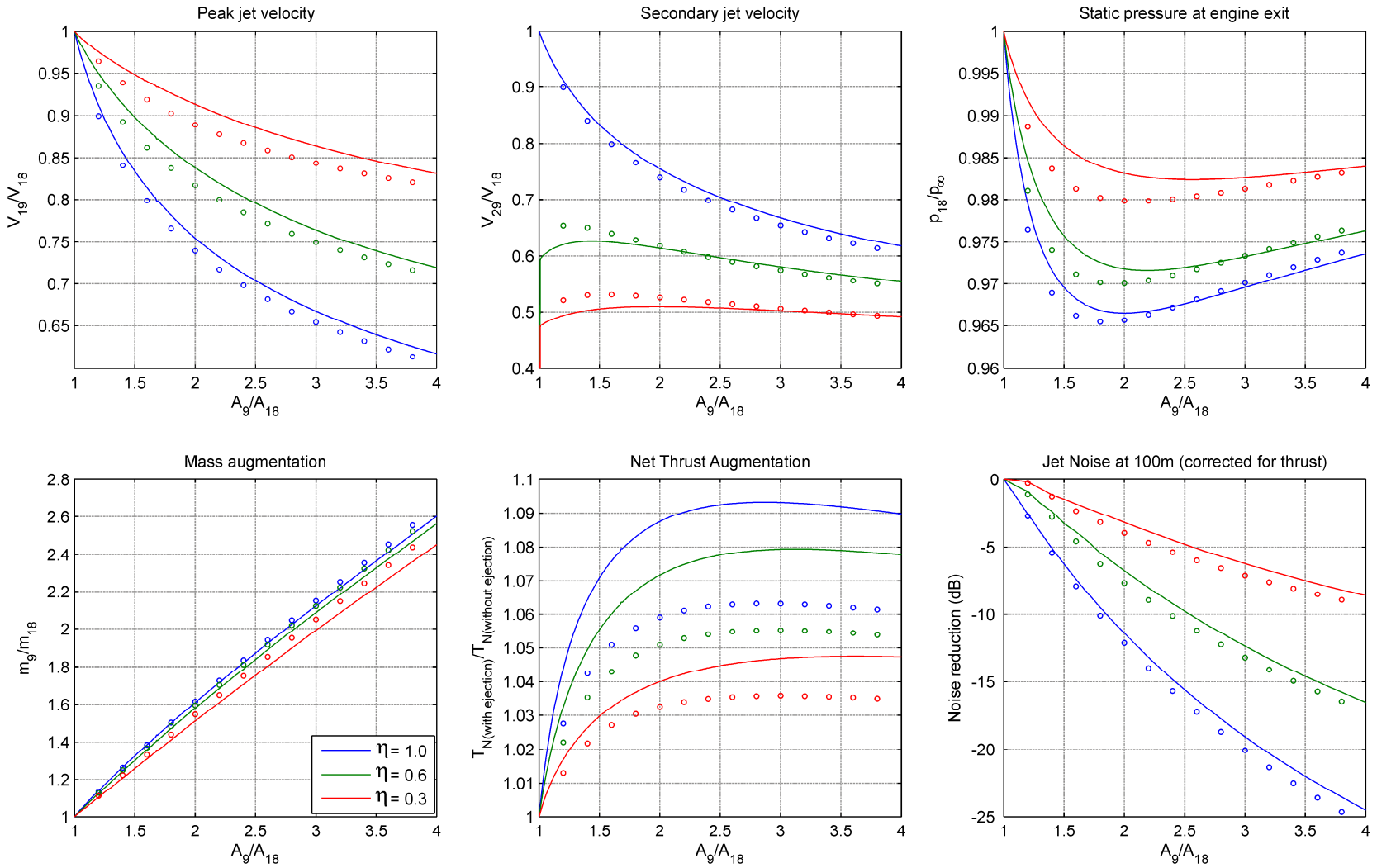

Figure 3-19: Prediction of ejector performance for V_∞=80m/s when driven by a core jet with 1.20 stagnation pressure rise and Tj=T_∞+22K

(Solid lines = incompressible, circles = compressible, ISA sea level conditions, incompressible pressure ratio set to 1.198 to give identical performance with no ejector, see Appendix C for definition of locations 9, 18, 19 and 29.)

	Variant	Sideline	Flyover	Top of Climb	Start of Cruise
Altitude	C	200m	300m	12,192m	12,192m
	A		250m		
Conditions	-	ISA+12K		ISA+10K	ISA
Velocity	C	80m/s (V_R=70m/s)		Mach 0.8	Mach 0.8
	A	75m/s (V_R=65m/s)			
Weight	-	160,000kg		156,800kg	
Airframe Parameters*[1]	C	A_{wing} = 283.3m^2, L_1 = 7.7m, L_2 = 24.5m, h_{rudder} = 9m			
	A	A_{wing} = 885.6m^2, L_1 = 7.3m , L_2 = 26.4m, L_3 = 19.0m			
Lift to Drag ratio	C	18		21	
	A	21		24	
Angle of climb	-	8.0°	See eqn 3.2	0.36°	0°
PR_{IN}	-	0.995			
PR_{OUT} *[2]	C	0.99			
	A	0.98			
ΔT_0 *[3]	C	76 / (FPR-1)			
C_{FG}	-	0.99			
η_p	-	92%			

*1 See Appendix E for definition of airframe parameters.
Conventional aircraft values based on Boeing 767-200ER approximations

*2 Factors of 0.99 and 0.98 are duct losses with all-lifting body design utilising longer ducts for noise reduction. Changes in PR_{OUT} from core mixing not included at this time.

*3 Values of ΔT_0 due to core mixing estimated using GasTurb and discussed in more detail in Appendix D.

Table 4-1: Baseline aircraft parameters; Conventional two-engine (C) and three-engine all-lifting body (A)

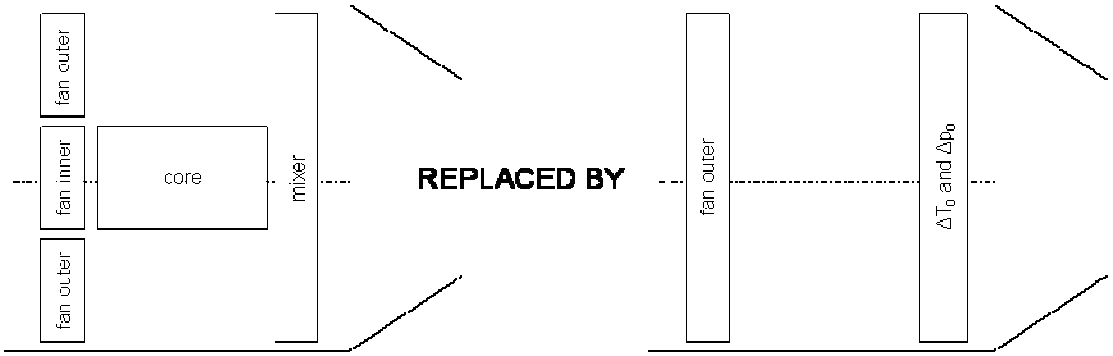

Figure 4-1: Modelling of core as temperature and pressure correction in UHBR engine

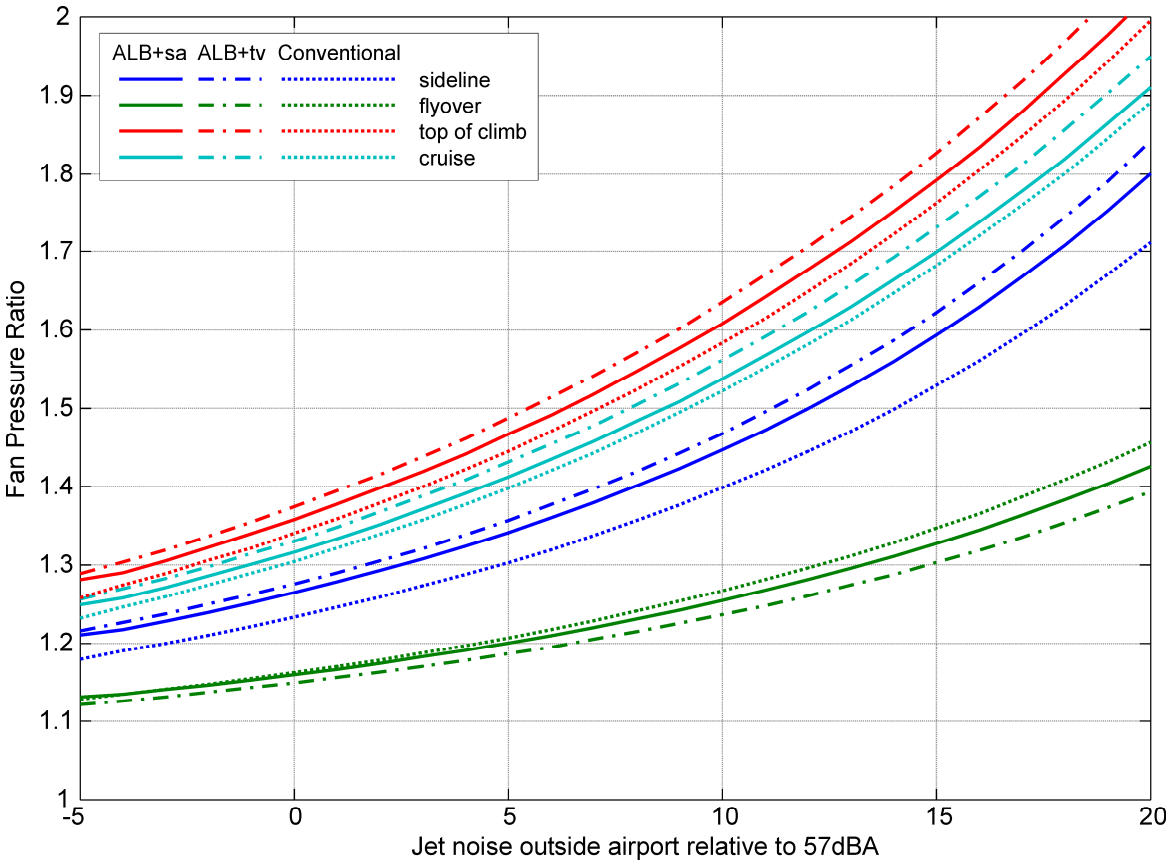

Figure 4-2: Resulting FPR for three aircraft variants at sideline, flyover, top of climb and cruise conditions when operating with fixed nozzle area and meeting specified take-off jet noise level.

(ALB+sa = three-engine all-lifting body airframe using split aileron to correct engine out yaw,
ALB+tv = three-engine all-lifting body airframe using thrust vectoring to correct engine out yaw,
Conventional = two-engine conventional airframe)

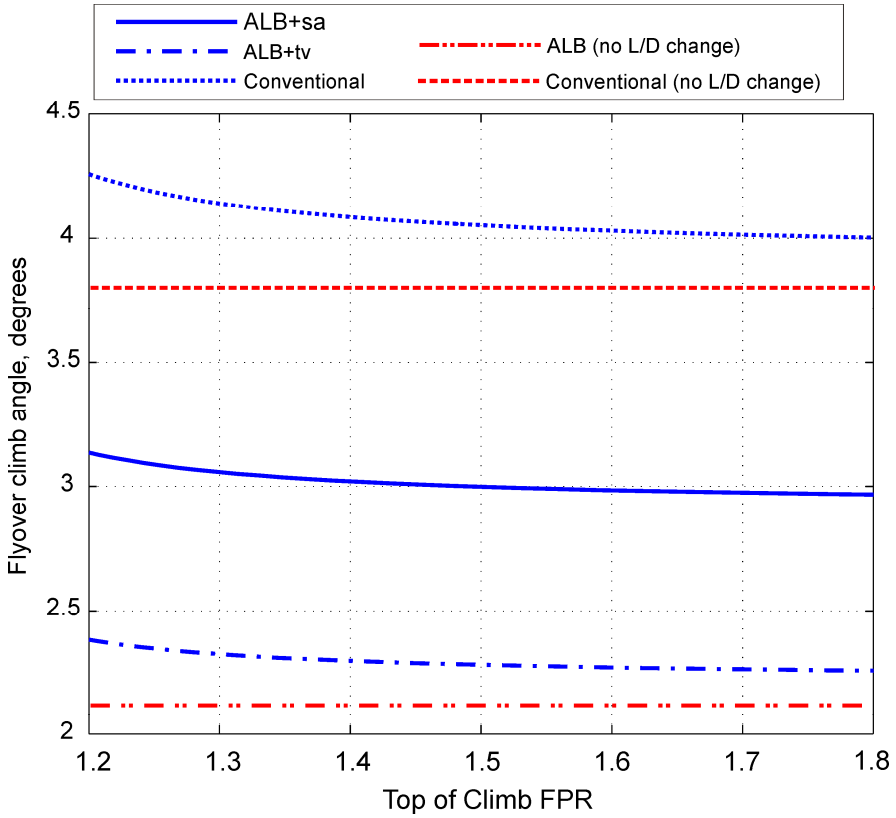

Figure 4-3: Impact of drag increase following engine out on pre engine out climb angle for 2 engine conventional and 3 engine all-lifting body aircraft. Windmill drag calculations based on Top of Climb fan face Mach number of 0.66.

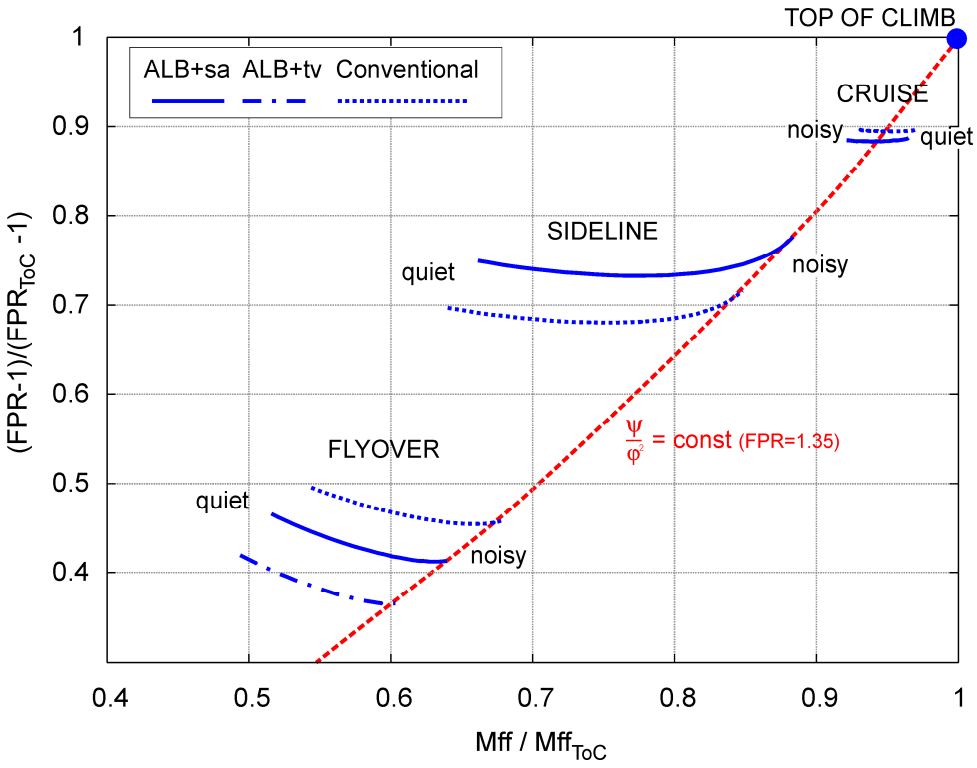

Figure 4-4: Locus of operating points on fan map for aircraft variants operating with fixed area nozzle

(ALB+tv and ALB+sa lines coincident for sideline and cruise locations)

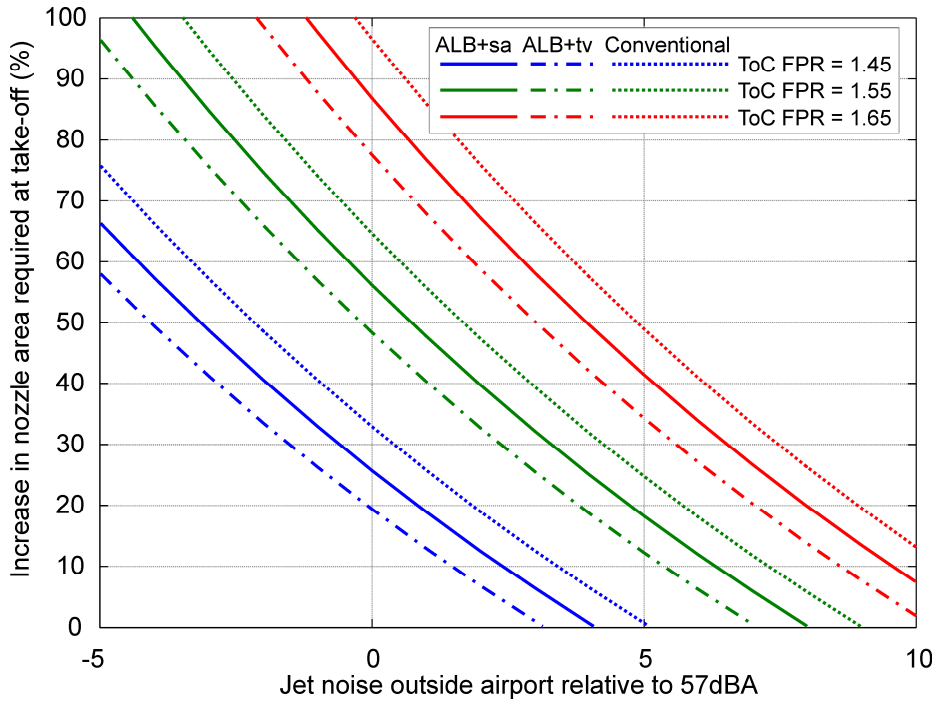

Figure 4-5: Change in nozzle area between take-off and top of climb required to meet specified take-off noise level and top of climb FPR

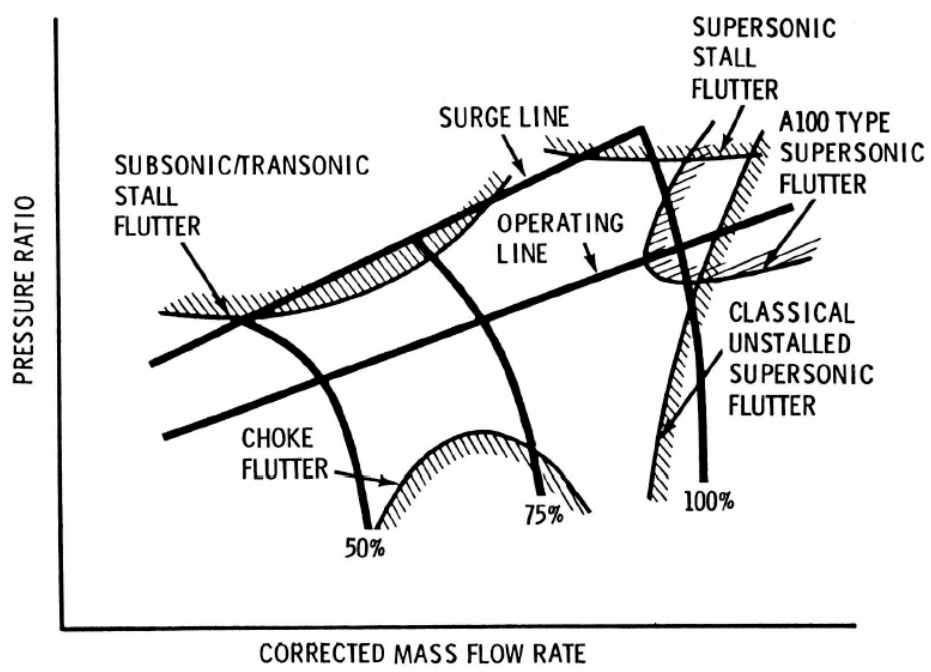

Figure 4-6: Types of Fan/Compressor Flutter (Snyder and Burns 1988)

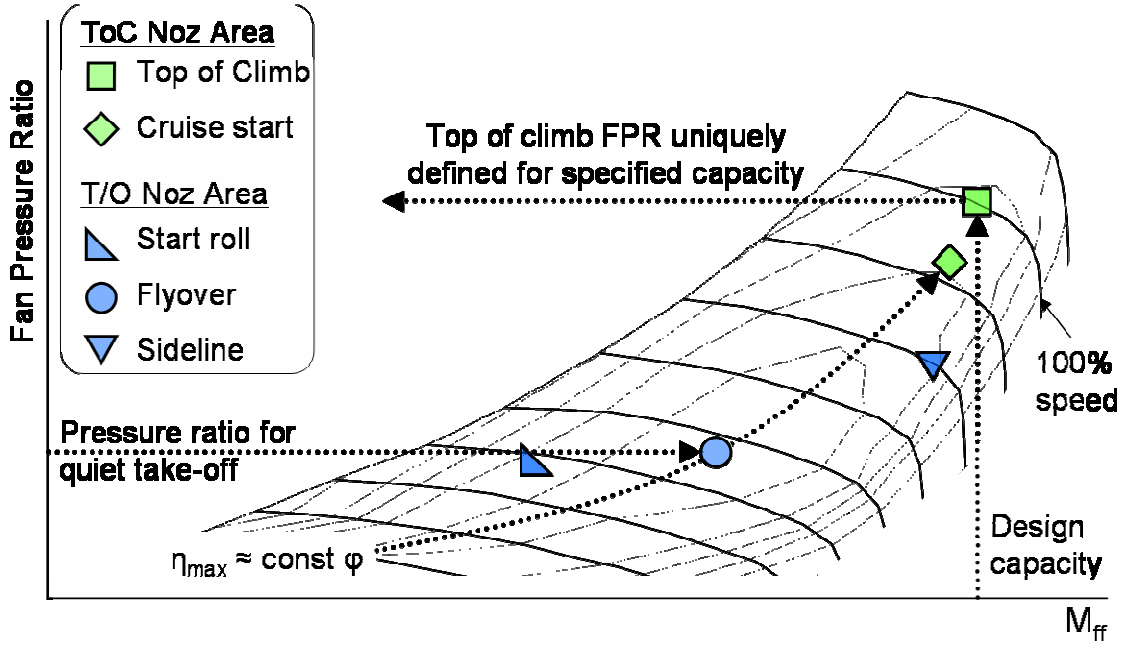

Figure 4-7: Fan operation with two nozzle areas; Top of Climb (ToC) and Take-off (T/O).

Top of climb FPR is uniquely specified by setting take-off nozzle area to meet noise target, matching flyover and cruise flow coefficients and specifying ToC design capacity.

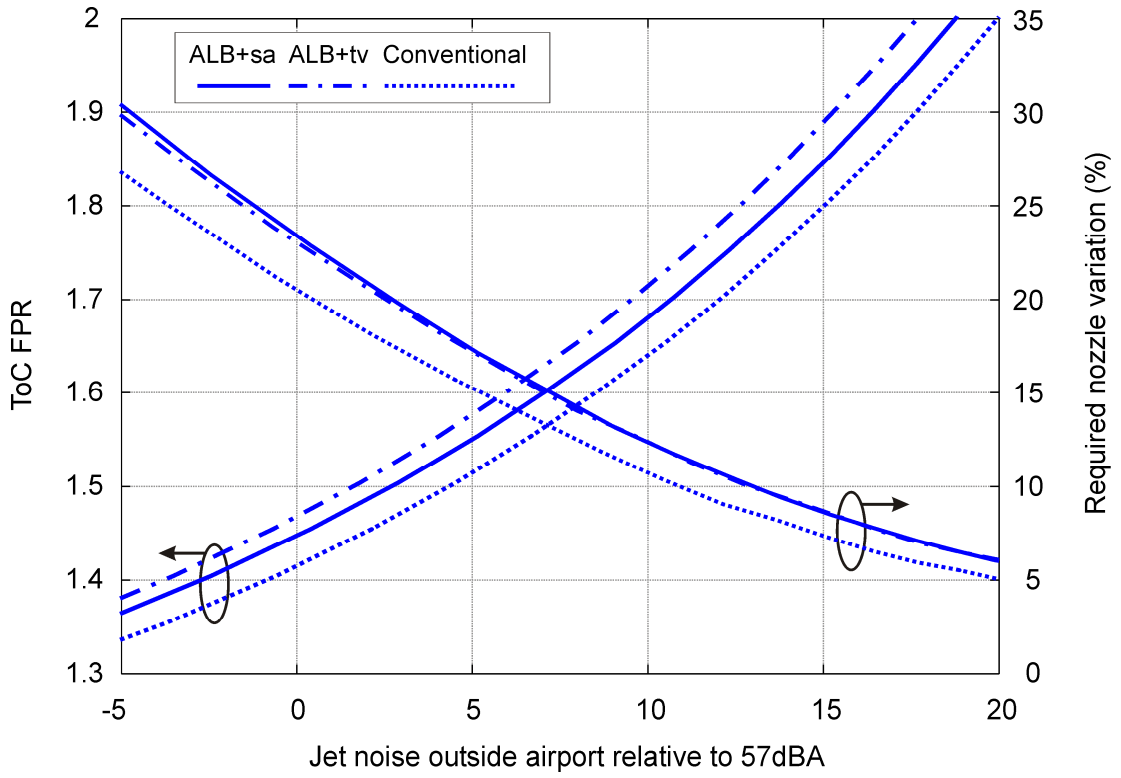

Figure 4-8: ToC FPR and nozzle variation required to meet a specified take-off jet noise target at the same time as setting $\varphi_{flyover} = \varphi_{cruise}$ (for equal ToC and cruise nozzle areas)

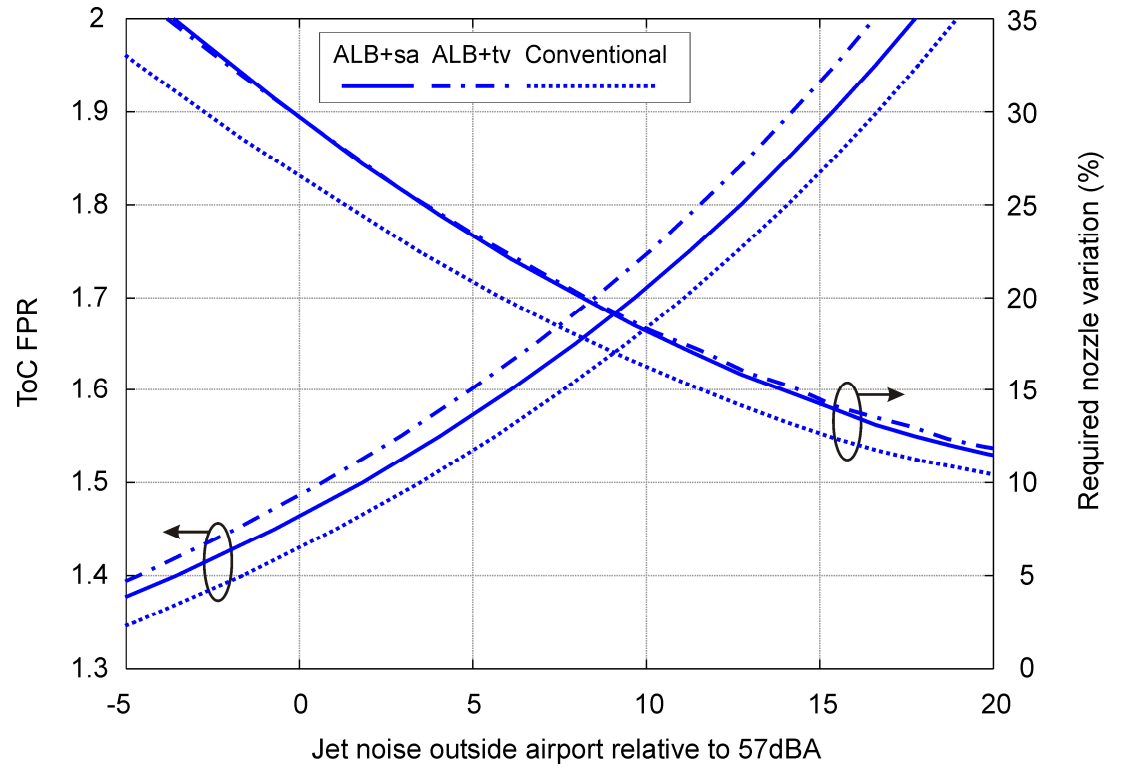

Figure 4-9: ToC FPR and nozzle variation required to meet a specified take-off jet noise target at the same time as setting $\varphi_{flyover} = \varphi_{cruise} + 0.05$ (for equal ToC and cruise nozzle areas)

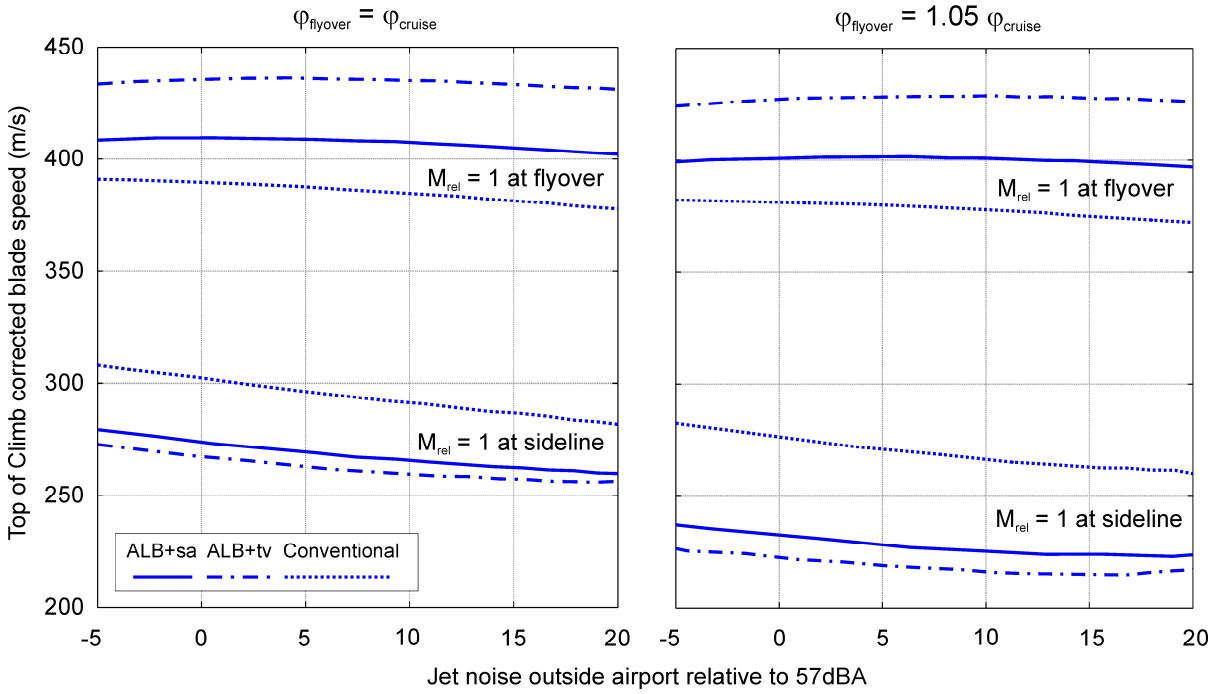

Figure 4-10: Required ToC corrected blade speed to satisfy M_{rel}=1 at sideline or flyover

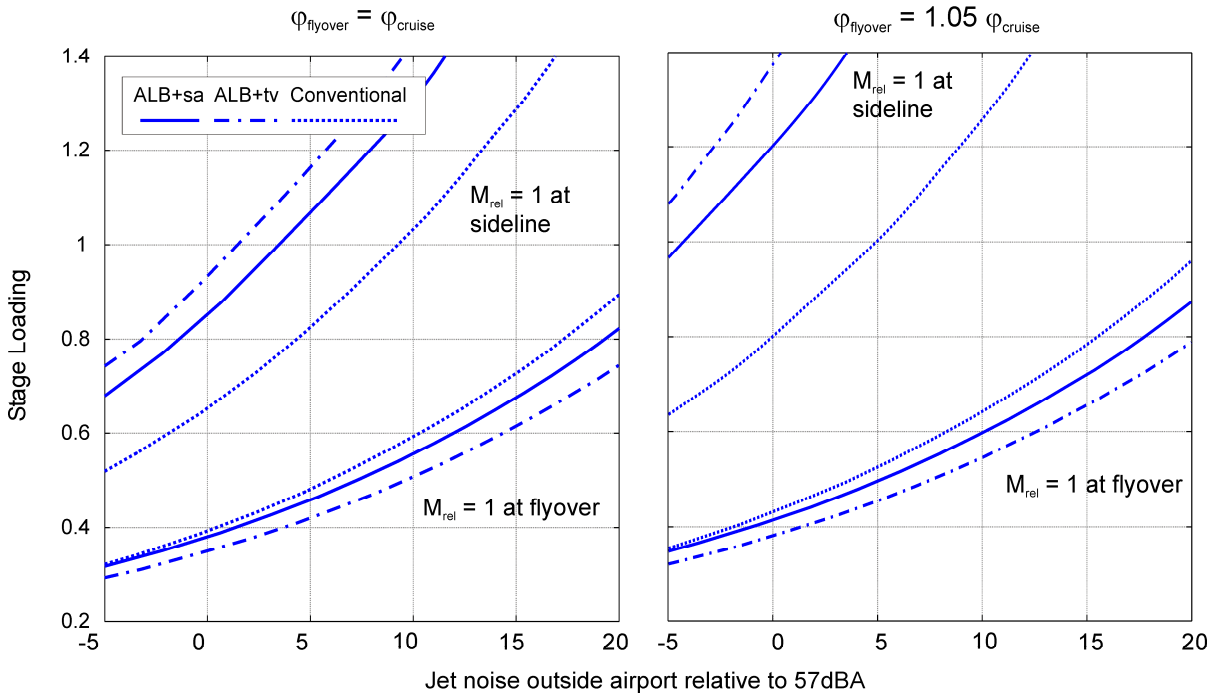

Figure 4-11: Required ToC stage loading to satisfy M_{rel}=1 at sideline or flyover

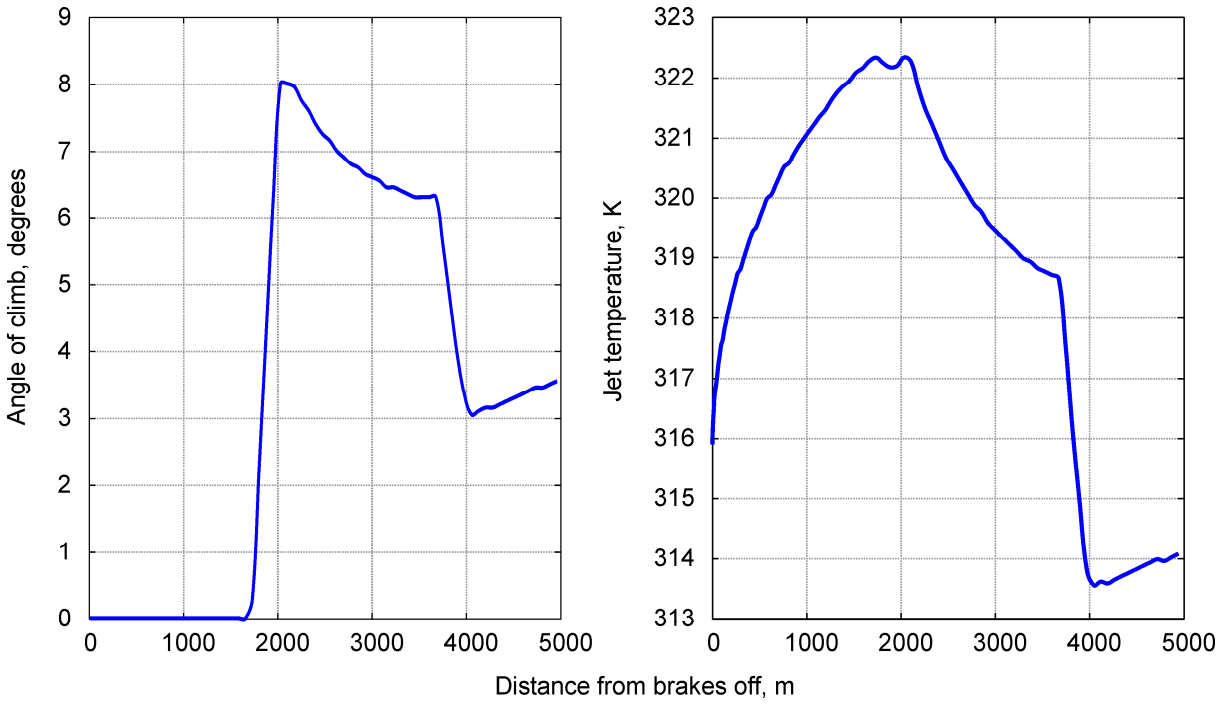

Figure 4-12: Optimised take-off performance of ALB+sa aircraft with ToC FPR of 1.442 under 57dBA jet noise limit.

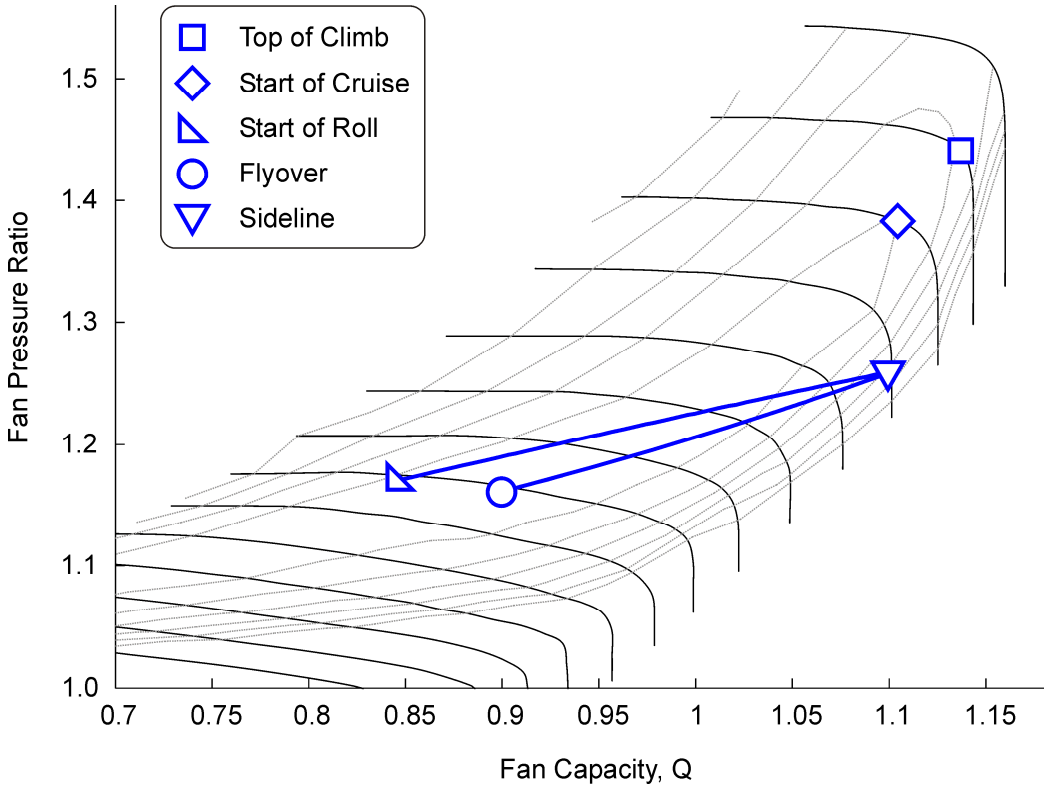

Figure 4-13: Fan operation of ALB+sa aircraft with ToC FPR of 1.442 under 57dBA jet noise limit. Fan characteristic was used to match cruise and flyover flow coefficients only. Stage polytropic efficiency set to a constant value of 0.92.

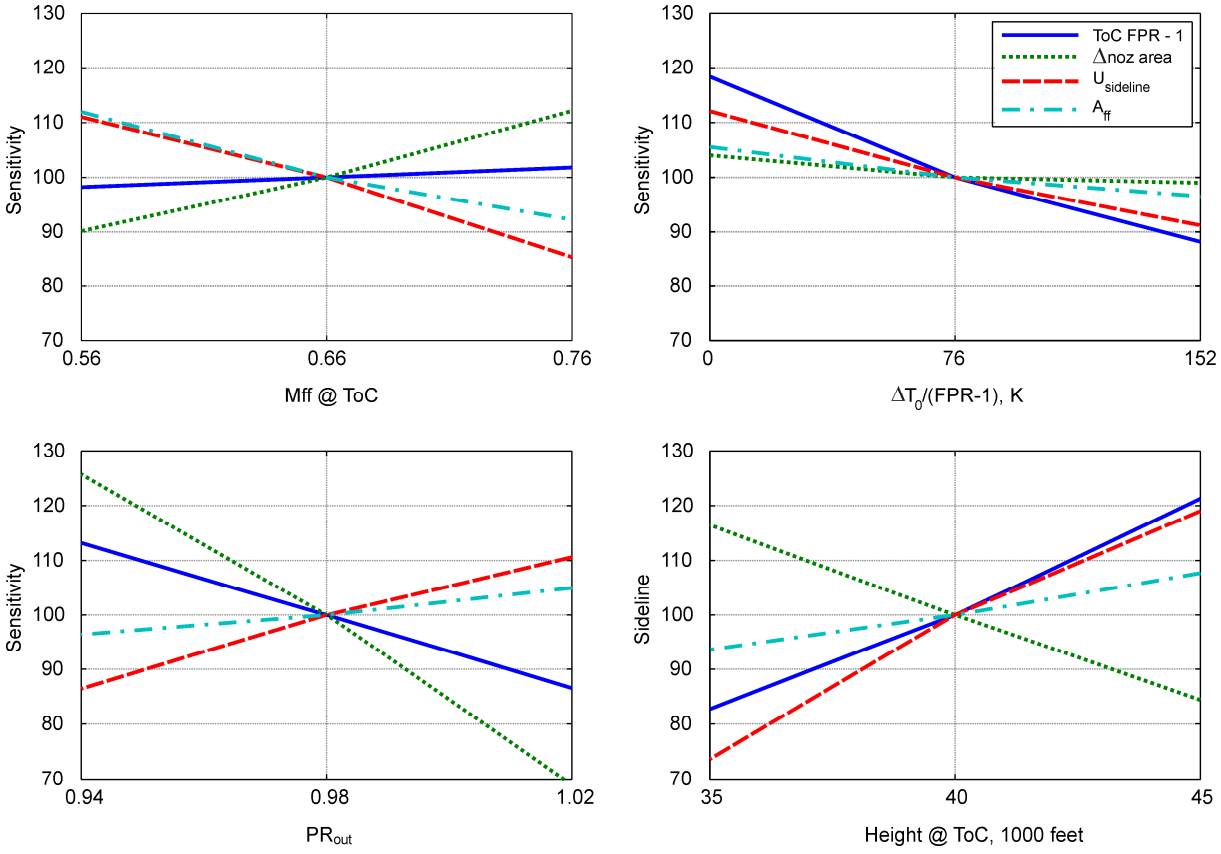

Figure 4-14: Impact of modifying input parameters when matching cruise and flyover flow coefficients whilst meeting take-off jet noise level of 57dBA.

Sensitivity = 100 * (property / baseline value of property). Baseline is split aileron all-lifting body with data from table 4-1. Properties are (i) top of climb FPR minus one, (ii) percentage change in nozzle area required between ToC and take-off, (iii) ToC fan tip speed that would give M_{rel}=1 at sideline condition and (iv) fan face area.

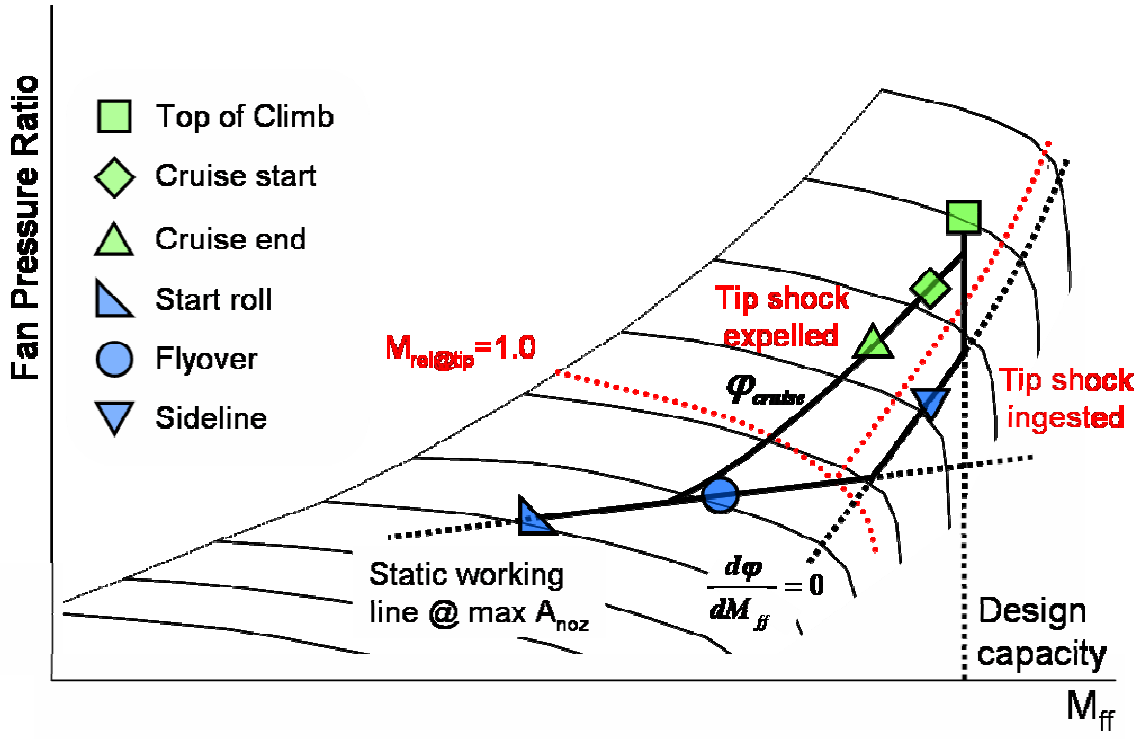

Figure 4-15: Fan operation with continuously varying nozzle area

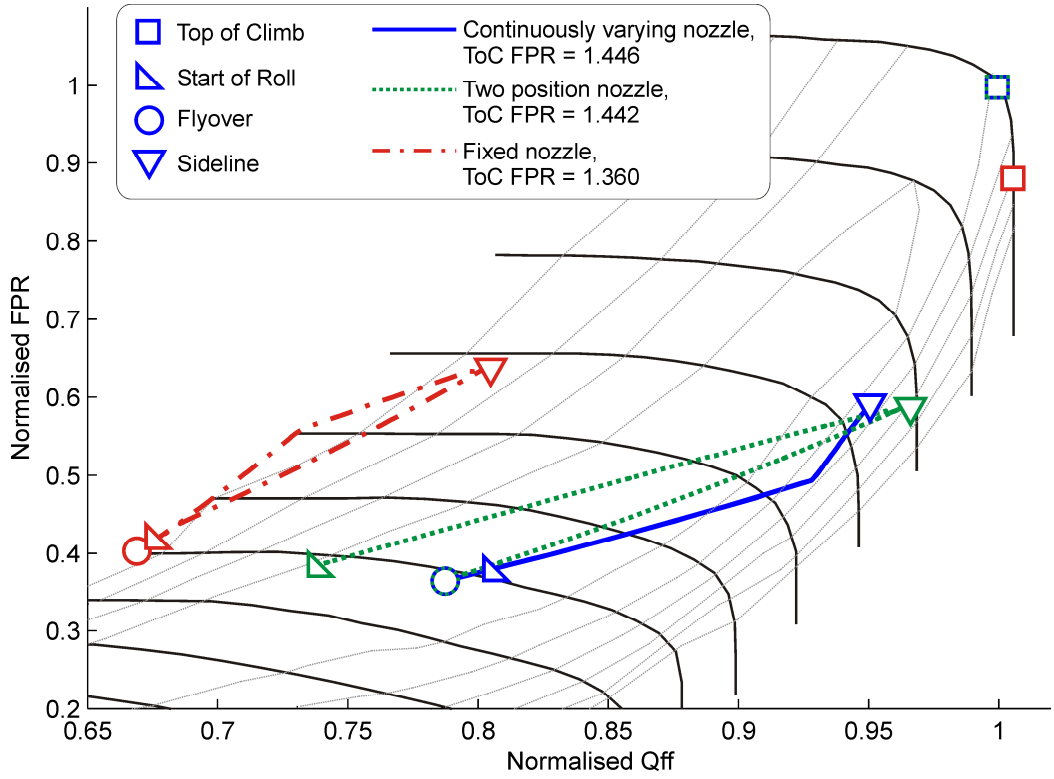

Figure 4-16: Comparison of fan operation for the ALB+sa aircraft under 57dBA jet noise limit when operating with a (a) a continuously varying nozzle area, (b) a two position nozzle and (c) a fixed nozzle

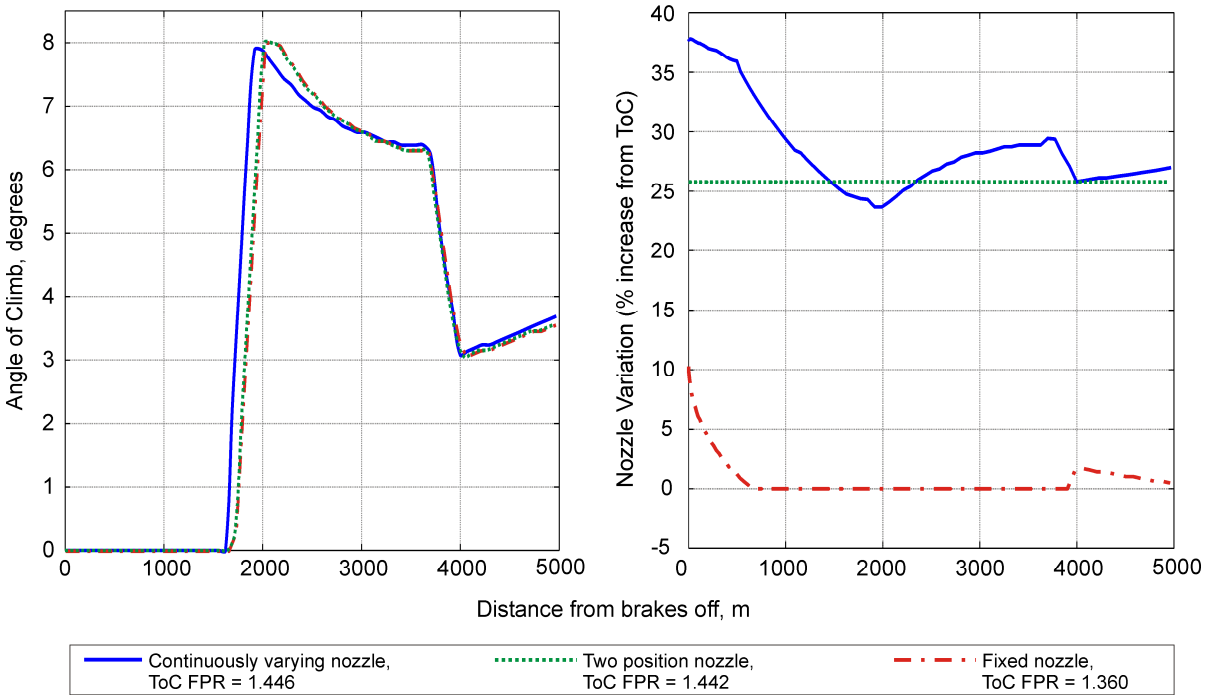

Figure 4-17: Comparison of take-off performance for the ALB+sa aircraft under 57dBA jet noise limit when operating with a (a) a continuously varying nozzle area, (b) a two position nozzle and (c) a fixed nozzle

Parameter	Value	Description
INMACH	0	Inlet absolute flow angles fixed
INVR	-1	$d^2P/dm^2=0$ and $dVr/dm=0$ at inlet
ISTEP	3	Non-uniform timestepping
ISMTH	2	Combined 2^{nd} and 4^{th} order smoothing
IPOUT	0	Static exit pressure applied at hub + radial equilibrium
ILOS	9	Loss subroutine 9 applied (Denton 1990)
FT	0.5	Timestep Multiplying factor
SF	0.01	Smoothing factor in pitchwise and spanwise directions
SFX	0.01	Smoothing factor in streamwise direction
DAMP	10	Negative feedback
CLIM	0.0001	Convergence criterion (average percentage change in meridional velocity)
RFIN	0.1	Relaxation factor for inlet pressure (reduced to 0.02 at low speed near stall)
REYNO	$1.5x10^6$	Reynolds number based on mid span meridional chord and exit velocity
REL	0.5	Relaxation factor on changes in viscous forces
FTRANS	0.001	Fully turbulent boundary layers
FACSEC	0.8	Multiplying factor on 4^{th} order smoothing
Mixing Length Limits	0.03 to 0.05	

Table 5-1: Multall calculation control parameters

Design Streamline	Approx mass flow from hub	0%	10%	30%	50%	70%	90%	100%
LE axial position	m	0.700	0.700	0.697	0.680	0.655	0.623	0.607
Axial chord	m	0.325	0.325	0.303	0.280	0.266	0.257	0.2601
LE radius	m	0.3000	0.4333	0.6129	0.7609	0.8801	0.9849	1.0334
TE radius	m	0.3600	0.4699	0.6384	0.7710	0.8838	0.9778	1.0160
Tangential Lean	% ax. chord	0	0.0165	0.0660	0	-0.0743	-0.2145	-0.3300
LE metal angle	degrees	23.5	29.5	40.9	47.3	52.3	56.7	58.5
Mid chord metal angle	degrees	-10.1	-0.925	26.15	40.29	49.585	56.285	58.225
TE metal angle	degrees	-30.1	-17.5	14.0	33.5	44.8	53.95	56.22
LE thickness	% ax. chord	0.0042	0.0042	0.0046	0.0049	0.0049	0.0044	0.0041
TE thickness	% ax. chord	0.0030	0.0030	0.0029	0.0027	0.0025	0.0022	0.0021
Max thickness	% ax. chord	0.0748	0.0622	0.0468	0.0366	0.0292	0.0234	0.0215
Location max thickness	% ax. chord	0.38	0.41	0.48	0.52	0.54	0.56	0.57

Table 5-2: Key fan rotor design parameters

		Design Streamtube				
		10% area	30% area	50% area	70% area	90% area
Top of Climb	M_{IN}	0.92	0.81	0.74	0.67	0.59
	φ_{IN}	-33.7°	-31.8°	-30.1°	-28.6°	-28.4°
	Re*	$4.9x10^6$	$4.7x10^6$	$4.5x10^6$	$4.2x10^6$	$3.8x10^6$
Cruise	M_{IN}	0.86	0.76	0.69	0.62	0.57
	φ_{IN}	-31.6°	-28.9°	-26.5°	-24.3°	-22.3°
	Re*	$4.6x10^6$	$4.4x10^6$	$4.1x10^6$	$3.8x10^6$	$3.5x10^6$
Take-off	M_{IN}	0.88	0.75	0.67	0.59	0.53
	φ_{IN}	-25.3°	-20.9°	-17.3°	-14.0°	-11.0°
	Re*	$4.2x10^6$	$3.9x10^6$	$3.6x10^6$	$3.2x10^6$	$2.9x10^6$
Swirl angle range		8.4°	10.9°	12.8°	14.6°	17.4°

* Reynolds number normalised for a blade chord of unity.

Table 5-3: OGV inlet design conditions for Mises

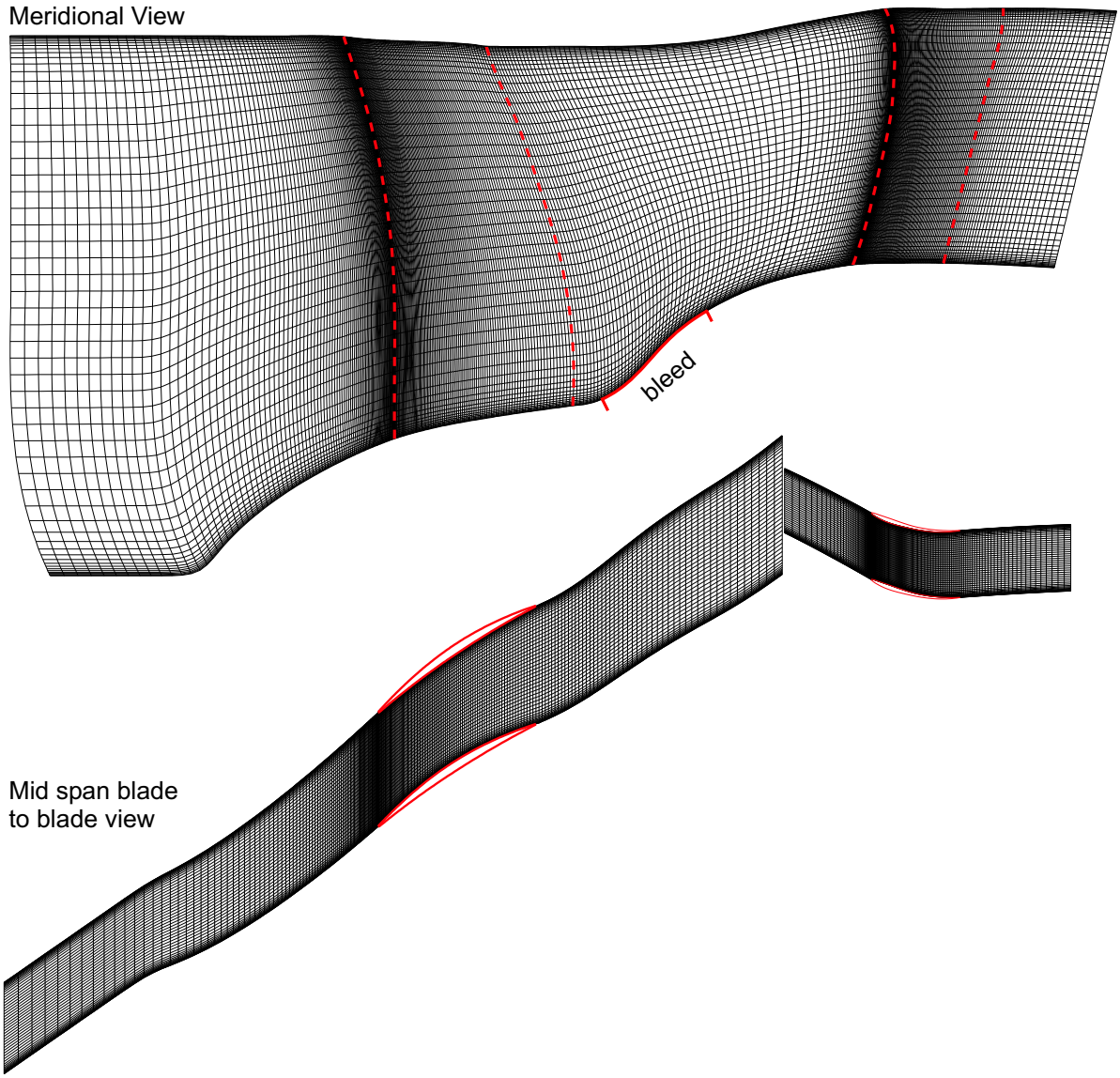

Figure 5-1: Fan Rotor mesh used in Multall

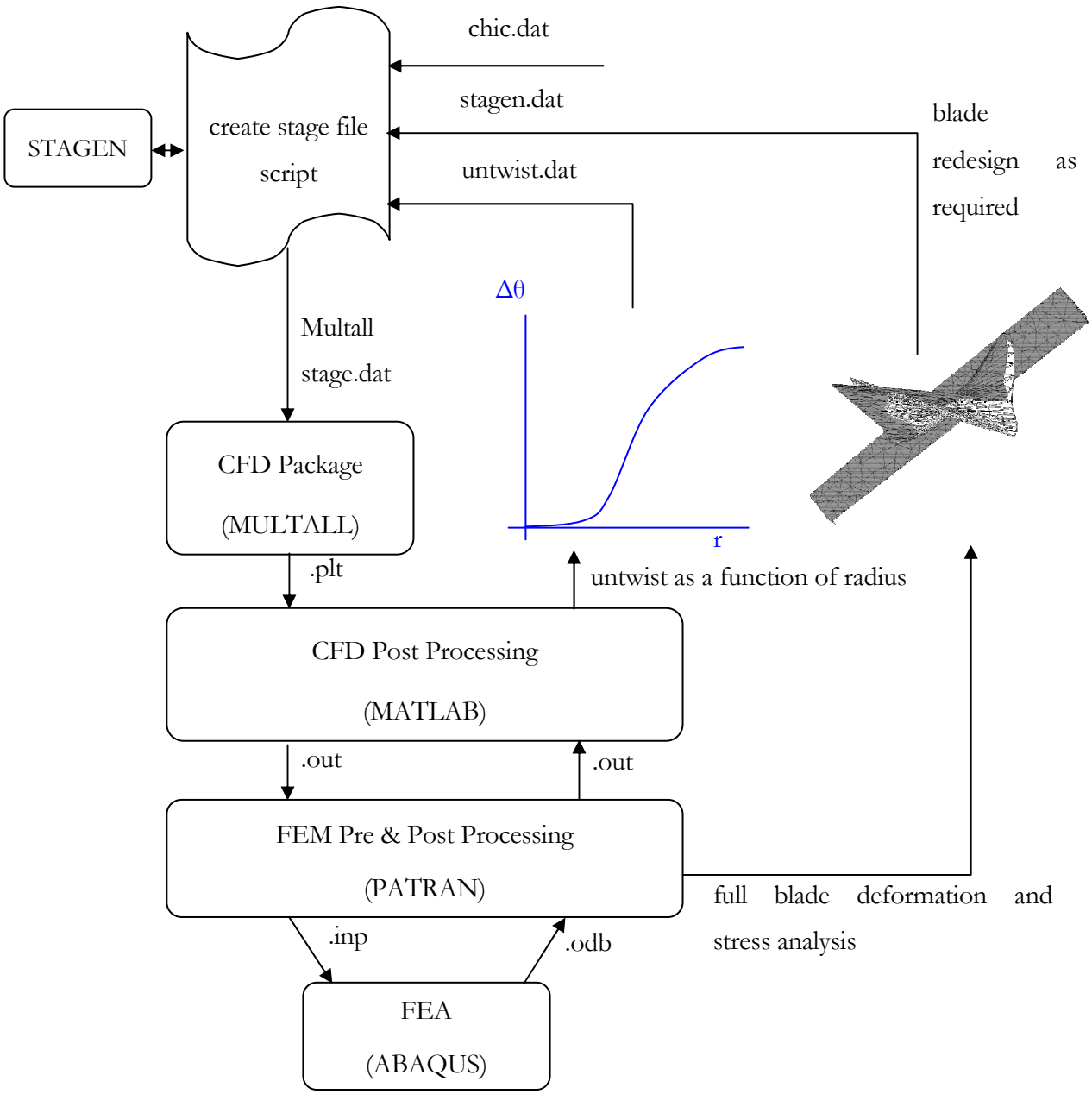

Figure 5-2: Inclusion of rotor blade deformation into design process

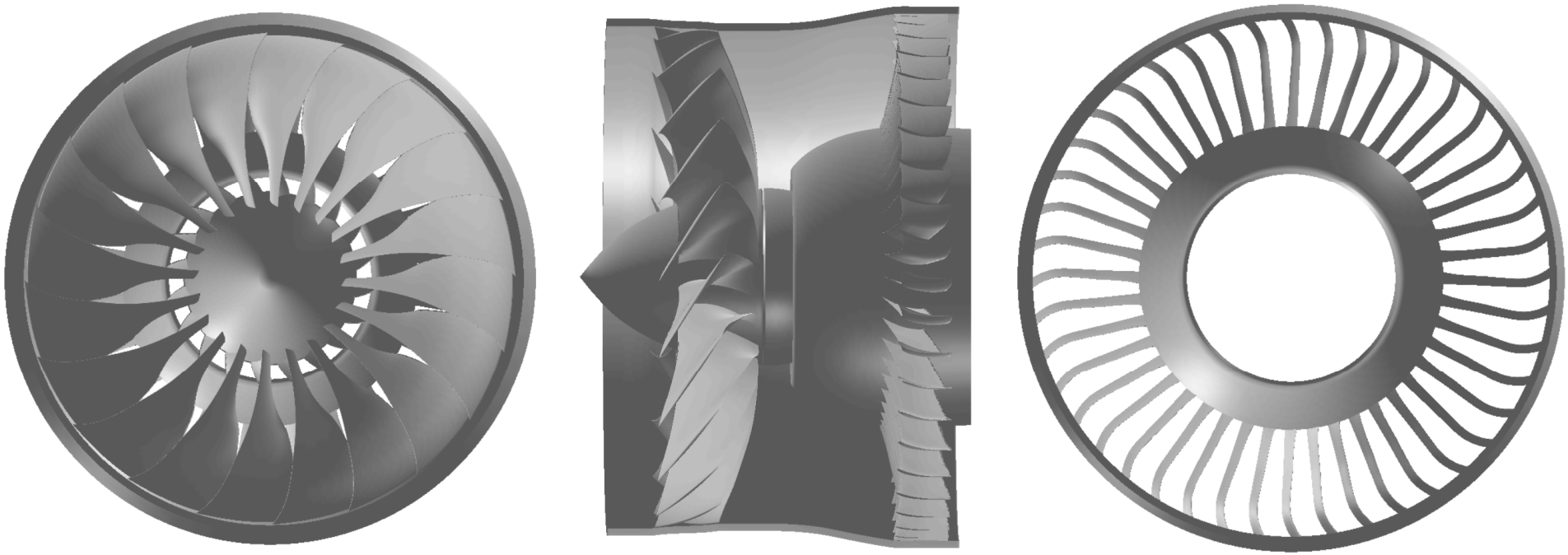

Figure 5-3: Final fan stage model

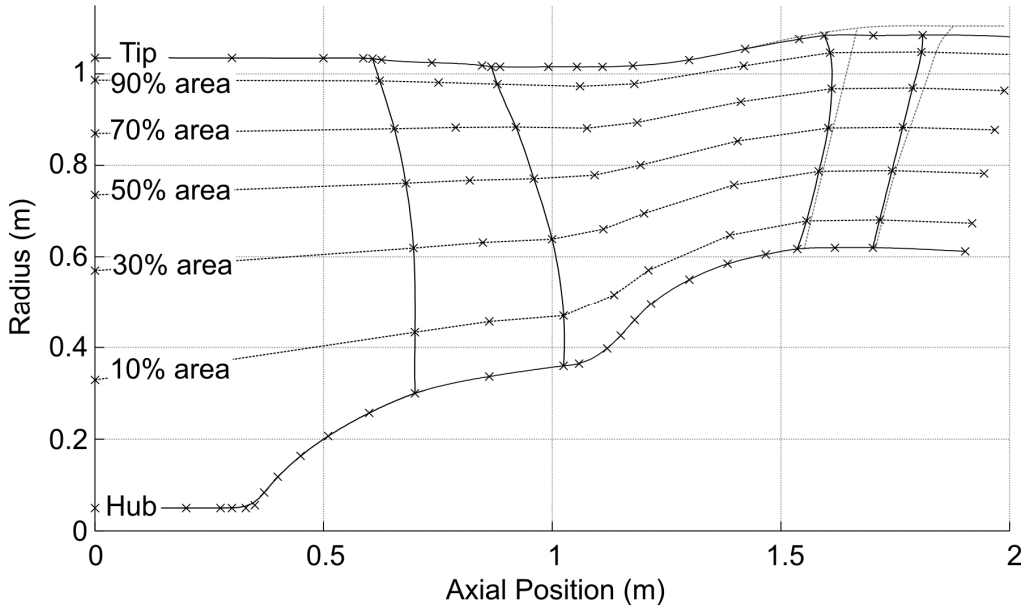

Figure 5-4: Design Streamlines
(also shown is the earlier version of the OGV design that was used for broadband noise estimation)

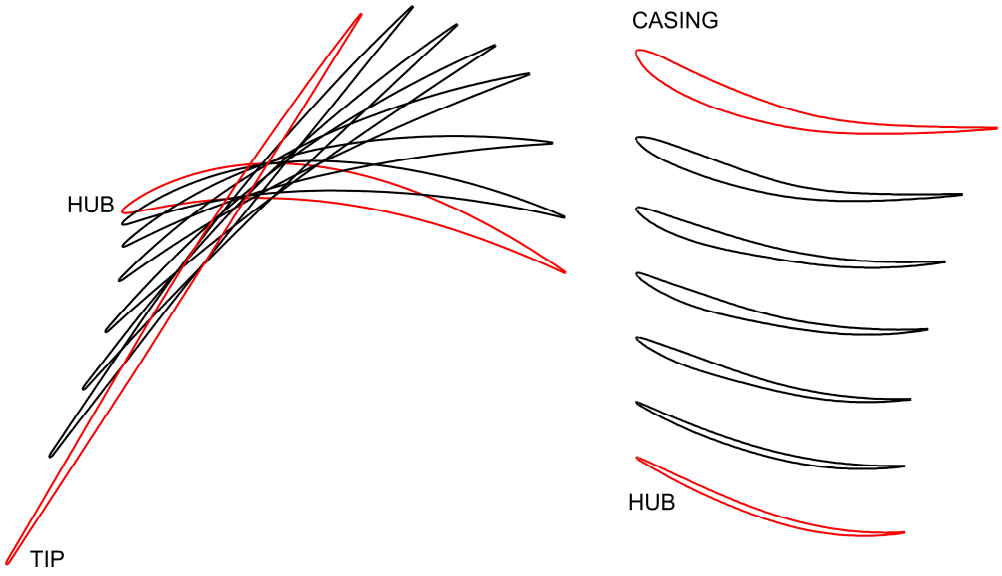

Figure 5-5: Rotor and OGV Blade Sections

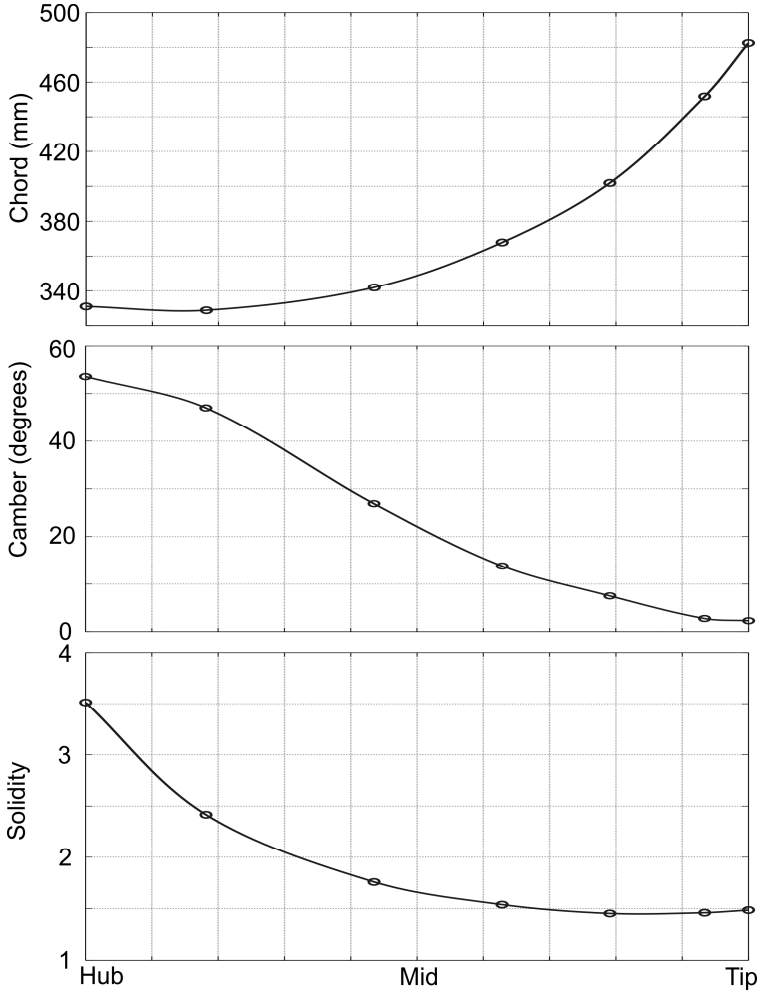

Figure 5-6: Variation in fan chord, camber and solidity from hub to tip

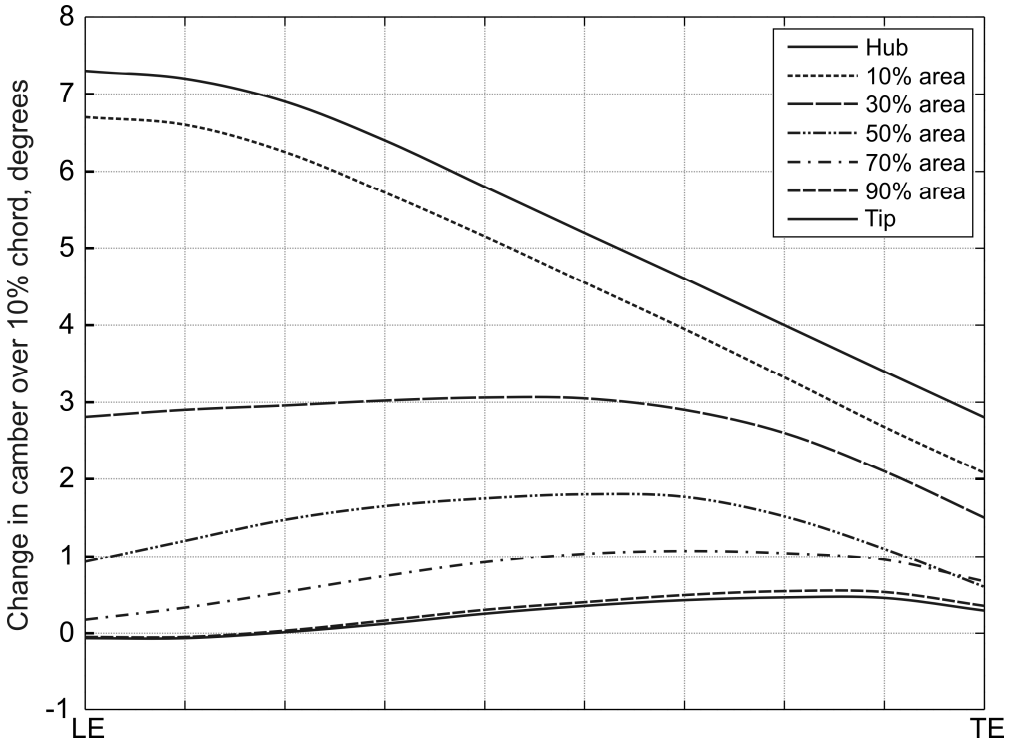

Figure 5-7: Distribution of camber along blade chord

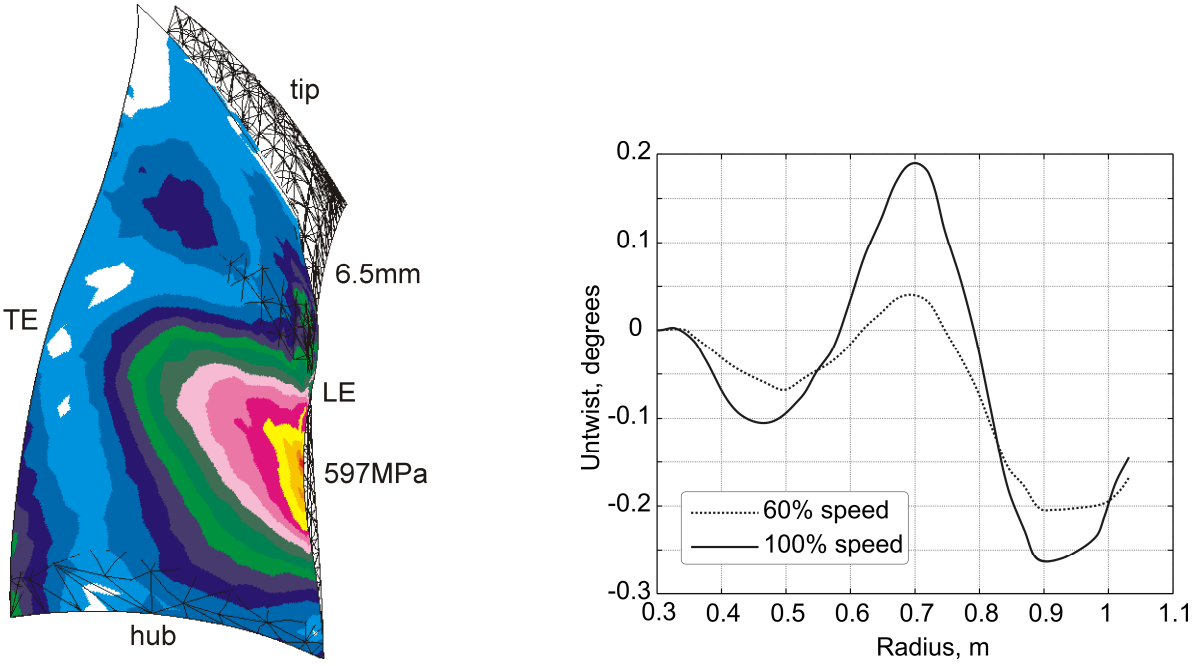

Figure 5-8: Fan blade stress and deformation

Left hand sketch is at top of climb conditions. For right hand figure, positive untwist is the direction a blade without sweep would rotate under centrifugal loading.

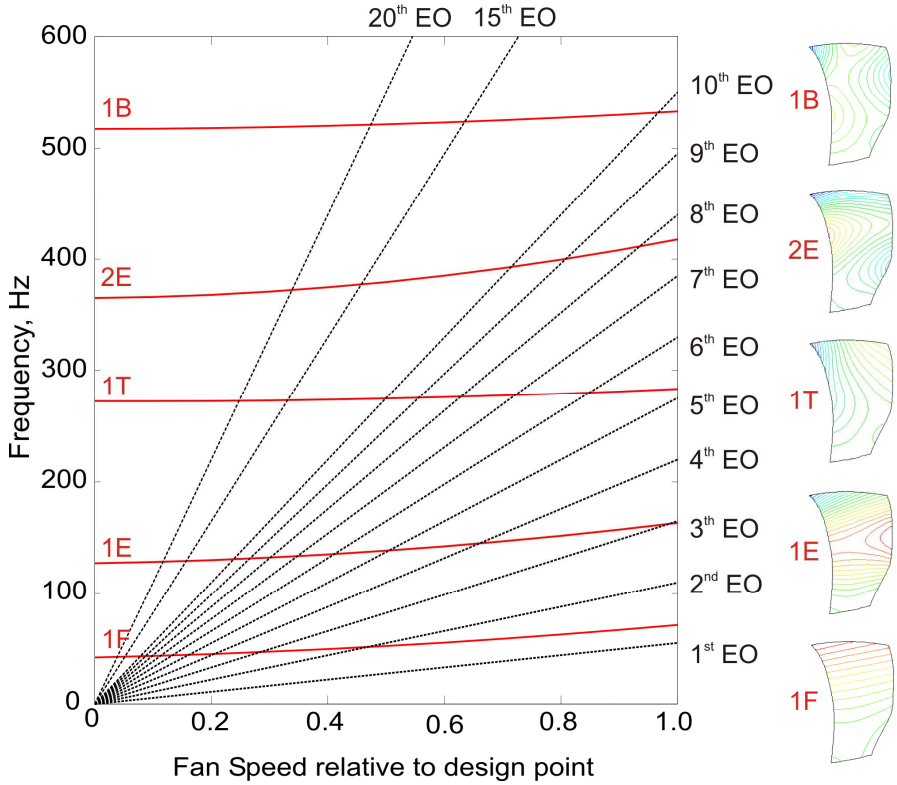

Figure 5-9: Fan blade Campbell Diagram

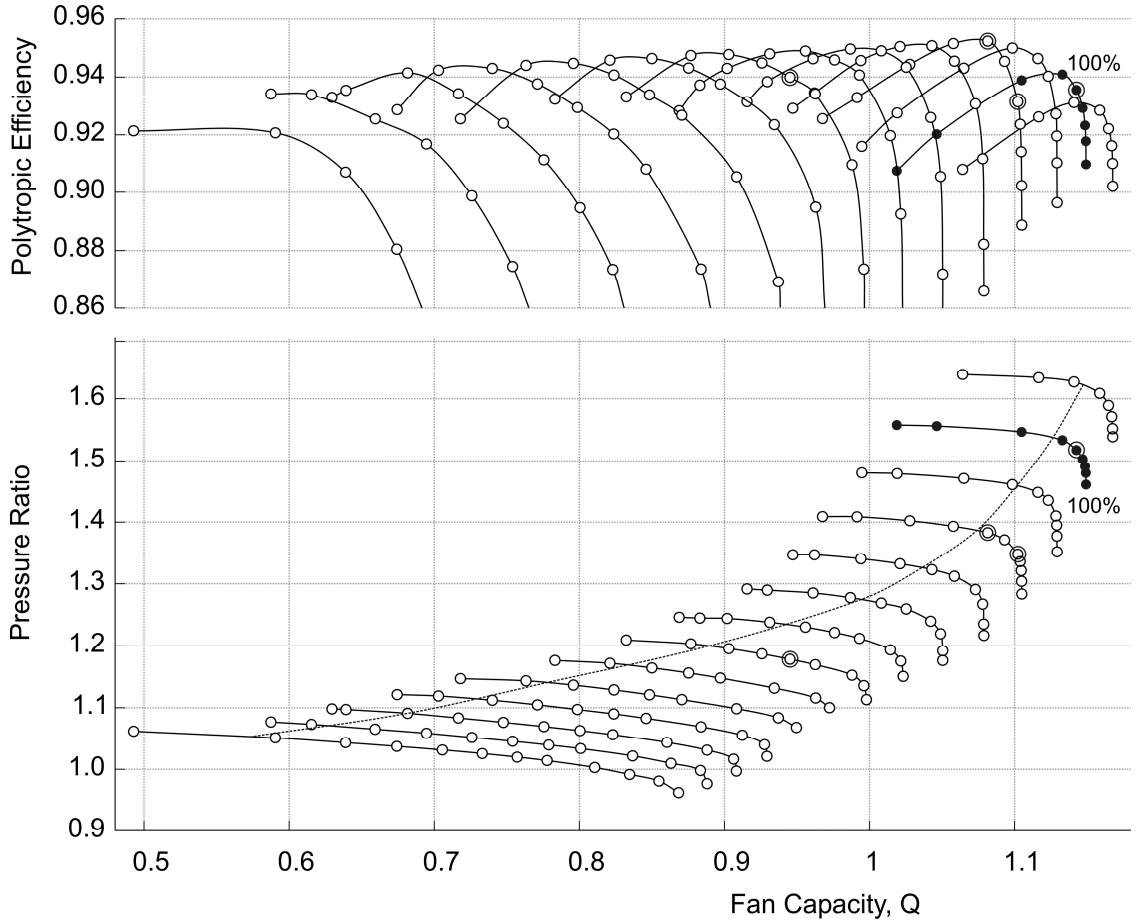

Figure 5-10: Fan Rotor Map

(Lines of corrected speed from 40% to 105% in 5% increments. Trace of peak efficiency shown on pressure ratio plot.
Points highlighted by additional circle correspond to top of climb (100% speed), cruise (90% speed near peak efficiency), sideline (90% speed at choke) and flyover (70% speed). These are shown in more detail in following plots.)

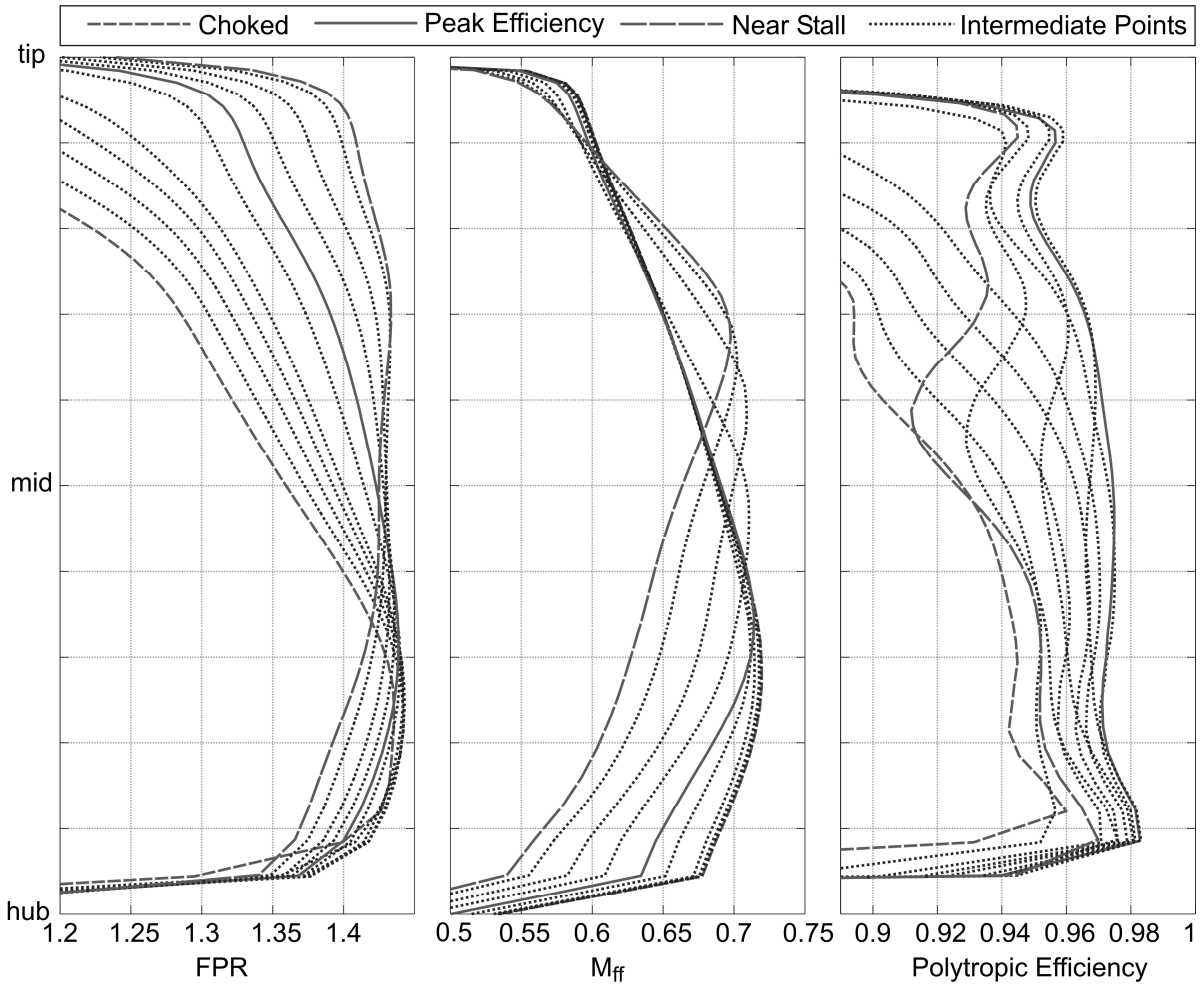

Figure 5-11: Radial variation in fan parameters at 90% corrected speed for a range of back pressures

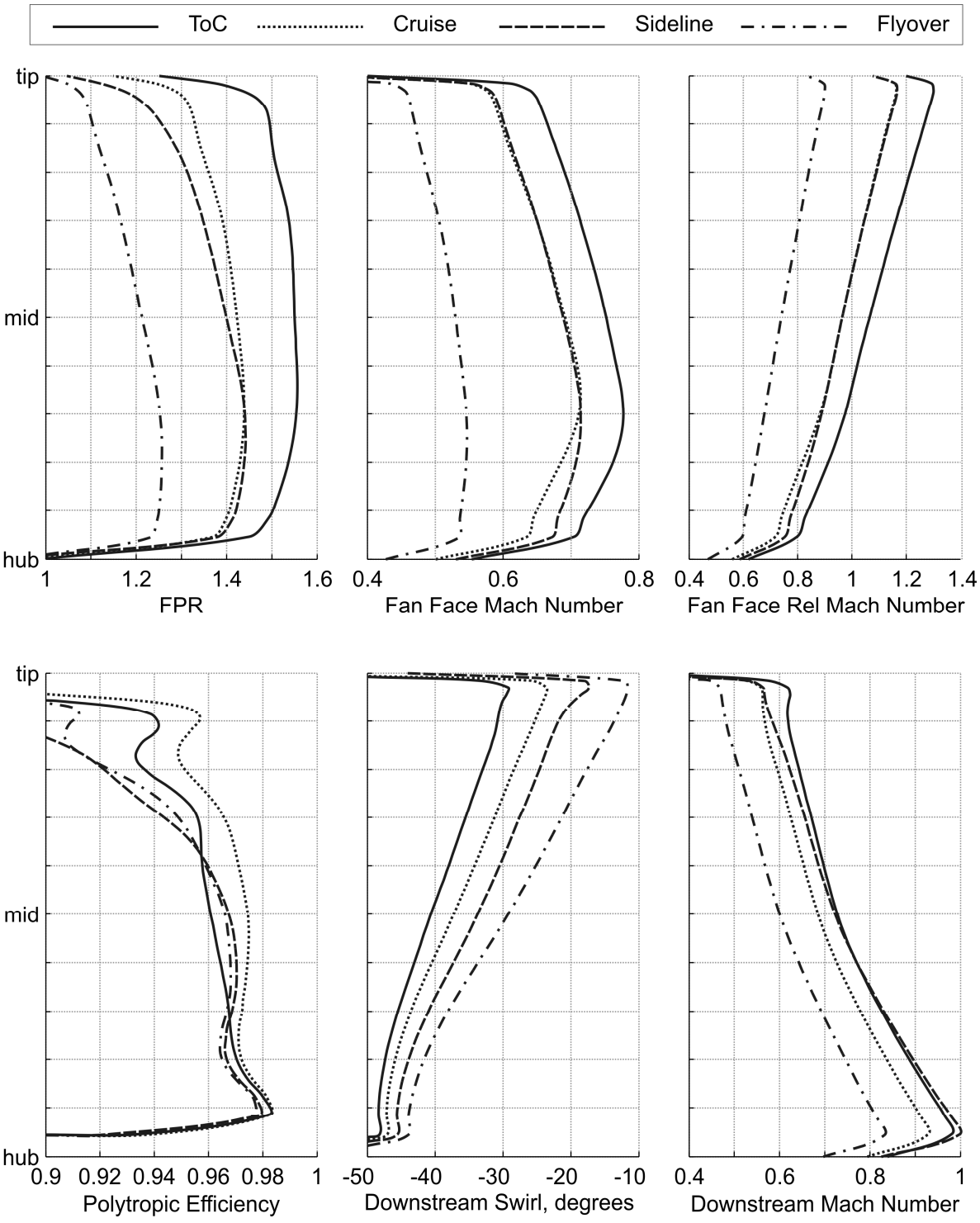

Figure 5-12: Radial variation in fan parameters at key operating conditions

(ToC @ 100% speed, 1.52 mass averaged PR, Cruise @ 90% speed, peak efficiency, Sideline @ 90% speed choked, Flyover at 70% speed near peak efficiency)

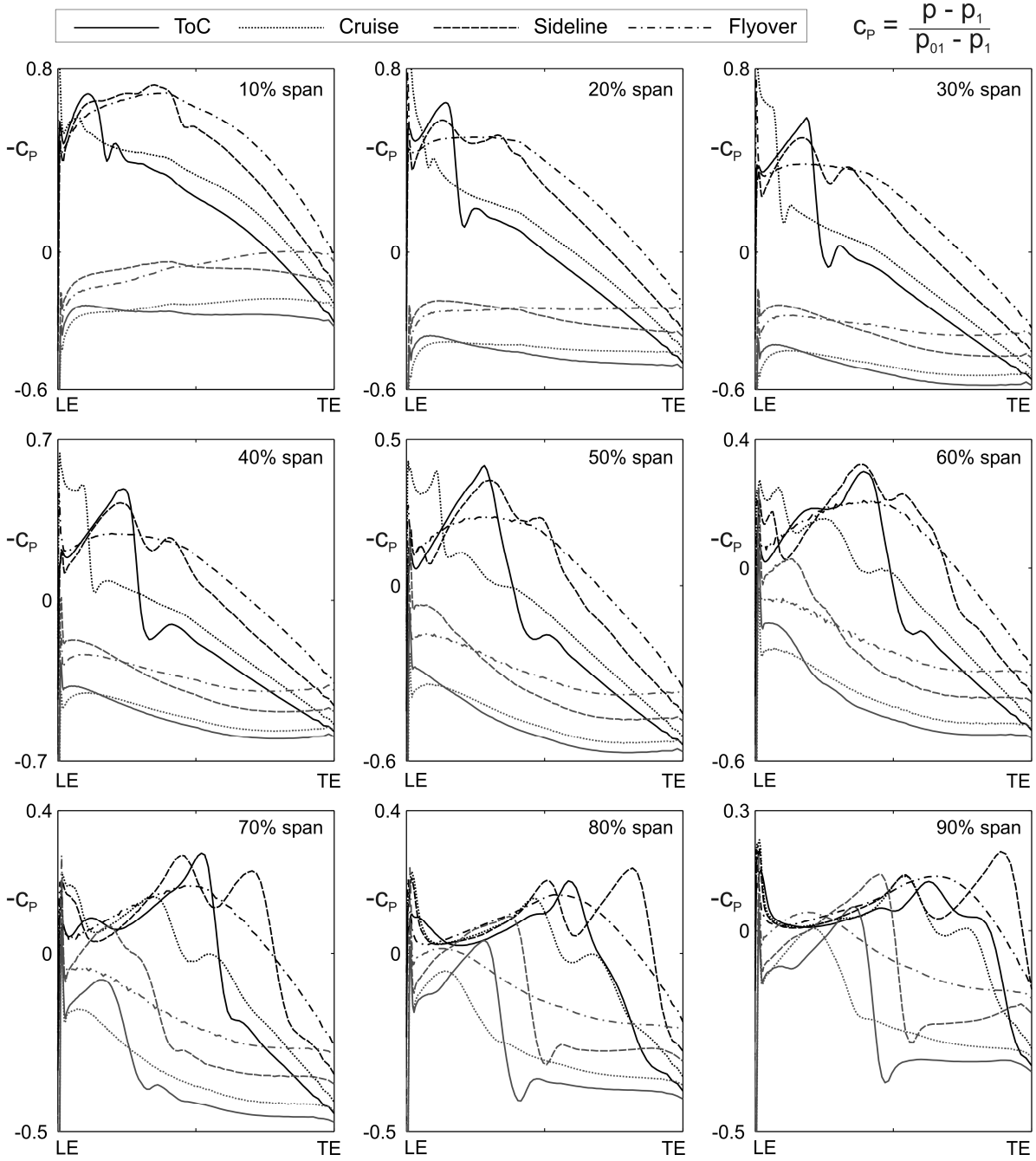

Figure 5-13: Pressure distribution on fan blade at key operating points

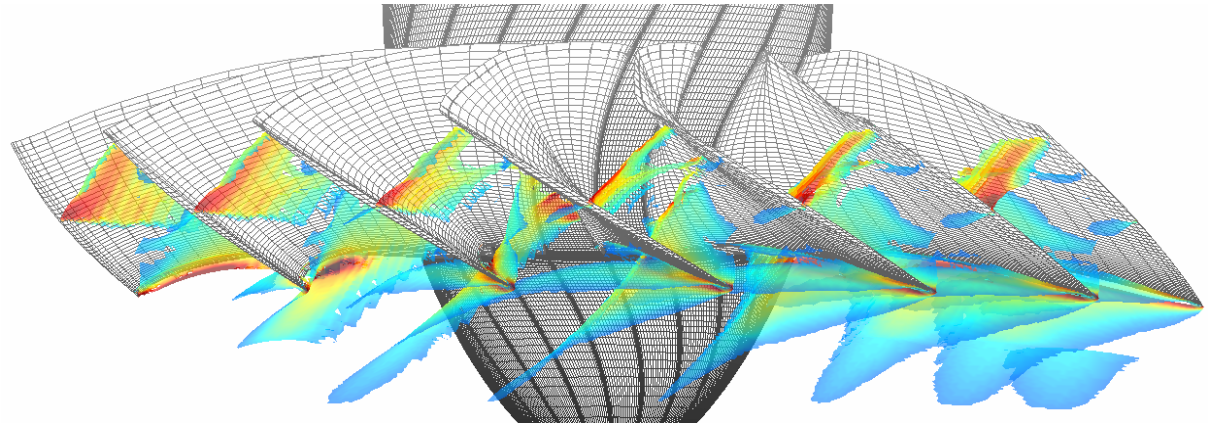

Figure 5-14: Shock Structure on fan at top of climb condition (100% corrected speed, 1.52 FPR)

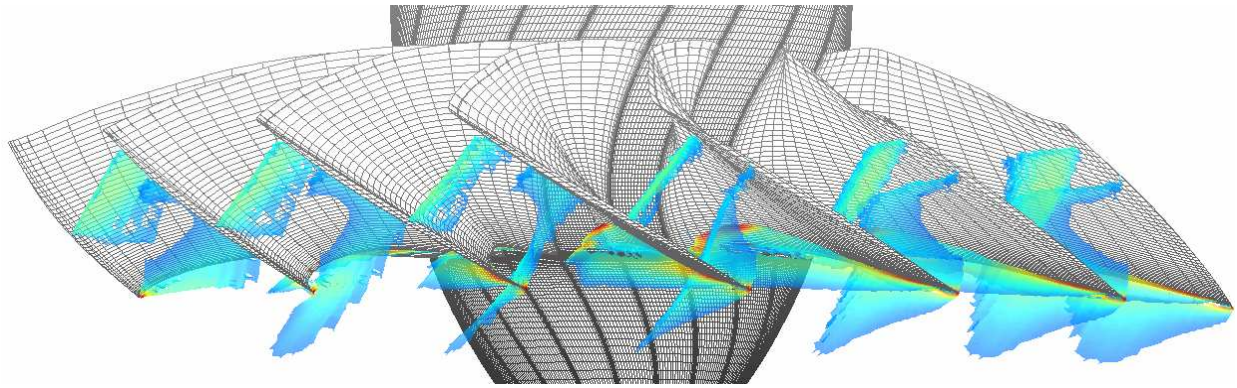

Figure 5-15: Shock Structure on fan at cruise condition (90% corrected speed, peak efficiency)

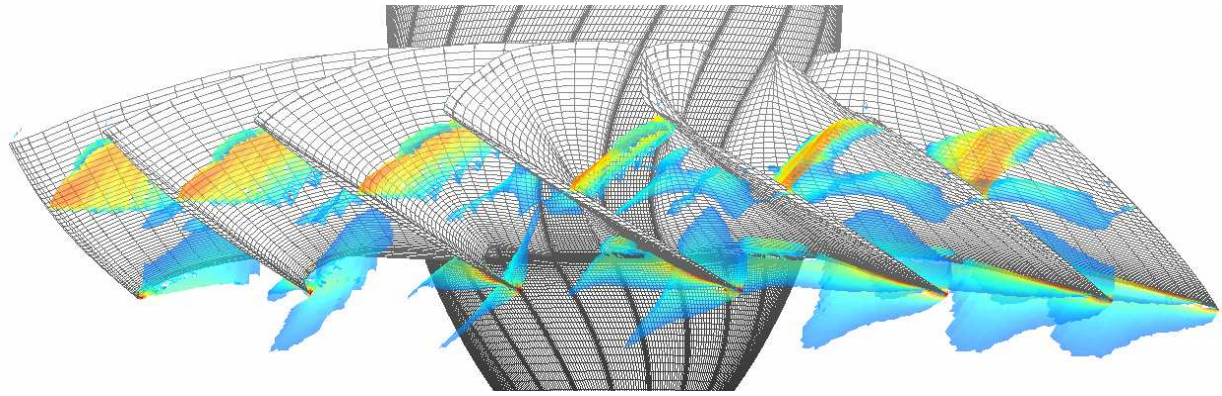

Figure 5-16: Shock Structure on fan at sideline condition (90% corrected speed, choked)

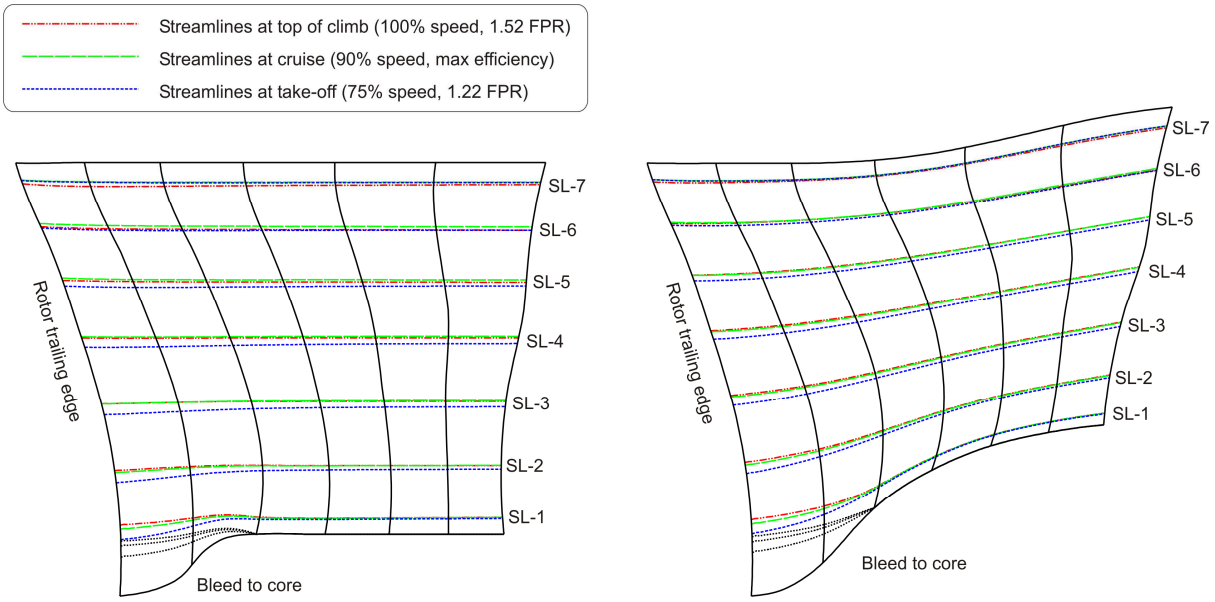

Figure 5-17: Duct design between rotor trailing edge and OGV leading edge.

Left hand sketch is initial fixed area, fixed radius design, right hand sketch is final fixed area, increasing radius design. Core flow was bled off for simplicity and the sketches show streamlines at three key operating conditions.

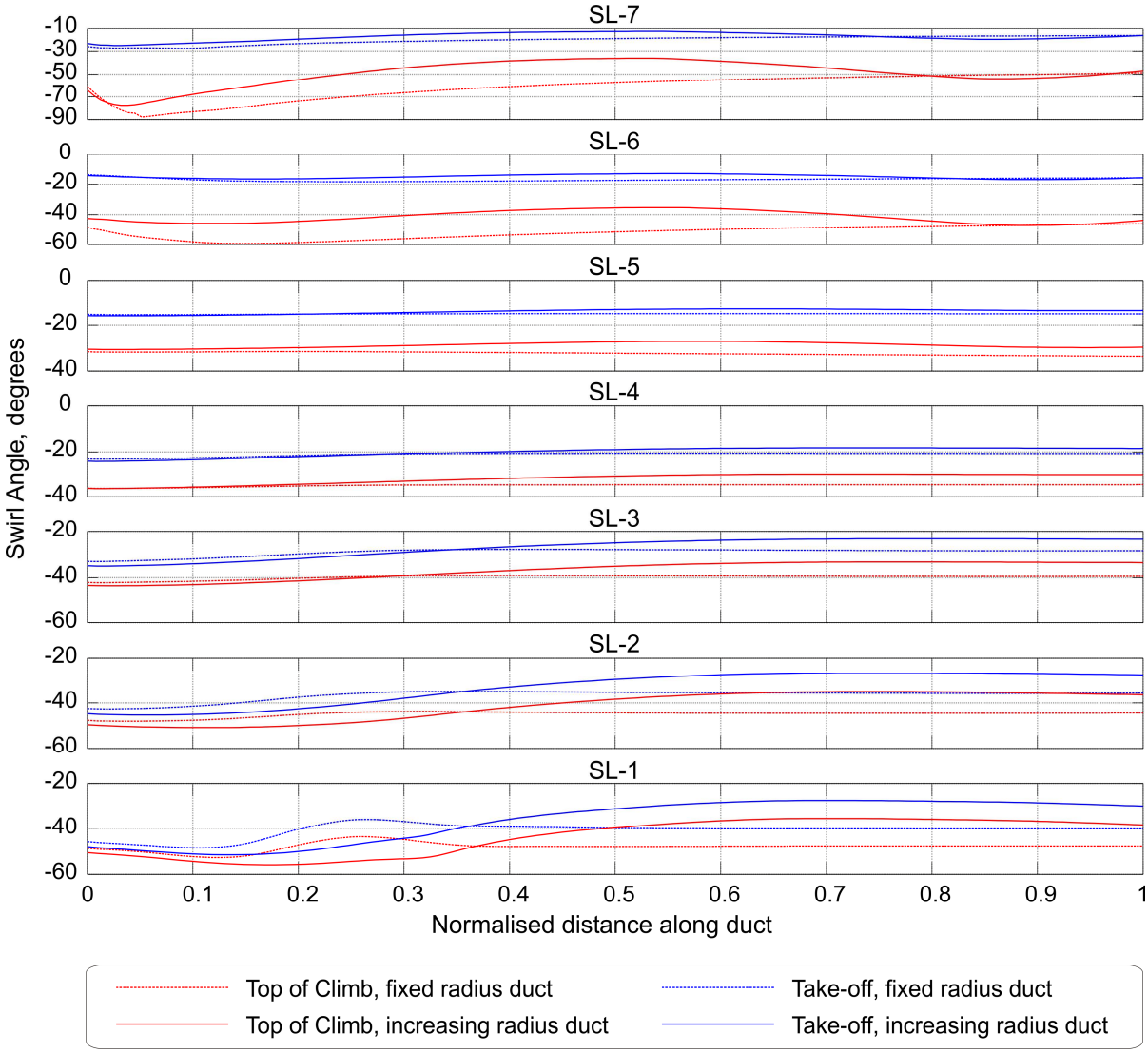

Figure 5-18: Variation in swirl along duct between rotor trailing edge location and OGV leading edge location for top of climb condition (maximum swirl) and take-off condition (minimum swirl).

Titles for each subplot refer to the streamlines shown in figure 5-17.

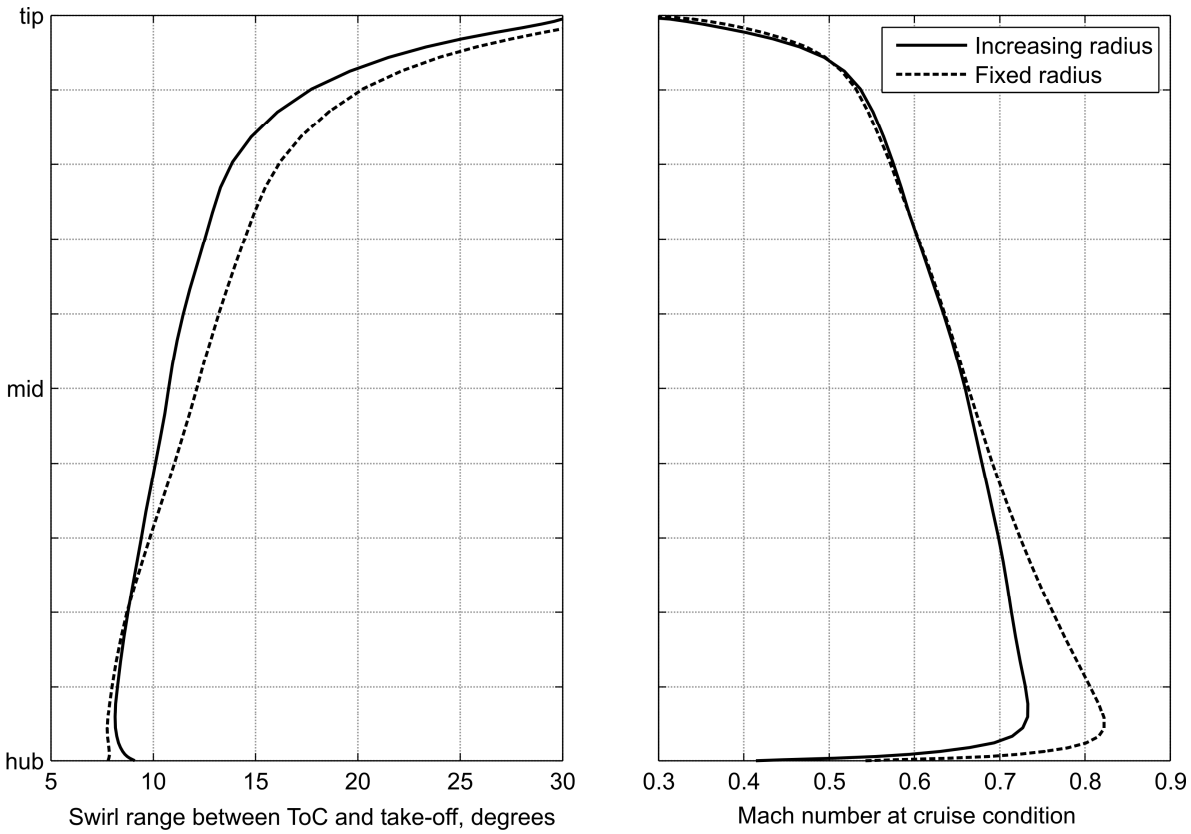

Figure 5-19: Comparison of duct exit conditions for fixed and increasing radius ducts

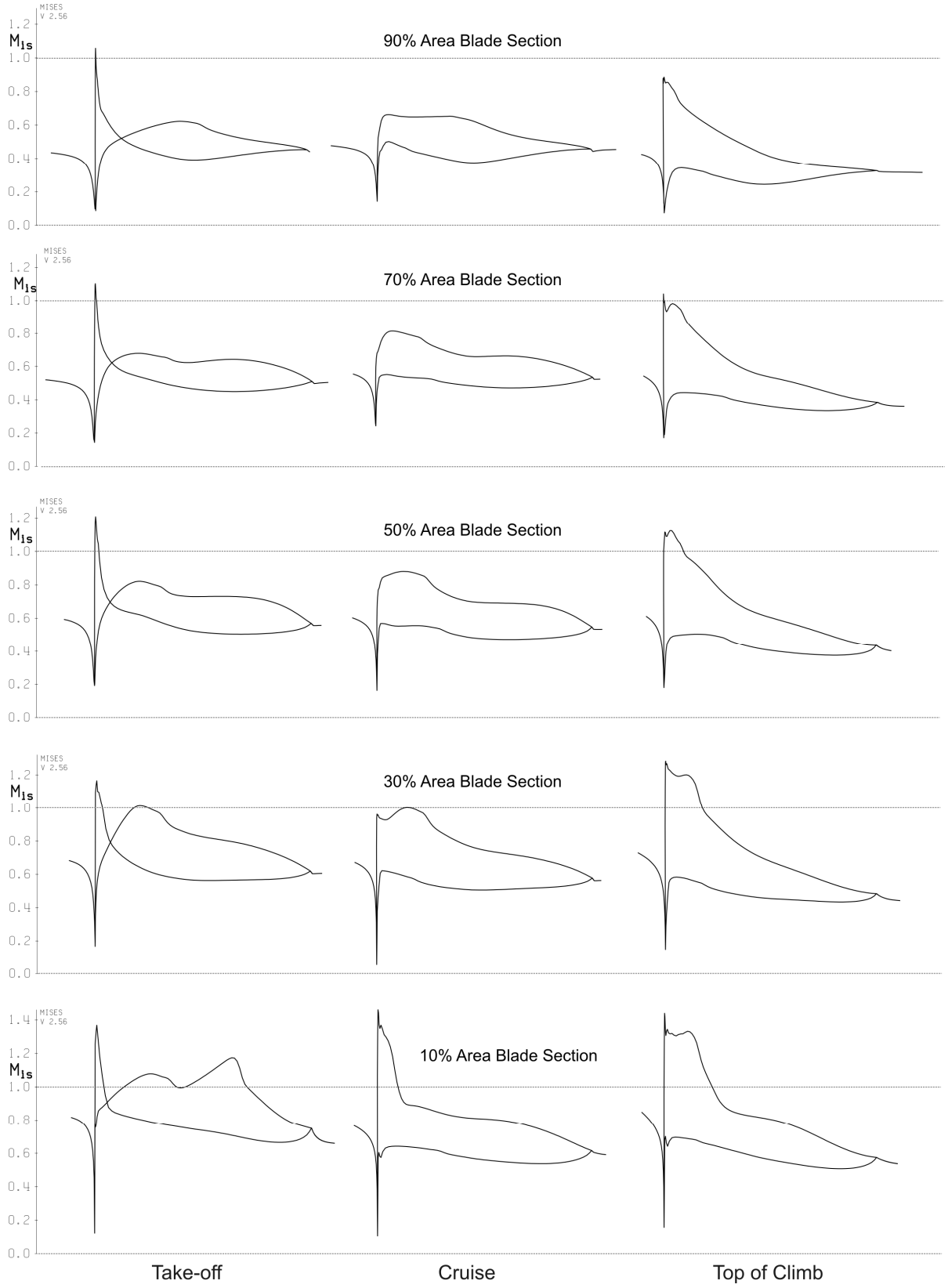

Figure 5-20: Estimated surface Mach number distribution on OGV design blade sections

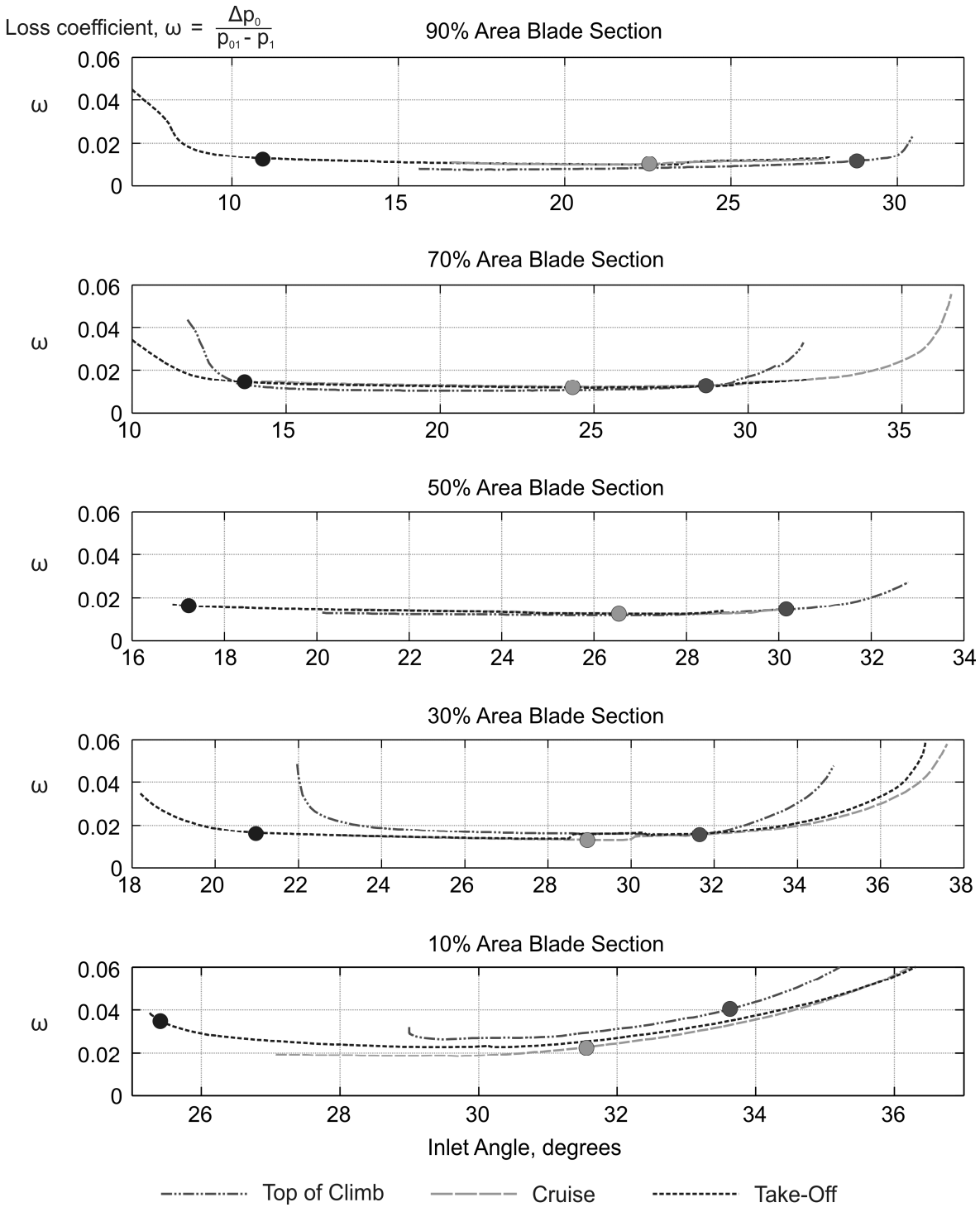

Figure 5-21: Estimated loss vs. inlet swirl angle for OGV design blade sections

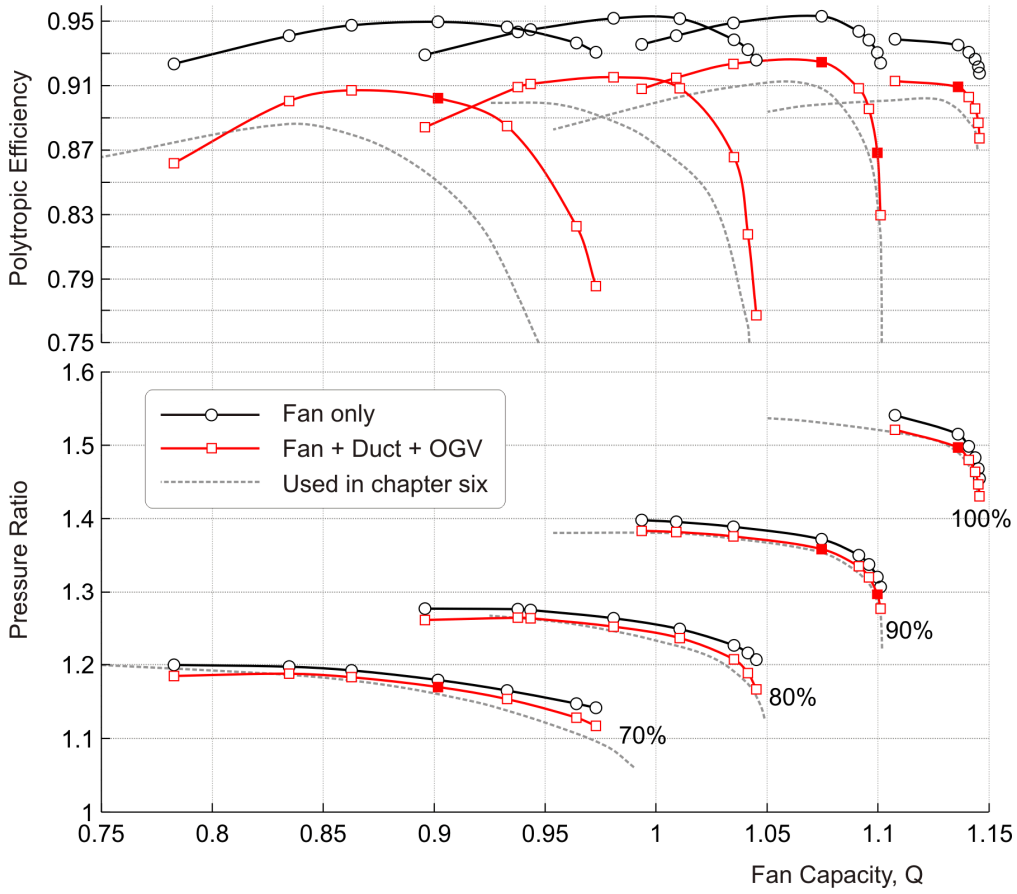

Figure 5-22: Fan stage map

Points highlighted by solid colour correspond to top of climb (100% speed), cruise (90% speed near peak efficiency), sideline (90% speed at choke) and flyover (70% speed). Note that the flyover position at 70% speed is different from that used when looking at rotor only performance (figure 5-10) in that it is at a lower capacity. This is to more closely match the final take-off operating line used in chapter six and shown in figure 6-11.

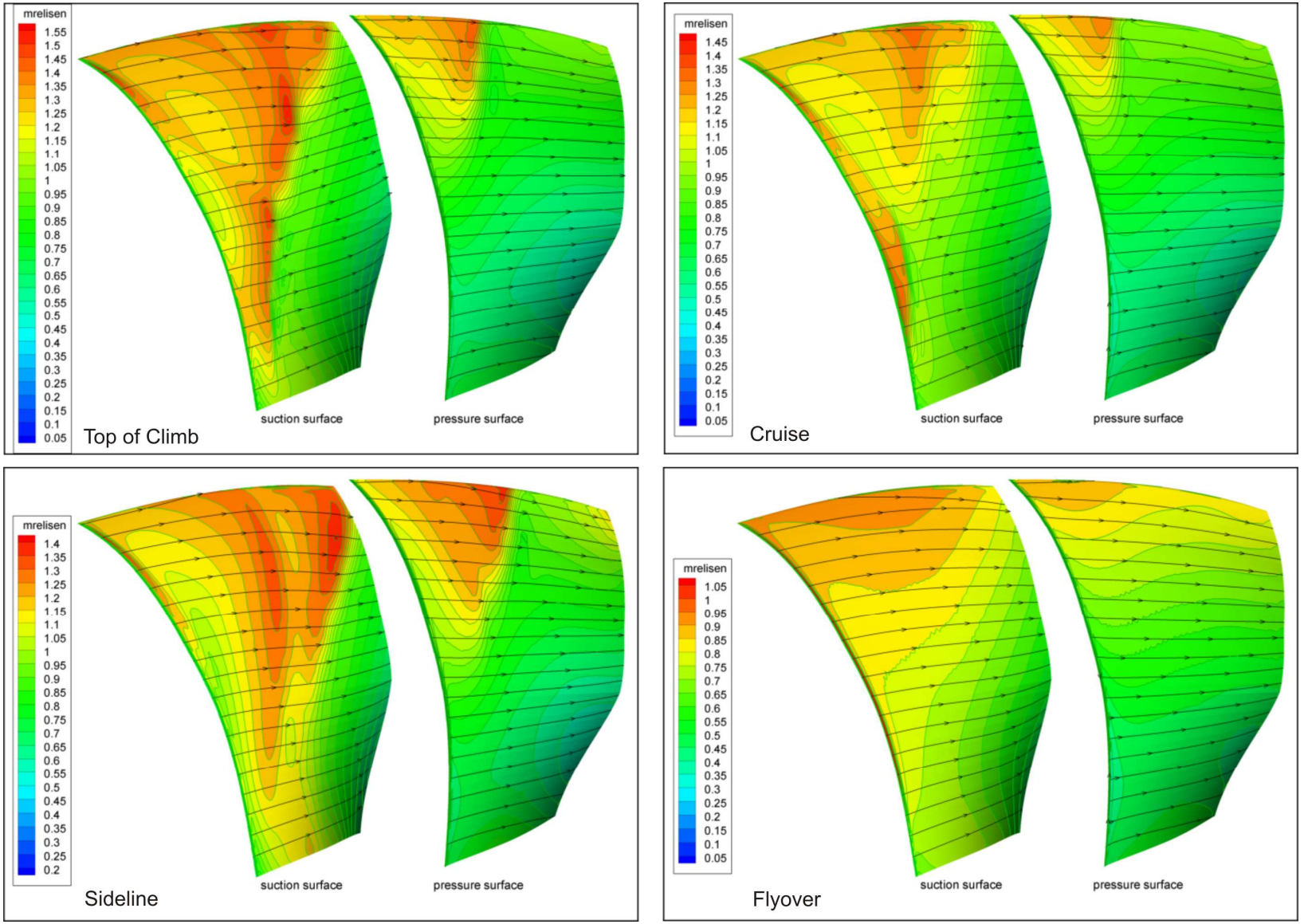

Figure 5-23: Contours of isentropic Mach number and streaklines on the fan at key operation locations

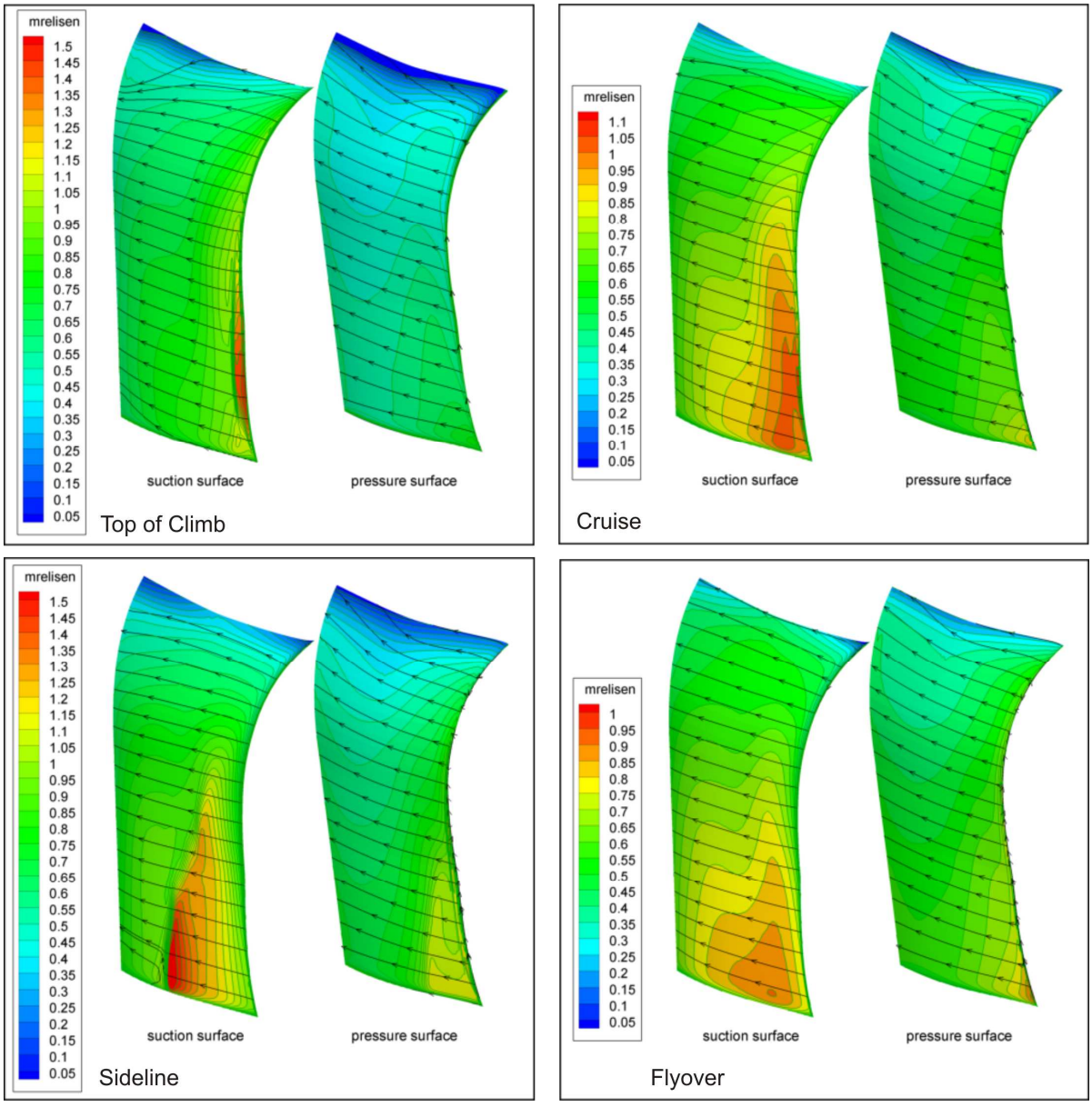

Figure 5-24: Contours of isentropic Mach number and streaklines on the OGV at key operation locations

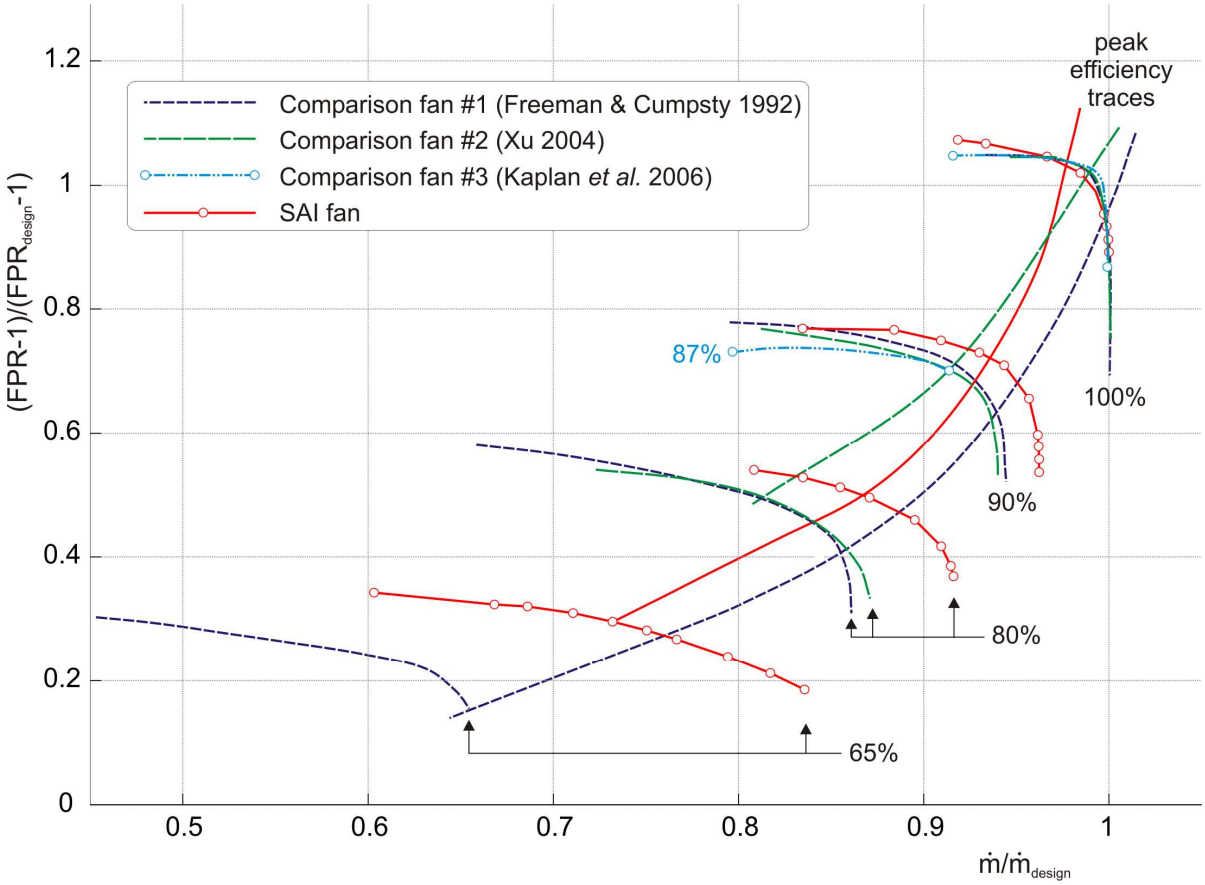

Figure 5-25: Comparison of fan performance with published maps of modern transonic fans

X-axis is corrected mass flow rate normalised to 100% speed choking mass flow rate. Y-axis is pressure rise of the fan normalised to 100% speed design point. Further details on each comparison fan in table below.

No	Source(s)	x-axis	y-axis	Normalised FPR	Normalised M_{ff}	100% $N/\sqrt{\theta}$	htr
-	SAI	Core+ bypass	Fan only, bypass flow only	1.52	0.668	371m/s	0.29
#1	Freeman and Cumpsty (1992) and Cumpsty (2003)	Core+ bypass	Fan only, bypass flow only	~1.80	*unknown*	455m/s	0.30
#2	Xu (2004), fig. 6 & Denton and Xu (2002)	Core + bypass	Fan only, core + bypass	~1.80	*unknown*	457m/s	*unknown*
#3	Kaplan *et. al.* (2006)	*not specified*	Fan and OGV	1.45	~0.7	328m/s	0.27

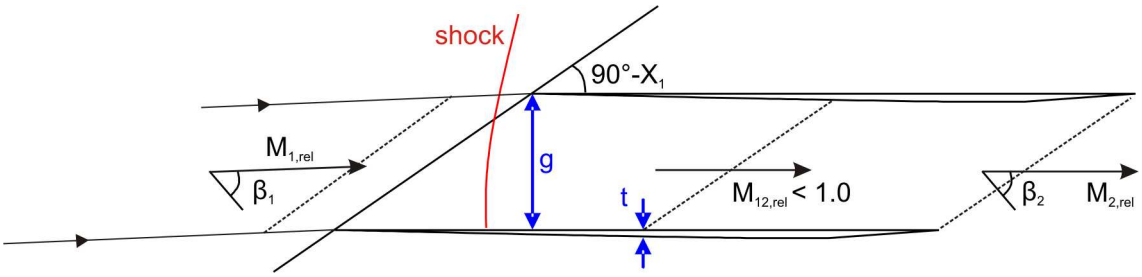

Figure 5-26: Operation with detached shocks (Freeman and Cumpsty 1992)

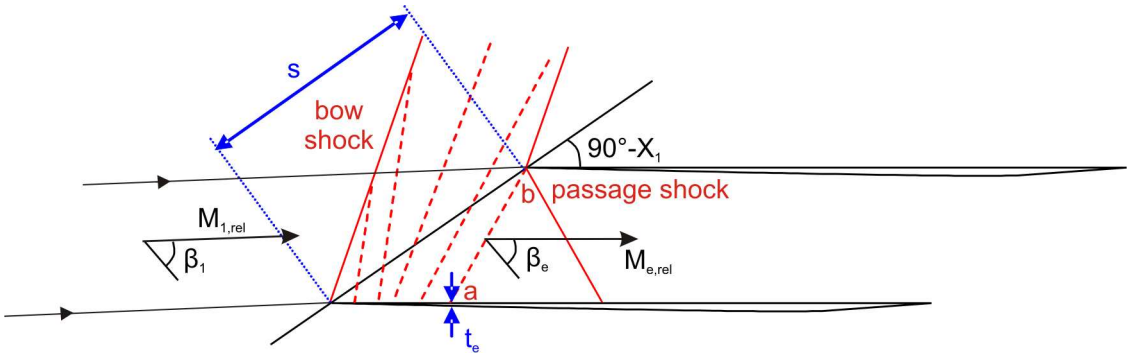

Figure 5-27: Operation with attached shocks – unique incidence

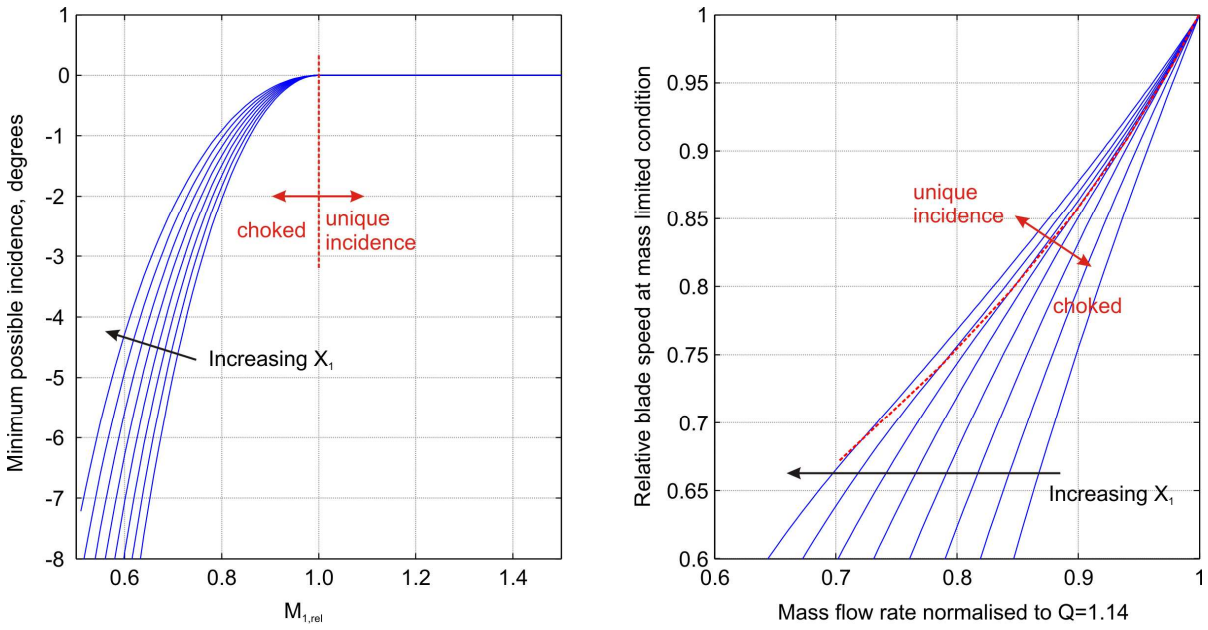

Figure 5-28: Mass flow limitation for a transonic zero thickness blade for metal angles from X_1=45° to X_1=66° in 3° increments.

Left hand subplot is created using models based on Figure 5-26 and Figure 5-27. Right hand subplot uses these results to find meridional and blade Mach numbers which are then used to find non-dimensional mass flow rate and blade speed. Finally, results are normalised for a notional design point capacity of Q=1.14.

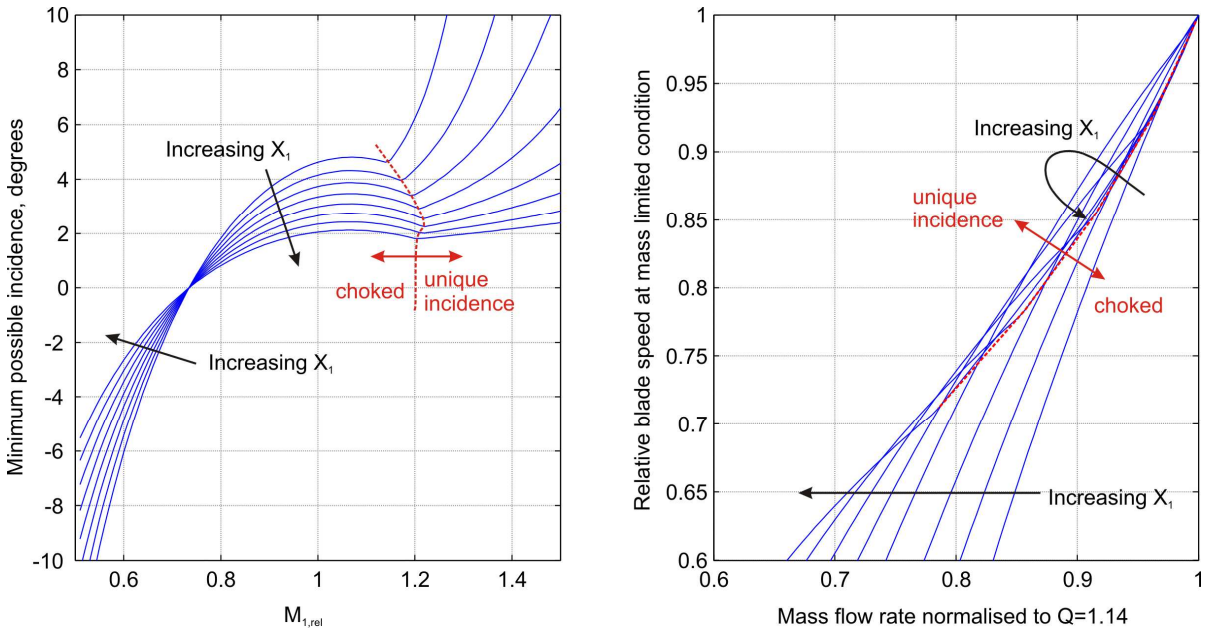

Figure 5-29: Mass flow limitation for a transonic non-zero thickness blade for metal angles from X_1=45° to X_1=66° in 3° increments, $t/g = 0.08$ and $(t_e+\delta_e^*)/s = 0.02$.

Left hand subplot is created using models based on Figure 5-26 and Figure 5-27. Right hand subplot uses these results to find meridional and blade Mach numbers which are then used to find non-dimensional mass flow rate and blade speed. Finally, results are normalised for a notional design point capacity of Q=1.14.

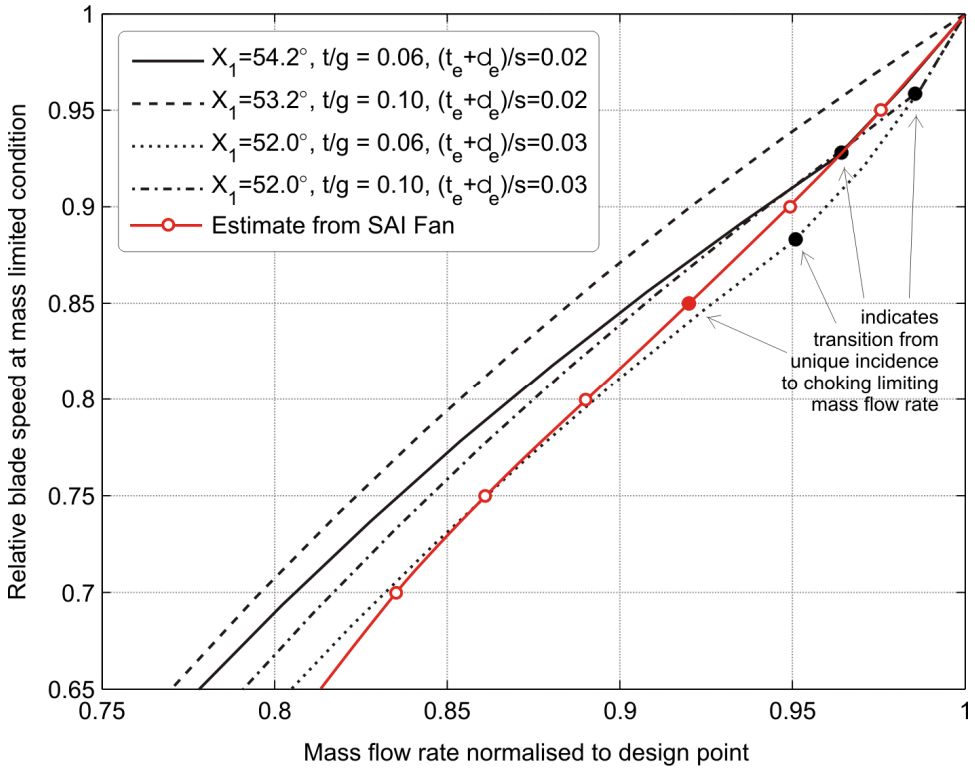

Figure 5-30: Impact of blade thickness on part-speed choking.
Results at 80% span for fan with 371m/s corrected tip speed, 0.29 hub to tip radius ratio and Q_{ff}=1.14 at design point. Inlet metal angle, X_1, set to meet design point capacity for specified speed and blade thicknesses.

Area	Parameter Name	Parameter Value
Aircraft	Take-off weight, m	160,272 kg
	Climb fuel	3,197 kg
	Cruise fuel	31,742 kg
	Wing Area	840 m^2
	Cruise Mach number	0.8
	Tire coefficient, μ	0.02
	Start of Cruise height	40,000ft (12,192m)
	End of Cruise height	45,000ft (13,716m)
	Rotation velocity, V_R	65m/s (optimising for jet noise) 57m/s (optimising for all noise)
Engines	Number of engines	3
	Fan Stage Pressure Rise at top of climb	1.467
	Design capacity, $Q_{ff,ToC}$	1.144 ($M_{ff,ToC}$ = 0.668)
	ToC Excess Thrust (thrust margin when climbing at 300 ft/min (1.52m/s) at ToC conditions)	6.6%
	Thrust coefficient, C_{FG}	0.9935
	Liner correction, forward	5 dB
	Liner correction, rearward	12.5 dB
Engine Geometry (figure 6-9)	D_{FAN}	2.20 m
	$D_{NOZ,MIN}$	1.77m
	$D_{NOZ,MAX}$	2.10 m
	L_{NAC}/D_{FAN}	~ 0.35
	L_{FAN}/D_{FAN}	~ 0.50
	L_{DUCT}/D_{FAN}	~ 2.00
	L_{NOZ}/D_{FAN}	~ 0.35
	x/L_{DUCT}	~ 0.50
Atmospheric	ΔISA at take-off	12 K
	ΔISA at top of climb	10 K
	ΔISA at cruise	0 K
Corrections	$PR_{out,zero}$ (core engine exit PR at M_∞=0)	0.931
	$PR_{out,ToC}$ (core engine exit PR at M_∞=0.8)	0.971
	$\Delta T_{0,zero}$	11.1 K
	$\Delta T_{0,ToC}$	39.2 K
	PR_{in}	0.995
Aircraft geometry for engine out calculation (appendix E)	L_1	7.3m
	L_2	26.4m

Table 6-1: SAI concept aircraft parameters (podded design)

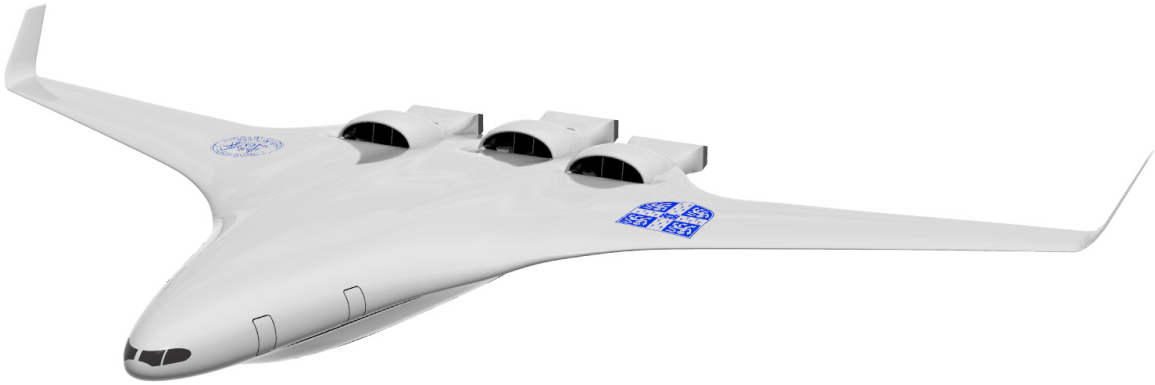

Figure 6-1: SAI Concept Aircraft #1 – high risk embedded design

Figure 6-2: SAI Concept Aircraft #2 – reduced risk podded design

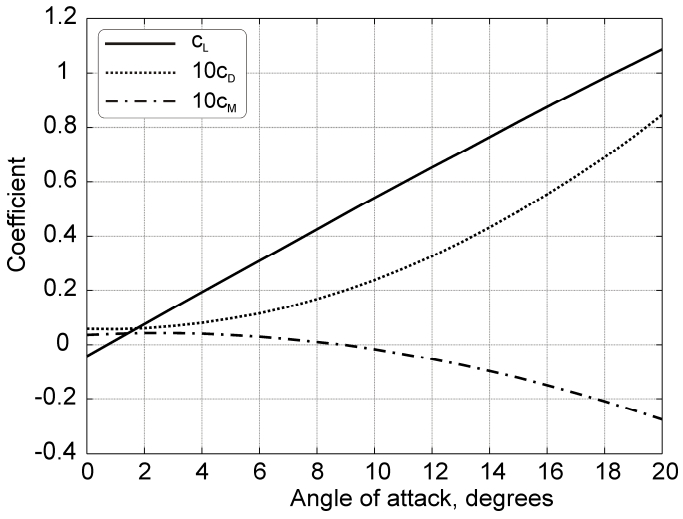

Figure 6-3: SAI Concept Aircraft c_L, c_D and c_M at take-off (both variants)
(c_M has nose down moment at high angle of attack)

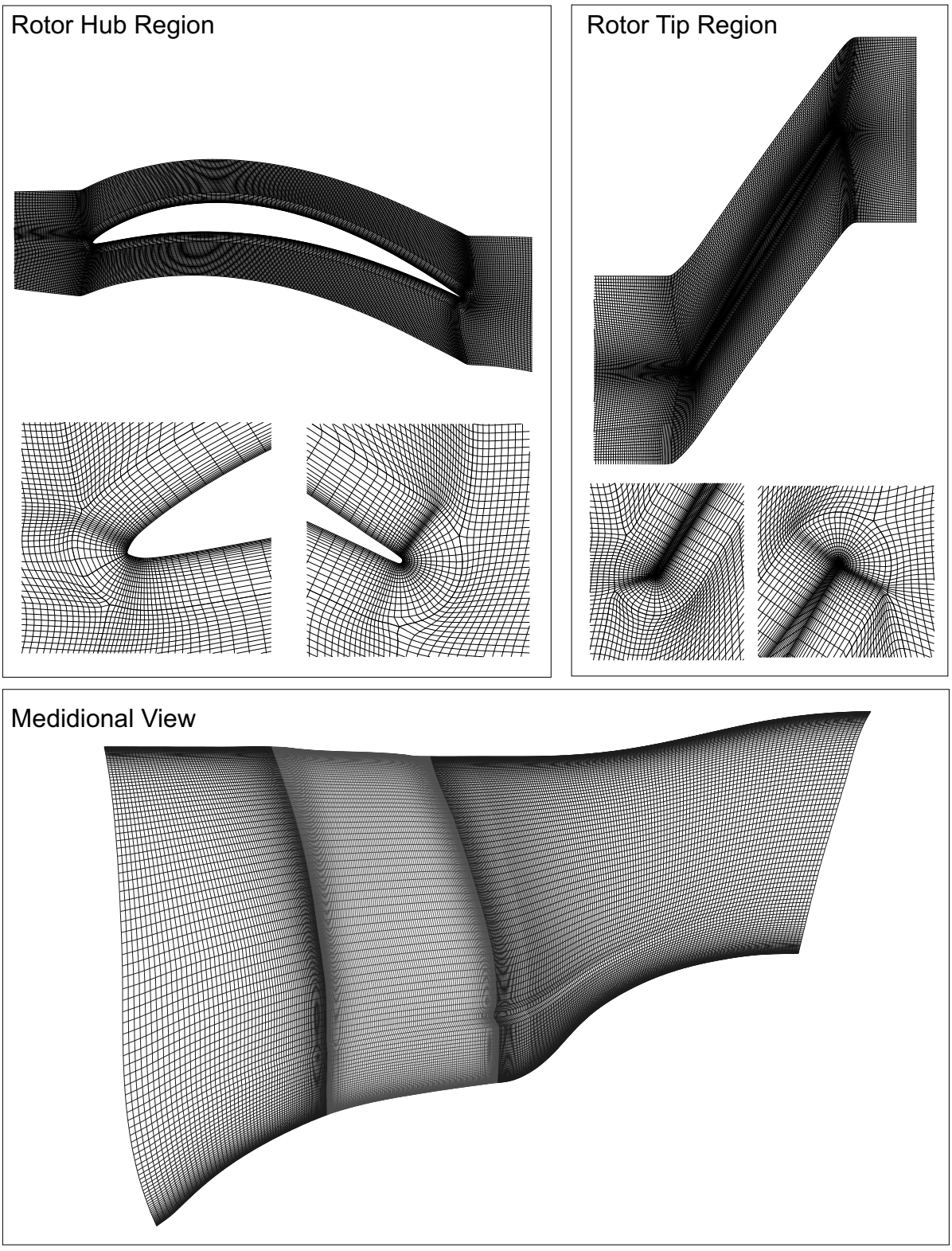

Figure 6-4: Details of grid used in Hydra

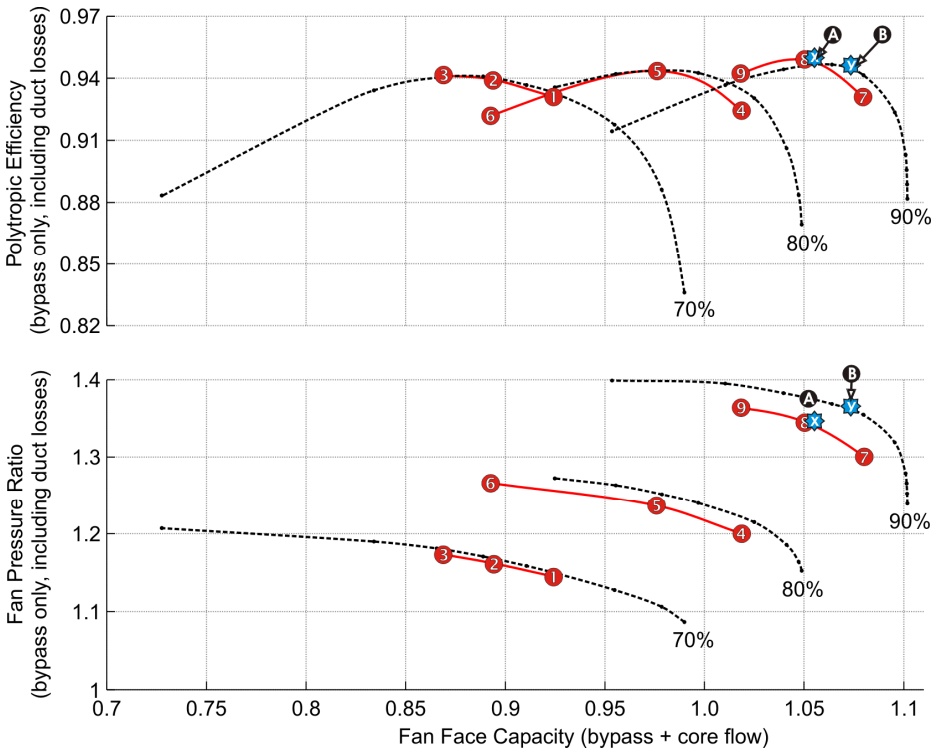

Figure 6-5: Comparison of mass averaged pressure rise and efficiency predictions from Multall and Hydra CFD codes.

Dotted lines and points A-B are from Multall, solid lines and points 1-9 are from Hydra, points X and Y are hydra with modified grid and boundary conditions – see text for details.

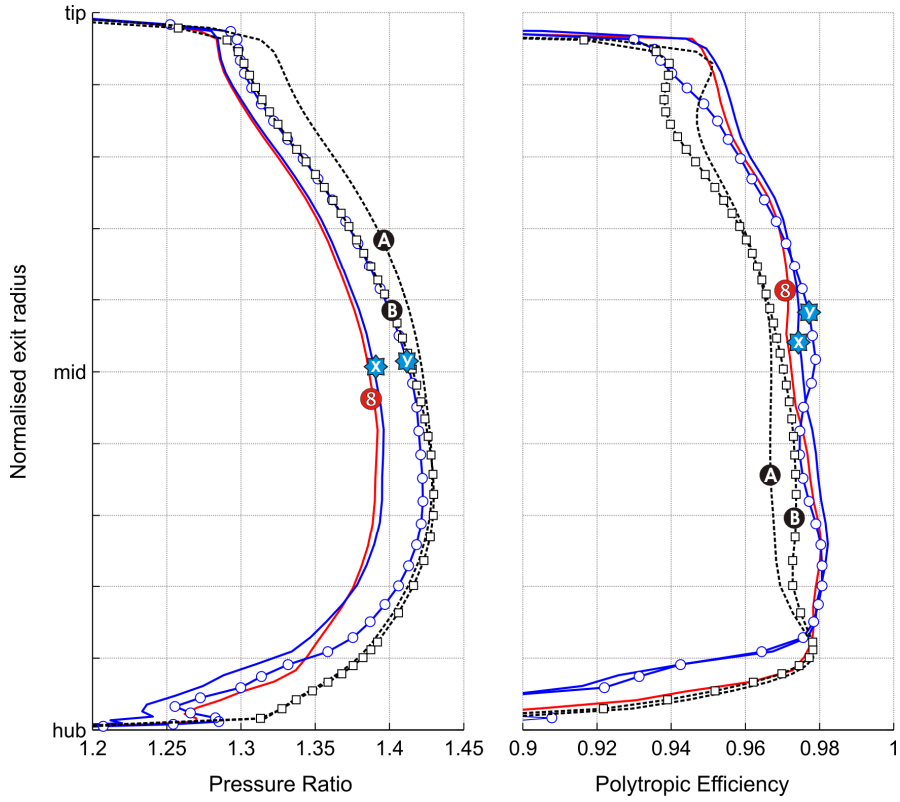

Figure 6-6: Comparison of radial variation in rotor only pressure rise and efficiency from Multall and Hydra CFD codes.

Points A and B are from Multall, points 8, X and Y are from Hydra. Ratio from inlet to rotor trailing edge..

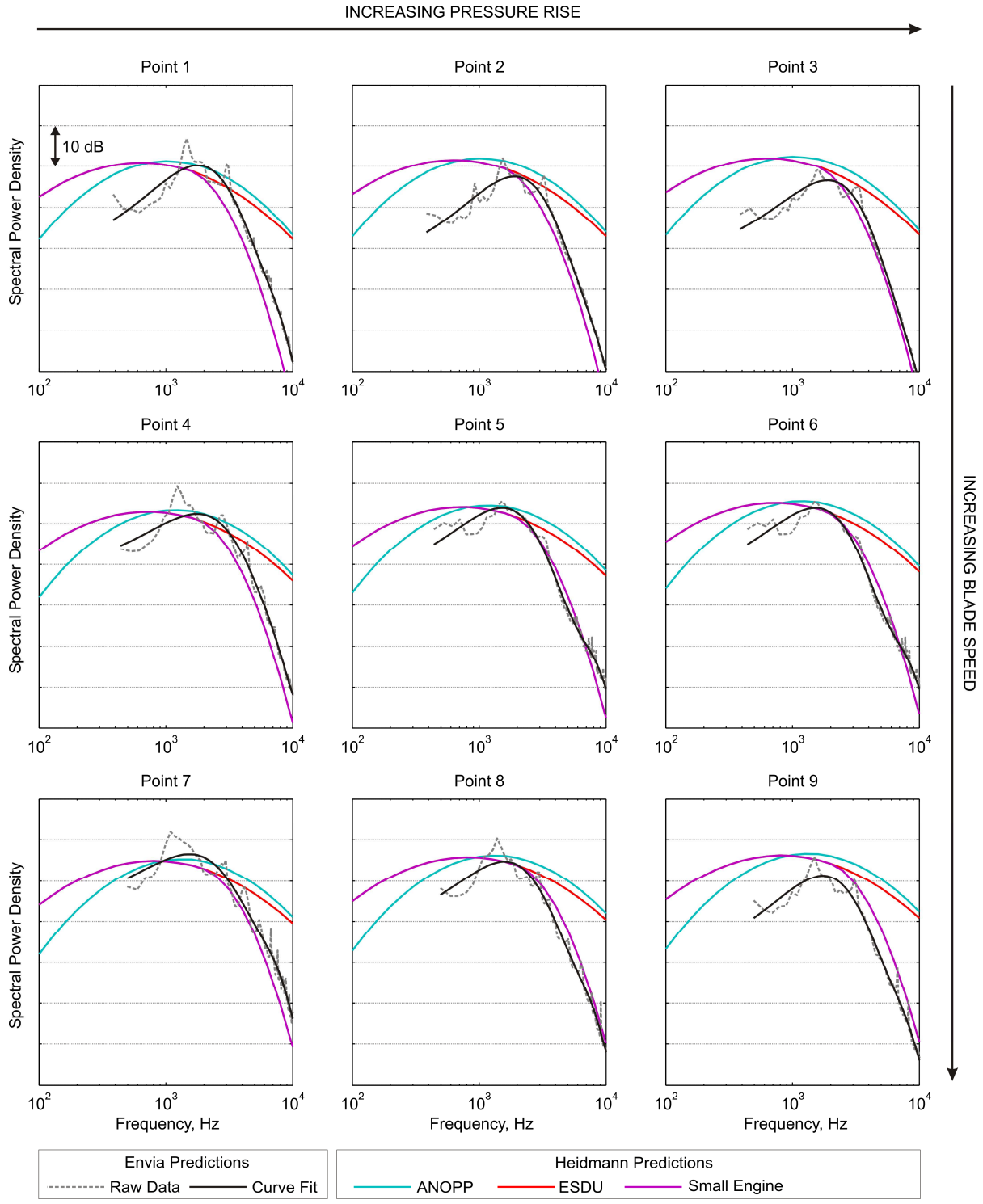

Figure 6-7: Comparison of in-duct acoustic power estimations for rearward propagating fan broadband noise.

Envia predictions are for rotor-stator interaction noise only, Heidmann predictions are for all broadband noise sources. See figure 6-5 *for location of points one to nine on fan map. All subplots cover the same noise range and are therefore directly comparable.*

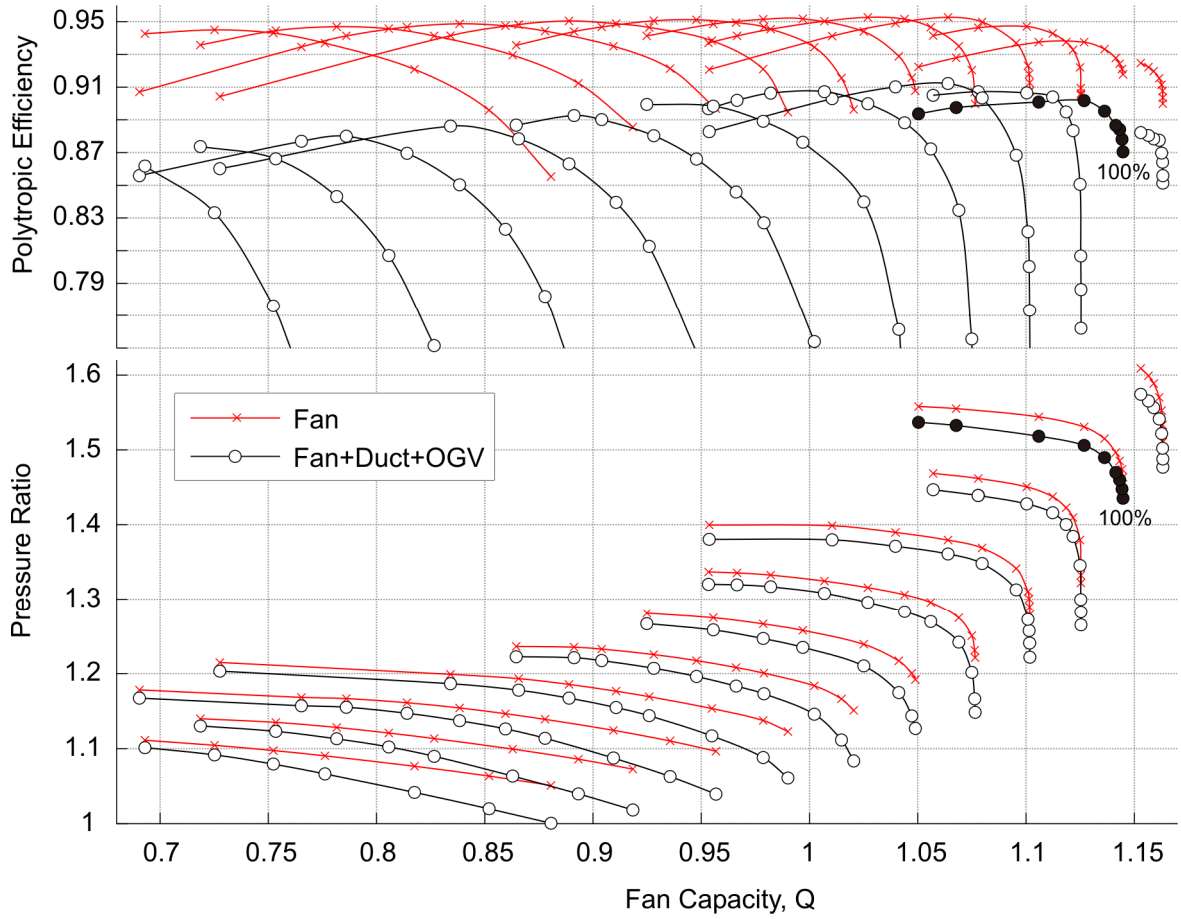

Figure 6-8: Fan Stage Map used in Take-Off Optimisation

(Lines of corrected speed from 55% to 105% in 5% increments. Fan Capacity is based on fan face conditions for all fan mass flow whilst pressure rise and efficiency values are for bypass flow only. Unlike for figure 5-10*, no attempt was made to extend characteristics towards stall.*

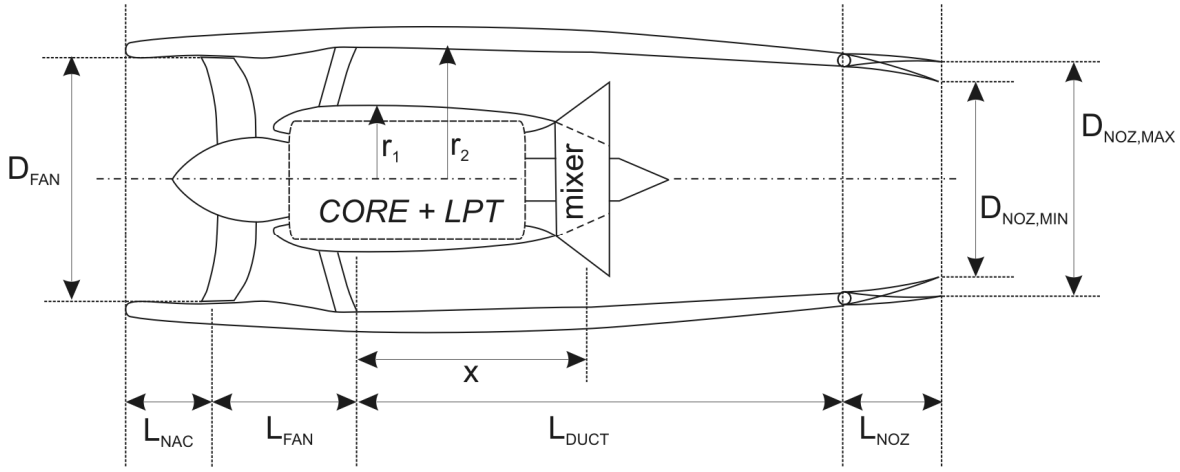

Figure 6-9: Engine cross-section

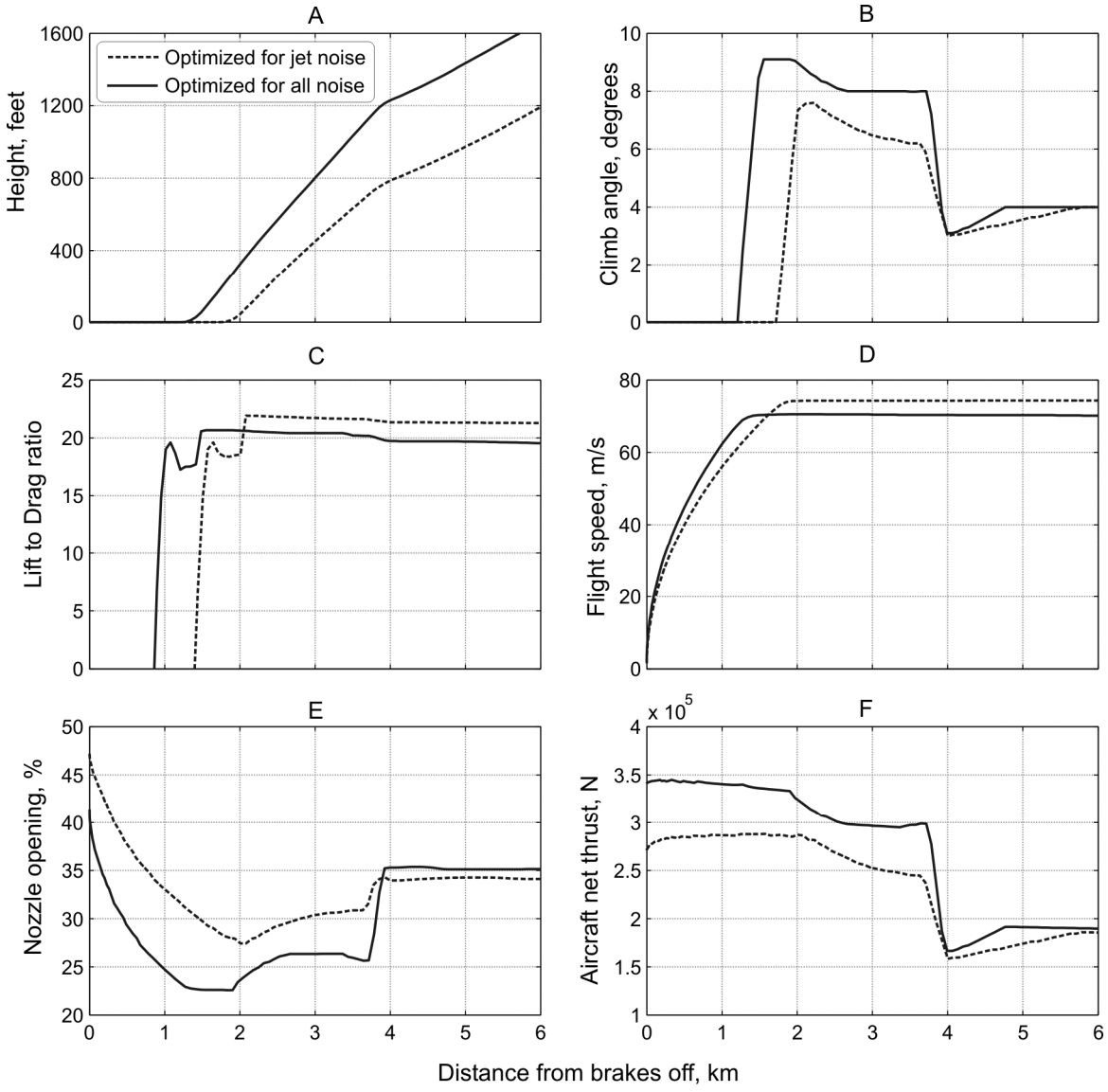

Figure 6-10: Variation in aircraft and engine parameters when taking off

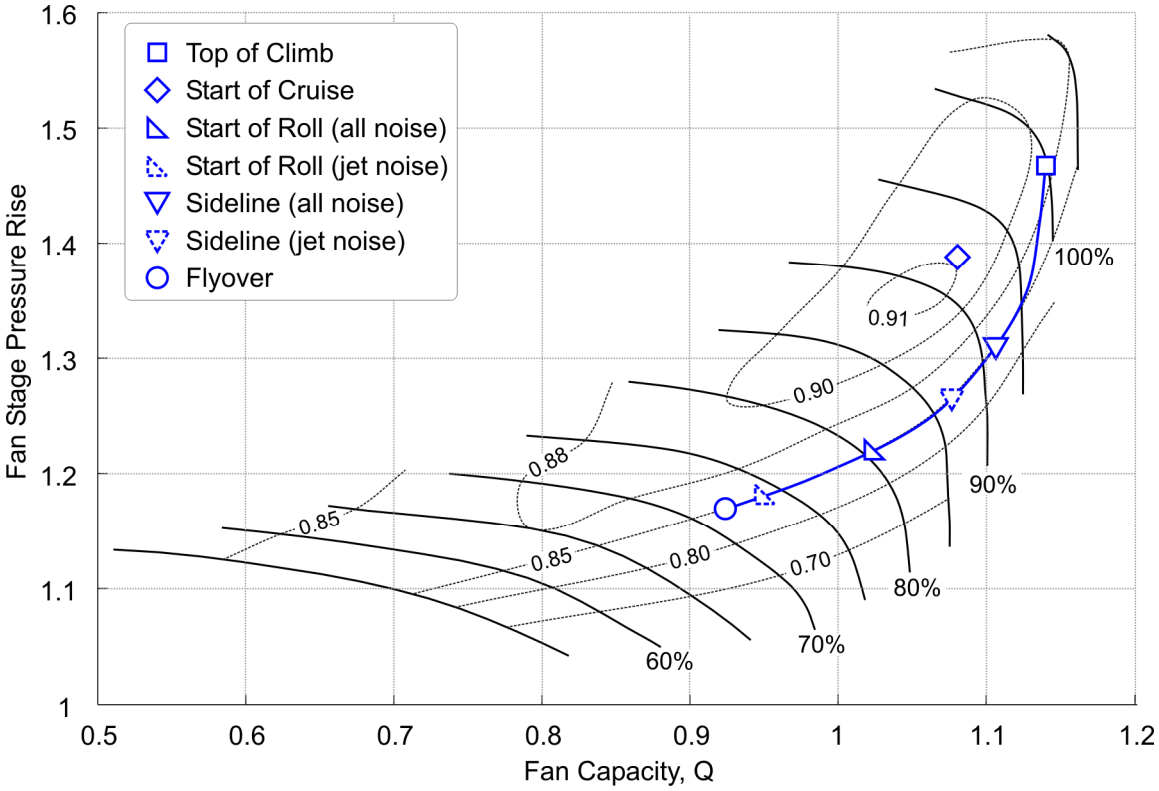

Figure 6-11: Fan operation between brakes-off and start of cruise with contours of polytropic stage efficiency

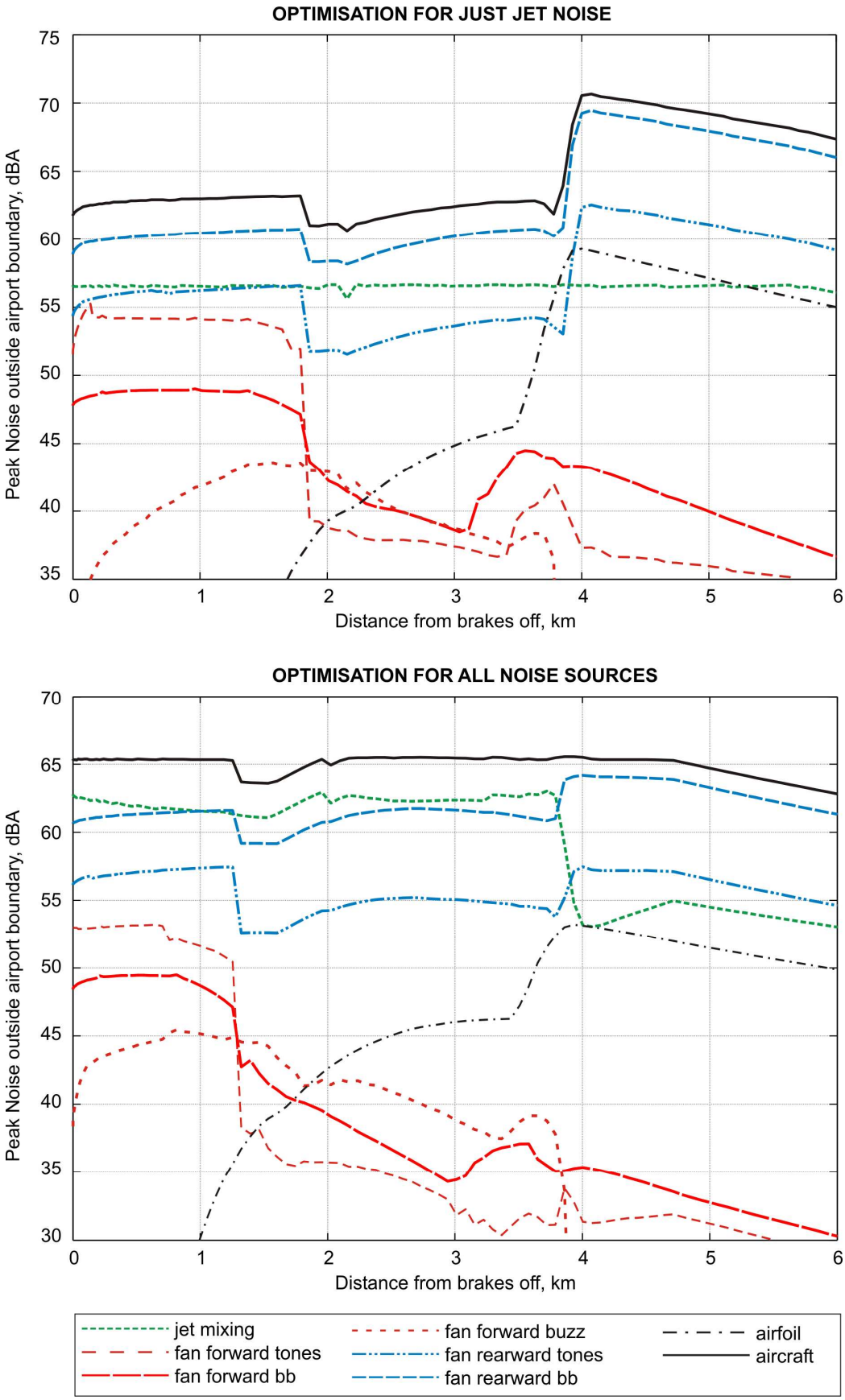

Figure 6-12: Estimated peak noise on the ground during take-off when optimising for just jet noise and when optimising for all noise sources

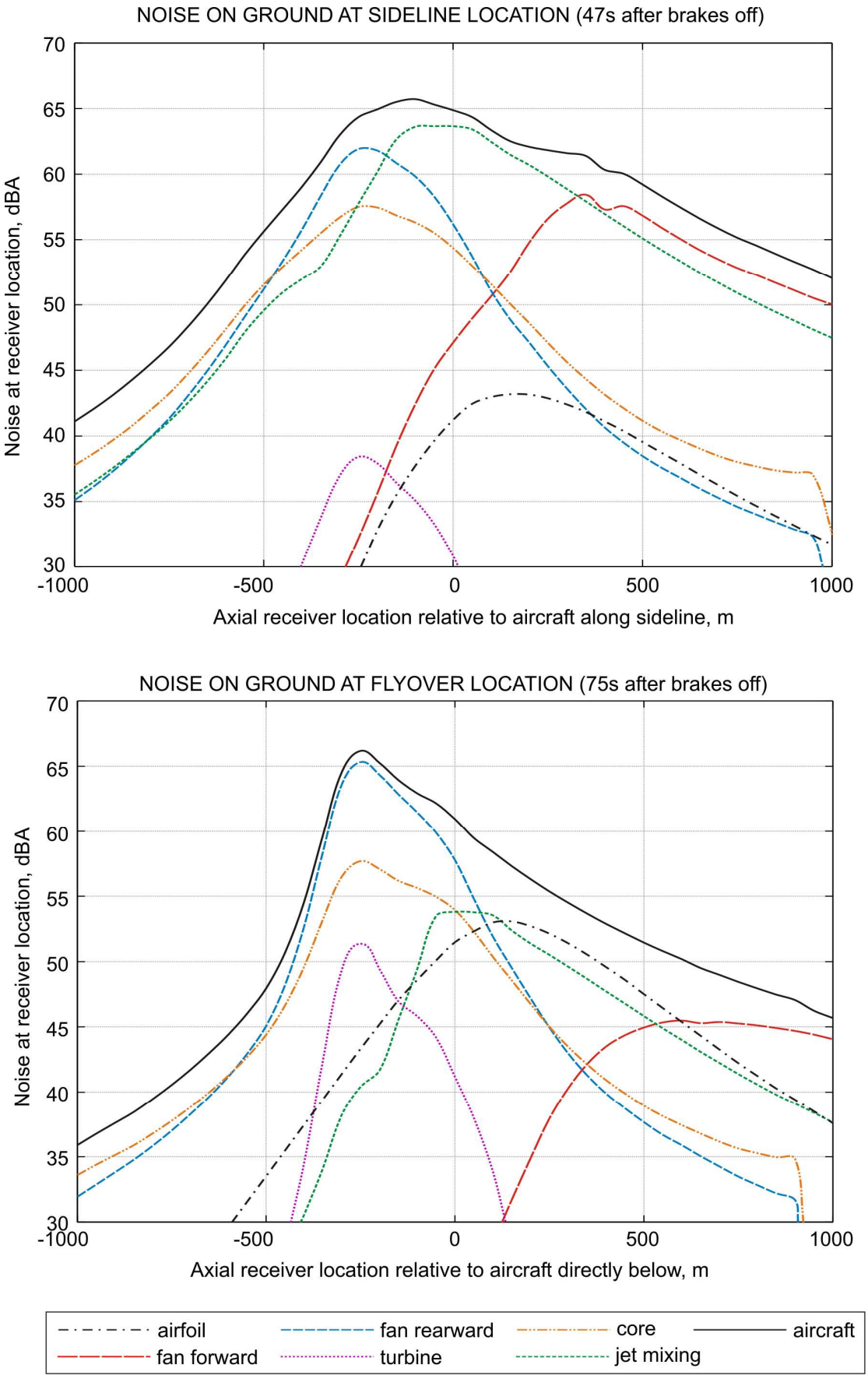

Figure 6-13: Noise footprints at sideline and flyover positions based on higher fidelity computations.

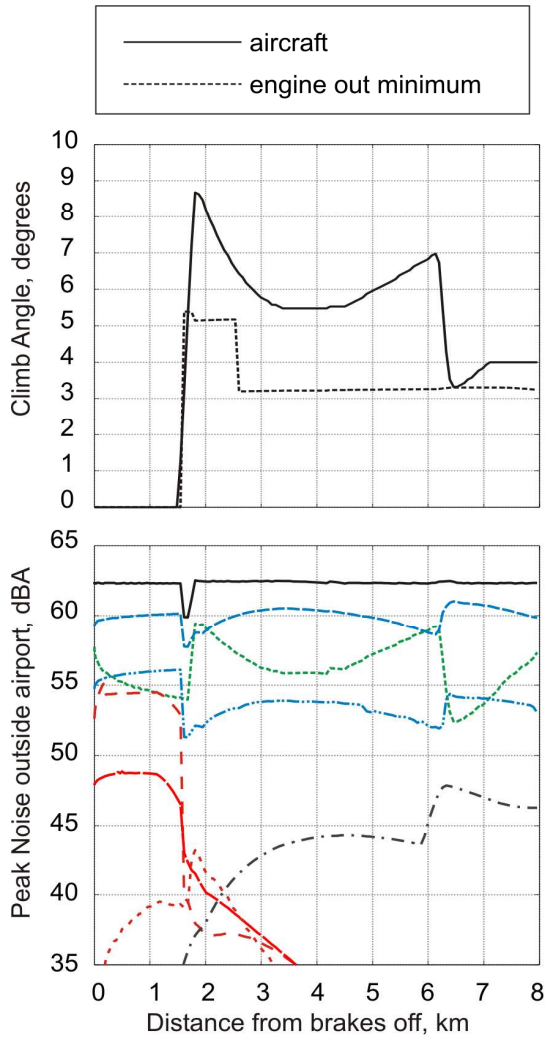

Figure 6-14: Take-off performance for a 6.5km flyover boundary

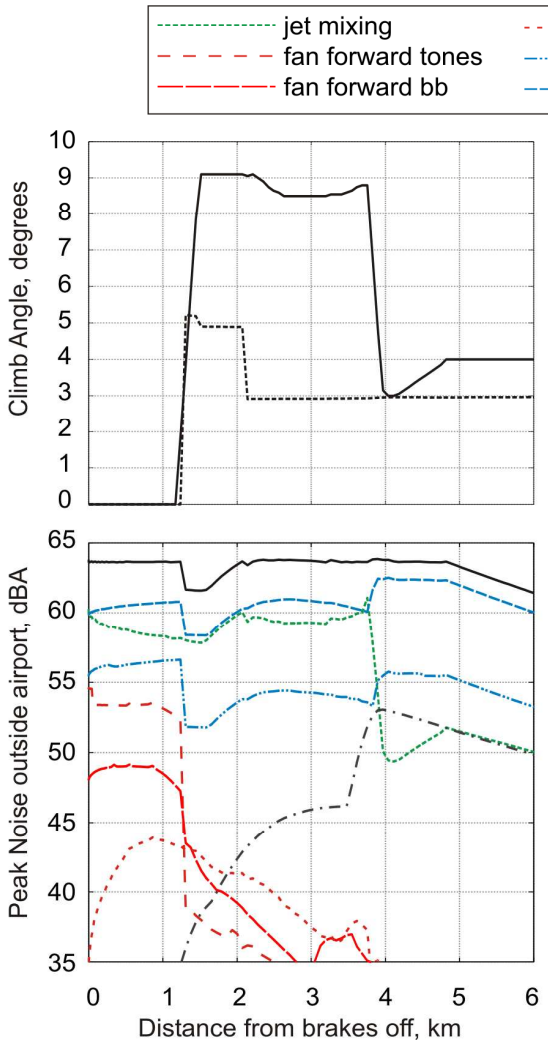

Figure 6-15: Take-off performance for baseline aircraft at 90% MTOW, ISA conditions

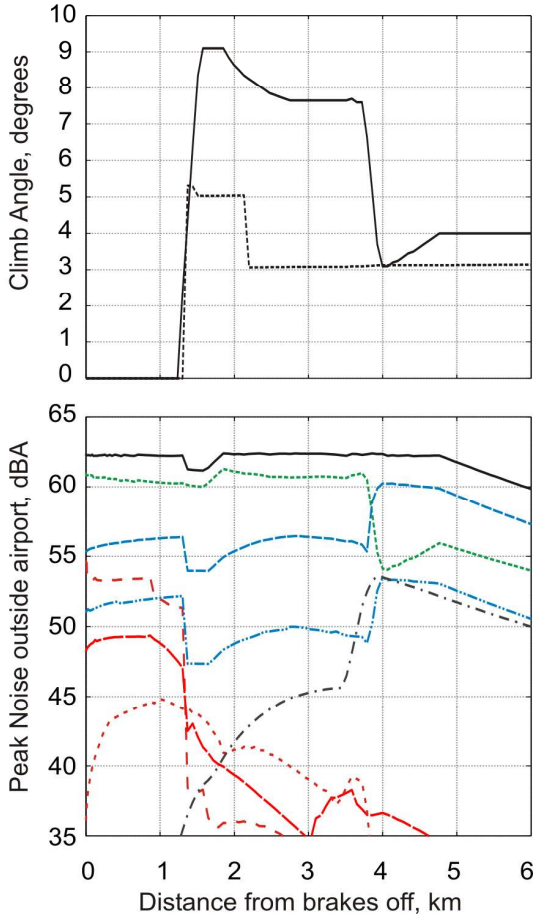

Figure 6-16: Take-off performance for an aircraft with +1 L/D annulus duct (-5dB fan rearward)

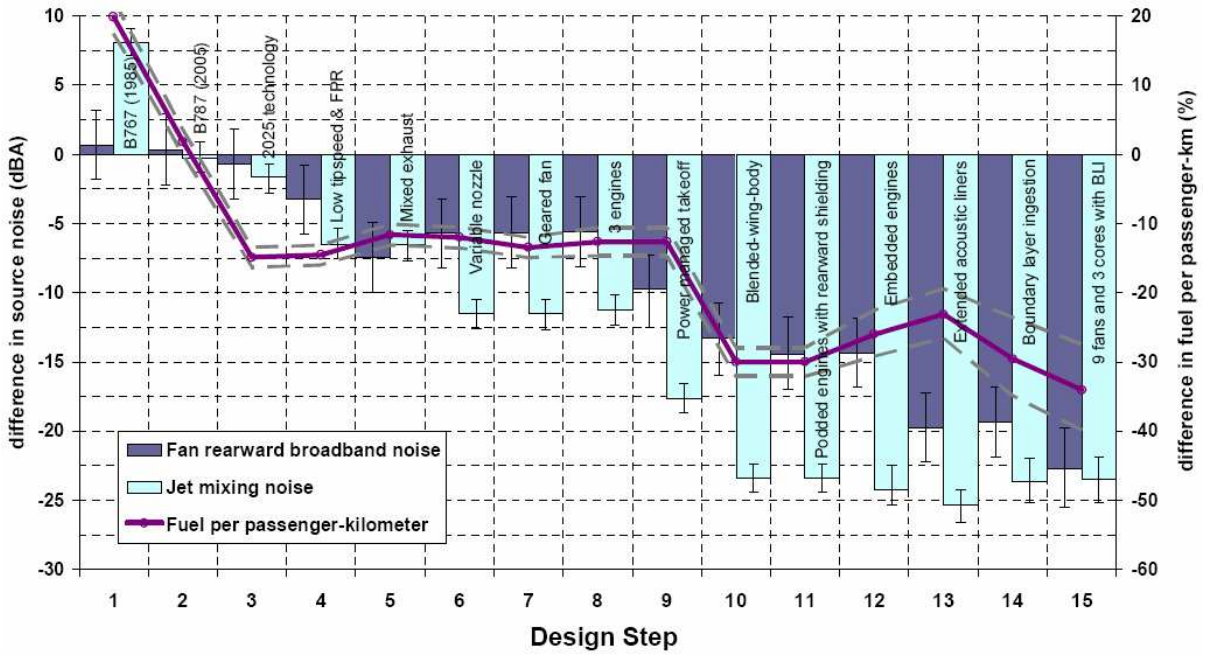

Figure 6-17: Mountains chart for take-off noise and fuel burn for earlier SAI aircraft (Schwartz 2006)

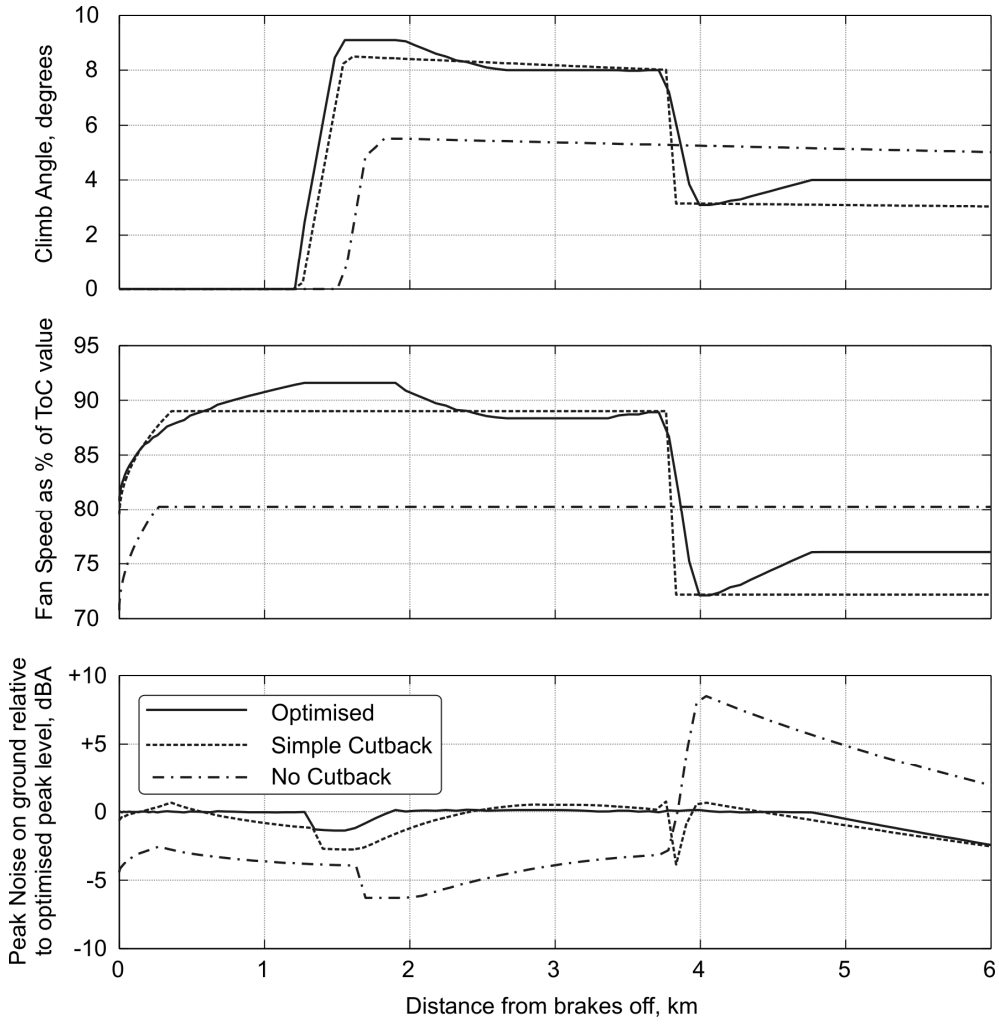

Figure 6-18: Impact of optimising take-off profile on aircraft and engine performance